Investigation of trace components in autothermal gas reforming processes

Von der Fakultät für Maschinenbau, Verfahrens- und Energietechnik

der Technischen Universität Bergakademie Freiberg

genehmigte

DISSERTATION

zur Erlangung des akademischen Grades

Doktor-Ingenieur
(Dr.-Ing.)

vorgelegt

von MSc. Ibrahim Kolawole Muritala
geboren am 14.08.1981 in Lagos, Nigeria

Gutachter: Professor Dr.-Ing. Bernd Meyer   (Freiberg)
                Professor Dr. Philipp Brüggemann   (Nürnberg)

Tag der Verleihung: 03.11.2017

Declaration

I hereby declare that I completed this work without any improper help from a third party and without using any aids other than those cited. All ideas derived directly or indirectly from other sources are identified as such.

In the selection and in the use of materials and in the writing of the manuscript I received support from the following persons:

....

....

....

Persons other than those above did not contribute to the writing of this thesis. I did not seek the help of a professional doctorate-consultant. Only persons identified as having done so received any financial payment from me for any work done for me.

This thesis has not previously been submitted to another examination authority in the same or similar form in Germany or abroad.

....

Ibrahim Kolawole Muritala

Acknowledgements

Contents

List of Figures

List of Tables

List of Abbreviations and Symbols

Abbreviations

AD   –   Amperometric detector, used in combination with IC

ASW   –   Aspen Simulation Workbook

ATR   –   Autothermal reforming of natural gas (catalytic)

AOX   –   Adsorbable organically bound halogens

BOD   –   Biochemical oxygen demand

CAS   –   Chemical Abstracts Service

CD   –   Conductivity detector, used in combination with IC

COD   –   Chemical oxygen demand or CSB – Chemischer Sauerstoffbedarf

DCS   –   Digital Control System

DIN   –   Deutsches Institut für Normung

DOC   –   Dissolved organic carbon

FAU   –   Formazine Attenuation Units

Gas-POX   –   Partial oxidation of natural gas

GasPro   –   GC column type

GC   –   Gas chromatography

HG   –   Hot gas or synthesis gas or hot synthesis gas or product synthesis gas

HP POX   –   High Pressure Partial Oxidation

IC   –   Ion chromatography

ICS   –   Ion Chromatography System

LC   –   local composition

LOQ   –   Limit of quantification

MPG   –   Multi-Purpose Gasification of heavy residual or oil gasification technology

MS5A   –   Molecular Sieve 5A, GC column type

n.n	–	Not detected
NRTL	–	Non-Random Two Liquid
PDH	–	Pitzer – Debye – Hückel
POX	–	Partial oxidation
ppbv	–	Parts per billion by volume
ppmv	–	Parts per million by volume
PPU	–	GC column type
RG	–	Raw gas or raw synthesis gas
STP	–	Standard Temperature and Pressure
SQL	–	Structured Query Language
TCD	–	Thermal conductivity detector, used in combination with GC
US EPA	–	United States Environmental Protection Agency
VOCs	–	Volatile organic compounds

Symbols

C_f	amount of carbon in feedstock
$\Delta_R H°$	Standard reaction enthalpy (for all reactants at 25°C and 1 bar)
γ^*_i	the unsymmetrical activity coefficient of ionic species i
G	Gibbs free energy
K_{eq}	Equilibrium constant
Q	Reaction quotient (real)
R	gas constant
T	absolute temperature
*	unsymmetrical
E	electrolyte
$\dfrac{G_m^{*E,PDH}}{RT}$	The Pitzer – Debye – Hückel formula, normalized to mole fractions of unity for solvent and zero for electrolytes, is used to represent the long-range interaction contribution.
$\dfrac{G_m^{*E,Born}}{RT}$	The Born equation is used to account for the Gibbs energy of transfer of ionic species from the infinite dilution state in a mixed-solvent to the infinite dilution state in aqueous phase.
$\dfrac{G_m^{*E,LC}}{RT}$	The local interaction contribution is accounted for by the Non-Random Two Liquid theory. The basic assumption of the NRTL model is that the nonideal entropy of mixing is negligible compared to the heat of mixing: this is indeed the case for electrolyte systems.
$\dfrac{G_m^{*E}}{RT}$	The excess Gibbs energy is given by adding NRTL expression for the local interactions, the Pitzer – Debye – Hückel expression, and the Born equation.
K_{eq}	Equilibrium dissociation constant
H_e	Henry's constant for the solubility of gas in pure water (Henry volatility)
P_i	Partial pressure of that species in the gas phase
m_eq	calculated equilibrium concentrations (molality)
m_real	calculated reaction quotient or calculated real concentrations (molality)
t/h	metric tonnes per hour
X_i	Molar mixing ratio in the aqueous phase

1 Introduction

1.1 Background

Gasification of carbonaceous compounds has been applied commercially around the world for years as it offers significant environmental advantages over competing technologies. With a lot of technical improvement and development on going, gasification provides potential pathways for producing commodity chemicals, synthesis of fuels and power generation. The process routes begins with the synthesis gas or syngas generation step, which can be through autothermal non-catalytic partial oxidation of natural gas (Gas-POX), autothermal catalytic reforming (ATR) of natural gas, or autothermal non-catalytic gasification of liquid hydrocarbons (Oil-POX). The produced syngas during gasification mainly consist of CO and H_2. Components like H_2O, CO_2, CH_4, N_2, trace compounds such as H_2S, COS, NH_3, HCN and others are present in the product synthesis gas (hot gas), which must be removed up to a certain threshold.

The studies of raw synthesis gas will be unfinished without thorough elucidation of trace components, which can impact on the downstream processes for raw gas treatments [Higman et al., 2003], [Stiegel et al., 2006] and [Miller et al., 2008]. Trace component analysis in gasification processes are important part of elemental component balances in order to understand the fate of these participating compounds in the feedstock. Depending on the feedstock composition and process parameters [Furimsky, 1999] and [Reed et al., 2001], these trace components can vary as they exist in the feed (e.g. as sulphur, nitrogen etc.) and / or are produced during gasification (e.g. as COS, HCN etc.). Although, there is a dearth of literatures on trace compounds studies relating to the gasification of natural gas processes. Trace components formation can occur as by-products of gasification for example during partial oxidation of natural gas at elevated temperature, the impact of raw synthesis gas water quench process can lead to the formation of organic acids like formic acid and several other components [Pitchai et al., 1986] and [Brüggemann, 2010].

Furthermore, research in the area of trace components studies in gasification processes with respect to hot synthesis gas quenching and raw synthesis gas are:

a) the studies of the influence of different operating parameters and the performance of the quench during pressurised black liquor gasification combined with catalytic process, which focuses on the final raw synthesis gas composition was done by [Wiinikka et al., 2012]. The major gas components (CO, H_2, and CO_2) of the final raw synthesis gas were influenced by the

system pressure (15 – 30 bar) in the gasifier and after cleaning in a counter current condenser gas cooler. The effects of the raised system pressure led to the increase in the concentration of minor gas components H_2S and COS in the gasifier [Wiinikka et al., 2012].

b) [Hoekman et al., 2013] developed characterization methods for sampling of organic and inorganic trace components in the raw synthesis gas produced from thermal conversion of biomass (rice hull and wood chip feedstocks). These traces were detected to be in the low ppb range. Cost-effective innovations are been developed in the cleaning and conditioning of hot gas in one reactor by integrating it with the fluidized bed steam gasification of biomass operating at 800 – 900°C. The purpose of this is to produce syngas, which is required for use in fuel cells. The finding shows that H_2S and alkali concentrations (inorganic traces) present in the hot gas from the gasifier can be limited to values above 100 ppbv and values below 100 ppmv respectively [Stemmler et al., 2013].

c) Straw char and glycol were gasified in a 60 kW pilot-scale atmospheric entrained flow gasifier [Pudasainee et al., 2014] to measure trace metals emission concentration, distribution into particle and gas phase in syngas. In the Sasol – Lurgi MK IV FBDB gasifier [Bunt et al., 2008], [Bunt et al., 2009] and [Bunt et al., 2010], Fact-Sage thermodynamic equilibrium modelling was used to simulate the trace metal elements behaviour under coal gasification process. These metals were distinctly categorized into volatile, semi-volatile, and non-volatile elements. It is possible for these volatilized metals to condensed on various components of the gasifier and results to reduction in the life of the gasifier [Bucko Z. et al., 2000], [Nishiyama et al., 2006], [Mondal et al., 2011] and [Cui et al., 2013] especially during the exposure of steels and alloys to carbon monoxide (CO)-rich gases at 450 – 700 °C [Stahl et al., 1996].

d) [Öhrman et al., 2014] analysed and measured H_2S, benzene, acetylene, ethylene, methane, soot and other traces present in the synthesis gas and the waste water during high temperature (1130 – 1340 °C and at 2 bar absolute pressure) gasification of milled soft stem wood powder from a pilot scale pressurized entrained flow oxygen blown biomass gasifier. The black residues collected from the surface of the quench water were dried and analysed in a thermo gravimetric analyser connected to a mass spectrometer. It was observed that the soot, quench water and cold synthesis gas have low amount of naphthalene, phenanthrene, fluoranthene, pyrene and other materials. Also, an earlier research from a pilot scale pressurized black liquor gasifier [Öhrman et al., 2012] indicates a reduction of COS from 400

ppm in the gasifier to 100 ppm after the quench, leading to an increase in the concentration of H_2S in the quench water due to the hydrolysis of COS. Particles comprising of Fe, S and Ni were detected to ensue from the corrosion of stainless steel piping and process equipment in the plant [Öhrman et al., 2012].

e) A new development to collect, identify and quantify traces in hot gas stream generated from biomass gasification was achieved [Woolcock et al., 2015]. The method applied time-weighted average (TWA) passive sampling with retracted solid-phase microextraction (SPME) and gas chromatography. The amount of trace tar compounds were quantified for a single analyte (for benzene at 115 °C) and at temperatures approaching 300 °C standard gas stream, validated on a pilot scale gasification and gas cleaning process with accurate prediction of gas stream concentrations in the ppb range at higher temperatures [Woolcock et al., 2013].

f) Based on some assumptions, a mathematical model of a column for retaining NH_3 and CO_2 into condensing water in a counter current organic solvent scrubber during biomass gasification at temperatures between 850 – 900 °C was developed [Pröll et al., 2005]. Decrement in NH_3 and CO_2 concentration in hot synthesis gas was realized. The goal was to reduce the amount of NH_3 in the hot synthesis gas by adjusting operating parameter in order to avoid additional gas cleaning steps [Pröll et al., 2005]. Gas-liquid equilibrium interaction between the condensate and the hot synthesis gas in the scrubber was applied based on NH_3-CO_2-H_2O model studies by [Edwards et al., 1975].

g) The controlling of the pH of water applied to quench and to scrub raw synthesis gas was reported during the production of synthesis gas by partial oxidation of hydrocarbons as raw synthesis gas exit the reaction zone between 700 – 1650 °C [Kimberly et al., 1989]. The patent gave claims to the formation of acidic compounds (formic acid) during quench operation and basic compounds (ammonia) during partial oxidation.

h) [Chih-Hao et al., 2003] employed the use of ammonia injection to minimize waste water treatment in order to have fewer amounts of metal contents in the effluent (grey water) of the quench water during the non – catalytic partial oxidation reaction of hydrocarbonaceous fuels (with preferred operating temperature of about 1200°C – 1500°C and most preferred pressure from 20 – 90 bar). This approach allows the recovery and recycling of more of the effluent water during gasification. [Anindra et al., 2015] utilized a carbon dioxide injector source to adjust the pH of the quench water. This was achieved by a configuration of pH

sensor to measure the pH of the grey water with a control valve to adjust the flow of the acidified water into the grey water. The process treats the black water from the quench chamber to generate grey water and soot.

Taking a critical look at the several gasification process plants operating world-wide and those at the planning stage [Shoko et al., 2006] and [Mondal et al., 2011], the total syngas production capacity was reported to be around 428,866,510 Nm^3/day [IGO et al., 2003]. The amounts of traces that are formed during gasification of natural gas are at low level in ppm. But the yearly consumption of natural gas for gasification is large, which provides the potential for these traces into the environment and calls for concerns.

In spite of all these, understanding of traces formation during gasification and quench operations can help in the choice of the downstream syngas treatment and utilization processes. Consequently, the corrosion effects on plant facilities, poisoning of catalysts and most importantly their discharge via effluents and their presence, which results from the accumulated build-up of these trace compounds could be mitigated and controlled when their sources and sinks are analytically identified.

1.2   Objective of the Work

The task of the present work is to investigate the effects of quenching operation on the trace components before and after the water quench operations during the autothermal non-catalytic reforming of natural gas (Gas-POX). In order to achieve this, Aspen Plus simulation model of the quench chamber of the HP POX (high pressure partial oxidation) plant at the Institute of Energy Process Engineering and Chemical Engineering (IEC), TU Bergakademie Freiberg was developed to re-calculate the quench chamber input amount of different trace compounds from their output amount measured during test points of the Gas-POX campaigns. As these traces are undesired, the assessment of the results in this work should lead to the improvement in the understanding of trace components and concepts that could be employed to influence their formation and reduction.

1.3 Overview of the Work

Presented in Chapter 2 are the process and test conditions during the test campaign of the Gas-POX. The HP POX test plant features, gaseous feedstock characteristics including natural gas, methods used to analysed the gaseous product and aqueous phase products were discussed. After that, Chapter 3 emphasizes on the simulation and concepts that were utilized to develop the HP POX quench water system model with the support of tools like Visual Basic for Applications (VBA), and Python as an interface between Aspen Plus and Microsoft Excel. In addition, Chapter 3 gives detail information about the thermodynamic consideration with respect to the property methods and sensitivity analysis studies. Chapter 4 reviews some trace components present in the quench water. It discussed their dissolution as well as vapour-liquid equilibria properties as their distribution were influenced by quench water pH values and quench water temperature variations. In order to investigate the formation of organic acids that were analysed from the quench water effluent samples, chapter 5 focuses on the formation of formic acid and acetic acid in the quench water. Chapter 6 looks at the formation of nitrogen compounds in the gasifier during gasification and their resultant effects when hot synthesis gas was quench-cooled in the quench chamber. The last is chapter 7, which discussed the possible causes and effects that could be responsible for the formation of traces such as BTEX, PAHs and soot in the quench water effluent during gasification of natural gas and the results of the analysed quench water effluent samples during the test campaigns under review.

2 Process and test conditions

2.1 HP POX test plant

The HP POX (high pressure partial oxidation) test plant has been in operation for research since summer 2004. This semi-industrial scale test plant is located on the site of the Institute of Energy Process Engineering and Chemical Engineering (IEC), Technische Universität Bergakademie Freiberg. It belongs to the university and it was designed and erected by Lurgi GmbH (now a part of the Air Liquide group) [COORAMENT report, 2010]. Its operation modes includes: autothermal catalytic reforming (ATR) of natural gas at pressures up to 70 bar (g), autothermal non-catalytic partial oxidation of natural gas (Gas-POX) at pressures up to 100 bar (g), which is the focus of this work and autothermal non-catalytic gasification of liquid hydrocarbons (Oil-POX), which is known as Multi-Purpose Gasification (MPG) at pressures up to 100 bar (g). Presented in Fig. 2.1 is the HP POX test plant´s flow chart with the main plant facility and material flow.
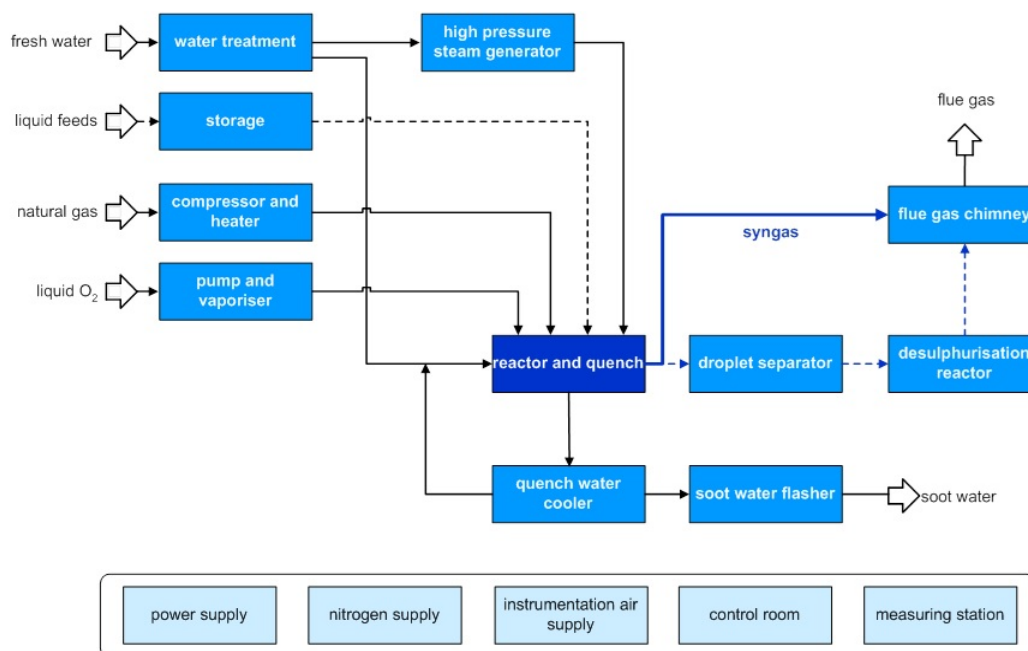
Figure 2.1: HP POX test plant main facility components and material flow courtesy of [Lurgi GmbH, 2008]

The HP POX test plant was specially designed to allow modification in its reactor geometry. Its combined pressure vessel in Fig. 2.2 consist of the reaction chamber (gasification unit) situated at the upper part of the pressure vessel and the quenching chamber below. The equipment allows for the variation of process parameters (pressure, temperature and quenching temperature) exceeding the

6

range generally employed in industrial practice [COORAMENT report, 2010]. During the ATR mode of operation, common reforming catalysts are usually filled in the lower part of reaction chamber. Also, natural gas is the feedstock during ATR and Gas-POX mode while liquid hydrocarbons are the feedstock in the MPG mode. In all these modes of operation, the feedstock mixes and reacts with oxygen and moderating steam. The oxygen is supplied as liquid oxygen which is pumped to the required pressure, evaporated and preheated before it is fed into the gasifier. Steam is supplied at high pressure from the water treatment facility after the production of deionized water that is used for the quenching process. The product synthesis gas which is also known as hot gas stream leaving the reactor is rapidly quench-cooled with quench water while the saturated raw synthesis gas is separated from the liquid phase in the quench chamber. Depending on the purpose of the experiment or test campaign, the product synthesis gas is flared at the flue gas chimney after sampling and measurements or used as feed for the gasoline synthesis test plant. The test plant has had over 8000 hours of operation over the years since installation. Furthermore, the test plant has a maximum thermal capacity of 5 MW, which corresponds to at the most 500 m^3 (STP)/h natural gas, or 500 kg/h liquid feed and it generates up to 1500 m^3 (STP)/h synthesis gas. An optical probe system (in Fig. 2.2) may be used to have visual access to the flame. This probe needs nitrogen flushing to keep the optics clear. This additional N_2 stream enters the reactor. The optical probe is mounted at the preheating burner port after heating the reactor refractory walls.
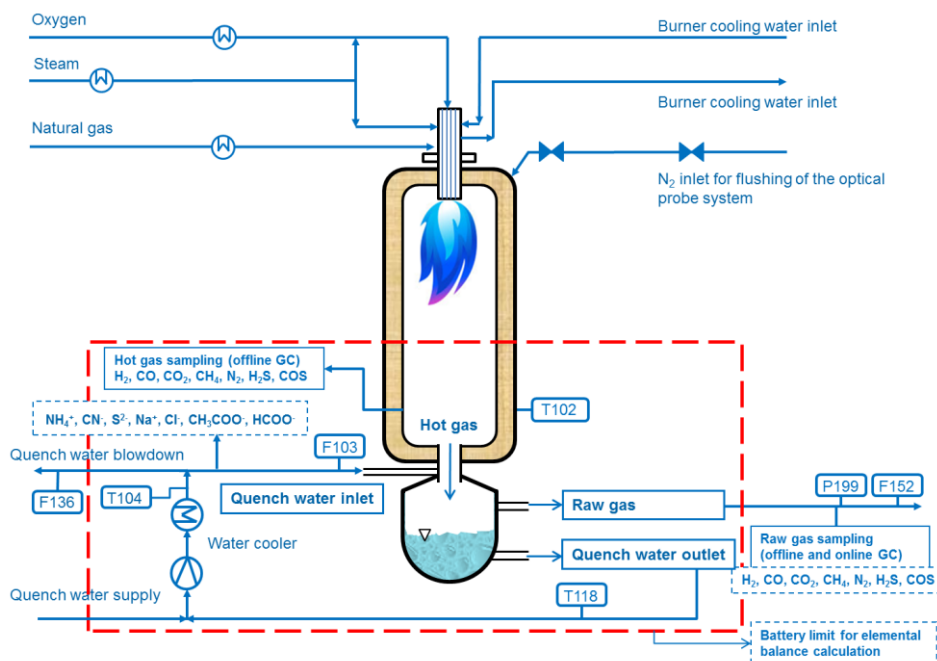
Figure 2.2: Simplified scheme of HP POX plant (including quench system) [Lurgi GmbH, 2008]

2.2 Test campaign procedure

The experimental results obtained during the test campaign activities on the HP POX test plant from April 2014 to March 2016 were used for these studies. In these periods, a total of 47 test points in the Gas-POX mode were obtained, they shall be the basis of this work and discussed in the later chapters. Measurement and sampling of feedstock, product synthesis gas, raw synthesis gas and quench water effluent were carried out during the test campaigns. In addition to all these measurements, the flows, temperatures, pressures and online analysis data of feeds, products and water cycles measured at the HP POX test plant were recorded and visualized using a DCS system. The data required for evaluating the test runs and for closing the balances were recorded every second and stored on an SQL server [Richter et al., 2015]. More information about other modes of operation of the HP POX test plant as well as the feedstocks analysis, gaseous phase products and aqueous phase product analysis can be found in [Meyer, 2007] and [Brüggemann, 2010].

2.2.1 Gas-POX operating parameter range

The Gas-POX operation mode of the HP POX ranges between 30 – 100 bar. Product synthesis gas outlet stream temperature goes up to 1450 °C. The feedstocks are natural gas, O_2 and steam. The natural gas is supplied at 12 bar via local gas distribution network and it is compressed (at most 113 bar) and preheated to 380 °C before entering the reactor.

Table 2.1: Outline of Gas-POX mode operating parameter range

Operating pressure	30 – 100 bar
Operating temperature	
Free space temperature	1450 °C
Outlet temperature	up to 1450 °C
Feedstock	
Natural gas	from 190 m³/h
Additional gases	
CO_2	up to 110 m³/h
N_2	up to 130 m³/h
Oxygen	from 80 m³/h
Steam	from 35 kg/h

2.2.2 Gas-POX experiments

The test runs in these studies focus on the variation of throughput of the natural gas residence time and the effect of the listed parameters on the synthesis gas composition as well as trace component formation:

- Pressure
- Temperature
- Feed ratio $O_2 : C_f$
- Feed ratio $H_2O : C_f$

Before the Gas-POX operation commences, it is possible to adjust the volume of the reactor by the addition of refractory bricks on the reactor wall.

Table 2.2: Outline of test runs operating mode and parameters of chosen test campaigns

Pressure	$H_2O : C_f$	$N_2 : C_f$	Points of investigation
bar (g)	mol / mol	mol / mol	
$50 - 60$	$0.2 - 0.5$	$0 - 0.007$	$O_2 : C_f$ (T) variation

2.2.3 Net reactions of partial oxidation

Partial oxidation (POX) process is the reaction of carbonaceous compounds (natural gas) and oxygen to be converted to synthesis gas according to following overall reaction:

$$C_nH_m + \frac{n}{2} O_2 \rightleftharpoons nCO + \frac{m}{2} H_2 \tag{2.1}$$

The methane and other hydrocarbons in natural gas like ethane, propane and butane in Table 2.3 react with a limited amount of oxygen which is not enough to completely oxidize the natural gas into carbon dioxide and water [Huff et al., 1994]. The reaction (2.1) can be summarized into series of basic chemical reactions such as partial oxidation of methane:

$$CH_4 + \frac{1}{2} O_2 \rightleftharpoons CO + 2 H_2 \qquad \Delta_R H^\circ_{298\,K} = \text{-35.7 kJ/mol} \tag{2.2}$$
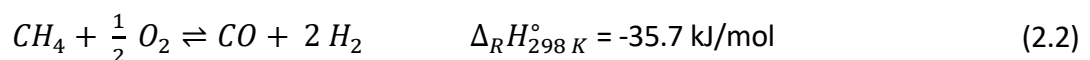
Partial oxidation of natural gas is an autothermal process involving in-situ partial combustion of natural gas at sufficiently high temperatures. The stoichiometry of the reaction is maintained to yield syngas mainly containing H_2 and CO and a $H_2 : CO$ ratio of 2 [Curry-Hyde et al., 1994]. It is possible to

have other reactions to take place where the feed gas reacts with CO_2 [Uchijima et al., 1994] to produce more syngas according to reactions (2.3)

$$CH_4 + CO_2 \rightleftharpoons 2\ CO + 2\ H_2 \qquad \Delta_R H^\circ_{298\ K} = 247.3\ \text{kJ/mol} \qquad (2.3)$$
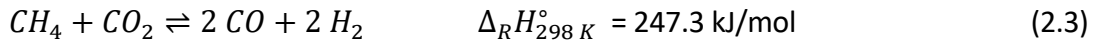
Reaction (2.3) is also called dry reforming or carbon dioxide reforming of methane.

$$CH_4 + H_2O \rightleftharpoons CO + 3\ H_2 \qquad \Delta_R H^\circ_{298\ K} = 206.2\ \text{kJ/mol} \qquad (2.4)$$
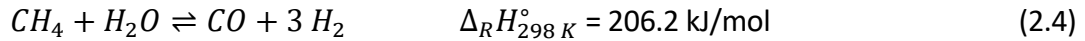
Reaction (2.4) is known as steam methane reforming; it is an endothermic reaction which means it requires heat supply to the process. This reaction offers the highest molar ratio of H_2/CO [Pitchai et al., 1986]. The reaction (2.2) occurs with the methane as the main constituent of the natural gas, steam and / or carbon dioxide combined to have the exothermal partial oxidation as well as the endothermal reforming reactions (2.3) and (2.4). In the instant that the gas is considered for subsequent synthesis, the water gas shift reaction (2.5) becomes important for adjusting $H_2 : CO$ ratio. Water gas process is used to produce hydrogen due to its economic benefits in Haber ammonia synthesis process with other types of water gas reported in [Smirniotis et al., 2015].

Carbon monoxide and steam reacts via shift reaction to produce an equimolar mixture of carbon dioxide and hydrogen.

$$CO + H_2O \rightleftharpoons CO_2 + H_2 \qquad \Delta_R H^\circ_{298\ K} = \text{-41.2 kJ/mol} \qquad (2.5)$$
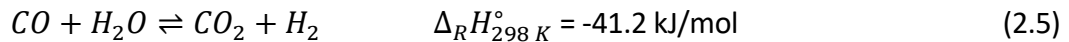
The reaction (2.6) is the total oxidation of methane and other hydrocarbons (in the natural gas), which is the main reaction in the zones of stoichiometric mixture in the flame.

$$CH_4 + 2\ O_2 \rightleftharpoons CO_2 + 2\ H_2O \qquad \Delta_R H^\circ_{298\ K} = \text{-802.3 kJ/mol} \qquad (2.6)$$
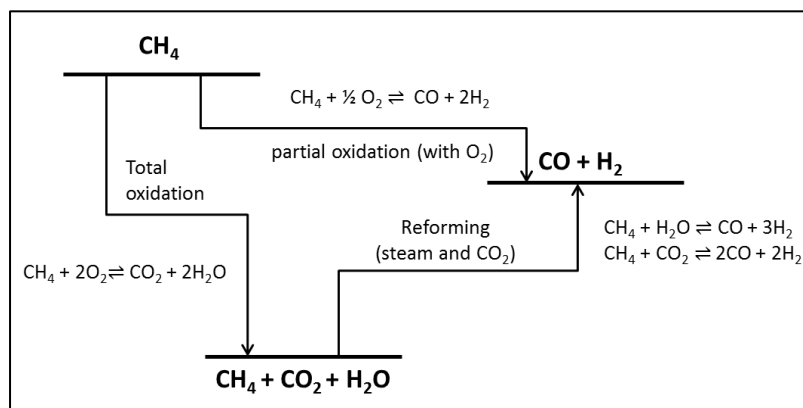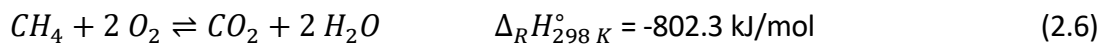
Figure 2.3: Overview of reactions of methane

Gasification processes for liquid feeds can be applied with little modification for partial oxidation of natural gas and other possible gaseous feedstocks [Higman et al., 2003]. But some considerations relating to feed preheating and the burner tends to differ. Generally, commercial production of syngas has been predominated by steam methane reforming (SMR) technology [Wilhelm et al., 2001] and partial oxidation of methane is an alternative technology especially the catalytic partial oxidation due to the fast heterogeneous reactions at lower temperatures [Zhou et al., 2010]. Although it requires high temperature [Pena et al., 1996], the unrequired catalyst cost associated with non-catalytic partial oxidation of methane gives it a great advantage. The concerns relating to the formation of carbon or soot and possible deposition on catalyst leading to the coking and deactivation of the catalyst in the steam reforming and catalytic partial oxidation processes have made non-catalytic partial oxidation of methane to be of great interest industrially over the former [Aasberg-Petersen et al., 2001] and [Zhou et al., 2010]. Although, the non-catalytic partial oxidation combines the catalytic steam reforming in an autothermal reforming (ATR) process [Aasberg-Petersen et al., 2003].

To improve the know-how relating to key process parameters in the production of syngas by non-catalytic partial oxidation of natural gas, several published researches [Konnov et al., 2004], [Zhou et al., 2010], [Guo et al., 2012], [Li et al., 2013], [Xu et al., 2014], and [Guiberti et al., 2016] have suggested a lot of findings and progress focusing on the upstream part of the gasification processes.

2.3 Gaseous feedstock characterization

The relevant properties of the feed input are discussed in this section. The feeds are natural gas, oxygen, and steam. The liquid oxygen and steam are of 99.5% purity and they serve as the gasification agents. The rest of the 0.5% liquid oxygen is assumed to be argon. As earlier stated, nitrogen is fed into the gasifier for the purpose of the optical probe apart from the negligible amount present in the natural gas as shown in Table 2.3 (see Appendix Table 9.1: Natural gas feed analysis method).

2.3.1 Natural gas feedstock composition

The natural gas used is supplied from two sources. Table 2.3 give the typical composition of the Russian and North Sea natural gas supplied to feed the HP POX test plant.

Table 2.3: Natural gas feedstock compositions

	Gas 1 (Russian)	Gas 2 (North Sea)
Molar composition (%)		
CH_4	97 – 99	88 – 90
C_2H_6	0.8 – 1.1	4 – 5
C_3H_8	0.3 – 0.4	0.5 – 1.0
∑(C_4H_{10} and higher)	0.1 – 0.2	0.1 – 0.2
N_2	0.6 – 0.8	2 – 4
CO_2	< 0.03	1 – 2

2.4 Analytical methods for gaseous products

2.4.1 Hot gas sampling

During operations, the product synthesis gas or hot gas stream exit the gasifier and it is cooled in the quench chamber. Moreover, for the sake of gas sampling, a part of the hot gas is sampled after indirect cooling in a water-cooled tube. Table 2.4 presents the analysis methods for products synthesis gas before quench operation.

Table 2.4: Product synthesis gas analysis method (hot gas before quench) [Brüggemann, 2010]

Sample	Anaylsis method and sampling time interval	Result
Product synthesis gas or hot gas before quench operations	GC-TCD (offline), MS5A column, Carrier gas: Argon, 2 hours	concentration of CH_4,N_2, H_2 (LOQ 100 ppmv)
	GC-TCD, PPU column, Carrier gas: Helium, 2 hours	CO_2, C_2H_6, C_2H_4, C_2H_2, C_3H_4, H_2S, COS (LOQ 20 ppmv)
	Absorption in aqueous H_2SO_4 solution for 2 – 6 hours per run, aqueous NH_3 concentration with IC according DIN EN ISO 14911	concentration of NH_3
	Absorption in aqueous NaOH concentration according DIN 38 405-D13	concentration of HCN
	Absorption in aqueous $C_4H_6CdO_4$(aq), aq. concentration according DIN 28 405-D26	concentration of H_2S
	Dräger tube according expected concentration range, 2 – 6 hours	approximate concentration of H_2S (LOQ 0.2 ppmv), NH_3 (LOQ 0.25 ppmv), HCN (LOQ2ppmv)

2.4.2 Raw synthesis gas analysis after quench

The composition of the raw synthesis gas was analyzed by the online and offline gas chromatography (multi-channel micro-GC 3000A). The online GC measures gas samples directly from the plant while the offline GC located in the laboratory analyses gas samples collected in gas bags from the plant at the same sampling location at intervals during the plant operation (see Table 2.5). Both online and offline GC were used to analyze raw synthesis gas with respect to CO_2, CO, H_2, CH_4, N_2, H_2S and COS.

Table 2.5: Analysis methods for raw synthesis gas [Brüggemann, 2010]

Sample	Analysis method and sampling time interval	Result
Raw synthesis gas after quench operations	GC-TCD (online), MS5A column, Carrier gas: Argon, Continuous sampling	concentration of H_2 (LOQ 100 ppmv)
	GC-TCD (online), MS5A column, Carrier gas: Helium, Continuous sampling	concentration of CH_4, N_2, CO, O_2 (LOQ 100 ppmv)
	GC-TCD (online), PPU column, Carrier gas: Helium, Continuous sampling	CO_2, H_2S, COS (LOQ 20 ppmv)
	GC-TCD (offline), MS5A column, Carrier gas: Argon, 2 hours	concentration of CH_4, N_2, CO, H_2 (LOQ 100 ppmv)
	GC-TCD (offline), PPU column, Carrier gas: Helium, 2 hours	CO_2, H_2S, COS (LOQ 20 ppmv)
	Dräger tube according expected concentration range, 2 – 6 hours	approximate concentration of H_2S (LOQ 0.2 ppmv), NH_3 (LOQ 0.25 ppmv), HCN (LOQ 2 ppmv)
	Absorption in aqueous H_2SO_4 solution for 2 – 6 hours per run, aqueous NH_3 concentration with IC according DIN EN ISO 14911	concentration of NH_3
	Absorption in aqueous NaOH concentration according DIN 38 405-D13	concentration of HCN
	Absorption in aqueous $C_4H_6CdO_4$(aq), aq. concentration according DIN 28 405-D26	concentration of H_2S

The raw gas samples were cooled and dried before online and offline GC sampling. It takes the offline GC a minimum of 4 minutes to analyze a gas bag and this was repeated 3 times for the two raw

synthesis gas sample bags making a total of 6 analyses for the offline GC at each of the chosen time points (time interval: 2 hours) within the test point. The average value of the 6 analyses of each of the chosen time points was taken for the offline GC. In order to ensure accuracy in the measurements, the final raw gas sample measurement was derived from the average of both the measured offline and online GC.

2.5 Aqueous phase product analysis

The analysis of the aqueous phase was carried out with the aid of ion chromatography (IC) (see Table 2.6). Section 2.5.1 gives the detail procedures for measuring CN^-, S^{2-} and NH_4^+ ions.

Table 2.6: Analysis methods for aqueous phase products [Brüggemann, 2010]

Samples	Analysis method	Sampling time interval	Result
Quenching water	IC-CD, DIN EN ISO 14911	2 hours	concentration of NH_4^+, $HCOO^-$, CH_3COO^-, Na^+, K^+, Mg^{2+}, Ca^{2+}, Cl^-, SO_4^{2-}, NO_3^-, NO_2^-, PO_4^{3-}, $S_2O_3^{2-}$, etc. in stabilized water phase
Quenching water	IC-AD, DIN 38405-D26 (S^{2-}), DIN 383405-D13(CN^-)	2 – 6 hours	CN^- and S^{2-} after distillative preparation
Quenching water	DOC, DIN EN 1484	selected experiments	dissolved organic carbon (DOC) concentration in water phase

The measured values (in blue) were used for the back calculation in the Aspen Plus set up for the HP POX test plant quench water system in Fig. 3.2 as well as chapter 4, 5 and 6.

2.5.1 Molecularly dissolved trace compounds and their ions trace analysis

The measurement represents the trace content according to quench water effluent stream for the overall NH_3, H_2S and HCN (see Table 2.6). Analyses of quench water samples were performed to check for the amount and constituent compositions of cations (NH_4^+) and anions (CN^- and S^{2-}) during the test campaign. Three different analytical procedures were used for NH_4^+, CN^- and S^{2-}. Quench water was collected in three different laboratory sample flasks with one being filled with a stabilizer solution of zinc acetate (for S^{2-} analysis), another flask with tablets of NaOH as stabilizer (for CN^- measurement) and an empty sample flask without stabilizer (for NH_4^+ and other ions).

The flask content used for analysis of NH_4^+ and other ions was filtered via a cartridge and then transferred into small sample test bottles and placed in the ICS – 2000 (for anions analysis) and ICS – 1500 (for cations analysis) coupled with the integrated system, which performs all types of ion chromatography separations using an electrical conductivity detector.

In the case of S^{2-}, the sampled solution (quench water sample with zinc acetate stabilizer) was consecutively pH value adjusted and cold stripped with nitrogen stream and then, the stripped H_2S is trapped in the absorption flask (high pH value) to stabilize the trapped species of H_2S as S^{2-}, which is then ready to be analyzed. The zinc acetate is reduced to zinc sulfide by H_2S present in the quench water sample. The use of zinc acetate to trap H_2S were widely reported in [Pomeroy et al., 1954], [Shanthi et al., 1996] and [Cassella et al., 1999].

In the case of CN^-, the sampled solution (quench water sample with NaOH stabilizer) was consecutively pH value adjusted, and then hot stripped at 158 °C in a laboratory distillation column. The stripped HCN is trapped in the absorption flask (high pH value) to stabilize the trapped species of HCN as CN^-, which is then ready to be analyzed. This method enables the analysis of trace HCN present in the aqueous phase to be carried out with new experimental findings by [Mai et al., 2010].

The separate samples of CN^- and S^{2-} were analyzed in the ion chromatography ICS – 3000 with amperometric detection with the support of Dionex Chromeleon data processing, data management and instrument validation software.

2.5.2 Other trace analysis

Information about the analysis made for other trace compounds like BTEX, PAHs and soot etc. shall be discussed later in chapter 7.

2.6 Limit of accuracy in measurement systems

In pilot scale or demonstration plants like the HP POX test plant, the designs are flexibility driven in order to have representative data collections during operation. Such flexibility provides the opportunity for new units to be added or quick modification with reconfiguration of the existing plant

and the possibility to test several operating conditions over a wide range. Regarding commercial-scale plants [Rietema et al., 1961], they are designed for the production of defined products quality at certain volume in order to maximize profit and minimize cost. Having the knowledge of the measurement errors associated with the plant facility or the measurement systems during experiment in the pilot scale plant is as important as the process itself. Then, estimate uncertainties of conversions or yields [Langensiepen et al., 1979] can lead to good assessment in the mass and energy balance with reduction of errors.

In the light of this, there are measurement errors that can be identified in different parameters relating to quantities measured, sampling, test and analysis in these kinds of experiments.
The steam or water content of the product synthesis gas leaving the reaction chamber cannot be measured directly and must be inferred as part of the calculatory reconciliation [Richter et al., 2015] between the reaction chamber elemental input and output. For example in biomass-to-liquid (BtL) process, the raw synthesis gas leaving the quench chamber contains some amount of steam different from that of the product synthesis gas from the gasifier [Trippe et al., 2011]. In the HP POX plant, the measured value of the raw gas volume flow rate was slightly corrected with the assumption that there was steam saturation according to quench water temperature [Richter et al., 2015].

The temperatures inside the gasification chamber were measured by R-type thermocouples. Due to differences inferred from multiple measurements, an estimated uncertainty of ±10 K [Brüggemann, 2010] was used as the absolute temperature at the reactor outlet. Also, the aging of these thermocouples were due to several test campaigns, which affects the tolerance of their measurements.

Presented below is Table 2.7, which gives an overview of relative accuracy for the measured value for temperature, pressure and flow of each feed and product stream as well as GC calibration for the measured main product synthesis gas compounds.

Table 2.7: Relative accuracy for the measured value for temperature, pressure and flow of each feed and product stream [Meyer, 2007] and [Brüggemann, 2010]

Measurement	Relative accuracy	Remarks
Flow of natural gas and product synthesis gas	0.3 %	Vortex flowmeters used for natural gas and product synthesis gas has a relative accuracy of 0.3 %
Flow of oxygen	2 %	Oxygen supply was measured by a Coriolis mass flowmeter has a relative accuracy of 2 %.
Flow of steam	1 %	The steam feeds by restrictors has a relative accuracy of 1 %.
Flow of nitrogen	2.5 %	The nitrogen that is used in flushing the optical probe in Fig. 2.2 was measured via a variable flowmeter has an approximated relative accuracy of 2.5 %.
Natural gas temperature	0.75 %	The natural gas temperature was measured by K-type thermocouple has a relative accuracy of 0.75 %.
Steam and oxygen temperatures	0.6 %.	The steam and oxygen temperatures were measured by resistance thermometers have relative accuracy of 0.6 %.
Pressure measurements	0.3 %	The pressure measurements were measured by pressure transducers has a relative accuracy 0.3 %.
GC calibration for the main product synthesis gas compounds	**Concentration range**	The evaluation of the GC calibration and its tolerances that were given by the manufacturer of the gas calibration system provided the relative accuracy values for the measured product synthesis gas compounds in the concentration range of: H_2 ±2 %, CO ±2 %, CO_2 ±2 %, CH_4 ± 5%, and N_2 ±5 %.
H_2	±2 %,	
CO	±2 %	
CO_2	±2 %	
CH_4	± 5%	
N_2	±5 %.	

2.7   Summary

The HP POX test plant operations and test campaign parameters were discussed. Series of chemical reactions relating to partial oxidation of methane were explained. The procedure for analyzing hot gas, raw gas and quench water samples during plant operations were reviewed. Also, discussed are the relative accuracy for the measured value for temperature, pressure and flow of feed and hot gas stream as well as GC calibration for hot gas components.

3 Simulation and methods

3.1 Test points calculation of the HP POX test campaign

The focus of this investigation is on the water quench operation processes during the Gas-POX operating mode of the HP POX test plant. This chapter describes the simulation tools employed for calculation and how results with the data from the test campaigns were used for the development of the models as well as considerations used in these studies. The first action is to simplify and take into account all aspect of the quench operations based on the quench chamber of the HP POX test plant in Fig. 2.2. The streams and their parameters were identified and implemented in the Aspen Plus model. In this, calculations were made for all the 47 test points of the considered campaigns using Microsoft Excel, Aspen Plus and the interface between Excel and Aspen Plus was via Visual Basic for Applications (VBA). On the other hand, the same approach was employed for Python, Microsoft Excel, and Aspen Plus. The interface between Excel and Aspen Plus was Python. Details of all these shall be discussed in later sections of this chapter.
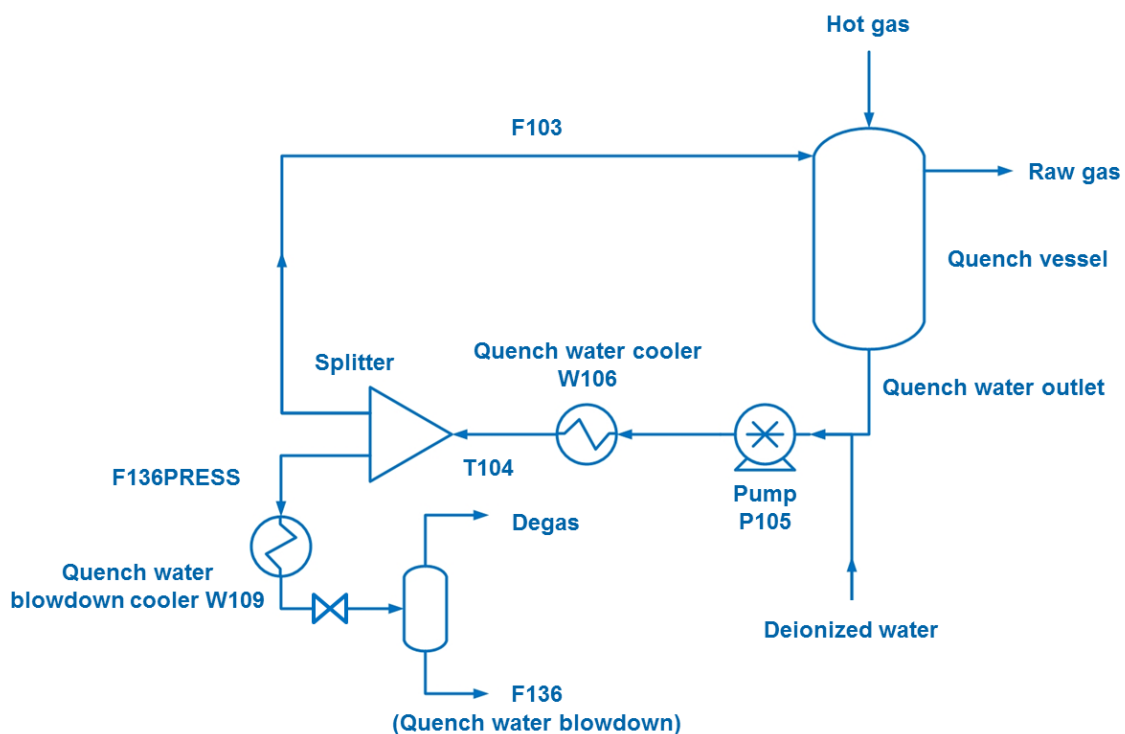
Figure 3.1: Simplified scheme for HP POX quench water system

The simplified process scheme of the quench chamber of the HP POX test plant can be seen in Fig. 3.1. The quenching of the hot gas stream is carried out by stream F103, which is a mixture of quench

water outlet and deionized water. Hot gas stream from the gasifier is quenched by stream F103 in the quench vessel. Leaving the quench vessel is the raw synthesis gas stream and the quench water outlet. The deionized water is mixed with the quench water outlet, pumped and cooled to have stream T104. Stream T104 splits into stream F103 and quench water blowdown stream F136PRESS. After cooling stream F136PRESS, this stream was depressurized and splits into stream F136, which is the depressurized quench water blowdown stream and Degas stream, which is gaseous evolution during depressurization and will be burnt in the flare.

3.1.1 Aspen Plus model for HP POX quench water system

This section contains an overview of original model, assumptions and a description of the model in Aspen Plus. Aspen is a process modelling tool that simulates industrial processes. It has a GUI for setting up the flowsheet, defining all the streams and units input and output parameters, and for running the simulation. More details about Fig. 3.2 can be found in Appendix Fig. 9.1 and Table 9.11.

Figure 3.2: Aspen Plus flow diagrams of simulated HP POX quench water system

Table 3.1: Description of blocks used in Aspen Plus simulation.

Unit	Name	Description
Flash	Quench	Rigorous 2 phase (vapour-liquid) equilibrium calculations.
RStoic	Reactor	Stoichiometric reactor based on known functional conversions or extent of reaction for the considered organic acids formation.
Pump	P105	Calculates the outlet pressure of the stream.
Cooler	W106	Calculates the enthalpy change of the stream for a given outlet temperature.
Splitter	SPLITOUT	Combines material streams and divides the resulting stream into two streams.
Cooler	COOLER	Calculates the enthalpy change of the stream for a given outlet temperature.
Design specification	DS – H_2S	Calculates the hot gas of H_2S inlet stream based on experimental data of S^{2-} concentration in the quench water sample (see Table 2.6 and Section 2.5.1).
Design specification	DS – NH_3	Calculates the hot gas of NH_3 inlet stream based on experimental data of NH_4^+ concentration in the quench water sample (see Table 2.6 and Section 2.5.1).
Design specification	DS – HCN	Calculates the hot gas of HCN inlet stream based on experimental data of CN^- concentration in the quench water sample (see Table 2.6 and Section 2.5.1).
Design specification	DS – F136	Specifies the deionized water flow based on measured value from F136.
Design specification	DS – F103	Specifies the flow of stream F103 based on measured value from F103.

Design specifications for the calculation of the content of H_2S, NH_3 and HCN in the hot gas after quench were implemented in Aspen Plus Design Spec functionality available in the flowsheeting options to meet the real measured trace in the quench water outlet data obtained from the HP POX test plant. These real data include laboratory analysis of some of the traces described earlier in Chapter 2 (Section 2.5.1).

The Electrolyte NRTL (ELECNRTL) equation of state embedded in the Aspen Plus software was used as the model`s property method for the calculation of the HP POX test plant quench water system cycle as illustrated in Fig. 3.2. ELECNRTL model can calculate activity coefficients for ionic species and molecular species in aqueous electrolyte systems likewise in mixed solvent electrolyte systems. Many new models developed for thermodynamic modelling of electrolyte solutions are mostly based on

Electrolyte NRTL model. The model gives an extensive excess Gibbs energy expression to represent the liquid-phase non-ideality for aqueous and mixed-solvent electrolyte systems [Chen et al., 2004], over the entire concentration range from pure solvents to saturated solutions or fused salts (extended to multicomponent solutions) [Jaretun et al., 1999] and [Jaretun et al., 2000].

The quench water outlet stream to be studied is a complex mixture or system, which contains dissolved gases and their ions. The electrolyte NRTL equation provides thermodynamically consistent model for aqueous electrolyte systems. This equation was developed with the local composition concept. This concept is similar to the NRTL (Non-Random Two Liquid) model for nonelectrolyte systems [H. Renon et al., 1968]. The explanation for local composition activity coefficients for multicomponent electrolyte systems can be seen in the Aspen physical property system manual [Aspentech manual: property method, 2012]. It is suitable for aqueous and mixed solvent application. With the initiation of electrolyte wizard in Aspen Plus, lists of aqueous species, salts, and possible reactions are displayed and can be chosen.

In electrolyte NRTL activity coefficient property method with only binary parameters, the equation satisfactorily represents physical interactions of true species in aqueous single electrolyte systems and multicomponent electrolyte systems over broad ranges of concentrations and temperatures. This property method can also represent infinitely dilute electrolyte systems (where it reduces to the Debye-Hückel model), nonelectrolyte systems (where it reduces to the NRTL model), and pure fused salts. The equation has been extended to model mixed solvent electrolyte-systems [B. Mock et al., 1984].

The electrolyte NRTL activity coefficient model comprises of three main contributions that enhances its capabilities. The first is the long-range force, which accounts for the electrostatic interactions of ion especially at low concentration and this implies a Pitzer – Debye – Hückel model. The second aspect of electrolyte NRTL activity coefficient model is known as Born contribution, which gives it the possibility to mixed aqueous – non aqueous electrolyte solvents. The third aspect is the local composition NRTL contribution, which is applied for short-range forces effective at higher concentrations of ions [Haghtalab et al., 2004].

Two fundamental assumptions of the model are: "The like-ion repulsion assumption" and "The local electroneutrality assumption". These led to adding the NRTL expression for the local interactions, the Pitzer-Debye-Hückel expression, and the Born equation to have equation (3.1) for the excess Gibbs energy:

$$\frac{G_m^{*E}}{RT} = \frac{G_m^{*E,PDH}}{RT} + \frac{nG_m^{*E,Born}}{RT} + \frac{G_m^{*E,LC}}{RT} \tag{3.1}$$

Solving equation (3.1) gives the main mathematical expression for Electrolyte NRTL activity coefficient model as in equation (3.2).

$$\ln \gamma_i^* = \ln \gamma_i^{*PDH} + \ln \gamma_i^{*Born} + \ln \gamma_i^{*,LC} \tag{3.2}$$

The complete form of the model can be found in [Chen et al., 1982], [Chen et al., 1986] and [Aspentech manual: property method, 2012]. γ_{i}^{*} denotes the unsymmetrical activity coefficient of ionic species i and the first, second and third terms on the right side of equation (3.2) are the activity coefficients introduced by the Pitzer – Debye – Hückel (PDH), Born and NRTL local composition models (LC) respectively.

Also, in the activity-coefficient approach for computing vapor-liquid equilibrium, Henry's law is used to represent the behavior of dissolved gases or other supercritical components. Aspen Plus has built-in Henry's law parameters for a large number of component pairs. The solvents are water and other organic compounds.

These parameters are used automatically on the properties parameters binary interaction HENRY-1 form when one specifies or designates these components as Henry's components on the Components Henry-Comps form.

Dissociation occurs in the electrolytic system of the quench water effluent and can be enhanced as a result of the interactions among the various species present.

3.2 Gas-POX 201 VP1 quench water system model simulation by Aspen Plus

Presented in this section is the calculation for test point Gas-POX 201 VP1 which is the first of the 47 test points. Fig. 3.1 and Fig. 3.2 give general schematics of the model in Aspen Plus. This chosen test point VP1 was further considered for the presentation of species distribution. Calculations of species distributions during sensitivity studies originating from this test point were analysed. The trace components molecule and ions are presented in Chapter 4. More information about the results of these studies shall be discussed in Chapter 4.

3.2.1 Measured and calculated input parameters

The measured and calculated streams for the HP POX test plant quench water system cycle streams are presented in Table 3.2. The operating parameters of the streams measured during the test point Gas-POX 201 VP1 (*) and the results obtained from the quench water system model in Aspen Plus (**) were used for the purpose of further studies especially the sensitivity analysis.

Table 3.2: HP POX test plant quench water cycle parameters Gas-POX 201 VP1*

Streams	Operating parameters (* Measured values , ** Calculated values)			Phase
	Flow rate (t/h)	Temperature (°C)	Pressure (bar)	
Hot gas (HG)	0.82 **	1172 *	71 **	Gas
Raw gas (RG)	0.77 *	177.4 **	71 *	Gas
Degas (Quench water blowdown)	0.002 **	20 **	1 *	Gas
Quench water outlet	5.4 **	177.4 *	71 **	Aqueous
Stream T104 (Quench water cooled)	6.0 **	79.9 *	72 **	Aqueous
Stream F103 (Quench water inlet)	5.3 *	79.9 **	72 **	Aqueous
Stream F136PRESS (Quench water blowdown)	0.7 *	79.9 **	72 **	Aqueous
Stream F136 (Quench water blowdown)	0.7 **	20 °C *	1 *	Aqueous
Deionized water	0.6 **	105 *	72 **	Aqueous

The measured values (in blue) were used for the back calculation in the Aspen Plus set up for the HP POX test plant quench water system in Fig. 3.2 as well as chapter 4, 5 and 6.

3.2.2 Calculated sensitivity studies of species and their distribution for test point (VP1)

The sensitivity analysis tool results elucidate the behaviours of different traces between raw synthesis gas and quench water, which were influenced by quench water temperature variations from 130 °C to 220 °C at constant pressure (79.9 bar) and quench water pH values variation. Also considered are the influence of organic acids such as formic acid (HCOOH) and acetic acid (CH$_3$COOH). The selected components under consideration were CO$_2$, H$_2$S, NH$_3$ and HCN. The distributions of their molecularly dissolved and ionic species were studied.

The operating parameters of the streams as shown in Fig. 3.1 and Fig. 3.2 were used to develop the Aspen Plus simulation model based on the test point VP1 data of the campaign Gas-POX 201 from HP POX test plant during operation. While the addition of the pH regulation input into stream F103 was used for sensitivity analysis.

Beforehand, a combined configuration of the quench water system cycle Aspen Plus model, VBA and Microsoft Excel was used to make the calculations for all the 47 test points of the Gas-POX test campaigns. Test point VP1 data of the Gas-POX 201 test campaign were then chosen for sensitivity studies.

The simulation model was applied to conduct sensitivity analyses for CO$_2$, H$_2$S, NH$_3$ and HCN amounts in raw gas, degas, and F136. These amounts were related to the hot gas. Changing parameters are: quench water temperature and quench water pH values. pH value changes were realized with an additional stream comprising of sodium hydroxide (20 mass-% NaOH, 80 mass-% H$_2$O) or sulfuric acid (20 mass-% H$_2$SO$_4$, 80 mass-% H$_2$O) in two different sensitivity studies (see Table 3.3 and pH regulator via stream F103 input in Fig. 4.2). The initial calculated pH value of the quench water outlet stream was 6.17 for this test point.

Table 3.3: pH regulator parameters

Streams	Operating parameters		Phase
	Flow rate varied during sensitivity studies (t/h)	Temperature (°C)	
pH regulator – NaOH	From 0 – 0.20	20	Aqueous
pH regulator – H$_2$SO$_4$	From 0 – 0.20	20	Aqueous

The other sensitivity studies done were on varying quench water temperature and the effects on the trace components distribution in the streams (raw gas, degas, quench water outlet, stream T104, stream F103, stream F136PRESS and stream F136) and are presented in chapter 4.

3.3 Used calculation tools related to the work

3.3.1 VBA in Excel

Visual Basic for Applications (VBA) via Microsoft Excel provides the interface to link Aspen Plus and Microsoft Excel. VBA is a high level programming language that is oriented around an object framework and event driven execution. It is a large sub-set of the Visual Basic language. It is a macro language that is integrated tightly into supporting applications. The syntax and functionality is identical to straight Visual Basic [Aspentech manual, 2008].
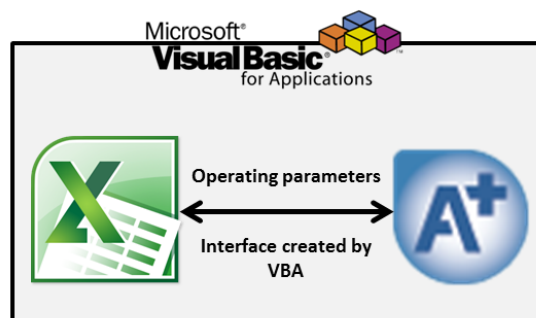
Figure 3.3: Integration of information and functions in VBA via Microsoft Excel to Aspen Plus model

Interfacing a process simulation tool like Aspen Plus and others with VBA in Microsoft Excel is widely applied in the industry, research and academics to simulate chemical process designs and operational changes. This creates the possibility to optimize the performance of a process. Consequently, the output data after the calculation can be saved in Microsoft Excel for further analysis [Rangaiah et al., 2016].

The approach in this work is to transfer the HP POX experimental data obtained during the test campaign into the developed Aspen Plus model in Fig. 3.1. For steady state simulation, Aspen Plus does not have an integrated function to perform the calculation of all the 47 test points along with their several parameters belonging to the streams and units at once. So, a need to implement the possibility of such functionalities arises. Therefore, the repeatability of calculation was major factor. Aspen Plus results are transferred back to Excel via the interface.

This approach had been in use by many engineers around the world as a possibility for the challenges faced when developing optimisation concepts for processes or improving facility operations with respect to huge databank of the system or a process under consideration. The need for flexible, intuitive and powerful tool to reduce the time consumed when performing monotonous calculations so as to increase accuracy and time for evaluation of results [Querol et al., 2011] and analysis are

inevitable. Thus, the VBA application was accessed via the development tool of Microsoft Excel. The information to be transferred in these cases were the operating parameters of components, streams and units, which were to be ran on the Aspen Plus model.

The Microsoft Excel file organizes and sends this information via VBA script in Excel to Aspen Plus. Then the result of the calculation goes back into Excel via VBA script. The process continues until the end. Fig. 3.3 presents the connectivity of VBA, Microsoft Excel and Aspen Plus: It is possible to use tools of Aspen Plus for optimization and sensitivity analysis during the calculation.

3.3.2   Python as interface between Aspen Plus and Microsoft Excel

During the course of this work, several attempts were made with the use of Python for the calculation of the 47 test points with the connectivity of Microsoft excel and Aspen Plus model. As earlier stated, the interface for this calculation was via Python.

The reason for the use of Python was due its high-level, interpreted, interactive and object-oriented scripting language. It was applied to calculate heat and mass transfer model for a catalyst particle to create a dynamic state scenario with a backward finite difference scheme [Durante et al., 2014].
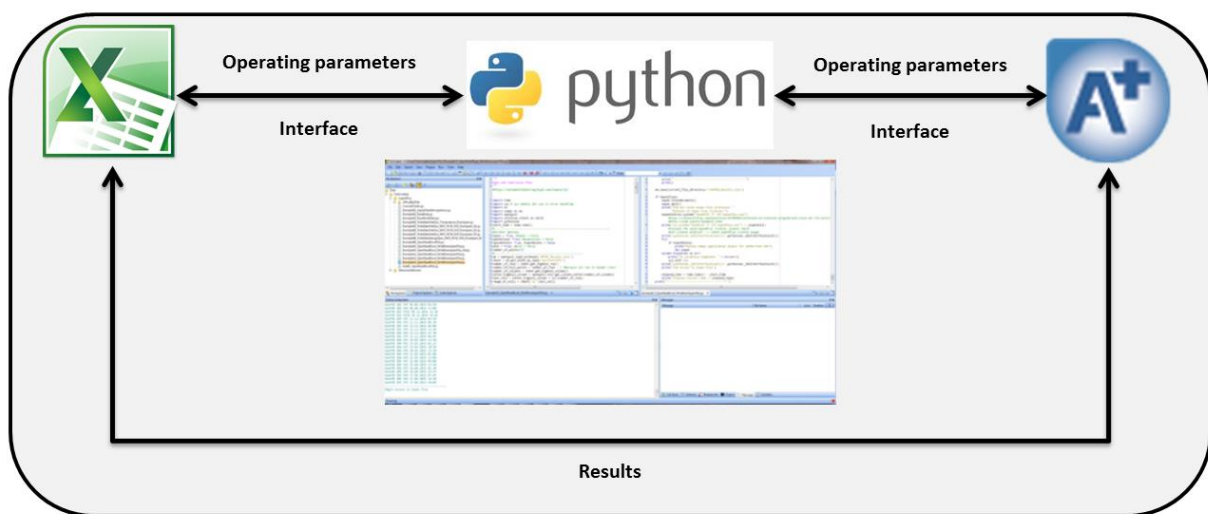
Figure 3.4: Integration of information and functions in Python via Microsoft Excel to Aspen Plus model

Python offers comfortable scripting, prototyping as well as interfacing environment. It is free open-source and it has a wide usage in the scientific community [Akesson et al., 2010]. The variable explorer in Aspen Plus model provides the Aspen Plus unit and stream variable node names, which must be implemented in the codes in Python. After transferring the variable values the Aspen Plus model can be ran. The results are transferred to Microsoft Excel after calculation for each test point.

3.3.3 Aspen Simulation Workbook

Aspen Simulation Workbook (ASW) provides easy and robust integration between AspenTech's process simulators and Microsoft Excel. It allows one to rapidly deploy models to a wider range of users without writing a single line of code [Aspentech: white paper, 2012]. In model building, it is necessary to ensure that the models are vigorous over a reasonably wide range of conditions. Relevant engineering judgement must be applied to keep the model as simple as possible for the intended application or purpose, resulting in a robust and interactive experience for the casual Excel-based user. ASW provides an easy mechanism for Excel connectivity to plant databases, allowing plant data to be retrieved on demand and applied to the simulation model.
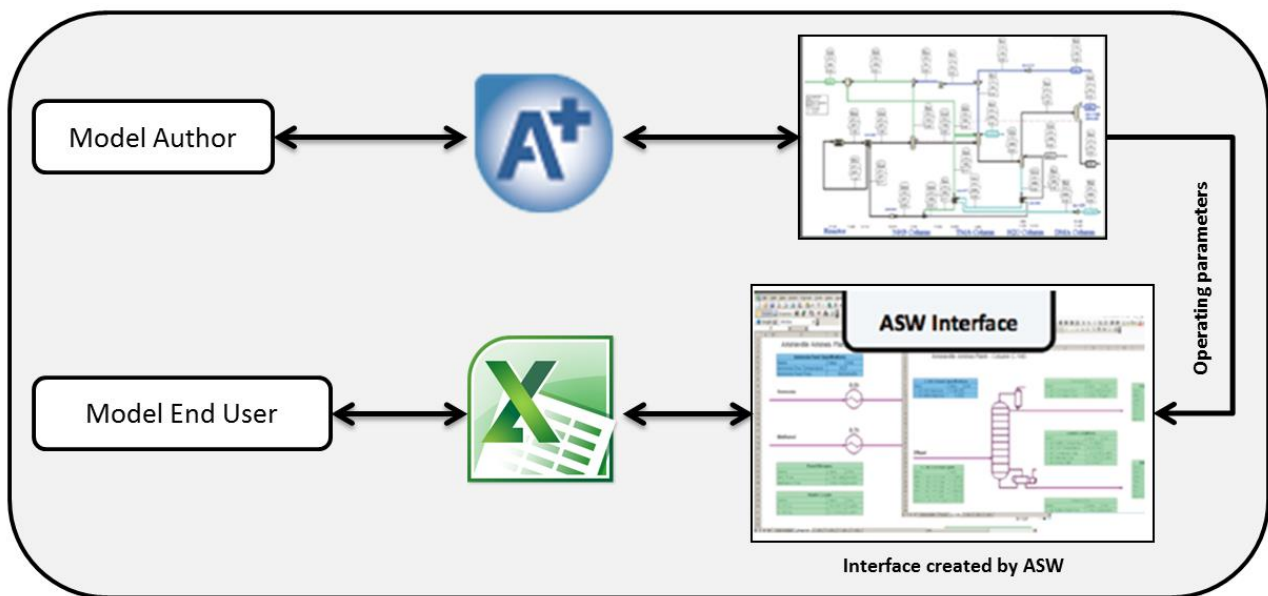
Figure 3.5: ASW enables Excel users to rapidly run scenarios using the underlying rigorous models to analyze plant data, monitor performance, and make better decisions.

ASW helps to link simulation models to plant data within the same Excel sheet allows the model user to:

- Populate simulation cases with measured plant data
- Send simulation results back to the plant information system using tags
- Overlay model predictions with plant data in plots and tables

The plant data tags can be linked to Excel using the standard features of most process historians such as Aspen InfoPlus. 21® [Aspentech: ASW in Aspen HYSYS, 2014]. The tuned models are then used in a predictive mode for what-if studies and other operational improvement scenarios. Consequently, the plant data tags can be updated each time a process simulation case is run from within ASW.

Subsequently, the simulation is complete, and then the tags mapped to model variables are updated with calculation results from the simulation.

The procedures for the use of ASW in this work are:

- The model must be ready, converged with no errors.

- Then initiate the ASW via Microsoft Excel organizer in the development tool tab.

- Configure the Aspen Plus model into the ASW simulation tab.

- Click the activate button to allow all configuration ready for scenario analysis.

- Then copy and paste the model variables from Aspen Plus to be considered for the calculation into the scenario analysis table.

- In the selection of the variables, at least one of both specified variable and model variable must be selected and copied into the scenario analysis table.

- Next is to right click on the Excel worksheet to initiate the scenario study wizard.

- On the scenario study wizard run active scenario and modify the table to ensure for a well-organized result after running the model.

ASW makes it easy to run hundreds of scenarios through the model to analyse historical data, analyse process sensitivity, check design cases, evaluate operating conditions, or evaluate a range of feedstocks. The scenario feature sets up is a table where the user can enter the values of several model inputs (columns) for several cases (rows). The scenarios are executed sequentially, with key simulation results filling in additional columns. The resulting table makes it very easy to compare a large number of cases. When used with historical plant data, the scenario feature makes it easy to identify changes in plant performance (e.g., changes caused by exchanger fouling over weeks or months), monitoring equipment, inferring properties, and more [Aspentech: white paper, 2012] and [Aspentech: ASW in Aspen HYSYS, 2014]. Moreover, due to the time consumption for configuration and running all the 47 scenarios, coupled with unavailable options in ASW to make calculations for Design-Specs, the ASW was not used for the calculation in this work. The configuration freezes up the computer, which makes the Microsoft Excel to crash and the entire ASW. Starting the entire process of configuring, copy and pasting several variable data make the whole process inefficient due to the sudden crash of the configured ASW, Microsoft Excel and Aspen Plus model.

3.4 Summary

The model of the HP POX plant was developed in Aspen Plus and configured with VBA in Microsoft Excel. The calculations for the 47 test points were made and the sensitivity analysis of Gas-POX 201 VP1 was further elaborated to study the effect of quench water temperature and pH value variations. Other tools used for the calculation in this work were discussed. The use of Python is promising, with further know-how, it is possible to develop more comprehensive sensitivity studies on all the 47 test point based on the knowledge from Gas-POX 201 VP1. Creating diagrams from the calculation directly from these configurations would save time spent on the development and analysis of profiles and results.

4   Trace components in quench water system

The usage of water in any gasification plant relies upon the type of feedstock and the downstream operations. For gasification plants that utilize heavy residues or coal feedstock, there will be net water consumption while in gasification plant that uses natural gas as feedstock, there can be a net production of water (especially in the autothermal reforming (ATR) mode) [Higman et al., 2003]. The gasification process that applies water to quench product synthesis gas or water scrubbing for raw synthesis gas are known to produce some wastewater effluent with dissolved H_2S, NH_3, HCN, heavy metals, and other specific trace components like chlorine and fluorine from coal feedstock [Gräbner, 2015]. This chapter focuses on the result of the sensitivity analysis performed on the Gas-POX 201 VP1 for the distribution of selected components namely H_2S, NH_3, HCN, and CO_2.

CO_2	NH_3	H_2S	HCN	H_2O	vapour (gas phase)
↑↓	↑↓	↑↓	↑↓	↑↓	
CO_2	NH_3	H_2S	HCN	H_2O	liquid (aqueous phase) molecularly dissolved

$$CO_{2\,(aq)} + H_2O \rightleftharpoons HCO_3^- + H^+ \qquad (4.1)$$

$$HCO_3^- \rightleftharpoons CO_3^{2-} + H^+ \qquad (4.2)$$

$$NH_{3\,(aq)} + H_2O \rightleftharpoons NH_4^+ + OH^- \qquad (4.3)$$

$$NH_{3\,(aq)} + HCO_3^- \rightleftharpoons NH_2COO^- + H_2O \qquad (4.4)$$

$$HCN_{(aq)} \rightleftharpoons CN^- + H^+ \qquad (4.5)$$

$$H_2S_{\,(aq)} \rightleftharpoons HS^- + H^+ \qquad (4.6)$$

$$HS^- \rightleftharpoons S^{2-} + H^+ \qquad (4.7)$$

$$CO_{\,(aq)} + H_2O \rightleftharpoons HCOOH_{\,(aq)} \rightleftharpoons HCOO^- + H^+ \qquad (4.8)$$

$$2CO_{2\,(aq)} + 4H_{2\,(aq)} \rightleftharpoons CH_3COOH_{(aq)} + 2H_2O \qquad (4.9)$$

$$CH_3COOH_{(aq)} \rightleftharpoons CH_3COO^- + H^+ \qquad (4.10)$$

Figure 4.1: Vapour-liquid equilibria system of CO_2, H_2S, NH_3, HCN and organic acids in the quench water and extended mechanisms according to [Kamps et al., 2001], [Alvaro et al., 2000], [Kuranov et al., 1996], [Xia et al., 1999] and [Edwards et al., 1978].

In these studies, considerations to the presence of organic acids like formic acid and acetic acid were included in the quench water. These organic acids shall be discussed in chapter 5. CO_2 is not a trace, its amount in the quench water effluent and its contribution to the formation of other ions and by-products cannot be neglected. Presented in Fig. 4.1 are equations (4.1) – (4.10). These equations are the reactions leading to the molecular dissolution of CO_2, H_2S, NH_3 and HCN from the hot gas into the quench water and the dissociation of their corresponding molecularly dissolved species that were considered in these studies. These components shall be discussed in the next session of this chapter. Table 4.2 – 4.5 represent the parameters of individual trace components and the calculated amount of traces originating from the measured ammonium, cyanide and sulfide from the quench water blowdown that were discussed earlier in chapter 3 for test point VP1 in Fig. 3.1 and Table 3.1.

Figures 4.6, 4.7, 4.9, 4.10, 4.12, 4.13, 4.15 and 4.16 represent the outcome of Aspen Plus sensitivity studies. The effects of varying quench water temperatures and pH values were calculated regarding the distribution of the trace components in the streams: raw gas, degas, quench water outlet, stream T104, stream F103, stream F136PRESS and stream F136 in Fig. 4.2.

The Sankey Diagrams shown in Figures 4.5, 4.8, 4.11 and 4.14 are the pictorial representation of each trace component flow present in the HP POX test plant quench water system cycle streams for test point VP1. Although, these diagrams are not drawn to scale collectively, each stream gives a visualized overview of the amount of traces present in them in relation to the entire quench water system cycle.

4.1   Physico-chemical parameters of quench water

The HPPOX quench is a direct quenching. The product synthesis gas from the gasifier enters the quench chamber at 1172 °C, and then quench-cooled. Leaving the quench chamber is the raw gas, which is saturated with water. The cleaning of raw gas and the further downstream processes (e.g. CO-shift) give syngas that may be used for synthesis for example methanol production or gas-to-liquids processes. The quench water effluent is collected in the chamber, split for discharging via the quench water blowdown stream and recycled according to Fig. 4.2. In addition to water quench, other types of direct quenching methods applied in gasification processes include gas and chemical quench. High cooling rate is achieved in all these direct quenching methods [Qian Zhu et al., 2015].

4.1.1 Quench water pH adjustment

It is important to note that the pH values variation is also known as pH adjustment in the chemical process industry or at times pH control. Due to the recycling of the quench water effluent to add up with the deionized water during the quenching process of the hot gas, there are possibilities to have changes in the pH values of the quench water effluents. These call for a need to look into the concept of pH adjustment in consideration to what is obtainable in the industry and reported by [Kimberly et al., 1989], [Chih-Hao et al., 2003] and [Anindra et al., 2015].

The concentration of traces in the recycled waste water is important when the reused water is introduced into the quenching process. Apart from water savings issues, the concentration of salts and the presence of organic compounds are critical to the improvement of the quenching process. Although, the HP POX plant quench cycle has no salt formation in the system. Depending on the particular process, the objectives of quenching includes: temperature control, prevention of consecutive reactions, retention of product compositions and impact on the process efficiency [Moulijn et al., 2013]. The capability to analyze the reuse effluent provides the opportunity to take precautions with respect to the presence of solids, acidic and corrosion reactions resulting from the effluent with metallic surfaces of plant facility [Ávila Filho et al., 2015]. As quench water retains these traces in the quench water cycle, dissolved ions may exceed the solubility product of some salts and form precipitation of inorganic particles (metallic salts). Although, these components were analysed to be in trace quantities, but they have the possibility to change the physiochemical property of the quench water system. Some industrial plants are designed to emit no waste water effluent streams due to the environmental risk assessment of the contaminants and effects on the ecosystem. This types of industrial plant are mostly located at the arid regions, where additional heat is applied to the effluent to be concentrated to form brine from the water treatment plant by evaporation process [Gräbner, 2015] with solid waste salt as residues. pH adjustments systems are manufactured and installed by many companies around the world for the neutralization of acid and base from any industrial wastewater source (See Appendix Fig. 9.6 for calculated pH values and Table 9.2: pH scale with examples of solution [NALCO 2008]).

Furthermore, at some point in many gasification processes especially, when coal or heavy residues are the feedstock, there is a need for washing water during the syngas treatment process. In coal gasification, chlorides, ammonia and other constituents of the gases are captured. While in heavy residues gasifiers, water is used for the removal of soot and the water is known to contain some

certain amount of hydrogen cyanide, ammonia and hydrogen sulfides. In any of the situations, the pH of the water needs to be adjusted especially in the overall effluent water treatment and flocculation step [Higman et al., 2003]. The controlling of quench water effluent pH [Kimberly et al., 1989] was proved in the recycling of quench water with an unacceptable acidic pH during partial oxidation of hydrocarbon feedstocks. This was achieved by retaining some amount of ammonia present in the water-quench scrubber that was used to cool synthesis gas and to remove the solid particulates of ash and soot. In the same studies [Kimberly et al., 1989], the formation of acidic compounds (formic acid) and basic compounds (ammonia) were reported during the quenching process. Another example of the pH adjustment was reported in [Anindra et al., 2015] when reducing impurities within the syngas using water and the quench chamber to produce black water. A carbon dioxide injector source to adjust the pH of the quench water was applied. The configuration was reported to consist of pH sensor to measure the pH of the grey water with a control valve to adjust the flow of the acidified water into the grey water (carbon dioxide injector). The process treats the black water from the quench chamber to generate grey water and soot [Anindra et al., 2015]. [Chih-Hao et al., 2003] employed the use of ammonia injection into the stream of soot water after filtering the soot. This was to minimize waste water treatment in order to have fewer amounts of metal contents in the effluent (grey water) of the quench water. This approach allows the recovery and reuse of more of the effluent water during gasification.

The results of the influence of quench water pH regulation on the trace components distribution will be presented in this chapter. This was achieved with the aid of the sensitivity analysis tools in Aspen Plus (pH regulator input in Figure 4.2). The simulation model was extended with an additional stream comprised of sodium hydroxide (20 mass-% NaOH, 80 mass-% H_2O) or sulfuric acid (20 mass-% H_2SO_4, 80 mass-% H_2O) in two different sensitivity studies (see Table 3.3). The calculated pH value of the quench water outlet stream given in Fig. 4.2 is 6.17 (for Gas-POX 201 VP1).

In the first case, 20 % NaOH solution input according to Figure 4.2 was used to increase the initial pH value of the quench water from 6.17 to 8, which resulted in more basicity in the quench water as the flow rate of the solution of NaOH was introduced from 0 – 200 kg/h. A similar procedure was done for the 20 % H_2SO_4 solution in water, and the resulting pH value of the quench water was reduced from 6.17 to 0.14. In both cases, the quench water temperature was kept constant at about 177.4 °C.
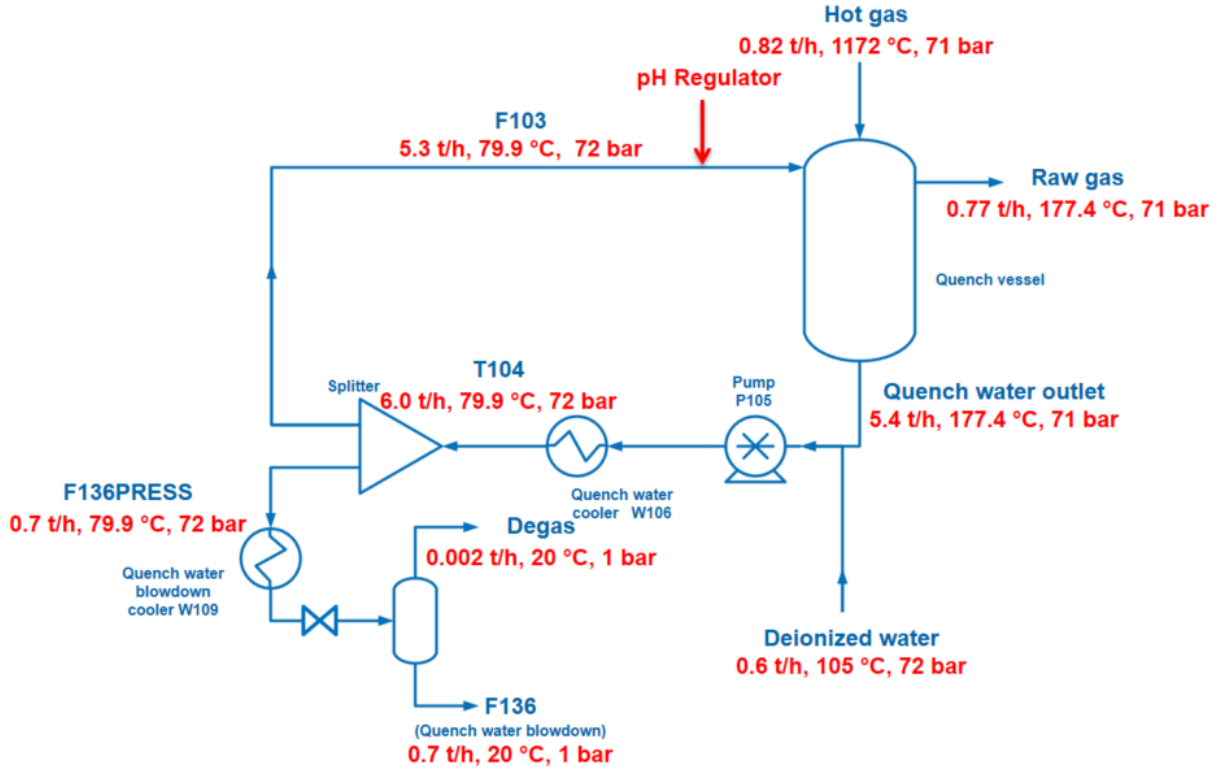
Figure 4.2: HP POX quench water system with pH regulator for sensitivity studies

Figures 4.7, 4.10, 4.13, and 4.16 present, the influences of changes in the quench water pH on the trace components distribution. The trace ratios in relation to the respective trace inlet via hot gas were included to study their characteristics.

4.1.2 Henry constant

In order to have the phase distribution of species, temperature dependent equation for volatile, weak electrolyte waste water containments like CO_2, NH_3, H_2S, HCN etc. were presented base on ionization and Henry's law constants [Yoo et al., 1986]. Several approaches are used to describe the solubility of a gas in water. Henry´s law constant can be defined via concentration:

$$H_e = \frac{P_i}{X_i}$$

(4.11)

H_e is the Henry volatility defined via aqueous-phase mixing ratio, P_i is the partial pressure of that species in the gas phase and X_i is the molar mixing ratio in the aqueous phase [Sander, 2015].

In addition, Henry's law is a limiting law that only applies for dilute solutions. The margin of concentration, which it is applied becomes narrower the more the system diverges from ideal

behavior. Henry's constant changes when the temperature of the system changes [Francis L. Smith et al., 2007] and [Perry et al., 1984]. This leads to temperature dependency of Henry's constant and why it is usually refer to Henry's law coefficient. The Henry's constant used for the studies were derived from [Edwards et al., 1978] for CO_2, [Alvaro et al., 2000] for NH_3, [Kamps et al., 2001] for H_2S, and [Rumpf et al., 1992] for HCN as it can be seen in Fig. 4.3 and Appendix (Fig. 9.2 and 9.3). These Henry's constants of the considered traces shall be discussed in relation to their behaviors in the HP POX quench water system according to Fig. 3.1. (See Appendix for comparison between Henry's constant derived from Aspen Plus and literatures according to Fig. 9.2 and 9.3)
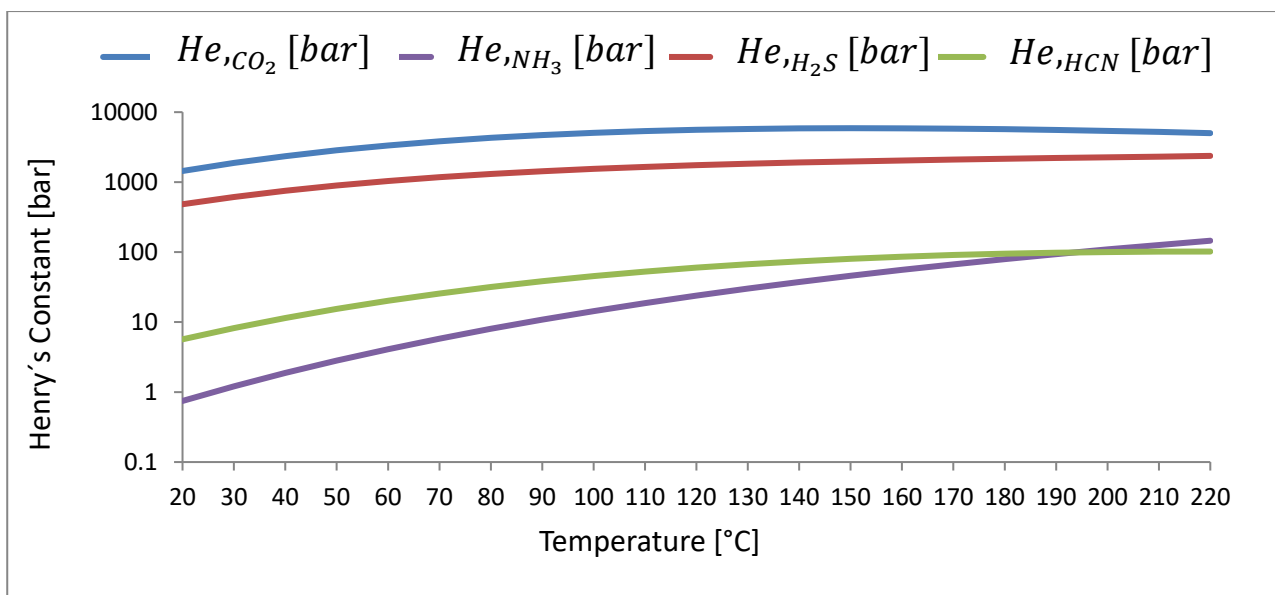
Figure 4.3: Henry's constant for CO_2, H_2S, NH_3 and HCN derived from [Edwards et al., 1978] for CO_2, [Alvaro et al., 2000] for NH_3, [Kamps et al., 2001] for H_2S, and [Rumpf et al., 1992] for HCN

4.1.3 Dissociation constant

The dissociation constant of a compound is the equilibrium constant for the dissociation of its compound into its components. For example water dissociation equilibrium [Tanaka et al., 2010], or self-ionization reaction is presented by:

$$H_2O \rightleftharpoons H^+ + OH^- \qquad (4.12)$$

Usually, it is expressed with chemical activities in place of concentration. The activity of water is generally taken to be 1 or unity [Nic et al., 2009] because most acid-base solutions are very dilute.

$$K_{\text{H}_2\text{O}} = \frac{a_{H^+}}{a_{H_2O}} \cdot a_{OH^-} \tag{4.13}$$

Equation (4.11) can be written as (when a_{H_2O} = 1):

$$K_{\text{H}_2\text{O}} = a_{H^+} \cdot a_{OH^-} \tag{4.14}$$

Presented in Figure 4.4 and Appendix (Fig. 9.4 and 9.5) are the dissociation constants derived from [Alvaro et al., 2000] for H_2O, NH_3 and NH_2COO^-, [Kamps et al., 2001] for CO_2, HCO_3^-, H_2S and HS^-, and [Edwards et al., 1978] for HCN (See Appendix for comparison between Dissociation constant derived from Aspen Plus and literatures according to Fig. 9.4 and 9.5). Fig. 4.4 presents the dissociation reaction of CO_2, NH_3, H_2S and HCN. $K_{\text{H}_2\text{O}}$ denotes the self-dissociation constant of water according to equation (4.12), (4.13) and (4.14), K_{CO_2} denotes the first dissociation constant of CO_2 according to equation (4.1) and (4.15),

$$K_{CO_2} = \frac{[HCO_3^-]\ [H^+]}{[CO_2]} \tag{4.15}$$

$K_{HCO_3^-}$ denotes the second dissociation constant of CO_2 according to equation (4.2) and (4.16),

$$K_{HCO_3^-} = \frac{[CO_3^{2-}]\ [H^+]}{[HCO_3^-]} \tag{4.16}$$

K_{NH_3} denotes the first dissociation constant of NH_3 according to equation (4.3) and (4.17),

$$K_{NH_3} = \frac{[NH_4^+]\ [OH^-]}{[NH_3]} \tag{4.17}$$

$K_{NH_2COO^-}$ denotes the carbamate formation reaction according to equation (4.4) and (4.18),

$$K_{NH_2COO^-} = \frac{[NH_2COO^-]}{[NH_3]\ [HCO_3^-]} \tag{4.18}$$

K_{HCN} denotes the dissociation constant of HCN according to equation (4.5) and (4.19),

$$K_{HCN} = \frac{[CN^-]\ [H^+]}{[HCN]} \tag{4.19}$$

K_{H_2S} denotes the first dissociation constant of H_2S according to equation (4.6) and (4.20), and

$$K_{H_2S} = \frac{[HS^-]\ [H^+]}{[H_2S]} \tag{4.20}$$

K_{HS^-} denotes the second dissociation constant of H_2S according to equation (4.7) and (4.21).

$$K_{HS^-} = \frac{[S^{2-}]\ [H^+]}{[HS^-]} \tag{4.21}$$
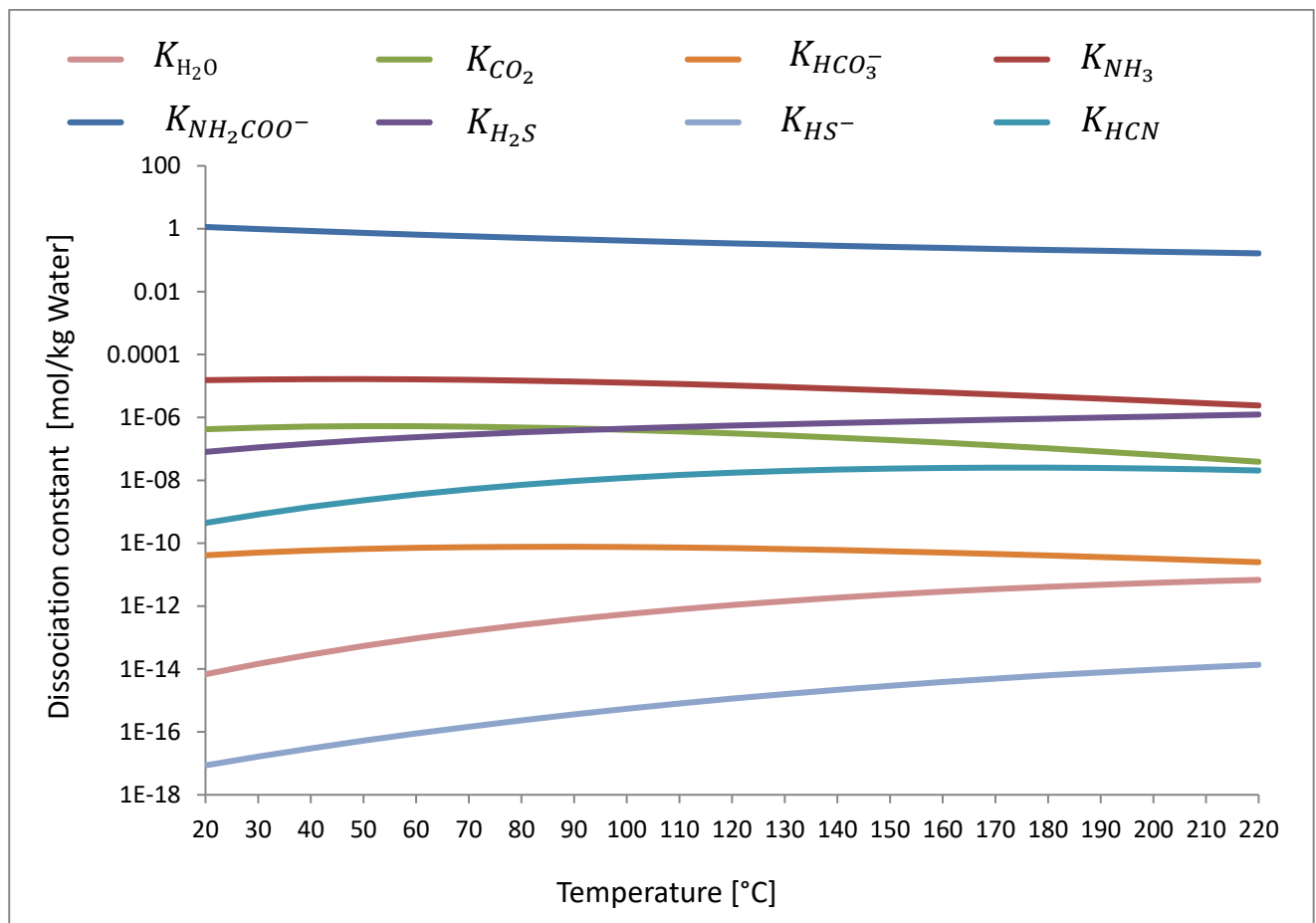
Figure 4.4: Dissociation constants for CO_2, H_2S, NH_3, HCN and H_2O derived from [Alvaro et al., 2000], [Kamps et al., 2001], and [Edwards et al., 1978]

Sections 4.2 – 4.4 focus on the behaviour of CO_2, NH_3, HCN and H_2S respectively based on the simulation results obtained from the sensitivity analysis for the quench water temperature and pH variation. The ratios of individual trace component present in hot gas stream to the following streams are given as: Raw gas/Hot gas = (RG/HG) flow rate ratio for raw gas, Degas/Hot gas = (DEGAS/HG)

flow rate ratio for degas stream and stream F136/Hot gas = (F136/HG) flow rate ratio for quench water blowdown stream.

4.1.4 Organic acids in quench water

This section is dedicated to give an overview of the organic acid components present in the quench water effluent sample (liquid phase) according to equation (4.8), (4.9) and (4.10). Details of these shall be discussed extensively in chapter 5. Table 4.1 presents the organic acids that were analyzed in the Gas-POX 201 VP1 quench water effluent sample. Aspen Plus automatically calculates the distribution of the ions in order to fulfil electroneutrality. The formic acid and it ions amount in the streams are given in Table 4.1 while the acetic acid is below threshold of measuring range for this test point.

Table 4.1: Organic acids distribution in streams for VP1 based on calculation from Aspen Plus.

Formic acid			
$HCOOH + \rightleftharpoons HCOO^- + H^+$			(4.22)
	HCOOH (kmol/hr)	HCOO$^-$ (kmol/hr)	Total $_{HCOOH\,(aq)}$ (kmol/hr)
QUENCH WATER (177.4 °C, 71 bar)	1.3E-04	2.2E-02	2.2E-02
T104 (79.9 °C, 72 bar)	2.2E-04	2.2E-02	2.2E-02
F103 (79.9 °C, 72 bar)	2.0E-04	2.0E-02	2.0E-02
F136PRESS (79.9 °C, 72 bar)	2.4E-05	2.4E-03	2.4E-03
F136 (20 °C, 1 bar)	4.6E-06	2.4E-03	2.4E-03
Acetic acid			
$CH_3COOH \rightleftharpoons CH_3COO^- + H^+$			(4.10)
	CH$_3$COOH (kmol/hr)	CH$_3$COO$^-$ (kmol/hr)	H$^+$ (kmol/hr)
QUENCH WATER (177.4 °C, 71 bar)	0	0	1.0 E-05
T104 (79.9 °C, 72 bar)	0	0	1.8E-05
F103 (79.9 °C, 72 bar)	0	0	1.6E-05
F136PRESS (79.9 °C, 72 bar)	0	0	1.9E-06
F136 (20 °C, 1 bar)	0	0	3.7E-07

4.2 Carbon dioxide (CO_2)

CO_2 is one of the principal components of the product synthesis gas generated from the gasifier apart from CO, H_2, H_2O and CH_4 [Higman et al., 2003]. It could be produced according to the water gas shift reaction in equation (2.5) and total oxidation of methane reaction in equation (2.6). Irrespective of the industrial gasification processes, some part of carbon will be converted to CO_2. Since CO_2 is a major by-product of gasification, there are efforts to reduce it from the source of production through absorption processes by washing the product synthesis with liquid solvent [Higman et al., 2003], [Ordorica-Garcia et al., 2009] and [Salkuyeh et al., 2013] or using solvent based CO_2 capture and sequestration technologies (CCS) [Kaldis et al., 2004], [Falcke et al., 2011] and [Li et al., 2012].

Experimental studies of solubility of CO_2 in aqueous solutions of water and organic acid are discussed in [Rumpf et al., 1997], [Kuranov et al., 1996], [Alvaro et al., 2000]. Certain formation of traces compounds occurs during the gasification process and some trace formation also occurs during quenching of the product synthesis gas in the quench chamber. Presented in Fig. 4.1 are the reactions (4.1), (4.2) and (4.4) of molecularly dissolved CO_2 in the liquid phase. Carbon dioxide from the product synthesis gas dissolves in stream F103 in the quench chamber according to Fig. 4.2. Some minute amount of formed carbonic acid (H_2CO_3) is highly unstable and subsequent acid-base chemistry lead to bicarbonate (HCO_3^-) and hydrogen ion (H^+). Bicarbonate dissociates to produces carbonate ion (CO_3^{2-}). Ammonia and bicarbonate reacts to form carbamate (NH_2COO^-).

The behaviour and the distribution of molecularly dissolved CO_2 and its ions in the quench water system shall be looked into as one of the gases from the product synthesis gas. In addition, the influence of the quench water temperature variation on the CO_2 and its species as well as quench water pH variation effects shall be discussed.

Table 4.2 presents the amount of CO_2 present in quench water cycle according to the results of the sensitivity analysis in the streams in Figure 4.2 for test point VP1. The gaseous streams are degas, hot gas and raw gas. The aqueous streams (liquid phase) include stream F103, quench water outlet stream, stream F136PRESS and stream F136. The total CO_2 around the quench water cycle is the sum of stream: F136, degas stream and raw gas stream, which is equal to the CO_2 outlet via hot gas. While the total amount of molecularly dissolved CO_2 is presented in equation (4.23).

Table 4.2: The distribution of CO$_2$ and its ions in all the streams

Stream names (Temperature, Pressure)	Stream total		CO$_{2,total}$	CO$_{2,total}$	CO$_{2,}$ molecularly dissolved	HCO$_3^-$	CO$_3^{2-}$	NH$_2$COO$^-$	pH value
	t/h	kmol/h	kmol/h	mmol/l	mmol/l	mmol/l	mmol/l	mmol/l	
QUENCH WATER (177.4 °C, 71 bar)	5.40	299.08	0.12	0.021	0.019 (94%)	1.2E-03 (5%)	2.4E-08 (0.0001%)	3.1E-07 (0.002%)	5.73
T104 (79.9 °C, 72 bar)	6.00	332.65		0.020	0.017 (84.5%)	3.2E-03 (15%)	1.1E-07 (0.0005%)	7.2E-08 (0.0004%)	5.53
F103 (79.9 °C, 72 bar)	5.30	296.38	0.11						
F136PRESS (79.9 °C, 72 bar)	0.70	36.26	0.014						
F136 (20 °C, 1 bar)	0.70	36.18	4.7E-03 (0.19%)	0.007	3.9E-03 (55.2%)	3.3E-03 (45%)	3.0E-07 (0.004%)	5.6E-08 (0.0008%)	6.24
DEGAS (20 °C, 1 bar)	0.002	0.09	9.0E-03 (0.36%)	0.102 (mol/mol)					
HOT GAS (1172 °C, 71 bar)	0.82	59.74	2.47 (100%)	0.041 (mol/mol)	$\frac{1}{M_{H_2O}} = 55500 \frac{mmol}{kg} \approx 55500 \frac{mmol}{l}$				
RAW GAS (117.4 °C, 71 bar)	0.77	57.05	2.45 (99.2%)	0.043 (mol/mol)					

The overall concentration of dissolved CO$_2$ in the liquid phase is:

$$\left[CO_{2\,(aq)\,total}\right]\frac{mol}{kg\ solvent} = \left[CO_{2\,(aq)\,molecues}\right] + \left[HCO_{3\,(aq)}^-\right] + \left[CO_{3\,(aq)}^{2-}\right] + \left[NH_2COO_{(aq)}^-\right] \qquad (4.23)$$

The Sankey diagram in Figure 4.5 indicates the flow of CO$_2$ and its compounds in the HP POX quench water system cycle based on the results obtained from the test point Gas-POX 201 VP1.
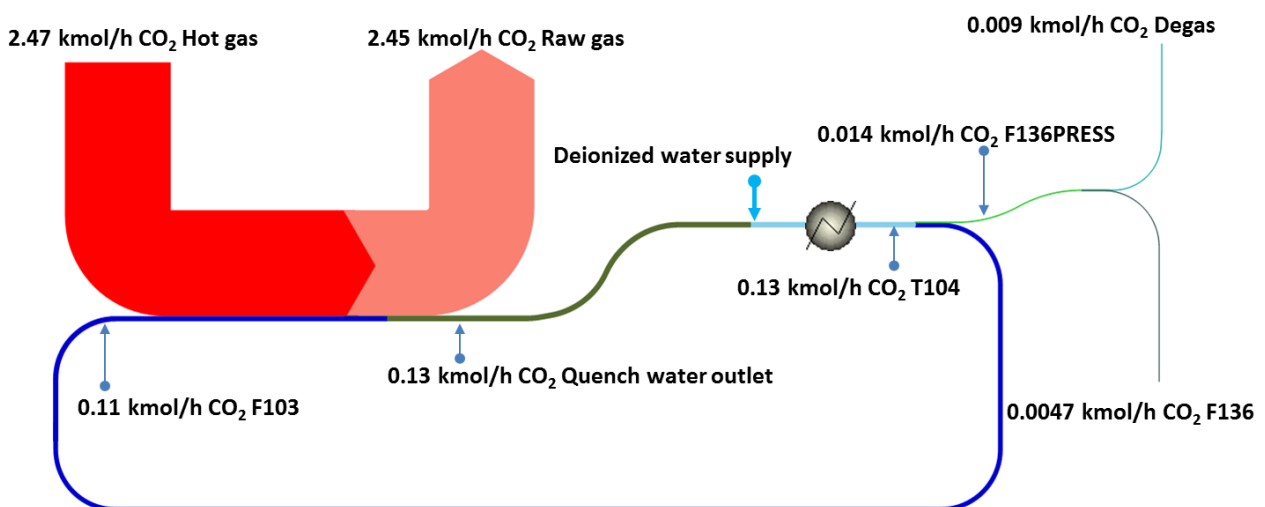
Figure 4.5: The flow of CO$_2$ in the quench water cycle (test point VP1).

It could be seen that virtually all the CO_2 originating from the gasifier with 2.47 kmol/h of CO_2 in hot gas remains in the raw gas stream with 99.2 % of CO_2 (2.45 kmol/h of CO_2).

4.2.1 Results of sensitivity study: quench water temperature variation effects on CO_2

The total dissolved CO_2 considered in each stream of the quench water cycle is the summation of molecularly dissolved: $CO_2(aq)$, $HCO_3^-(aq)$, $CO_3^{2-}(aq)$ and $NH_2COO^-(aq)$. The effects of quench water temperature variation on CO_2 as a result of the Aspen Plus sensitivity study are presented in Fig. 4.6. The ratios $CO_{2, F136}$ / $CO_{2, HG}$ and $CO_{2, DEGAS}$ /$CO_{2, HG}$ decrease with increase in quench water temperature as CO_2 first dissociation constant $HCO_3^-(aq)$ decreases. The Henry's constant of CO_2 increases with increasing temperature as it can be seen in Fig. 4.3 and also contributes to this effect. The ratio $CO_{2, RG}$ / $CO_{2, HG}$ remain almost unitary, almost all CO_2 from hot gas remains in raw gas stream. The pH value of the quench water decreases with increase in quench water temperature which was originally 6.17 at 177.4 °C and 72 bar. One reason for pH decrease in the quench water is also the increase of the self-dissociation constant of water with increasing temperature according to Fig. 4.3. At this point, it could be concluded that more of the CO_2 from the gasifier goes out of the quench chamber as the temperature of the quench water increases via the raw synthesis gas stream. A very little dissolved amount leaves the quench chamber via F136 while a minute amount is recycled into the quench system via F103. The dissolution of CO_2 in the quench decreases with increase in temperature of the quench water.
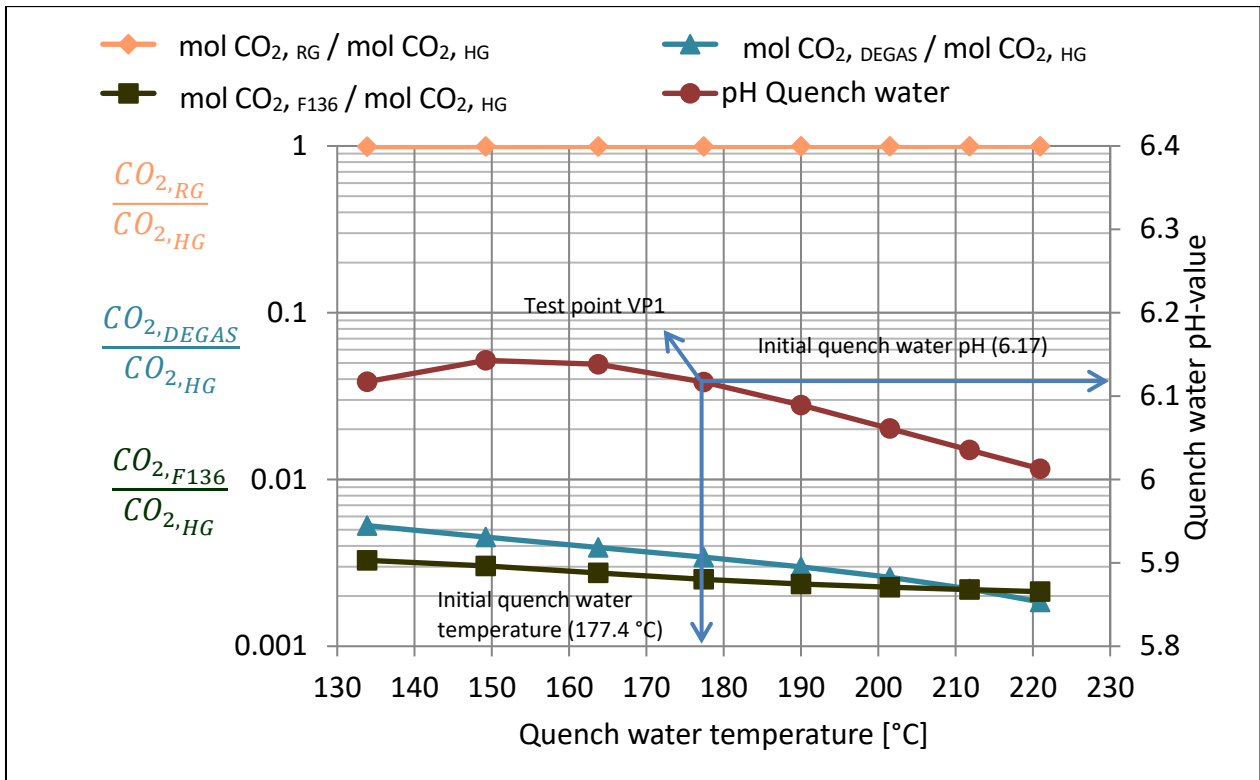
Figure 4.6: Calculated quench water temperature variation and effects on CO₂ distribution

In consideration to the increase temperature, an accumulation of dissolved CO_2 in the quench water might not happen in stream F103 over a long period of time when the quench water outlet is recycled and mixed with deionized water.

4.2.2   Results of sensitivity study: quench water pH variation influence on CO₂

Fig. 4.7 presents the influence of changes in the quench water pH on the CO_2 as a result of the Aspen Plus sensitivity study. It was observed that at low pH values from 0.14 to 7.7 nearly 100 % of CO_2 emanating from the hot gas leaves the quench chamber via the raw gas stream. At the pH value of 7.8, there was a decrease in CO_2 leaving via the raw gas stream. It was noticed that with increasing quench water pH values, CO_2 in the quench water blowdown stream F136 increase as more CO_2 goes into dissociation leading to a rise in the HCO_3^- formation. In Fig. 4.7, nearly the entire dissolved CO_2 remains in stream F136 exist then as HCO_3^- in aqueous solution. Consequently, the degas stream CO_2 content decreases with increasing quench water pH values from 7.8 to 8.
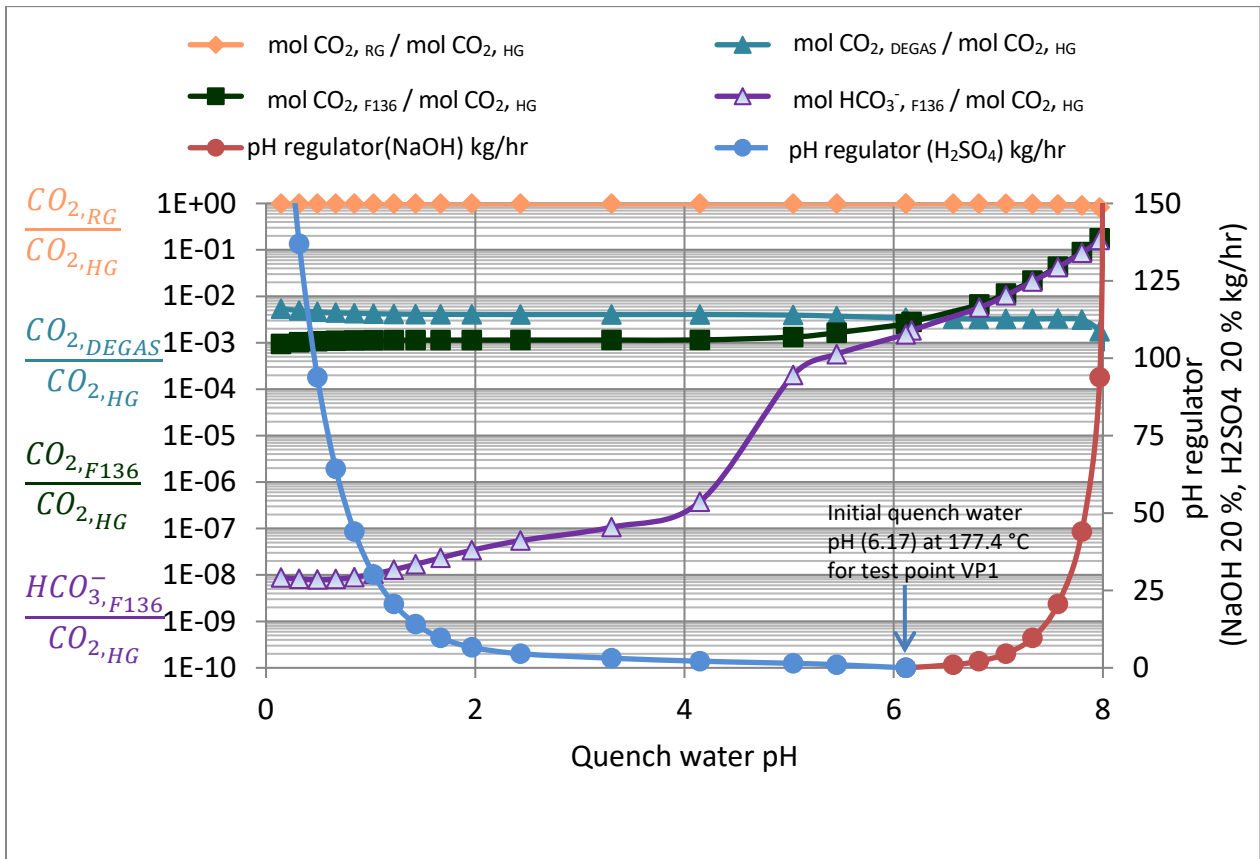
Figure 4.7: Calculated influence of pH regulation and effects on CO_2 distribution

The addition of basic pH regulator enhanced the washing down of CO_2 from the product synthesis gas and further dissociation produces HCO_3^- in the quench water chamber. Advancing this process could lead to the indirect scrubbing of CO_2 from the product synthesis gas and alleviating further concerns about CO_2 in the downstream process.

4.3   Nitrogen compounds

An unresolved problem in simplified integrated gasification combine-cycle (IGCC) process and processes operating at higher temperatures is the formation of nitrogen compounds especially ammonia and cyanides [Leppälahti et al., 1993]. It is important to take a look at these nitrogen compounds as they were measured during the test campaign. During operations, nitrogen is supplied into the gasifier as part of natural gas feed into the gasifier and for flushing the optical probe system. Consequently, the nitrogen is partially converted into NH_3 and HCN. In the downstream process of methanol production, the utilized catalysts are known to be sensitive to the both nitrogen compounds [Hiller et al., 2000] and [Bell et al., 2011].

The NH_3 molecules polarity and their ability to form hydrogen bonds enhance their high solubility in water. In aqueous solution, ammonia acts as a base by acquiring hydrogen ions from water to yield ammonium and hydroxide ions according to reaction (4.3) in Fig. 4.1. The vapour – liquid equilibrium behaviour of ammonia trace were investigated in [Hales et al., 1979], [Rumpf et al., 1999] and [Schäfer et al., 2007]. The aqueous solubility of ammonia, the ammonia-water thermodynamic constant and the generation of standard concentration of gaseous ammonia were reported by [Dasgupta et al., 1986]. Very high solubility behaviour of ammonia was observed in four different room-temperature ionic liquids (RTILs) and demonstrated in terms of thermodynamic excess functions base on [Yokozeki et al., 2007] equation-of-state (EOS) model.

HCN could lead to degradation of chemical solvent (used for acid gas removal) [Hiller et al., 2006] during raw synthesis gas treatment. Among the organic and inorganic cyano compounds [Dzombak et al., 2006], HCN is known to be of high toxicity. Due to varying literature values of HCN Henry constant, [Ma et al., 2010] measured the temperature dependence solubility of HCN in water to elucidate it equilibrium aqueous solubility. The experiment was carried out under severe precaution. The approached that was used to trap HCN in [Ma et al., 2010] was similar to those reported in Section 2.5.1.

4.3.1   Ammonia (NH_3)

The amount of NH_3 in the hot gas inlet to the quench water system, which satisfies the measured NH_4^+ outlet concentration, was calculated via design specification DS-NH_3 (Table 3.1 and Fig. 3.2). The total dissolved ammonia present in each stream of the quench water system cycle includes molecularly dissolved $NH_3(aq)$, $NH_4^+(aq)$, and $NH_2COO^-(aq)$. Reactions (4.3) and (4.4) present the chemical reactions of NH_3 and water to produce ammonium ($NH_4^+(aq)$) and carbamate ($NH_2COO^-(aq)$).

Table 4.3: The distribution of NH$_3$ and its ions in all the streams

Stream names (Temperature, Pressure)	Stream total (t/h)		NH$_{3, total}$	NH$_{3, total}$	NH$_{3, molecularly\ dissolved}$	NH$_4^+$	NH$_2$COO$^-$	pH value
	t/h	kmol/h	kmol/h	mmol/l	mmol/l	mmol/l	mmol/l	
QUENCH WATER (177.4 °C, 71 bar)	5.40	299.08	0.042	6.9E-03	3.7E-03 (29.2%)	3.3E-03 (70.8%)	1.5E-06 (0.004%)	5.73
T104 (79.9 °C, 72 bar)	6.00	332.65		6.8E-03	3.3E-05 (0.49%)	6.7E-03 (99.5%)	7.2E-08 (0.001%)	5.53
F103 (79.9 °C, 72 bar)	5.30	296.38	0.037					
F136PRESS (79.9 °C, 72 bar)	0.70	36.26	4.5E-03					
F136 (20 °C, 1 bar)	0.70	36.18	4.5E-03 (60%)	7.0E-03	4.8E-06 (0.07%)	7.0E-03 (99.9%)	5..6E-08 (0.0008%)	6.24
DEGAS (20 °C, 1 bar)	0.002	0.09	5.4E-09 (7.2E-5%)	6.1E-08 (mol/mol)	$\frac{1}{M_{H_2O}} = 55500\,\frac{mmol}{kg} \approx 55500\,\frac{mmol}{l}$			
HOT GAS (1172 °C, 71 bar)	0.82	59.74	7.5E-03 (100%)	1.2E-04 (mol/mol)				
RAW GAS (117.4 °C, 71 bar)	0.77	57.05	2.9E-03 (39%)	5.1E-05 (mol/mol)				

The overall concentration of dissolved NH$_3$ in the liquid phase:

$$[NH_{3\,(aq)\ total}]\ \text{mol/(kg solvent)} = [NH_{3\,(aq)\ molecules}] + [NH_4^+{}_{(aq)}] + [NH_2COO^-_{(aq)}] \qquad (4.24)$$

NH$_2$COO$^-$(aq) is one of the species of NH$_3$ formed from the reaction of bicarbonate and ammonium. The total molecularly dissolved NH$_3$ is the summation of NH$_3$(aq), NH$_4^+$(aq) and NH$_2$COO$^-$(aq). Fig. 4.8 presents the flow of ammonia from hot gas to the quench water cycle system for the test point VP1. It can be seen that 39% of the ammonia remains in the raw synthesis gas and the remaining is transferred into the quench water. Table 4.3 presents the proportion of the three ammonia participating species. It can be seen that more than 99% of molecularly dissolved NH$_3$(aq) is presented as NH$_4^+$(aq) except in the quench water outlet stream from the quench chamber, where the composition of molecular NH$_3$(aq)and NH$_4^+$(aq) are approximately 29% and 71% respectively. Among all these ammonia species NH$_4^+$(aq) is the most dominant in the aqueous phase of the quench water system cycle.

7.5E-03 kmol/h NH_3 Hot gas

2.9E-03 kmol/h NH_3 Raw gas

5.4E-09 kmol/h NH_3 Degas

Deionized water supply

4.5E-03 kmol/h NH_3 F136PRESS

0.042 kmol/h NH_3 T104

0.042 kmol/h NH_3 Quench water outlet

4.5E-03 kmol/h NH_3 F136

0.037 kmol/h NH_3 F103
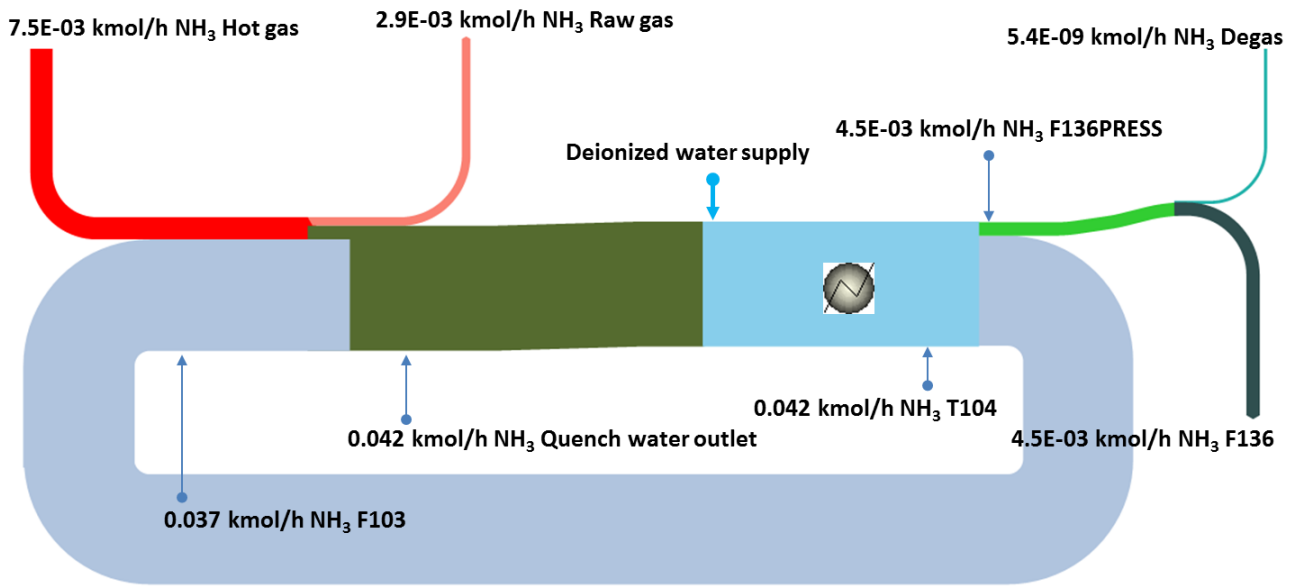
Figure 4.8: The flow of NH_3 in the quench water cycle (test point VP1).

4.3.2 Results of sensitivity study: quench water temperature variation effects on NH_3

The effects of quench water temperature variation on NH_3 as a result of the Aspen Plus sensitivity study are presented in Fig. 4.9. It was observed that the raw gas ammonia ($NH_{3, \text{Raw gas}}$) content increases with increasing quench water temperature. In the quench water blowdown stream (F136), NH_4^+(aq)were mostly represented, so the $NH_{3, \text{DEGAS}}$ / $NH_{3, \text{HG}}$ were very low as it can be seen in Fig 4.9.

Both the stream F136 and degas streams´ ammonia content decreases with increasing quench water temperature. The NH_3(aq) molecular solubility decreases with increase in quench water temperature as a result of the increase in NH_3 Henry constant (Fig. 4.3). The pH value of the quench water decreases with increase in quench water temperature, which was originally 6.17 at 177.4 °C and 72 bar.

The increase in the amount of $NH_{3 \text{ Raw gas}}$ was due to the increased temperature of the quench water, which enhances the ammonia to be in the vapour phase and thus leaving the quench chamber via the raw gas.
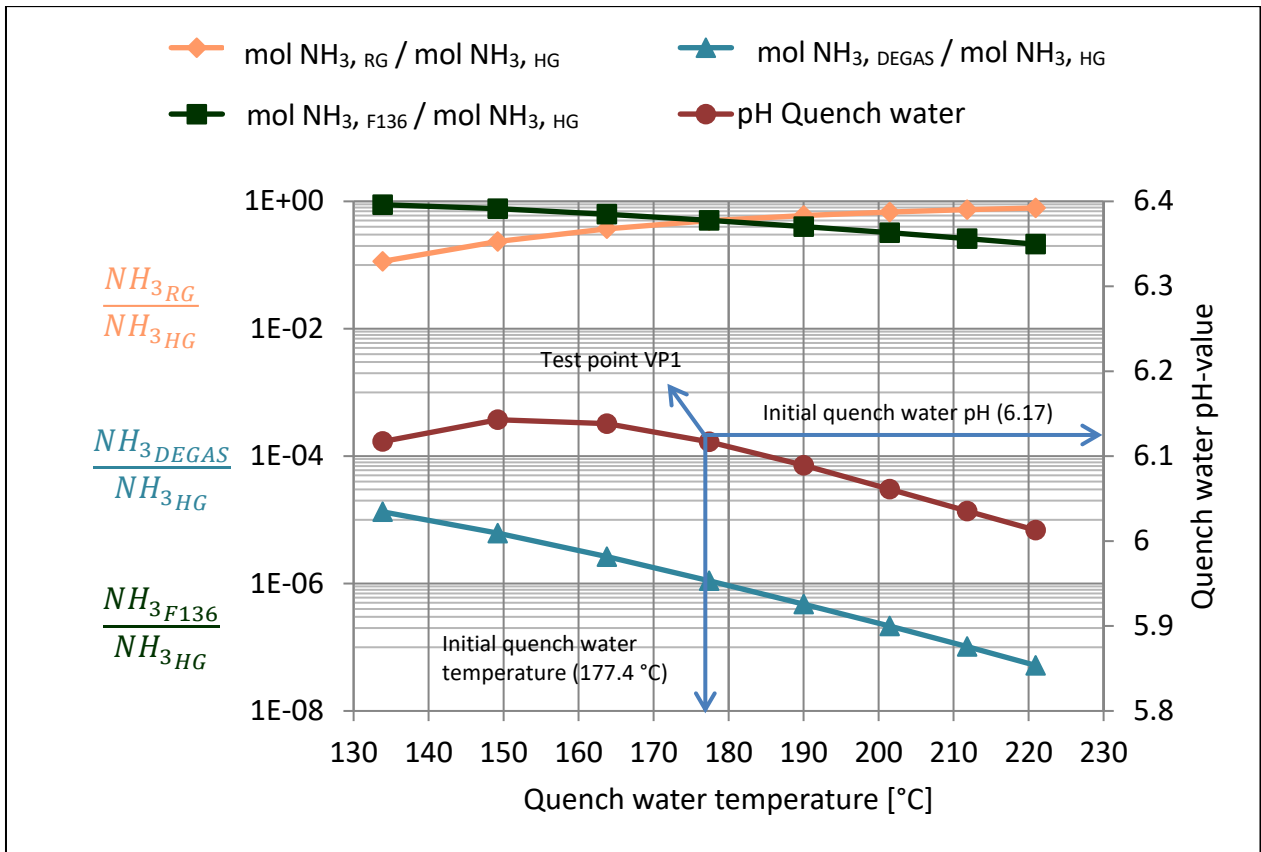
Figure 4.9: Calculated quench water temperature variation and effects on NH₃ distribution

4.3.3 Results of sensitivity study: quench water pH variation influence on NH₃

The influence of quench water pH variation on NH_3 as a result of the Aspen Plus sensitivity study is presented in Fig. 4.10. In comparison to what happened in the case of CO_2, the situation here was quite different as lower amount of NH_3 leaves the quench vessel via the raw gas stream at low pH values (between 0 – 6.17) when H_2SO_4 solution was introduced. On introducing NaOH solution, $NH_{3; Raw\ gas}$ increases, $NH_{3; F136}$ decreases and $NH_{3\ DEGAS}$ remains very minute. The NH_4^+ was the most NH_3 species present in stream F136 at low pH values.
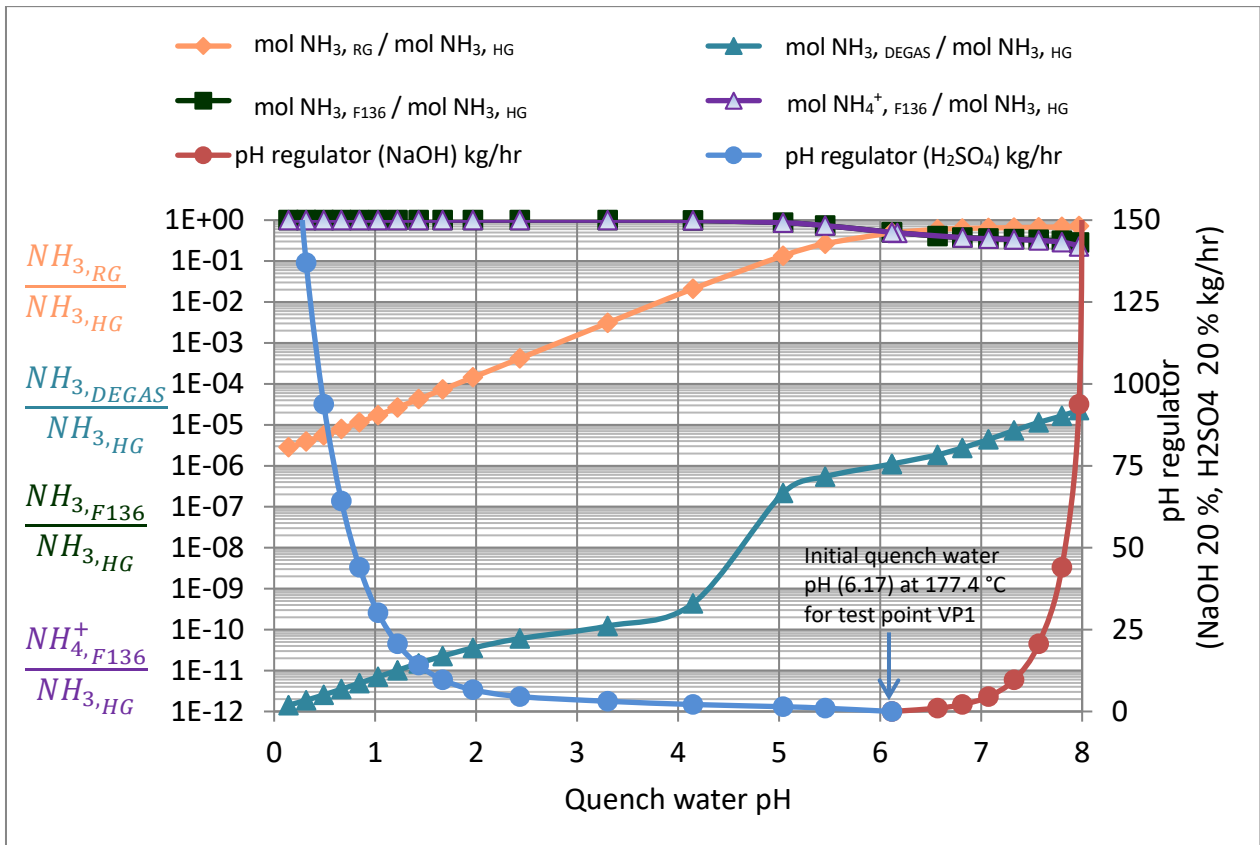
Figure 4.10: Calculated influence of pH regulation and effects on NH_3 distribution

4.3.4 Hydrogen Cyanide (HCN)

The amount of HCN in the hot gas inlet to the quench water system was calculated via design specification DS – HCN (Table 3.1 and Fig. 3.2). The total dissolved hydrogen cyanide present in each stream of the quench water system cycle includes molecularly dissolved HCN(aq) and CN^-(aq). Reactions (4.5) present the dissociation of HCN in water to produce CN^-(aq) and hydrogen ion (H^+(aq)).

Approximately 76 % of HCN remains in the raw gas for the test point VP1 (see Table 4.4). HCN molecule is highly soluble in water, its solubility decreases with increased temperature according to Fig.4.3. The total dissolved HCN in each stream of the quench water system cycle is the sum of molecularly dissolved HCN (aq) and CN^-(aq) according to equation (4.25).

The Sankey diagram in Figure 4.11 represents the flow of HCN and CN^- in the HP POX quench water system based on the results obtained from the Gas-POX 201 VP1. It could be seen that 76 % of the HCN $_{hot\ gas}$ leaves the quench chamber via the raw gas. The remaining HCN remains in the quench water mostly as molecularly dissolved species (Table 4.4).

Table 4.4: The distribution of HCN and its ions in all the streams

Stream names (Temperature, Pressure)	Stream total t/h	Stream total kmol/h	HCN_{total} kmol/h	HCN_{total} mmol/l	$HCN_{molecularly\ dissolved}$ mmol/l	CN^- mmol/l	pH value
QUENCH WATER (177.4 °C, 71 bar)	5.40	299.08	5.7E-04	9.5E-05	9.4E-05 (98.4%)	1.4E-06 (1.5%)	5.73
T104 (79.9 °C, 72 bar)	6.00	332.65			9.3E-05 (99.7%)	2.5E-07 (0.3%)	5.53
F103 (79.9 °C, 72 bar)	5.30	296.38	5.1E-04	9.3E-05			
F136PRESS (79.9 °C, 72 bar)	0.70	36.26	6.2E-05				
F136 (20 °C, 1 bar)	0.70	36.18	6.2E-05 (23.8%)	9.5E-05	9.5E-05 (99.9%)	8.1E-08 (0.09%)	6.24
DEGAS (20 °C, 1 bar)	0.002	0.09	5.9E-07 (0.2%)	6.8E-06 (mol/mol)	$\frac{1}{M_{H_2O}} = 55500\,\frac{mmol}{kg} \approx 55500\,\frac{mmol}{l}$		
HOT GAS (1172 °C, 71 bar)	0.82	59.74	2.6E-04 (100%)	4.4E-06 (mol/mol)			
RAW GAS (117.4 °C, 71 bar)	0.77	57.05	2.0E-04 (76%)	3.5E-06 (mol/mol)			

The overall concentration of dissolved HCN in the liquid phase:

$$[HCN_{(aq)total}]\ \text{mol/(kg solvent)} = [HCN_{(aq)molecules}] + [CN^-_{(aq)}] \tag{4.25}$$
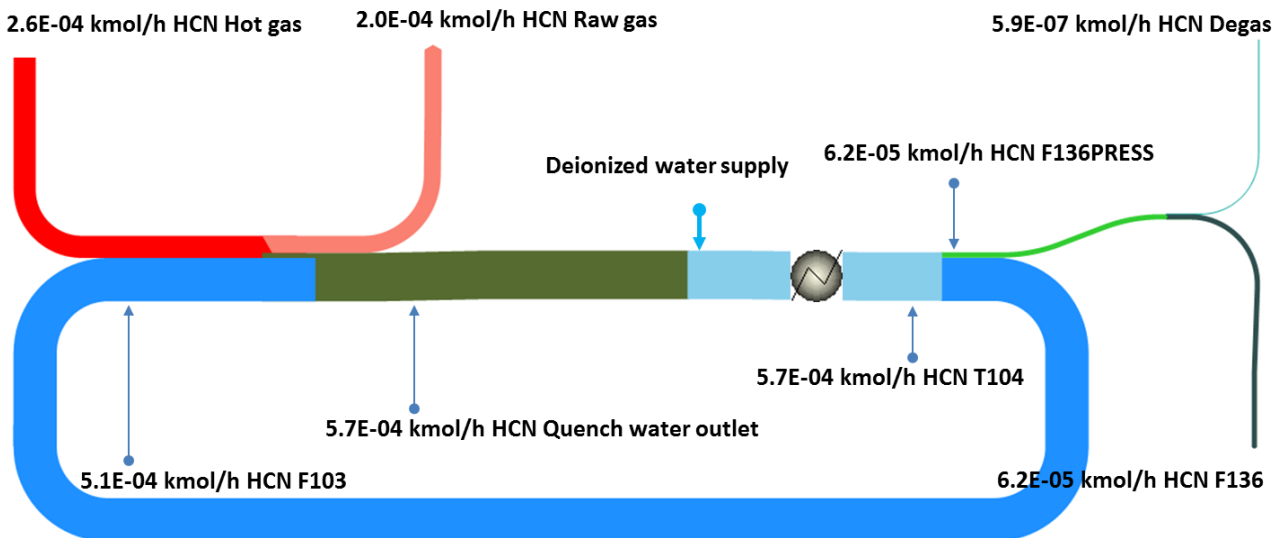
Figure 4.11: The flow of HCN in the quench water cycle (test point VP1).

4.3.5   Results of sensitivity study: quench water temperature variation effects on HCN

From the results in Fig. 4.12 and Table 4.4, it could be seen that as quench water temperature increases, more HCN from hot gas remains in raw gas ($HCN_{Raw\,gas}$ / $HCN_{Hot\,gas}$ increases) while HCN_{F136} and HCN_{DEGAS} decrease with increasing quench water temperature. The Henry constant of HCN increases with increase of quench water temperature (See Fig. 4.2).

Henry´s constant increase is the main dominant effect. In all the liquid phase streams (with respect to F103, T104, F136PRESS and F136) of the quench water system cycle, over 98% of the total dissolved HCN exist as molecularly dissolved HCN.
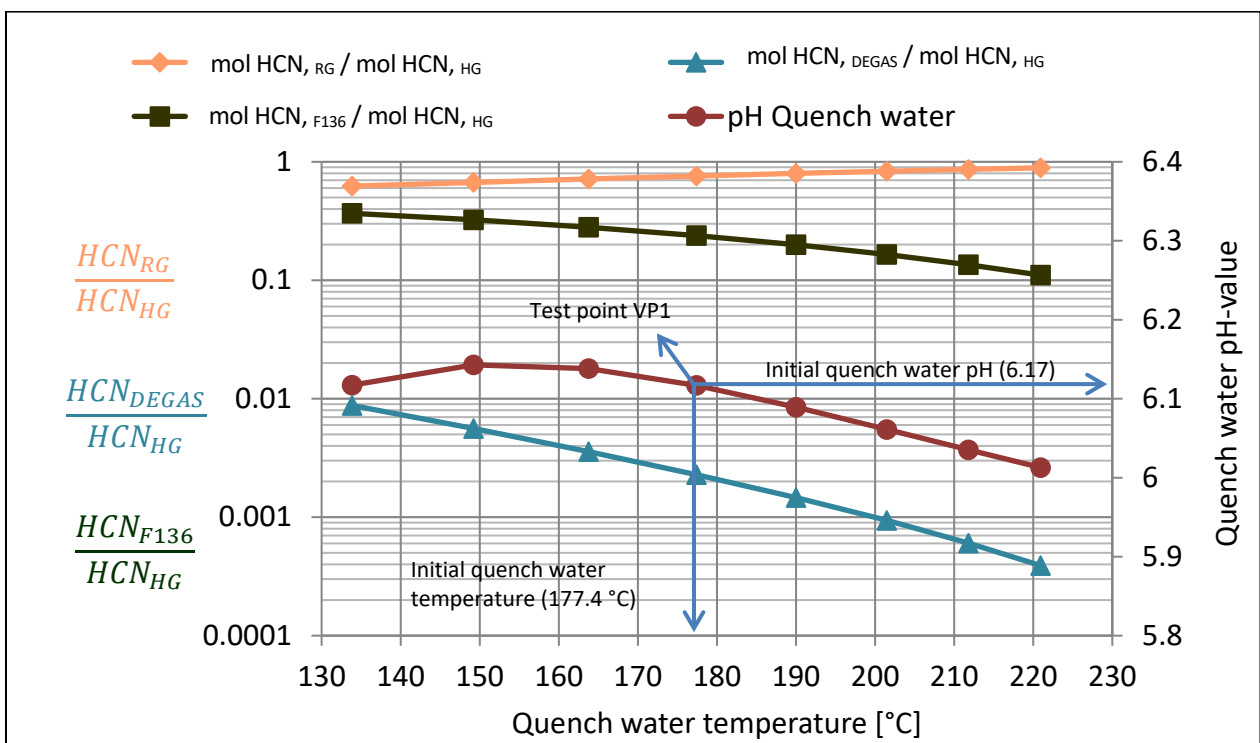
Figure 4.12: Calculated quench water temperature variation and effects on HCN distribution

4.3.6   Results of sensitivity study: quench water pH variation influence on HCN

There were no big changes when H_2SO_4 solution was introduced but the change mainly occurs when NaOH solution was introduced into the quench water via stream F103 (see Fig. 4.2). At this condition, $HCN_{Raw\,gas}$ decreases while dissolved HCN increases as more HCN in the liquid stream goes into dissociation leading to an increase in CN^- formation (see Fig. 4.13).
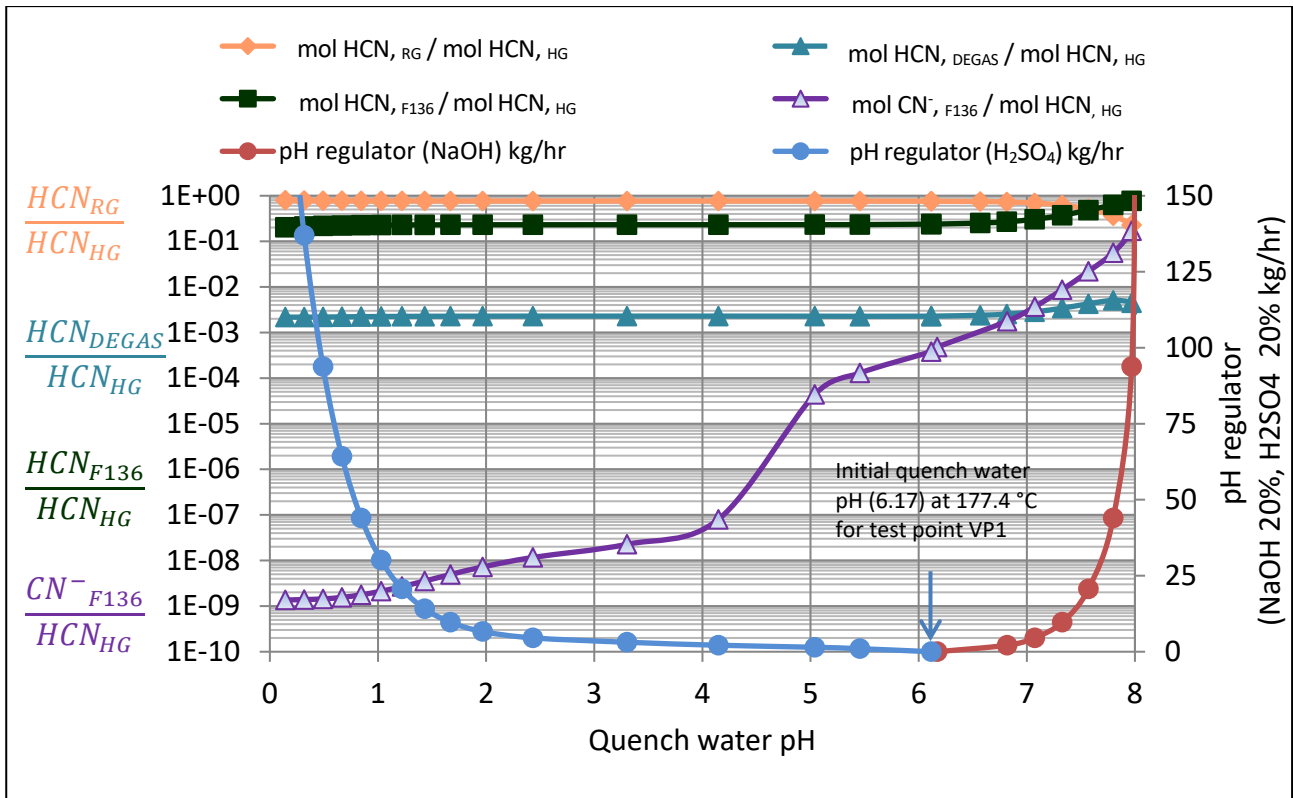
Figure 4.13: Calculated influence of pH regulation and effects on HCN distribution

4.4 Sulphur compounds: H_2S

In the downstream utilization of raw synthesis gas for the production of ammonia, methanol, gas-to-liquids or Fischer-Tropsch syntheses etc., sulfur compounds are precursor to catalyst poison. In methanol production it is applicable to have feed gas with less than 0.1 ppmv of H_2S in order to avoid poisonous effect on the catalysts [Gräbner, 2015].

Sulphur compounds in the natural gas present as H_2S are partly converted during gasification into COS. There is a relationship between H_2S and COS amount [Higman et al., 2003] in the raw synthesis gas, this relationship is evaluated based on the hydrogenation and hydrolysis reactions (4.26) and (4.27) respectively [Gräbner, 2015]:

$$H_2 + COS \rightleftharpoons H_2S + CO \qquad (4.26)$$

$$COS + H_2O \rightleftharpoons H_2S + CO_2 \qquad (4.27)$$

In liquid phase, Henry´s law was reported not to be applicable for H_2S in water [Wright et al., 1932] but H_2S behaves like other gaseous solutes, which undergoes electrolytic dissociation. But further experimental works by [Carroll et al., 1989] and [Rumpf et al., 1999] provide a good comparison and agreement as an adapted Pitzer model was used to correlate the new data for the excess Gibbs energy of an aqueous electrolyte solution.

The amount of H_2S in the hot gas inlet to the quench water system was calculated via design specification DS – H_2S (Table 3.1 and Fig. 3.2). In water, H_2S is known to be a weak acid that can go through the chemical reactions (4.6) – (4.7). The presence of hydrogen sulfide in the hot gas during the quench operations yield molecularly dissolved $H_2S(aq)$, $HS^-(aq)$ and $S^{2-}(aq)$ in the quench water stream after dissociation in water. The total dissolved H_2S is the sum of dissolved $H_2S(aq)$ molecules, $HS^-(aq)$ and $S^{2-}(aq)$.

Table 4.5: The distribution of H_2S and its ions in all the streams

Stream names (Temperature, Pressure)	Stream total		H_2S total	H_2S total	H_2S molecularly dissolved	HS^-	S^{2-}	pH value
	t/h	kmol/h	kmol/h	mmol/l	mmol/l	mmol/l	mmol/l	
QUENCH WATER (177.4 °C, 71 bar)	5.40	299.08	1.8E-05	2.9E-06	2.5E-06 (87.2%)	3.7E-7 (12.8%)	4.9E-12 (0.0001%)	5.73
T104 (79.9 °C, 72 bar)	6.00	332.65		2.9E-06	2.6E-06 (89.9%)	2.9E-7 (10%)	1.2E-14 (4E-07%)	5.53
F103 (79.9 °C, 72 bar)	5.30	296.38	1.6E-05					
F136PRESS (79.9 °C, 72 bar)	0.70	36.26	1.9E-06					
F136 (20 °C, 1 bar)	0.70	36.18	9.5E-07 (0.7%)	1.5E-06	1.3E-06 (86.0%)	2.0E-7 (13.9%)	2.9E-16 (2.0E-08%)	6.24
DEGAS (20 °C, 1 bar)	0.002	0.09	9.6E-07 (0.9%)	1.1E-05 (mol/mol)	$\dfrac{1}{M_{H_2O}} = 55500\,\dfrac{\text{mmol}}{\text{kg}} \approx 55500\,\dfrac{\text{mmol}}{l}$			
HOT GAS (1172 °C, 71 bar)	0.82	59.74	1.2E-04 (100%)	2.0E-06 (mol/mol)				
RAW GAS (117.4 °C, 71 bar)	0.77	57.05	1.1E-04 (98%)	1.9E-06 (mol/mol)				

The overall concentration of dissolved H_2S in the liquid phase:

$$\left[H_2S_{(aq)\,total}\right]\text{mol/(kg solvent)} = \left[H_2S_{(aq)\,molecules}\right] + \left[HS^-_{(aq)}\right] + \left[S^{2-}_{(aq)}\right] \tag{4.28}$$

The Sankey diagram in Figure 4.14 represents the flow of H_2S and its compounds in the HP POX quench water system cycle based on the results obtained from the Gas-POX 201 VP1. It could be seen

that virtually all the H_2S originating from the gasifier with 1.2E-04 kmol/h of H_2S in hot gas remains in the raw gas stream (98 % of H_2S, see Table 4.5).
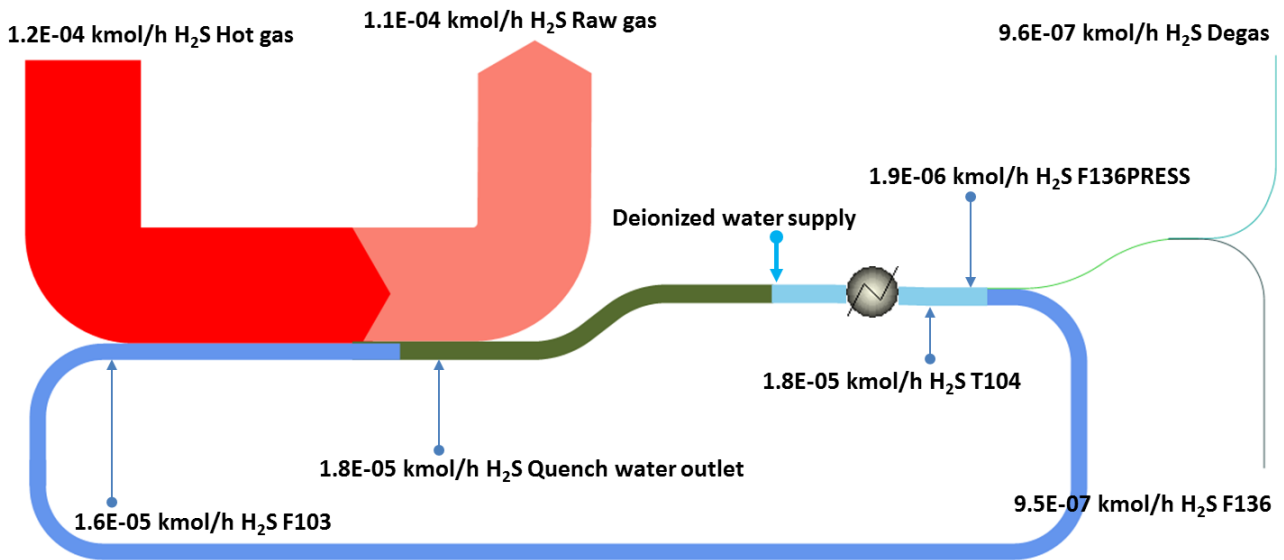
Figure 4.14: The flow of H_2S in the quench water cycle (test point VP1)

4.4.1 Results of sensitivity study: quench water temperature variation effects on H_2S

Figure 4.15 shows the result of the sensitivity studies regarding temperature change in the quench water. $H2S_{F136}$ and $H2S_{DEGAS}$ ratio with hot gas decrease with increase in quench water temperature. This observed change was due to the increase in the H_2S Henry constant in Fig. 4.2. The amount of the HS^-(aq) and S^{2-}(aq) are low compared to that of molecularly dissolved H_2S.
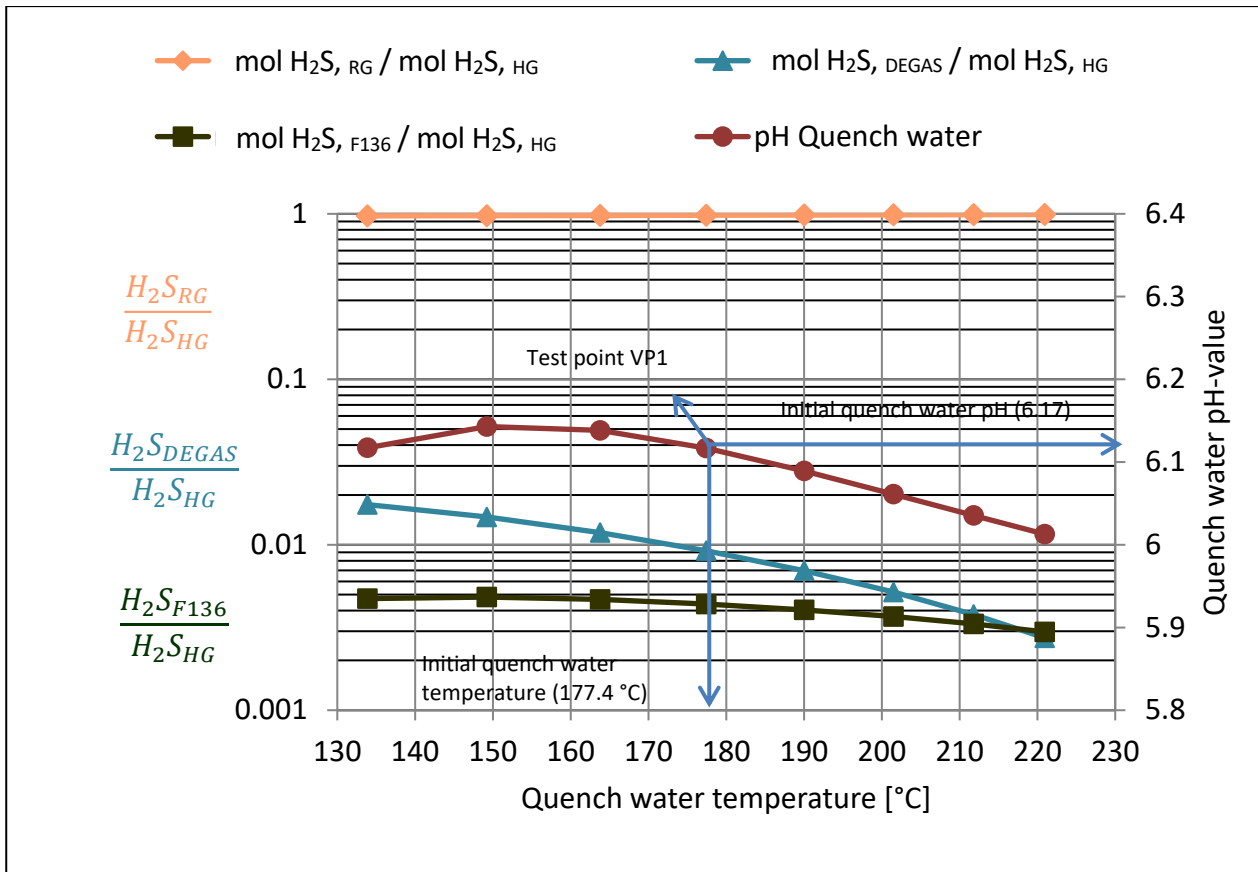
Figure 4.15: Calculated quench water temperature variation and effects on H_2S distribution

4.4.2 Results of sensitivity study: quench water pH variation influence on H_2S

$H_2S_{Hot\ gas}$ remains nearly complete as $H_2S_{Raw\ gas}$ at low pH values of the quench water in Figure 4.16. A pronounced drop in raw gas H_2S was observed when the quench water pH was 7.5 and the decrease continues as pH value further increases. For degas stream, there were no noticeable changes when H_2SO_4 solution was introduced as pH value regulator but the changes occur when the initial quench water pH value was increased from 6.17 to 8 by introducing NaOH solution. In stream F136, H_2S increases as more H_2S goes into dissociation leading to an increase in HS^- formation in the aqueous solution.
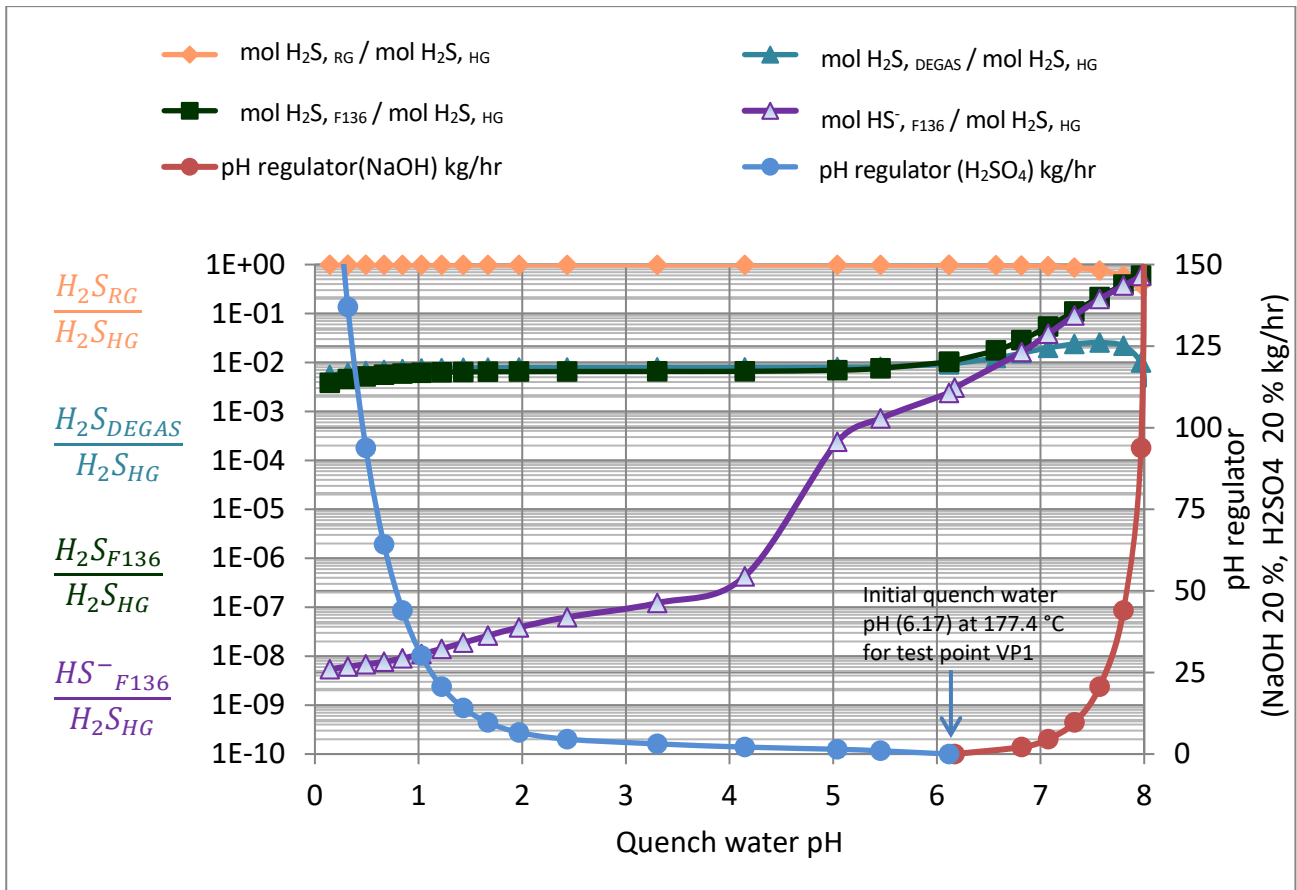
Figure 4.16: Calculated influence of pH regulation and effects on H₂S distribution

4.5 Summary

Whenever the quench water temperature increases, the quench water pH values reduce among others because of an increasing self-dissociation of water. There is a complex interaction between changing Henry constant and dissociation constants of the dissolved species, which led to the decreased in the overall solubilities of H_2S, HCN, NH_3 and CO_2 in the blowdown stream F136 and to increasing H_2S, HCN, NH_3 and CO_2 content in the raw gas.

The chosen ELECNRTL model in Aspen Plus also takes into account the activity coefficient of the molecularly and ionically dissolved species and the solvent (water).

The increases in quench water temperature, lead to the increase of CO_2, H_2S, NH_3 and HCN in the raw gas stream:

Whenever the pH value of the quench water inlet F103 was increased with the introduction of a NaOH solution or reduced with a H_2SO_4 solution; the amounts of CO_2, H_2S and HCN present in the quench

water blowdown stream increase or reduce respectively. These conversely led to a decrease or respective increase in the amount of these components present in the raw gas stream.

In contrast to the acid compounds (CO_2, H_2S, and HCN), NH_3 decreases in the quench water blowdown stream and increases in the raw gas stream when NaOH solution was introduced and contrarily for the case of H_2SO_4 solution.

To design an optimum quench operation process, the solubility of weak electrolyte gases like basic gas (ammonia) and sour gas (carbon dioxide, hydrogen sulphide and hydrogen cyanide), their vapour – liquid equilibria (VLE) behaviour and other physiochemical properties such as Henry´s constants are important. Henry's constants of the trace gases and chemical reaction equilibrium constants in the solvent mixtures of the quench water must be studied on individual bases to have a better understanding of the behaviour of these trace gases and their species. Although, it is complex to describe the behaviours of all the trace components present in the quench water system together but an individual approach will guide to come to an optimum decision especially when other test points are further investigated.

5 Organic acids trace studies in quench water

The formation of the traces of formic acid (HCOOH) and acetic acid (CH_3COOH) shall be discussed in this chapter. The quenching of the hot gas leaving the gasifier unit is a direct quenching method, which takes place in the HP POX quench chamber. This provides the interaction between the components of the hot gas (at 1172 – 1444 °C and from 51 – 81 bar) and quench water (stream F103: liquid phase at 141 – 194 °C) in the quench chamber during the test campaigns according to Fig. 3.1. Also discussed are possible reaction mechanism that might be responsible for the formation of these organic acids and how they interact with other components present in the quench water.

In gasification processes, the high partial pressure of CO favours the formation of formic acid in the liquid phase [Higman et al., 2003], which results in the lowering of the pH of the aqueous medium. Consequently, the presence of formic acid and acetic acid for example may influence the corrosivity of alkanolamine solvents employed for cleaning and purifying natural gas or in the CO_2 capture [Kittel et al., 2012] as well as their effects when they are accumulated around process plant surfaces. These lead to the increase of corrosion rate and results to increase of acid in the aqueous medium [Pearson et al., 2016]. In addition, several methods were developed to purify significant amount of water in Fischer-Tropsch process. Apart from benzene, toluene, xylenes, styrene, acetaldehyde and so on, formic acid and acetic acid were among the acid contaminant that were required to be removed from the process water or cooling water in the reaction section of the Fischer-Tropsch synthesis [David et al., 1973] and [William et al., 2010]. These hydrocarbons were formed during the Fischer-Tropsch synthesis. The treatment comprises of a liquid-liquid extraction in order to remove some fraction of these organic acids from the water stream [Luis et al., 2004], [Lino et al., 2008] and [Ivan et al., 2014]. Although, all these cases are typical examples that occur in the aforementioned industrial processes based on facts from literatures. They are not part of what happens in the HP POX test plant.

5.1 Organic acids interaction with ammonia compounds in the quench water

The presence of traces of formic acid species (HCOOH, $HCOO^-$), acetic acid species (CH_3COOH, CH_3COO^-), other acid species and ammonia species (NH_3, NH_4^+) in the quench water effluent mixed with the deionized water provides the medium for acid-base chemical reactions during the quench operations. These interaction enhance neutralization effects [Wang et al., 2005], which is common to industrial waste water effluents for examples in coal gasification at about 60 bar [Higman et al., 2003]. Test point VP1 has a calculated pH value of 6.17 (see Appendix Fig. 9.6: Calculated pH values, temperature range and species). The calculated pH values change from test point to test point as a

result of the acid-base interactions in the quench water and changes in the distribution of various molecularly dissolved components as well as their ions and due to different quench water temperatures. The ammonia formed in the gasifier partly goes into dissolution in the quench chamber and interacts with these organic acids and other acid species. Experiments on formic acid and acetic acid interaction with ammonia and water were reported by [Becker et al., 1963] and [Rablen et al., 1998] with peculiar aggregation properties [Imberti et al., 2010] at molecular level in consideration to the strong hydrogen bond formation they exhibit [Soffientini et al., 2015].

The figures discussed in this chapter are based on reactions (4.8), (4.9) and (4.10) as well as the results derived from the calculations from the Aspen Plus model of the quench water system (see Appendix, Fig. 9.7: Aspen Plus flow sheet setup for organic acid compounds calculations and Table 9.12). Part of these organic acid dissociate in the quench. The formation of formic acid according to equation (4.8) was also report by [Brüggemann, 2010] together with kinetic mechanisms for the formation of formic acid.

$$CO_{(aq)} + H_2O \rightleftharpoons HCOOH_{(aq)} \rightleftharpoons HCOO^- + H^+ \tag{4.8}$$

$$2CO_{2\,(aq)} + 4H_{2\,(aq)} \rightleftharpoons CH_3COOH_{(aq)} + 2H_2O \tag{4.9}$$

$$CH_3COOH_{(aq)} \rightleftharpoons CH_3COO^- + H^+ \tag{4.10}$$
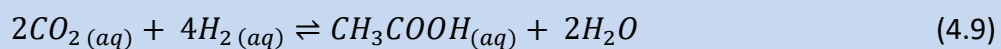
The equilibrium (m_eq) denotes the concentration of the acid calculated in Aspen Plus separately in an equilibrium reactor. The calculated equilibrium concentrations (m_eq) do not influence the calculated quench water species distribution based on analysed values and are only compared with the real values (m_real). While the so called real (m_real) denotes reaction quotient, which is the concentration of the acid or base formed based on the amount of these component measured and analysed in the laboratory and re-calculated in Aspen Plus with the help of design specification tools.

Fig. 5.1 and 5.2 present the concentration of formic acid, the concentration of ammonia and the quench water temperature in the quench chamber during the hot gas quenching. These profiles are based on the result from the Aspen Plus model of the quench water system for the 47 test points under consideration (see Appendix Table 9.3: Gas-POX test campaigns and with designated serial numbers).
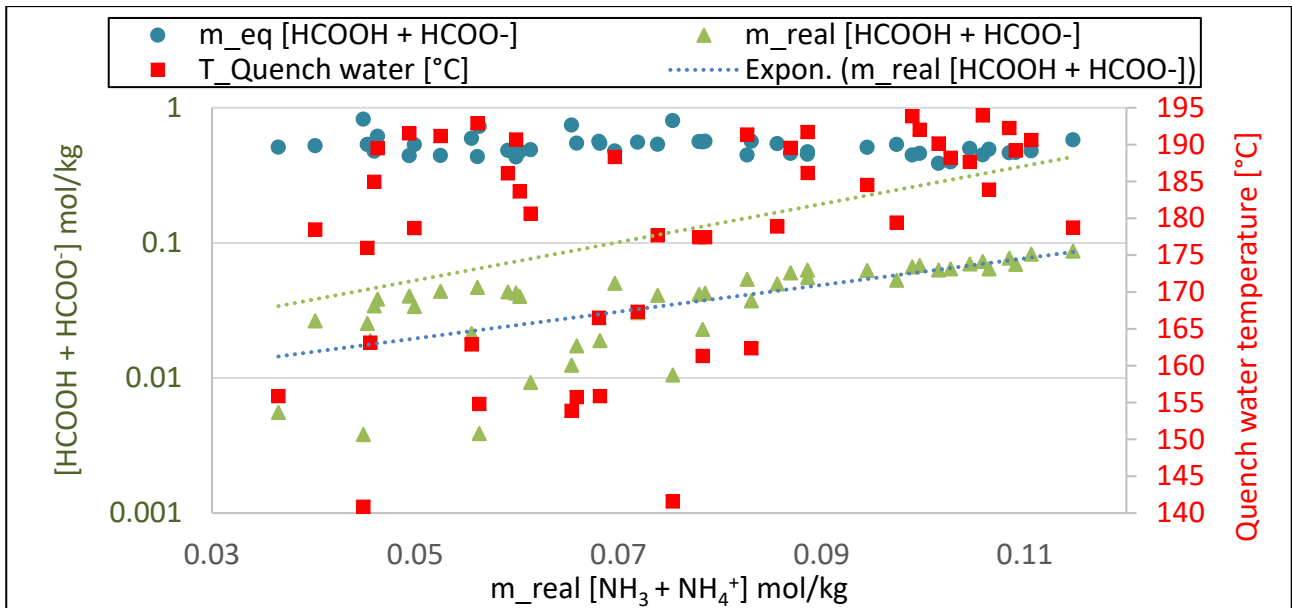
Figure 5.1: Aspen Plus back-calculated (real) formic acid concentration, quench water temperature and the calculated equilibrium formic acid concentration against back-calculated (real) ammonia concentration for the 47 test points (using amongst others sampled $HCOO^-$ and NH_4^+ values according to Table 2.6).

From Figure 5.1, it could be observed that there is a correlation (see Appendix: Table 9.4; r = +0.81) between the increase of the real formic acid concentration and the increase in the concentration of ammonia in the quench water. The calculated equilibrium formation of formic acid decreases with increasing temperature of the quench water (see Fig. 5.2). It can be observed that both the equilibrium and real formation of formic acid becomes closer as ammonia concentration increases. Figure 5.2 show the dependency of the real ammonia formation as temperature of the quench water increase. It could be observed that the real formation of formic acid and ammonia show a correlation from 140 °C to 195 °C (see Appendix: Table 9.4). In this, it could be concluded that there is a buffer characteristics of the species present in formic acid ($HCOOH$ is a weak acid and $HCOO^-$ a weak base) and ammonia (NH_4^+ is a weak acid and NH_3 is a weak base). According to [Alexander et al., 1948], during these kinds of interaction in the aqueous phase of the quench water, ammonium formate as an ammonium salt might be formed and decompose when there is further increase in temperature. Although, the quench water system under consideration in this dissertation is a dilute system with no salt formation during or after the quench operation. In the literature studies of the mechanism of the Leuckart reaction [Alexander et al., 1948], the appearance of ammonium formate at 120 °C to 130 °C, the elimination of water by ammonium formate to form formamide when heated and the possibilities

of reaching equilibrium at 165 °C was reported. These types of reactions (Leuckart) occur during the conversion of carbonyl compounds to form amino derivatives [Alexander et al., 1948]. Also, the decomposition of formamide formed from ammonium formate produces carbon monoxide (CO) and ammonia at temperatures above 120 °C [Gibson, 1969]. More comment about formamide and other traces formation from its decomposition can be found in [Nguyen et al., 2013], [Becker et al., 1963] and [Gibson, 1969] in the Appendix (see comment on formamide).
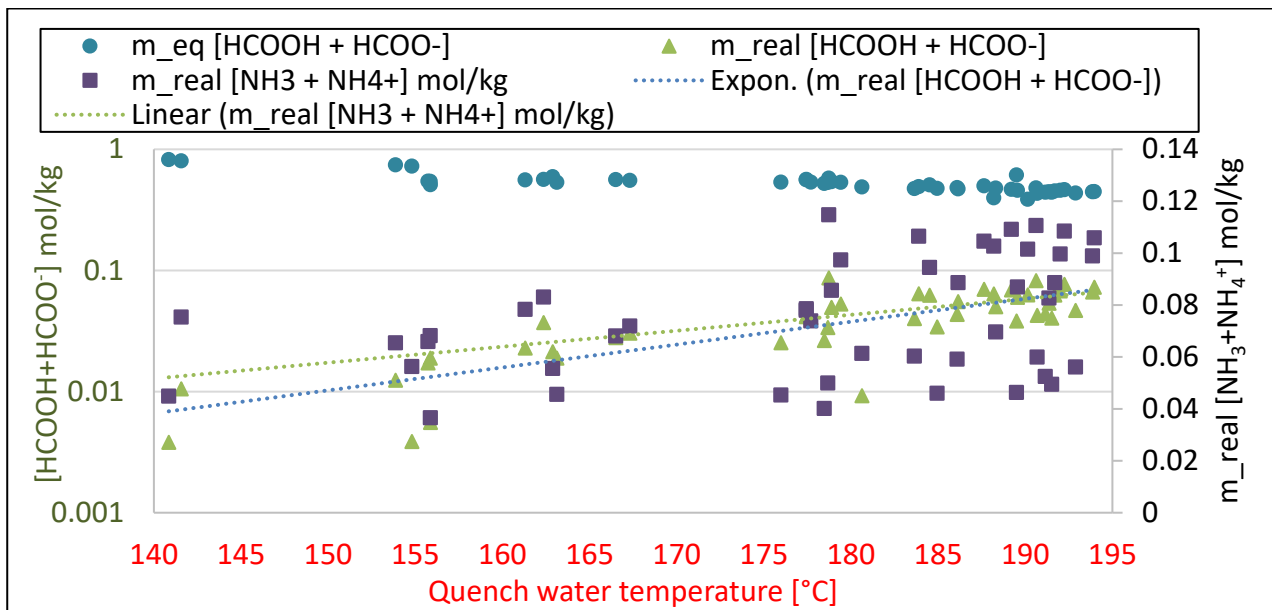
Figure 5.2: Aspen plus back-calculated (real) formic acid concentration, back-calculated (real) ammonia concentration and the calculated equilibrium formic acid concentration against quench water temperature for the 47 test points (using amongst others sampled $HCOO^-$ and NH_4^+ values according to Table 2.6).

Fig. 5.3 and 5.4 present the concentration of acetic acid, the concentration of ammonia and the quench water temperature in the quench chamber during the hot gas quenching. In the analysed quench water to detect the presence of acetic acid, it was observed that the amount of the acetic acid in the first thirteen test points were below the threshold of measuring range. This led to have the real concentration of acetic acid which is based on the laboratory analysis of the quench water and implemented in Aspen Plus to be unseen for the first thirteen test points (see Appendix Table 9.3: Gas-POX test campaigns and with designated serial numbers and see also Fig. 5.9).

It can be seen in Fig. 5.3 that the concentration of the equilibrium and real acetic acid are far apart from each other. The calculated equilibrium concentration of acetic acid produced in the quench water is between 0.0465 mol/kg and 0.0826 mol/kg. While the real concentration of acetic acid is produced in the quench water is between 1.34E-10 mol/kg and 0.0009 mol/kg.
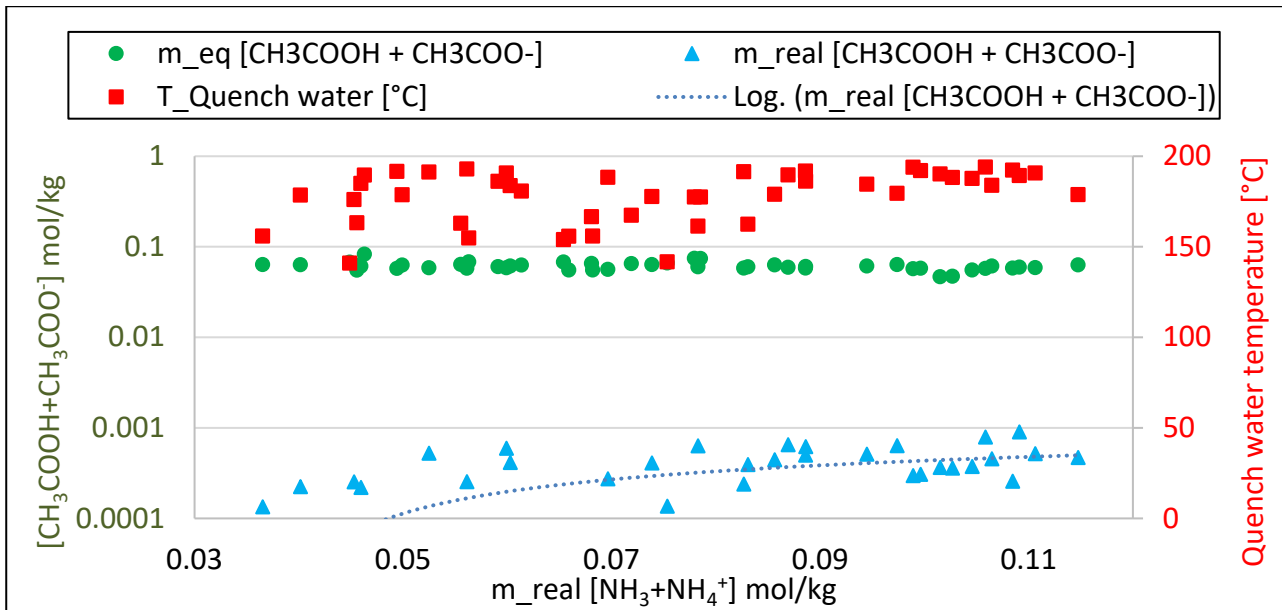
Figure 5.3: Aspen plus back-calculated (real) acetic acid concentration, quench water temperature and the calculated equilibrium acetic acid concentration against back-calculated (real) ammonia concentration for the 47 test points.

There is a correlation between the between the increase of the real acetic acid concentration and the increase in the concentration of ammonia in the quench water (see Appendix: Table 9.4; positive moderate correlation r = +0.60).
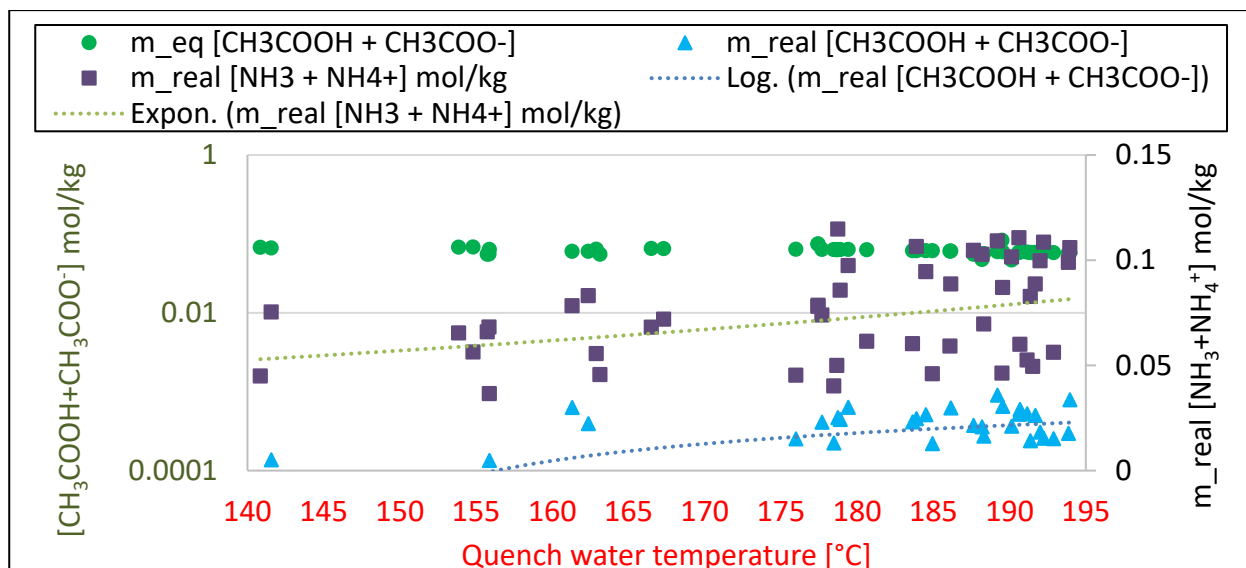
Figure 5.4: Aspen plus back-calculated (real) acetic acid concentration, back-calculated (real) ammonia concentration and the calculated equilibrium acetic acid concentration against quench water temperature for the 47 test points.

In Fig. 5.4, there is positive weak correlation between the increase of real acetic acid concentration and increasing temperature of quench water (see Appendix: Table 9.4; r = +0.49).

The acid-base correlation between equilibrium acetic acid concentration, ammonia concentration and temprature are negative weak correlation on like that of the formic acid, which are negative weak or strong correlations as in Fig. 5.2 (see Appendix: Table 9.4). Although, ammonia concentration increases as quench water temperature increases (see Appendix: Table 9.4 and Section 4.3.2).

There are measured concentrations of total formic acid and total ammonia in quench water systems but hot inlet gases from two different feedstocks in [Brüggemann, 2010], which can be compared with Fig. 5.2 in this chapter.

5.2 Formic acid

Several reaction mechanisms leading to the formation of formic acid in high temperature water had been proposed in the literature [Pitchai et al., 1986] with free radicals playing important role in oxidation of methane. CO is known as a precursor for the formation of formic acid [Gräbner, 2015]. During the process of reducing evaporator scaling when recovery liquids and solids from effluent

discharge in partial oxidation gasification, [Webster et al., 2000] reports that the CO present in the product synthesis gas reacts with water under high temperature and high pressure condition in the scrubber to form formic acid based on reaction (4.8).

In the production of hydrogen, formic acid can be used as a raw material due to it readily soluble behaviour in water especially at high temperature, where the decarboxylation pathway strongly predominates [Lu et al., 2011]. The formation of formic acid begins with the dissolution of CO gas present in the hot gas in the quench according to the summarized reaction (4.8).

Decarboxylation and dehydration are pathways for the decomposition of formic acid in the temperature range from 175 °C to 260°C [McCollom et al., 2003] based on reaction (5.2) and (5.3) respectively.

$$HCOOH_{(aq)} \rightleftharpoons CO_{2\,(aq)} + H_2 \qquad (5.2)$$

$$HCOOH_{(aq)} \rightleftharpoons CO_{(aq)} + H_2O \qquad (5.3)$$

Studies on aqueous-phase oxidation of formic acid and formate by [Bjerre et al., 1992] indicated that when there is dissolution of formic acid in water, decarboxylation is strongly dominant [Yu et al., 1998]. The dehydration is dominated in the gas phase [Akiya et al., 1998] and [Maiella et al., 1998]. The conjugate base of fomic acid is formate. Both are known to be the simplest form of organic acid and acid anions. Formate is formed by any of the reduction of molecularly dissolved HCO_3^- or CO_2 or hydration of CO or by the acid–base reaction of formic acid and ammonia [McCollom et al., 2003].

$$HCOO^-_{(aq)} + H_2O \rightleftharpoons HCO_3^- + + H_2 \qquad (5.4)$$

$$HCOO^-_{(aq)} + H^+ \rightleftharpoons CO_{2\,(aq)} + H_2 \qquad (5.5)$$

$$HCOO^-_{(aq)} + H^+ \rightleftharpoons CO_{(aq)} + H_2O \qquad (5.6)$$

$$HCOO^-_{(aq)} + NH_4^+_{(aq)} \rightleftharpoons HCOOH_{(aq)} + NH_{3\,(aq)} \tag{5.7}$$
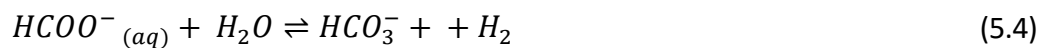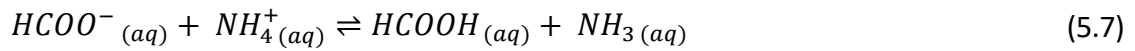
Although, most of the reaction discussed above occurs within similar temperature range of the HP POX quench water but they are enhanced by the presence of specific catalysts over a long period of time (800 hours) [McCollom et al., 2003]. In geologic environments, the longer period of time suggest that the system attained equilibrium between CO_2, H_2 and formate at a temperature of about 260 °C [McCollom et al., 2003].

The HP POX quench water residence time after quenching the hot gas in the quench chamber last for 5 minutes and there is no catalyst involvement but there are possibilities to have the metallic wall or surface of the quench chamber acting as catalyst.

5.2.1 Trace of formic acid in quench water

Fig 5.5 present the calculated concentration of the equilibrium and real formation of formic acid present in the quench water for the 47 test point and quench water temperature. Lesser amount of the formic acid is formed in the back calculated real concentration in comparison to the equilibrium calculation.
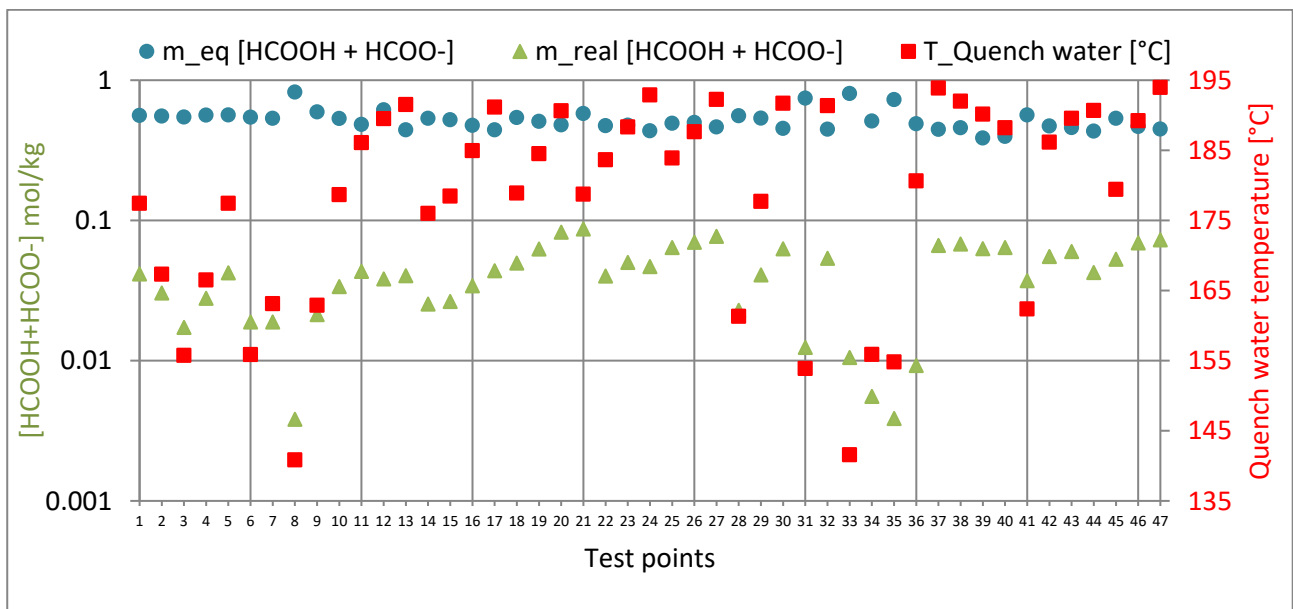
Figure 5.5: Concentration of formic acid (Aspen plus calculated m_eq and back-calculted m_real) formation in the quench and quench water temperature for the 47 test points.

Figure 5.6 illustrates the formic acid concentration in the quench as a function of quench water temperature. The real formic acid formation increases slowly as quench water temperature increases (r = +0.79). On the other hand, the calculated equilibrium formation of formic acid sharply decreases with the increase in the quench water temperature (r = -0.83).
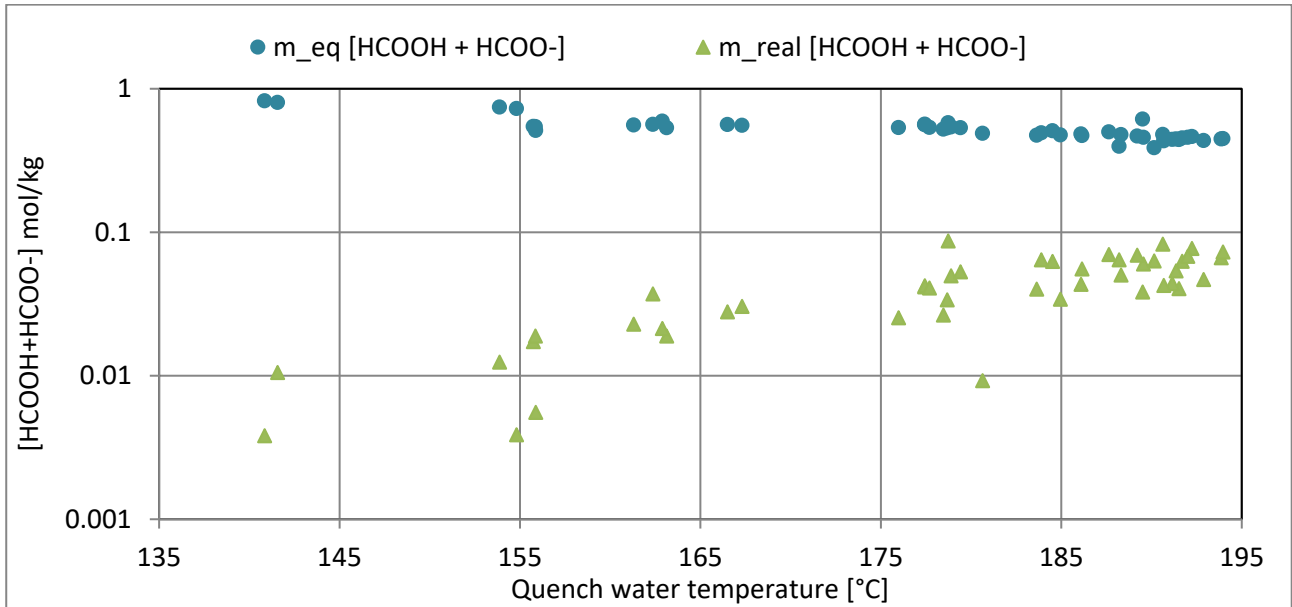
Figure 5.6: Concentration of formic acid (Aspen plus calculated m_eq and back-calculted m_real) in the quench against quench water temperature for the 47 test points (as in Fig.5.2).

The formation of formic acid is kinetically limited in the temperature range of the quench water system. It is possible for the real formation of formic acid to attain equilibrium if there is a further temperature increase beyond 195 °C. This fact could be inferred from the hydrothermal experiments conducted by [McCollom et al., 2003] to investigate organic acid formation in aqueous geologic fluids, which play significant role in a variety of geochemical processes.
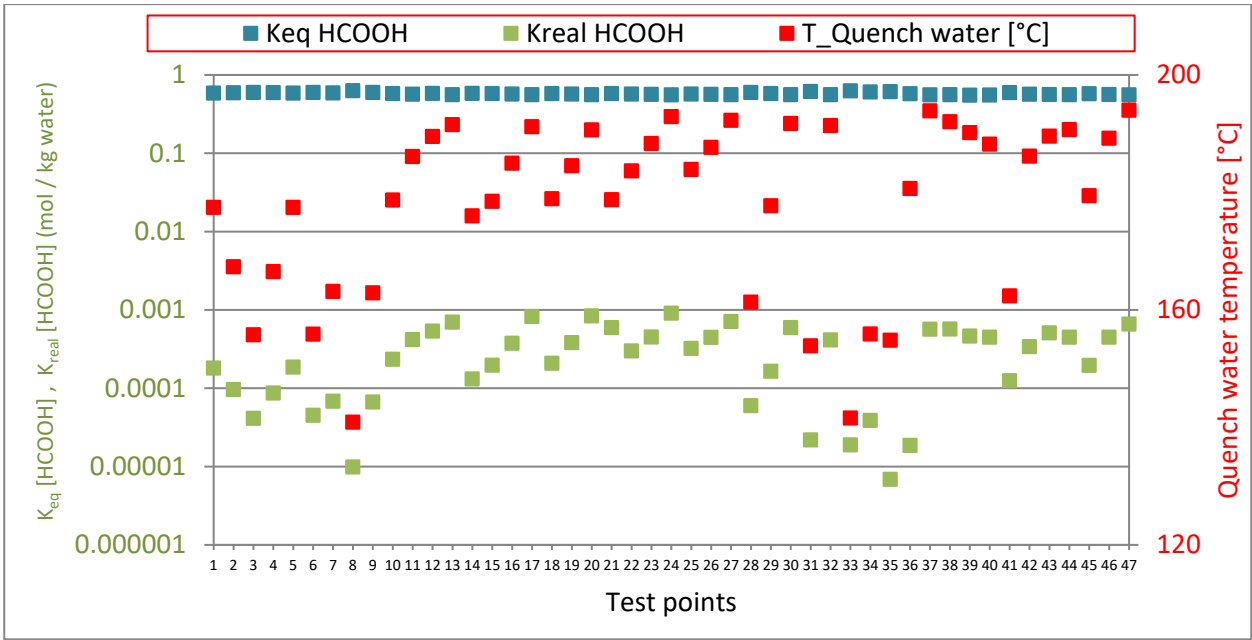
Figure 5.7: Comparison between formic acid equilibrium constant (Keq), reaction quotient (Kreal) and the quench water temperature for the 47 test points.

From equation (4.8) at equilibrium and neglecting the activity coefficients and setting activity of water to 1 (a_{H_2O} = 1):

$$K_{eq} = \left[\frac{[HCOOH]}{[CO]}\right]_{eq} \tag{5.8}$$

For the back calculated real formation of formic acid (real or reaction quotient)

$$K_{real} = \left[\frac{[HCOOH]}{[CO]}\right]_{real} \tag{5.9}$$

Figure 5.7 shows the K_{eq} and K_{real} values for formic acid for each test point and the quench water temperatures.
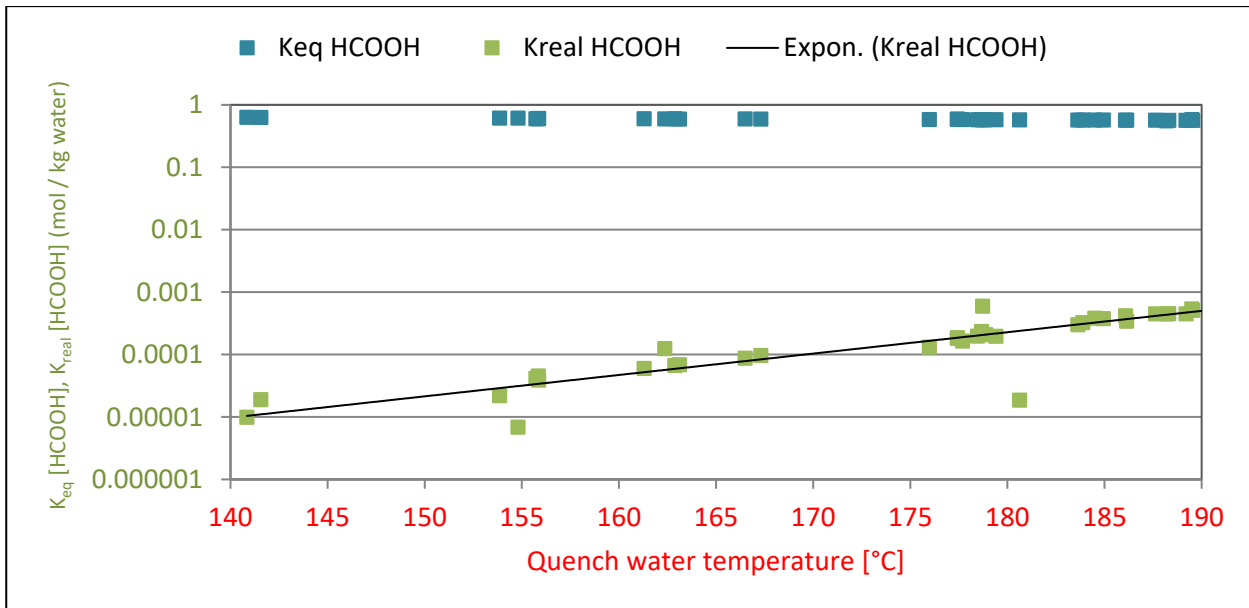
Figure 5.8: Comparison between formic acid equilibrium constant (Keq) and reaction quotient (Kreal) against quench water temperatures for the 47 test points.

It can be observed from Fig. 5.8 that the equilibrium constants inferred from Aspen Plus calculations remain the same throughout the increase in quench water temperature (r = -0.97). While the reaction quotients increases steadily as temperature increases (r = +0.83). This indicates the formation of more formic acid as temperature increases from 140°C to 190 °C.

5.3 Acetic acid

Acetic acid is a weak acid, which can dissociate and form ions [Park et al., 2006]. Reports on its dissociation mechanism and how it enhances the corrosion rate of mild steel at metal surface of industrial plant facilities by accelerating the cathodic reaction was previously discussed by [Tran et al., 2014]. Due to its presence in industrial cooling water, acetic acid changes the pH, BOD and COD of the water. Experimental studies to remove acetic acid from industrial waste water by means of sorption was proposed by [Dar et al., 2013] and by means of catalytic distillation [Xu et al., 1999] shows the high efforts required in the removal of dilute acetic acid from water. Several adsorption experiments for the removal of acetic acid were reported by [Zhang et al., 2016] and [Özcan et al., 2013] as alternatives to the problem encountered in the process to extract acetic acid from aqueous solutions of water. This is due to the close boiling point of two compounds (water and acetic acid)

and research in this field has gained significant importance over the past decades. In the petrochemical and fine chemical industries, the recovery of dilute acetic acid from aqueous stream has been one of the major challenges as conventional distillation [Lei et al., 2004] system remains uneconomical for it recovery [Gangadwala et al., 2008]. A theoretical study for removal of acetic acid from waste water via reactive distillation process was proposed earlier by [Gangadwala et al., 2007]. The outcome show the complexity required to maintain steady state and better improvement than the azeotropic distillation model. The formation of acetic acid in the quench water is represented in reaction (4.9) and (4.10). The CO_2 from the hot gas undergoes hydrogenation in liquid phase to form acetic acid.

Other methods leading to the formation of acetic acid in aqueous phase from the reactions involving any of CH_4, CO_2, H_2 and catalyst are widely reported in [Wu et al., 2013], [Li et al., 2002], [Wang et al., 2004], [Wieringa et al., 1939] and [Iglesia et al., 2001].

The thermal decarboxylation of aqueous solutions of acetic acid is expected to occur in contact with various surfaces of catalyst between 335 °C and 355 °C [Bell et al., 1994] based on reactions (5.10) and (5.11) to form bicarbonate.

$$CH_3COOH_{(aq)} \rightleftharpoons CH_4 + CO_2 \tag{5.10}$$

$$CH_3COO^-_{(aq)} + H_2O \rightleftharpoons CH_4 + HCO_3^- \tag{5.11}$$
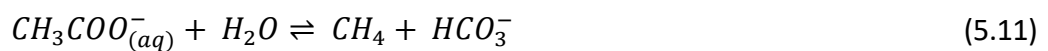
Also experiments from [Bell et al., 1994] informed that some significant fraction of acetic acid decomposition may occur through oxidation based on reaction (5.12).

$$CH_3COOH + 2O_2 \rightarrow 2CO_2 + 2H_2O \tag{5.12}$$

[Zhang et al., 2017] investigated a complete reaction of acetic acid steam reforming for hydrogen production based on catalytic activity (Ni and Co) with CH_3COCH_3, CH_4 and CO as the main by-products as represented in the following reactions [Basagiannis et al., 2007] occurring at higher temperatures above 850 °C:

$$CH_3COOH + 2H_2O \rightarrow 2CO_2 + 4H_2 \tag{5.13}$$

$$2CH_3COOH \rightarrow CH_3COCH_3 + H_2O + CO_2 \tag{5.14}$$

$$CH_3COOH \rightarrow CH_4 + CO_2 \tag{5.15}$$

$$CH_3COOH \rightarrow 2H_2 + 2CO \tag{5.16}$$
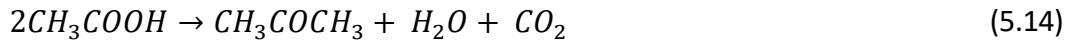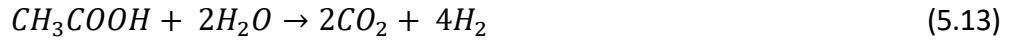
Reaction (5.13) was suggested to be one of the decomposition reactions of acetic acid [McCollom et al., 2003]. Other formation and decomposition of acetic acid were proposed by [Bennett et al., 2007] as acetic acid is categorized amongst astrobiologically important molecules. Reaction (5.16) occurs with the influence of La_2O_3 and Al_2O_3 materials acting as catalyst [Basagiannis et al., 2007].

5.3.1 Trace of acetic acid in quench water

Fig 5.9 present the calculated concentration of the equilibrium and the concentration of the calculated real acetic acid present in the quench water for the 47 test point and quench water temperature.
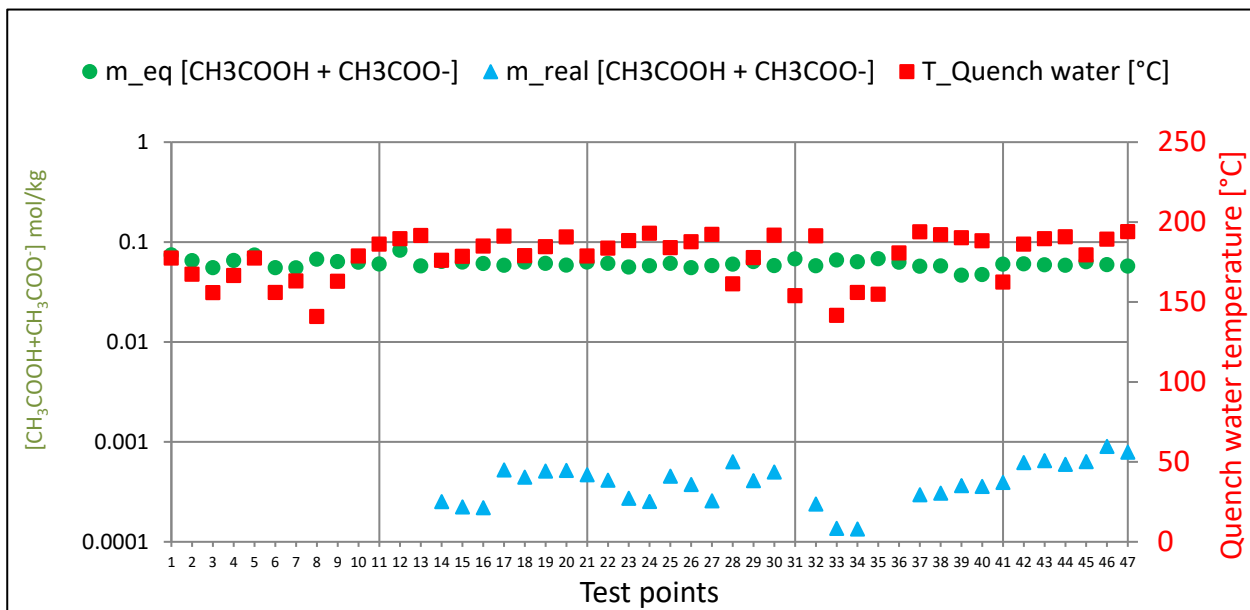
Figure 5.9: Concentration of acetic acid (Aspen plus calculated m_eq and back-calculted m_real) in the quench and quench water temperature for the 47 test points.

It could be observed in Fig. 5.9 that lesser amount of the acetic acid concentration is formed in the calculated real values in comparison to the equilibrium values.
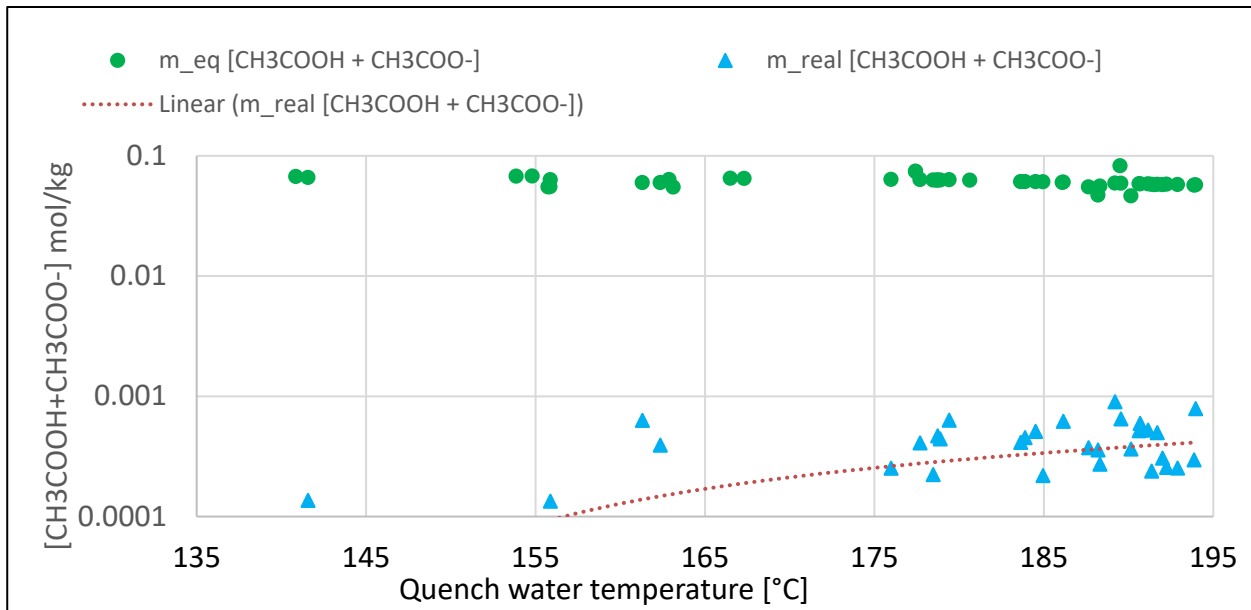
Figure 5.10: Concentration of acetic acid (Aspen plus calculated m_eq and back-calculted m_real) in the quench against quench water temperature for the 47 test points (as in Fig.5.4).

Figure 5.10 illustrates the concentration of acetic acid in the quench. The real acetic acid formation increases slowly as quench water temperature increases (r = +0.49). On the other hand, the calculated equilibrium formation of acetic acid decreases with the increase in the quench water temperature (r = -0.30).

In this, the formation of acetic acid is limited by the temperature of the quench water. There is a weak approach between the calculated real and equilibrium concentration of acetic acid with increasing quench water temperature. Reaction (4.9) represents the formation of acetic acid in the quench water as implemented in Aspen Plus.
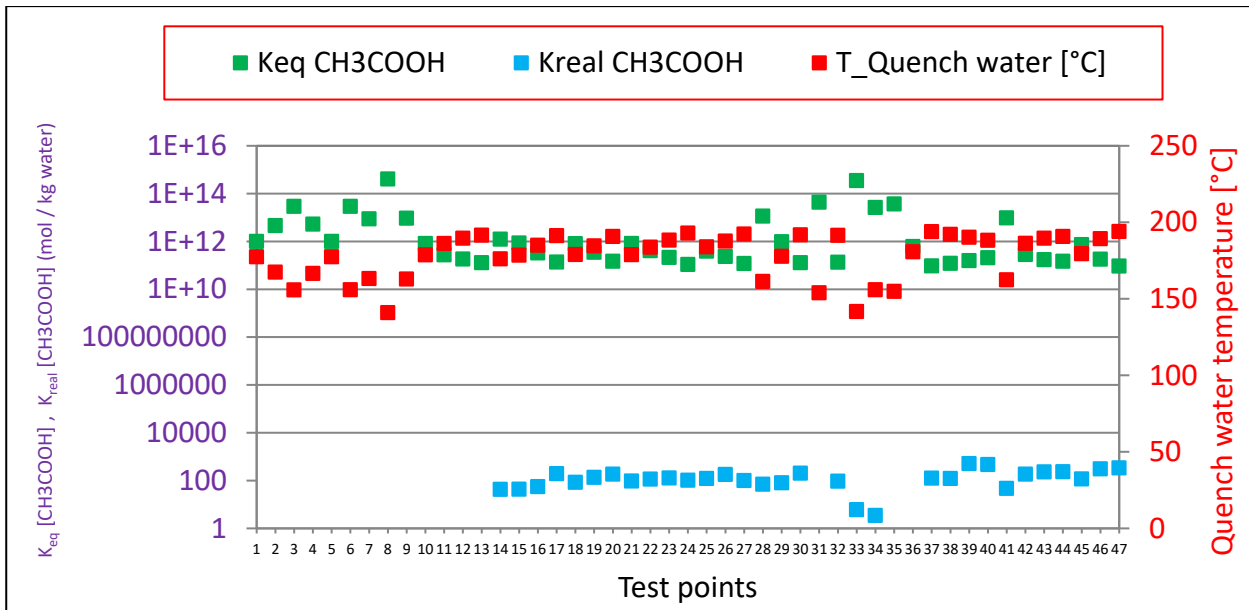
Figure 5.11: Comparison between acetic acid equilibrium constant (Keq), reaction quotient (Kreal) and the quench water temperature for the 47 test points.

From equation (4.9) at equilibrium:

$$K_{eq} = \left[\frac{[CH_3COOH]}{[H_2]^4\,[CO_2]^2}\right]_{eq} \tag{5.17}$$

For the formation of acetic acid not at equilibrium (real or reaction quotient)

$$K_{real} = \left[\frac{[CH_3COOH]}{[H_2]^4\,[CO_2]^2}\right]_{real} \tag{5.18}$$

Figure 5.11 indicates K_{eq} and K_{real} for acetic acid for each test point and their quench water temperature. There is temperature dependency observed for the K_{eq} as the equilibrium constants increase as quench water temperature reduces in the range between 140 °C to 190 °C (Fig.5.12).

It can be observed from Fig. 5.12 that the equilibrium constant inferred from Aspen Plus simulation decreases gradually as the increase in quench water temperature increases (r = -0.62). While the reaction quotient tends to increase steadily as temperature increase (r = +0.56). This indicates the formation of more acetic acid in the non-equilibrium calculation as temperature increases from 140°C to 190 °C (see Appendix: Table 9.4).

71
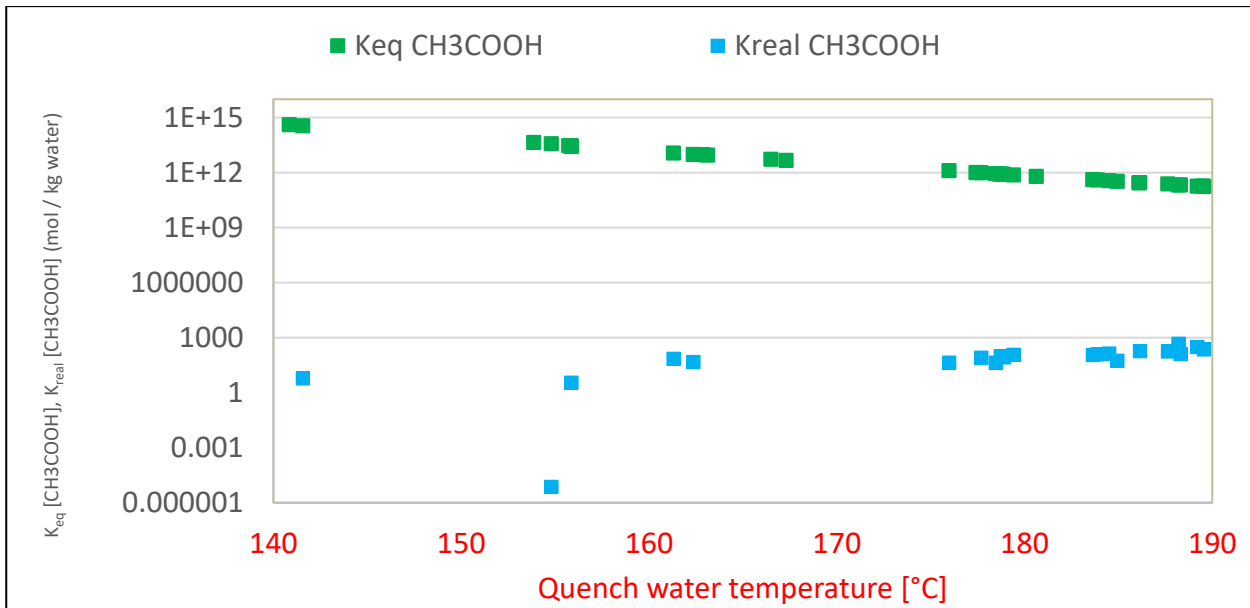
Figure 5.12: Comparison between acetic acid equilibrium constant (Keq) and reaction quotient (Kreal) against quench water temperatures for the 47 test points.

5.4   Summary

The formation of organic acids in the quench water during the hot gas quenching was discussed based on results obtained from Aspen Plus. Meanwhile, there are no published works on formic acid and acetic acid formation in non-catalytic partial oxidation of natural gas and the product synthesis gas quench operations. These organic acids formation are widely reported in many hydrothermal process conditions in aqueous geological fluid specifically in the geochemical processes and in the presence of minerals or metals (acting as catalyst) [McCollom et al., 2003].

Sequel to the literature studies, there are possible reactions that may occur leading to the formation of these trace compounds after quench operation especially after the end of each test campaign or plant shutdown. This period provide the longer residence time for the formation to take place. The presence of phenolic compounds in the quench water need to be investigated as their reactions are pathways to the formation of both formic acid and acetic acid as reported by [Man et al., 2011].

Acid-base interaction between acid compounds and basic compounds present in the quench water must be further looked into as the salt produced from these reactions can cause damage to the plant facility as well as other possible corrosion effects for other system than the investigated quench water

system. The salt formation is not to be expected in the HP POX quench where the ionic species are diluted.

The interaction between traces of organic and inorganic compounds present in the quench water must be further investigated, as there is buffering benefit that could be derived from the trace amount of organic acid to regulate the pH of the quench water against basic compounds (neutralization).

6 Temperature approach studies for NH₃ and HCN formation in gasifier

The focus of this chapter is to discuss conversion of fuel-nitrogen into nitrogen compounds in the gasifier during gasification based on the results from the Aspen Plus simulation (see Appendix Fig. 9.8: Aspen Plus flow sheet setup for nitrogen compounds calculations and Table 9.12). There are two possible ways nitrogen enter into the gasifier during the test campaign. Nitrogen stream is used to keep the optical probe clear, which is applied to visualize the flame during plant operations. Also, nitrogen is supplied into the gasifier as a component in natural gas feedstock input (see Table 2.3). N_2 is partially converted into NH_3 and HCN. These two compounds constitute important consideration for the downstream utilisation of the syngas.

6.1 Nitrogen compounds: NH₃ and HCN

In several gasification processes, bound nitrogen in the complex structure of different fuels is liberated and reacts. The consequence of these different homogeneous and heterogeneous reactions led to the formation of these nitrogen compounds [Leppälahti et al., 1995]. In terms of natural gas, there are no chemically bound fuel nitrogen present [Higman et al., 2003] when compared with coal, biomass or sewage sludge. It is generally assumed that bound nitrogen in aromatic rings is released as HCN and the nitrogen from amines appears as NH_3 [Gräbner, 2015]. There is a dearth of data and published works on autothermal gasification of natural gas relating to the conversion of the fuel-nitrogen during gasification. But there are many facts that have been published about nitrogen compounds formation for other gasification feedstock especially fuels like coal [Chang et al., 2006], biomass [Simell et al., 1996], [Hansson et al., 2004], heavy residue [Abdul R. et al., 2004], with recent findings about sewage sludge [Schweitzer et al., 2017], [Liu et al., 2017], [Ma et al., 2017] and [Thomsen et al., 2017]. Nitrogenated aromatic compounds present in sewage sludge has been linked to the formation of PAHs and nitrogenated PAHs by [Fullana et al., 2003] and [Cao et al., 2010].

Nitrogen is sometime used in some gasification process to moderate the temperature by adding it to the oxygen [Higman et al., 2003]. Irrespective of the gasification process, there are studies that has proved that all fuels produced more NH_3 than HCN [Leppälahti et al., 1995] under all the conditions, whereas less HCN [Cao et al., 2013] and [Xu et al., 2012] is produced. Although, this fact varies with respect to the fuel`s characteristics and composition. In the work of [Hämäläinen et al., 1996] during

pyrolysis and gasification of coal, between the two nitrogen compounds produced, HCN is liberated as a major product with high concentration of NH_3 measured, which was believed to be formed from HCN during devolatilization reaction [Hämäläinen et al., 1996]. The major identified factor responsible for the formation of coal-nitrogen components in the gas phase and within the solid particles was the presence of H radicals when coal particles are heated in a fluidized-bed / fixed-bed reactor, which was reported in an experiment by [Chang et al., 2006]. It is observed that N radicals from char-nitrogen and the H radicals from H_2O and the rupture of the nitrogen containing heteroaromatic ring systems contribute to the formation of NH_3 and HCN [Chang et al., 2006].

In non-catalytic autothermal reforming of natural gas, the formation of these nitrogen compounds is as a result of the thermal HCN and NH_3 formation, which is reported to be a function of the actual temperatures in the flame zone and burner performance in the gasifier [Higman et al., 2003]. When the hot gas is quenched, some traces of ammonia and hydrogen cyanide remains in the quench water effluent as ammonia has a very high solubility in water. Trace of ammonia in the syngas is highly undesirable as it can lead to the formation of amines on catalyst during methanol synthesis. Trace of HCN is know to be one of the catalyst posion in Fisher-Tropsch process. In general, there is a lot of capital and operating cost [Hongrapipat et al., 2014] for gas cleaning and removal that are associated with the presence of these nitrogen compounds in the treatment of raw gas or syngas before further utilization.

Futhermore, several experimental results show that the mechanism and formation of NOx (nitrogen oxides) precursors during the pyrolysis of coal gave better understanding about the formation of NH_3 and HCN [Kambara et al., 1993], [Hämäläinen et al., 1994], [Chang et al., 2003] and [Liu et al., 2017]. Although, care must be taken as nitrogen oxides are know to form resin with unsaturated hydrocarbons in the gas phase especially in the liquid nitrogen wash of ammonia plant [Higman et al., 2003]. These formed resins are prone to extreme unplanned explosions [Slack et al., 1973]. But in the process where there is raw gas shift are applied; NOx (nitrogen oxides) and the unsaturated hydrocarbons are hydrogenated on the catalyst [Higman et al., 2003].

Also, [Cataldo et al., 2009] investigated the thermal decomposition of formamide in gas phase to produce HCN polymer and further prolong heating at 185°C or 220°C formed an insoluble black product while the gaseous product released during the decomposition of formamide were CO_2, CO and NH_3 (see Appendix: comment on formamide).
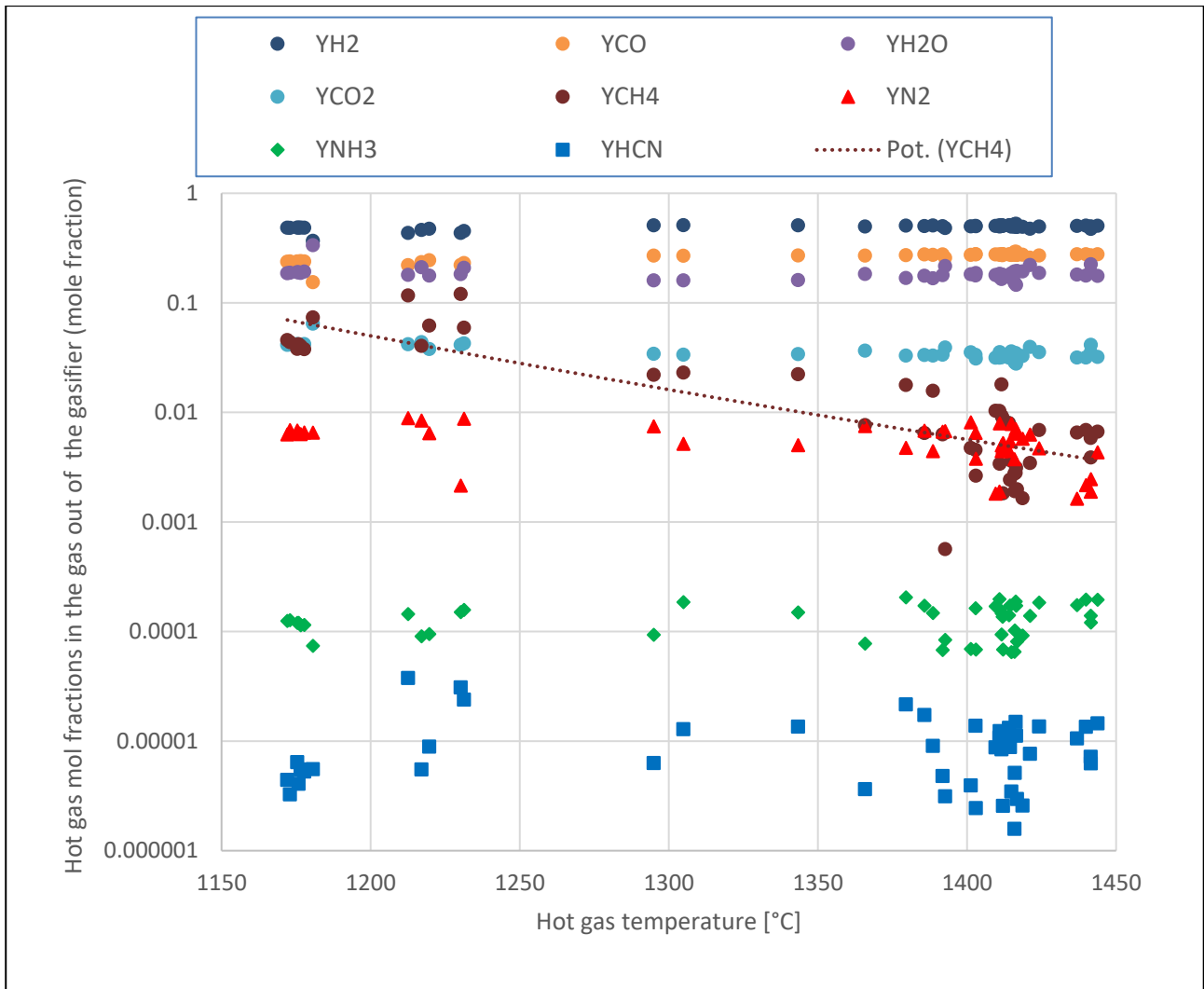
Figure 6.1: Mole fraction of gas compoents in the hot gas outlet out of gasifier against hot gas temperature for the 47 test points

Figure 6.1 present the gas component mole fractions of the gasifier outlet gas (hot gas) against the hot gas temperatures from 1150 °C to 1450 °C for all the 47 test point. It could be observed that mole fraction of hydrogen (Y_{H_2}) range from 0.44 to 0.49, which make it the most dominant of all the product synthesis gases. After hydrogen, the next is carbon monoxide (CO) with the mole fraction from (Y_{CO}) range from 0.19 to 0.22. Next to CO is water (steam), as the yield of gases in the gasifier is refered to as wet gas, the Y_{H_2O} range from 0.33 to 0.22. The mole fraction of CH$_4$ follows a sharp decrement from 0.11 to 0.0006. This strong drecrease in CH$_4$ is due to its increasing consumption leading to the formation of H$_2$, CO, H$_2$O and CO$_2$ based on the reactions in Section 2.2.3.

Furthermore, the mole fraction of nitrogen (Y_{N_2}) range from 0.001 to 0.009. N_2 is partly conversed into NH_3 and HCN. Y_{NH_3} is 20 times lesser than Y_{N_2} while Y_{HCN} is over 600 times lesser than Y_{N_2}. This confirms the formation of more NH_3 than HCN as the nitrogen compounds.

6.2   Ammonia (NH₃) formation in the gasifer

Figure 6.2 presents, the calcuated reaction quotient of NH_3 formation (real or non-equilibrium) from the gasifier as one of the component of the hot gas and the hot gas temperature for all the 47 test point under consideration, as well as the equilibrium constant of the NH_3-formation. Based on equation (6.1), some part of N_2 in the gasifier reacts with hydrogen and convert into NH_3.

$$\frac{1}{2} N_2 + \frac{3}{2} H_2 \rightleftharpoons NH_3 \qquad (6.1)$$

From equation (6.1), the forward reaction is exothermic and the backward reaction in endothermic.
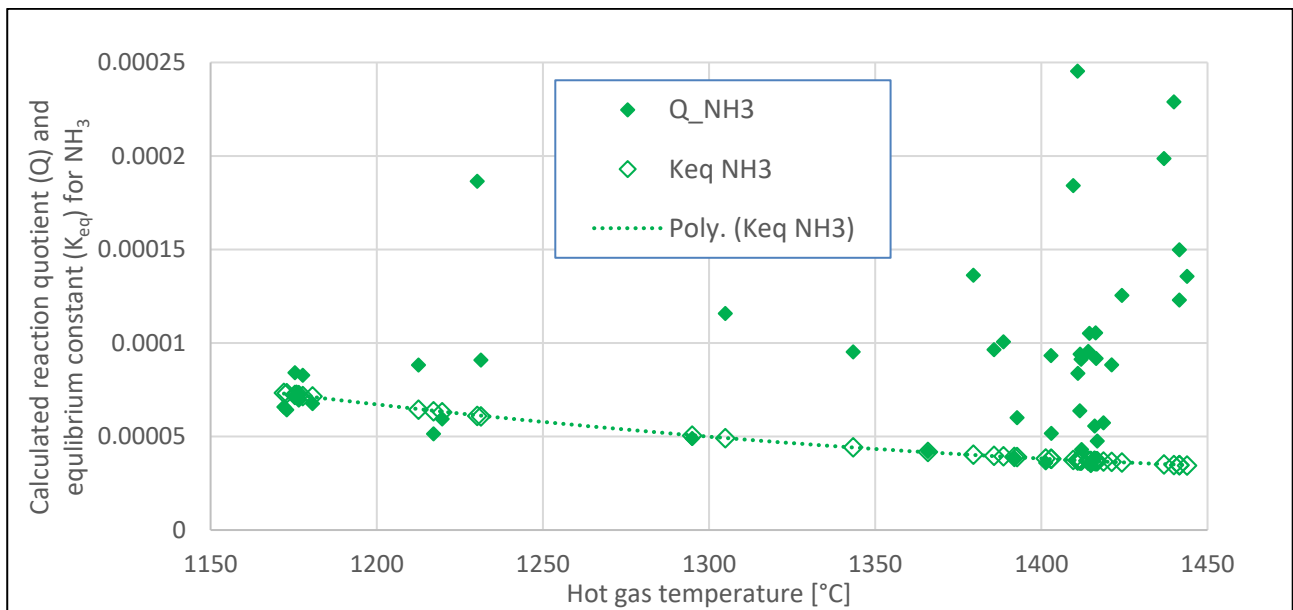
Figure 6.2: Calculated reaction quotient (Q) and equlibrium constant (K_{eq}) for NH_3 against hot gas temperature for the 47 test points (see Fig. 9.10 in Appendix)

Since the component under consideration are in the gas phase, the Q and the K_{eq} of NH_3 formation can be express in terms of partial pressure as in equations (6.2) and (6.3). From a general observation, it could be seen that the calculated equilibrium constant (K_{eq}) of NH_3 gradually decreases as the hot gas temperature increases (see line Poly. K_{eq} NH_3, a consequence of the exothermic forward reaction

of the considered equation (6.1)). The calculated reaction quotients are unexpectedly mostly larger than the equilibrium constants at the same respective hot gas temperature. This indicates that in most considered test points there is unexpectedly more NH_3 present than at equilibrium condition.

$$K_{eq} = \left[\frac{P_{N_2}^{1/2} \, P_{H_2}^{3/2}}{P_{NH_3}} \right]_{eq} \tag{6.2}$$

$$Q_{NH_3} = \left[\frac{P_{N_2}^{1/2} \, P_{H_2}^{3/2}}{P_{NH_3}} \right]_{real} \tag{6.3}$$
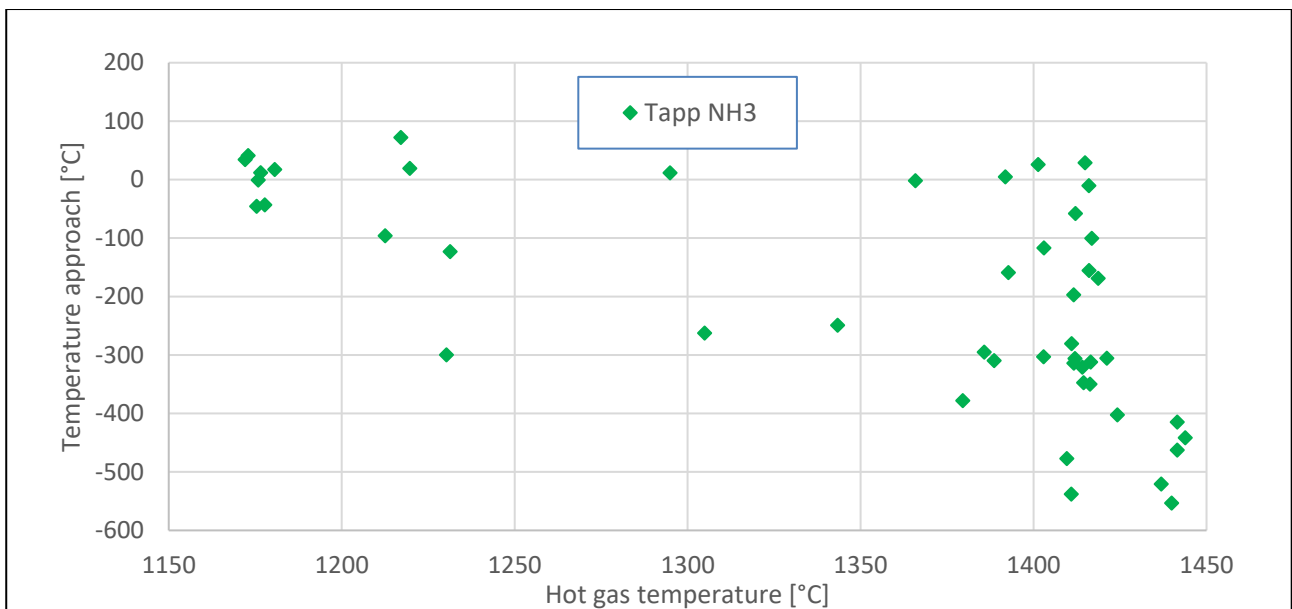
Figure 6.3: NH_3 temperature approach against hot gas temperature for the 47 test points (see Fig. 9.11 in Appendix)

Since the kinetic data for NH_3 formation are not available from the literatures, the temperature approach was used. The forward reaction (6.1) is exothermic and the backward reaction is endothermic. Hence, temperature approach (Tapp) less than zero according to Figure 6.3 correspends to larger calculated reaction quotients than the equilibrium constants at the respective hot gas temperature according to Figure 6.2. Mostly, all the test points have negative approaches with the exception of few test points, which includes: test points 1, 4, 5, 8, 9 and a few others.

6.3 Hydrogen cyanide (HCN) formation in the gasifier

Equation (6.4) present the reaction between carbon monoxide and ammonia leading to the formation of HCN. The Q and the K_{eq} of HCN formation (the reaction quotient and the equilibrium constant) can be expressed in terms of partial pressures as in equations (6.5) and (6.6). Figure 6.4 presents the calulcuated reaction quotients and the equilibrium constants of HCN from the gasifier.

$$CO + NH_3 \rightleftharpoons HCN + H_2O \qquad (6.4)$$
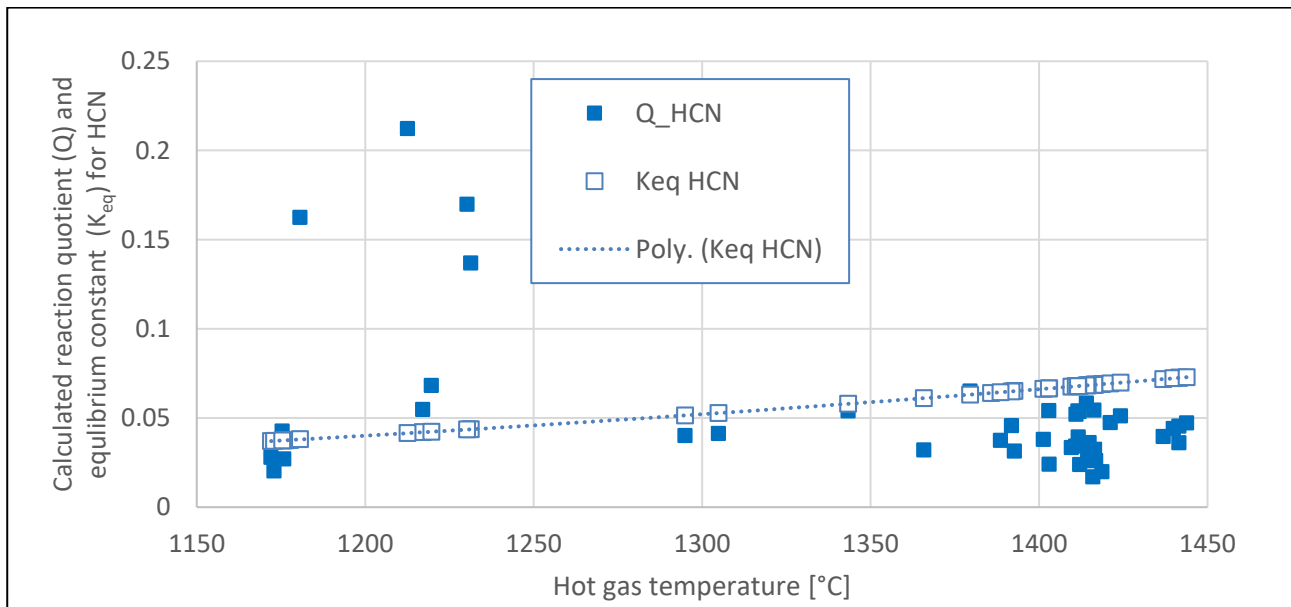
Figure 6.4: Calculated reaction quotient (Q) and equlibrium constant (K_{eq}) for HCN against hot gas temperature for the 47 test points (see Fig. 9.13 in Appendix)

$$K_{eq} = \left[\frac{P_{HCN} \, P_{H_2O}}{P_{CO} \, P_{NH_3}} \right]_{eq} \qquad (6.5)$$

$$Q_{HCN} = \left[\frac{P_{HCN} \, P_{H_2O}}{P_{CO} \, P_{NH_3}} \right]_{real} \qquad (6.6)$$
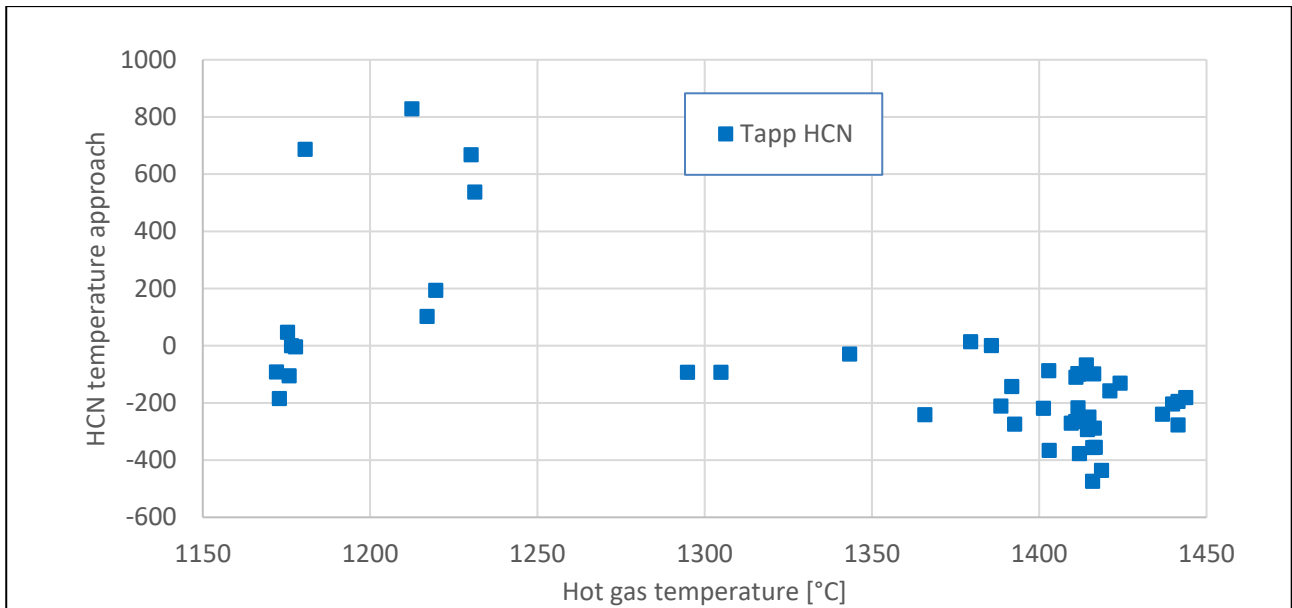
Figure 6.5: HCN temperature approach against hot gas temperature for the 47 test points (see Fig. 9.14 in Appendix)

From Figure 6.4, it could be seen that the calculated K_{eq} of HCN formation increase gradually with increaseing hot gas temperatures (a consequence of the endothermic forward reaction of equation (6.4)) and are mostly above the reaction quotient Q_{HCN} except for few test points between hot gas temperature ranging from 1176 °C and 1217 °C. This indicates that in most considered test points there is as expected less HCN present in the reaction quotient Q_{HCN} than at equilibrium condition. From equation (6.3), the forward reaction is endothermic and the backward reaction is exothermic. Similarly to Figure 6.3 (for Tapp NH_3), most of the test points have negative temperature approaches (Tapp HCN) in Figure 6.5 with the exception of a few test points between hot gas temperature ranging from 1176 °C and 1217 °C. But in case of HCN formation according to equation (6.4)these negative temperature approaches indicate that there is mostly less HCN present than at equilibrium condition, contrary to the NH_3-formation in Section 6.3 of this chapter, where the negative temperature approaches in Figure 6.3 for reaction (6.1) imply more NH_3 present than at the respective equilibrium conditions (see Figure 6.2). The reasons are the exothermic forward reaction of equation (6.1) and the resulting decrease of K_{eq} NH_3 with temperature in Figure 6.2, contrary to the endothermic forward reaction of equation (6.4) and the resulting increase of K_{eq} HCN with temperature in Figure 6.4. A consequence of the different K_{eq} inclinations are negative NH_3 temperature approaches in Figure 6.3 for Q NH_3 > K_{eq} NH_3 in Figure 6.2 and negative HCN temperature approaches in Figure 6.5 for Q HCN < K_{eq} HCN in Figure 6.4.

6.4 Discrepancies between back-calculated reaction quotients and equilibrium constants of the NH_3 formation

During the course of the investigation about the nitrogen compounds formation in the upstream part of the quench process (i.e. in the hot gas leaving the gasifier), the simulation work had found discrepancies between back-calculated reaction quotients and equilibrium constants of the NH_3 formation according to equation (6.1). The calculated reaction quotients of the NH_3 formation are unexpectedly mostly larger than the equilibrium constants at the same respective hot gas temperature (see Section 6.2). In the following Sections 6.4.1 and 6.4.2 the calculated equilibriums constants (see equations (6.2) and (6.5)) of the reactions according to equations (6.1) and (6.4) as displayed in Figures 6.2 and 6.4 are used to calculate imaginative hot gas equilibrium mole parts of the nitrogen components under different constraints:

1. The equilibrium constants according to equations (6.2) und (6.5) for reaction equations (6.1) and (6.4) are used to calculate the equilibrium distribution between N_2, NH_3 and HCN. As a constraint, the gasification reactions between the other hot gas components according to Section 2.2.3 do not succumb to an equilibrium approach. That means the calculated equilibrium distribution between N_2, NH_3 and HCN according reaction equation (6.1) and (6.4) leads only to a marginally calculated change in the hot gas H_2, CO, H_2O and also N_2 amount and the hot gas bulk component mol parts because of the low hot gas N_2, NH_3 and HCN mol parts (see. Fig. 6.1) and the low amount of conversion of N_2 into NH_3 (negligible change in N_2 amount respective mole fraction according to Fig. 6.6).

2. As a further constraint only the equilibrium constants according to equation (6.5) for reaction equation (6.4) are used to calculate the equilibrium distribution between NH_3 and HCN (i.e. without achieving equilibrium distribution between N_2 an NH_3 according to reaction equations (6.1)). In this case even the change between real and calculated equilibrium NH_3 mol amount and mol parts is marginally low because of the the low amount of conversion of NH_3 into HCN (compare Y_{NH3} in Figures 6.1 and 6.7, negligible change in NH_3 amount respective mole fraction).

6.4.1 Case 1: calculated equilibrium distribution between N_2, NH_3 and HCN

Presented in Figure 6.6 are the calculated equilibrium mole fractions and real mole fractions for N_2, NH_3 and HCN (equilibrium mole fractions according to equations (6.2) und (6.5)). The discrepancies

between back-calculated reaction quotients and equilibrium constants of the NH_3 formation according to equation (6.1), i.e. mostly Q NH_3 > K_{eq} NH_3 in Fig. 6.2, also render the discrepancies Y_{NH3} > $Y_{NH3, eq}$ for most test points (in Fig. 6.6). Unexpected relations Y_{HCN} > $Y_{HCN, eq}$ ($Y_{HCN, eq}$ resulting from concomitant and complementary calculated $Y_{NH3, eq}$ values) also occur for many test points for the HCN formation according to reaction equation (6.4).
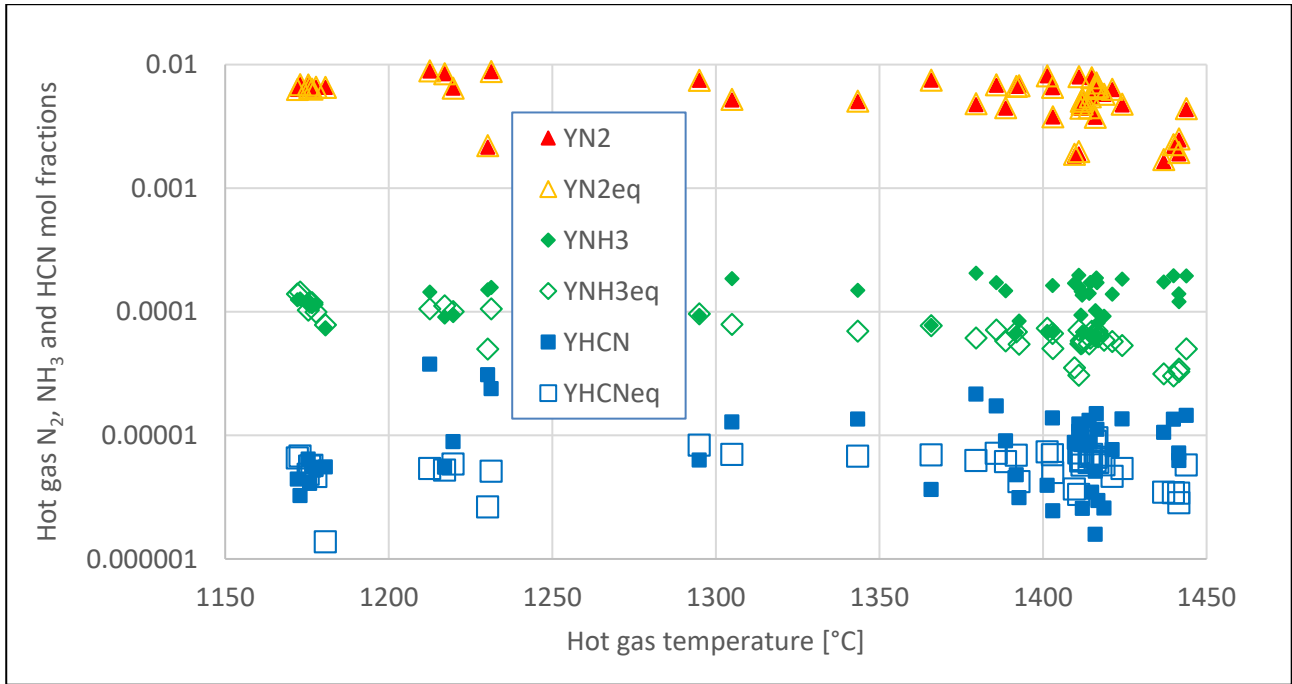
Figure 6.6: Comparison between calculated real and equilibrium hot gas N_2, NH_3 and HCN mol fractions against their respective hot gas temperature (case 1).
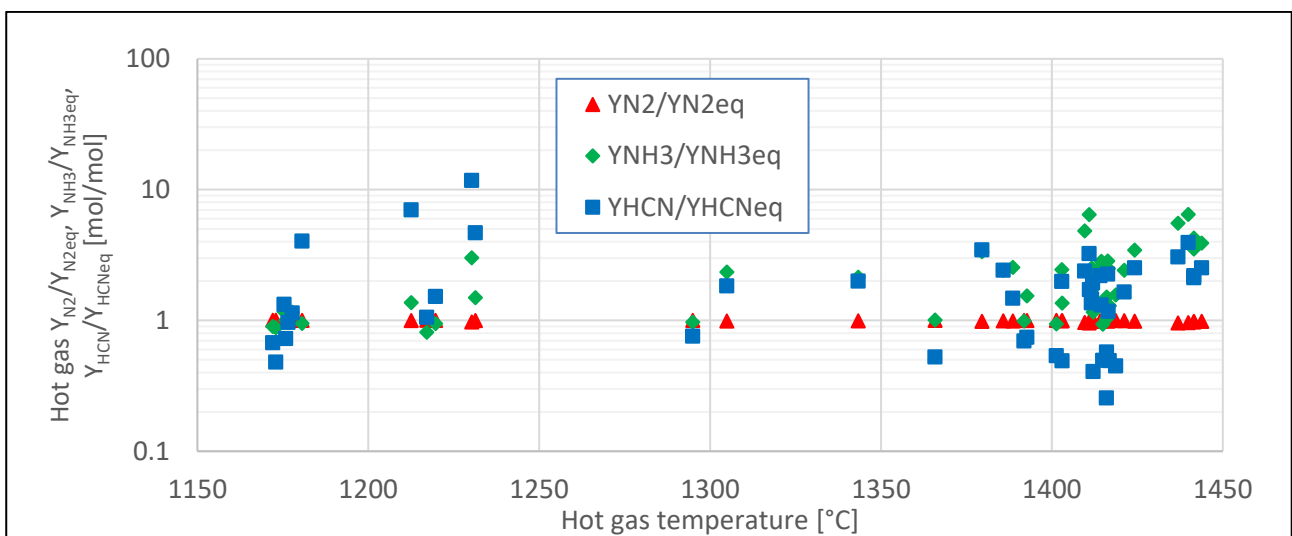
Figure 6.7: Relations between back-calculated real and equilibrium hot gas N_2, NH_3 and HCN mol fractions (for chemical equilibrium according to equations (6.1) and (6.4)) against their respective hot gas temperature (see Case 1, Section 6.4.1, and Fig. 6.6)

6.4.2 Case 2: calculated equilibrium distribution between NH₃ and HCN

Presented in Figure 6.8 are the calculated equilibrium mol fractions and real mol fractions for NH_3 and HCN (equilibrium mol fractions according to equation (6.5)) without achieving equilibrium distribution between N_2 an NH_3 according to reaction equations (6.1).

Relations $Y_{HCN} < Y_{HCN, eq}$ ($Y_{HCN, eq}$ resulting from assumed real Y_{NH3} values) occur for most test points for the HCN formation according to reaction equation (6.4). That means, if the Aspen Plus back-calculated hot gas NH_3 mol fraction Y_{NH3} really exceed $Y_{NH3, eq}$ (i.e. hot gas $Y_{NH3} > Y_{NH3, eq}$) than the expected relations $Y_{HCN} < Y_{HCN, eq}$ are mostly fulfilled. For an overview of each of the 47 test points see Fig. 9.9 and Fig. 9.12 in Appendix.
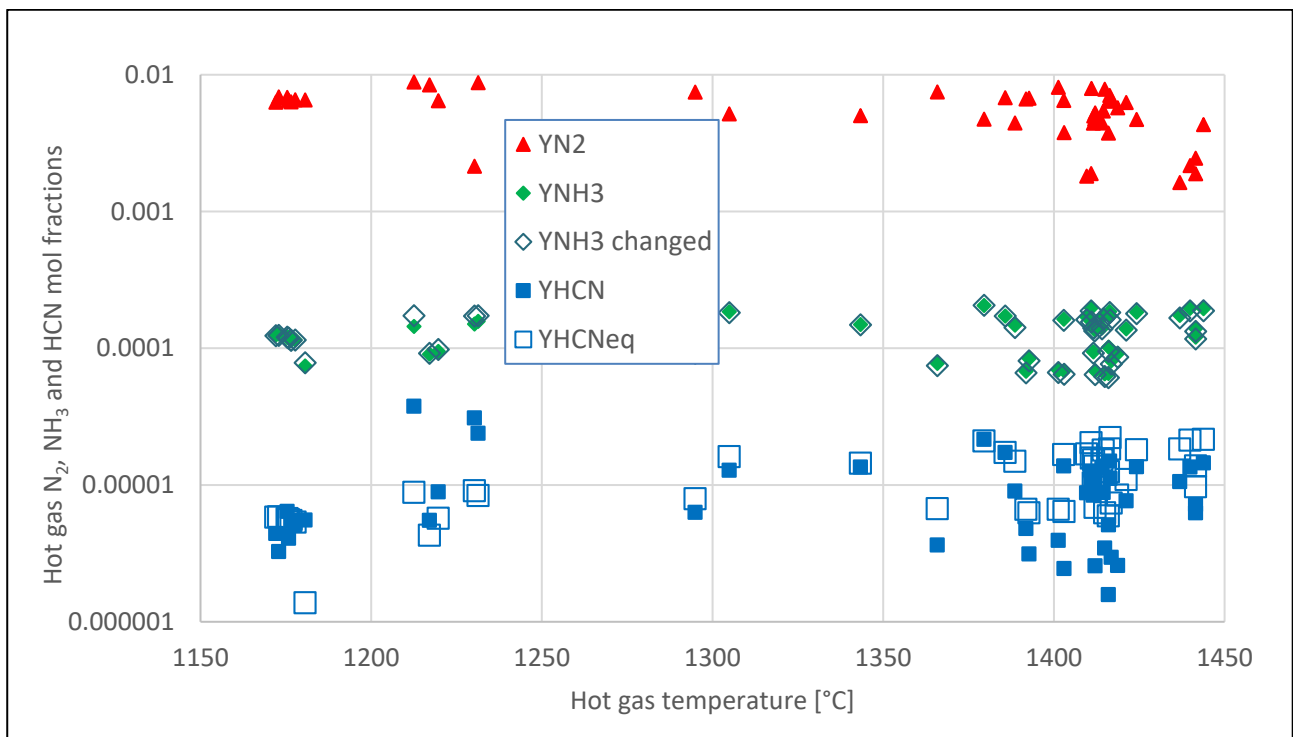
Figure 6.8: Comparison between calculated real and equilibrium hot gas HCN mol fraction against their respective hot gas temperature (case 2).
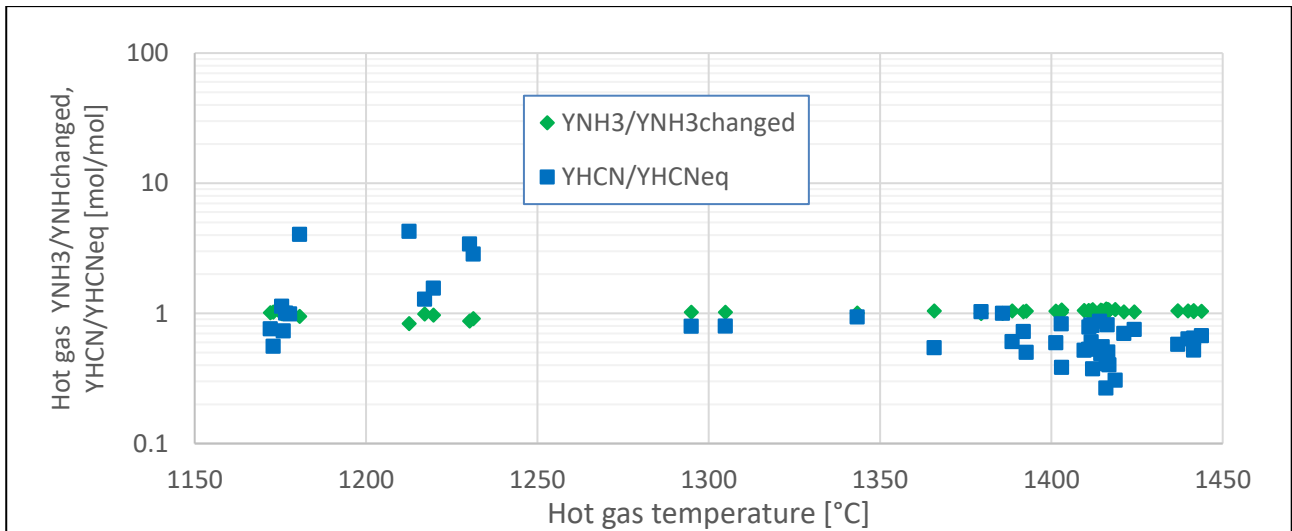
Figure 6.9: Relations between back-calculated real and equilibrium hot gas HCN mol fractions, and change in NH$_3$ mol fractions (for chemical equilibrium according to equation (6.4)), against their respective hot gas temperature (see. Case 2, Section 6.4.2 and Fig. 6.7)

6.5   Summary

Based on the findings in this chapter about the formation of more NH$_3$ and HCN in the reaction quotient than equilibrium condition, these are indications showing the formation of more NH$_3$ after the hot gas exit the gasifier. Consequently, NH$_3$ reaction with CO leads to the formation of HCN (equation (6.4)). The question in this situation is to ask where the unexpected increase in the formation of NH$_3$ comes from.

The NH$_3$ and HCN content in the hot gas outlet out of the upstream POX reactor were back-calculated via Aspen Plus Design Specifications using as constraint, the ammonium and cyanide content in the quench water samples from the quench water system (as explainend in Sections 2.5 and 2.5.1). This implies the possible hypothesis that this back-calculation not only encompasses the NH$_3$ content in the hot gas from the POX gasifier but also include a possible supplementary amount of NH$_3$ formation according to equation (6.1) in the gas phase of the quench chamber itself. NH$_3$ formation according to equation (6.1) is a moderately exothermic process (see Table 9.5, Fig. 9.15 and Fig. 9.16 in the appendix) which is favoured by temperature decrease according to Le Chatelier's principles. The possibility of another reaction, the moderately exothermic homogeneous water–gas shift reaction during water quench processes of hot gas outlets from gasifiers, was for example studied and presented in the literatures [Uebel et al., 2016a] and [Uebel et al., 2016b]. In analogy to this

mentioned water–gas shift reaction during water quench processes, it could be postulated by the hypothesis that the moderately exothermic homogeneous gas reaction of ammonia formation according to equation (6.1) also takes place in the water quench processes (at least in the first moment of these quench processes, as long as the concomitant temperature drop does not lead to too much deceleration of the reaction kinetics of the equation (6.1) reaction) and (see Section 4.3.2 and Section 4.3.3).

Figure 6.10 presents the gas concentration of nitrogen, ammonia, HCN and hot gas temperature against the 47 test points. In these are the comparsion between the reaction quotient and equilibrium constant of ammonia and HCN for case 1 and case 2 (see Section 6.4.1 and 6.4.2) for each test point with their respective hot gas temperature and nitrogen concentration.
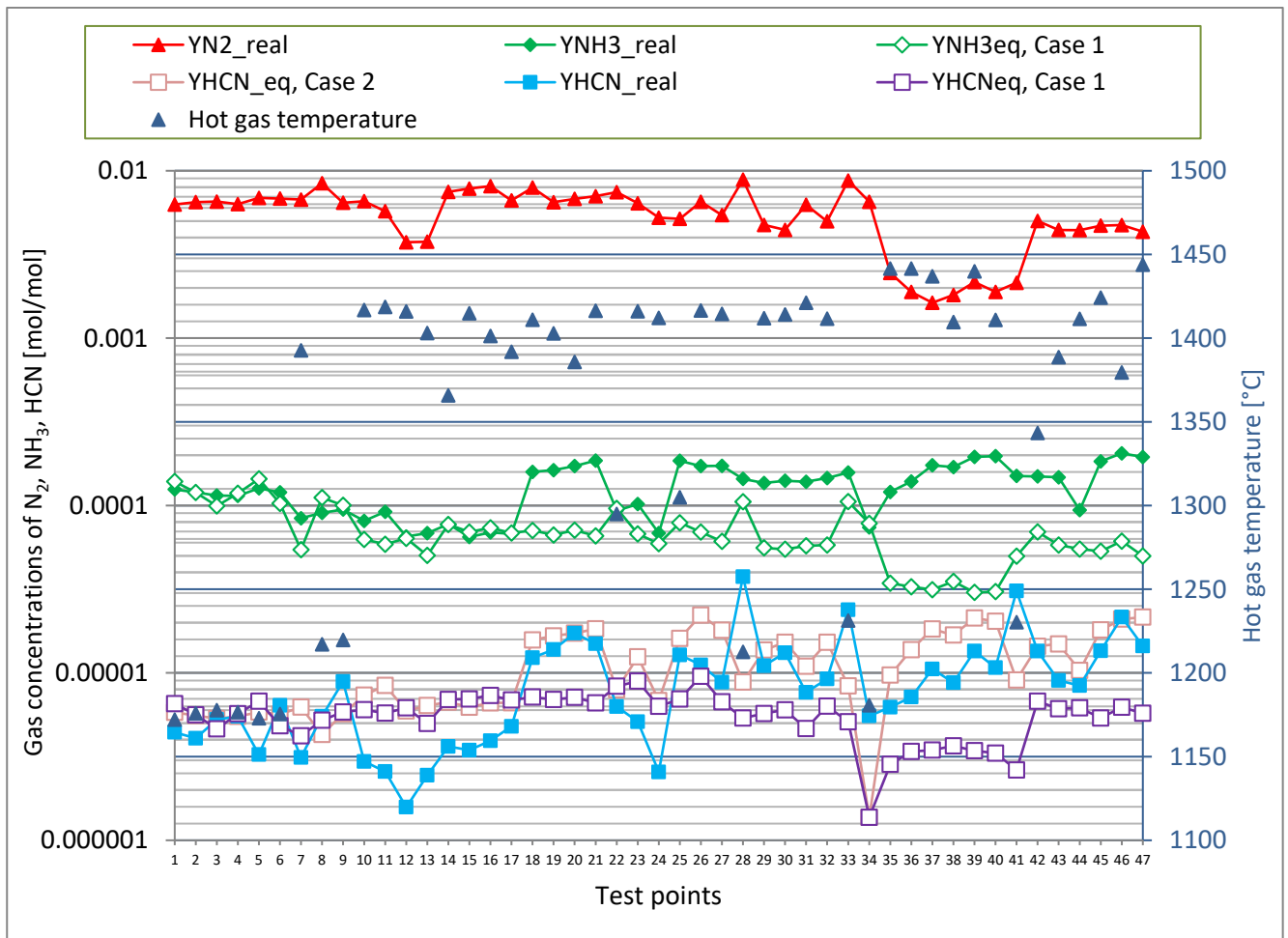
Figure 6.10 Comparison between NH_3 and HCN formation (mole fraction) calculated equilibrium constant (K_{eq}) and calculated reaction quotient (Q), N_2 consumption and hot gas temperatures for the 47 test points (case 1 and case 2).

7 Traces of BTEX, PAHs and soot in quench water

The objective of this chapter is to discuss the results of the laboratory analysis of the quench water. The quench water samples from the HP POX test campaigns Gas-POX 203 – 207 (See laboratory analysis results in Appendix Tables 9.7 for BTEX, Tables 9.9 for PAHs and Table 9.10 for soot) were analysed by an accredited laboratory. Also discussed in this chapter are the processes that could be responsible for the formation of the product synthesis gas trace particulates of soot and traces of organic compounds of BTEX and PAHs in the quench water.

BTEX, PAHs and soot are often present in wastewater [Dórea et al., 2007] from chemical and petrochemical industries as well as hot gas stream from biomass gasification [Torretta et al., 2015]. The degree of the formation of these compounds differs based on the feedstock for a particular gasification process. The fossil-based solid feeds like coal, petroleum residue as well as renewable feedstocks such as the lignocellulosic biomass [Bhavya et al., 2015], [Hermann et al., 2007], [Wiinikka et al., 2006] and [Wiinikka et al., 2004], waste from chemical pulp and paper production are known to produce more BTEX, PAHs and soot than gaseous feedstock like natural gas [Raimondi et al., 2009], [Lederer et al., 2015] and [Steynberg et al., 2006]. In the partial oxidation of natural gas, a very little amount of carbon is formed and this carbon is free of metals [Higman et al., 2003], which simplify the soot capture [Higman et al., 2002].

The difference in the amount of BTEX, PAHs and soot formed in many gasification processes can be from the effect of different operation conditions, feedstock and / or feed preparation processes, the design of their burners, and product synthesis gas quenching methods. Usually, gasification processes does not only produce the main constituent of syngas alone but a large number of intermediate by-products of decomposition and oxidation formed, which are then not further decomposed.

Due to the high toxicity of these compounds to human health and the environment, many stringent regulations have been imposed on concentration of these compounds inside wastewaters for the safe discharge [Lin et al., 1999]. Several methods like condensation, catalytic oxidation, adsorption, thermal oxidation, membrane separation and absorption have been employed for removing these organic compounds from wastewaters.

The thermochemical processing of coal and production of chemically complex wastewater were reported by [Jin et al., 1999] and [Parkhurst et al., 1981] to evaluate and identify the toxicity of the effluent discharged and effect on the aquatic ecosystems. It was confirmed that volatile phenols and ammonia were the major chemicals that led to the toxicity of the effluent discharged from the coal gasification plant. PAH compounds as constituent of coal tar [Yang et al., 2006] and [Zhang et al., 2006] was removed by its acidification demulsion during the pre-treatments of coal gasification waste water.

High concentration of PAHs and other undesirable compounds were confirmed [Gai et al., 2008], [Pinto et al., 2014] and [Hsu et al., 2016] in emissions and waste water relating to the gasification of coal. In response to the operating parameter during the thermochemical conversion of biomass, several tar species were created [Asadullah et al., 2014], [Woolcock et al., 2013] and [Torres et al., 2007]. In order to reduce the tar content from the hot gas obtained from an experimental gasifier, thermal cracking was applied. Large part of the tar and other C_xH_y compounds were converted to soot by polymerization [Houben et al., 2002]. In order to remove tar from biomass gasification during experiment, a comprehensive compounds in tar were developed. Toluene, naphthalene, phenol and pyrene representing all the one-ring compounds, two-ring compounds: phenolic and other heterocyclic compounds and three-rings and higher compounds were included in the comprehensive tar compounds [Supawat et al., 2014]. This approach offers the gas clean-up technology that could be applied downstream of the gasifier reactor in order to have the syngas quality.

Presented in the Appendix (Tables 9.7 for BTEX, Tables 9.9 for PAHs and Table 9.10 for soot) are the laboratory analysis results obtained from the HP POX quench water effluent samples during the Gas-POX 203 – 207 test campaigns. Despite the fact that the some amount of traces of BTEX, PAHs and soot were below the threshold of measuring range, the next sections of this chapter give a detail study of each of the trace compounds that were analysed.

7.1   Quench water behaviour

Figure 7.1 presents an overview of the HP POX test plant quench water system. All products and by-products of the gasification process (Gas-POX mode) enters the quench chamber via the hot gas stream. The quench chamber has a volume of 1 m³, a liquid level measurement with a mean residence

time of about 5 minutes. The hot gas stream temperature during the test campaign under review (Gas-POX 201 – 207) range from 1172 – 1443 °C, pressure range from 51 – 81 bar and flow rate from 0.4 – 0.9 t/h. The analysed quench water samples were collected at the quench chamber´s quench water stream outlet every one hour during each test campaign. The quench water outlet stream leaves the quench chamber at 5.2 – 5.4 t/h, 141 – 194 °C and pressure range from 51 – 81 bar. Stream F103 supplies the quenching water and it enters the quench chamber at the rate of 5.3 t/h, pressure range from 61 – 82 bar and temperature range from 79 – 80 °C.
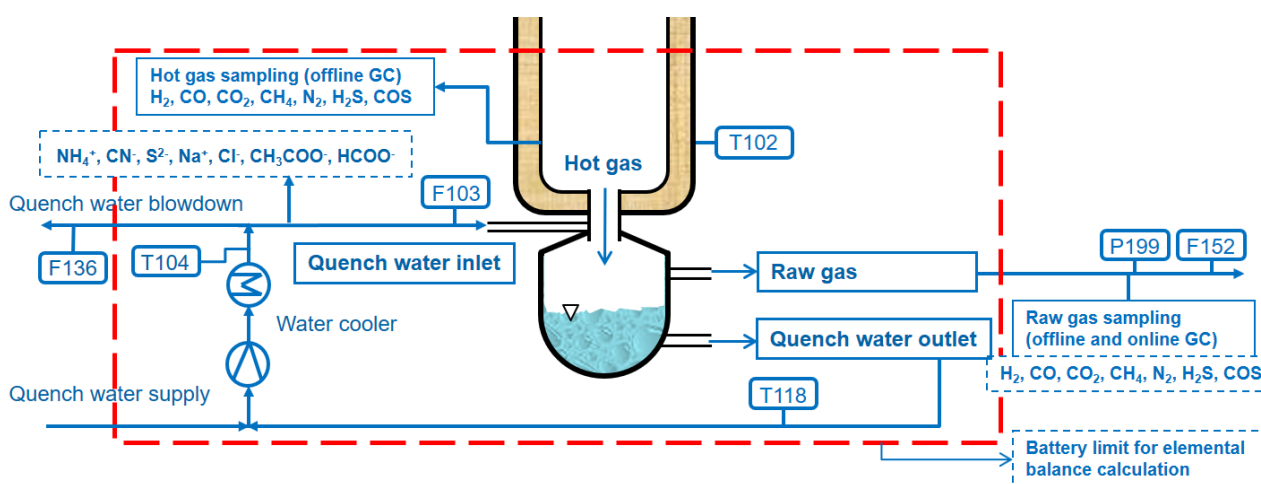
Figure 7.1: HP POX test plant quench water system

7.2 BTEX compounds

Benzene, toluene, ethylbenzene and xylene (BTEX) are part of the designated chemicals by the US EPA [Lin et al., 1999] and [Xu et al., 2003] as priority chemicals that need to be reduced to a very low level in industrial wastewaters for safe discharge. The treatment of BTEX-containing wastewater is an integral part of wastewater treatment of the chemical and the petrochemical industries. The presence of these volatile organic compounds (VOCs) like benzene, toluene, ethylbenzene, and meta- (m), para- (p), and ortho- (o) xylene in industrial processes are continuously monitored following the European directive 2002/69/EC in the European Union member states [Zalel et al., 2008]. This is to limit the emissions of benzene at national regulations. The International Agency for Research on Cancer (IARC) classifies benzene as group 1, ethylbenzene as group 2B, toluene, styrene and xylenes as group 3 carcinogens.

Table 9.6 (in Appendix) presents the content of the aromatics analyzed in the quench water effluent. These aromatics are known to be responsible for the formation of carbonaceous particles similar to soot particles [Mohammed et al., 2016] and [Raj et al., 2015] and deactivate catalyst in the low – temperature multistage catalytic section (beds) of Claus process [John et al., 2001]. They can withstand high temperature environment of the Claus furnace [Mohammed et al., 2015]. They are present in automobile exhaust, emissions from coal and oil burning as well as petrochemical plants. The sources of BTEX ranges from the production of plastics, resins, lubricants, rubber, adhesives, detergents, coatings, paint, and so on. A study to understand the fate of BTEX between gaseous and aqueous phase in a dynamic system were quantitatively determined [Sostaric et al., 2016], [Am Daifullah et al., 2004] and [Allou et al., 2011]. Their dissolution is complicated mainly due to the presence of suspended compounds. The findings show that the dissolution is not the only major mechanism of gaseous BTEX uptake in aqueous phase but the formation of hydrogen bonds between VOCs and atmospheric water [Sostaric et al., 2016] and air–water interfacial adsorption [Kim et al., 1998]. The atmospheric water may be the gasifier or quench chamber environment and the air-water interfacial may be the transition between gas and liquid phase to have aqueous solution.

The reaction mechanism for the formation of BTEX in gasification and other industrial processes are very scares. Many mechanisms have been proposed for the formation of benzene from different reacting species, radicals and smaller hydrocarbon fragments. Benzene is the simplest form of the BTEX. Reaction (7.1) [Olsvik et al., 1994] happens to be the most important reaction in the formation of benzene and mostly leading to the formation of coke [Holmen et al., 1995]. Another formation of benzene via chemically activated addition and isomerization reactions have been illustrated by [Westmoreland et al., 1989]. [Vourliotakis et al., 2008] indicates that the syngas produced by POX reforming is mainly constituted by H_2, CO, H_2O, CO_2 and a non-negligible percentage of C_2H_2, which is considered to be a major soot precursor. The role of propargyl (C_3H_3) and cyclopentadienyl (C_5H_5) radicals in the formation of benzene in combustion of aliphatic fuels were reported by [Richter et al., 2000]. In all the available mechanisms that have been proposed for the formation of benzene, reaction (7.1) is highly significant among several reaction mechanisms [Holmen et al., 1995], [Richter et al., 2000] and [Olsvik et al., 1994] where (7.1) occurs as the only irreversible reaction among others in the model.

$$C_2H_2 + C_4H_{\dot{5}} \rightleftharpoons C_6H_6 + H^{\cdot} \tag{7.1}$$

7.2.1 BTEX in quench water effluent

During the test campaigns of Gas-POX 203 – 207, traces of the BTEX were present in the quench water effluent samples. Presented in Fig. 7.2 and 7.3 are the measurement results of the test points and individual component of the BTEX respectively. The beginning of the test campaigns had witnessed the production of BTEX in the analyzed quench water effluent. The profiles in Fig. 7.2: Gas-POX 203 VP, Gas-POX 204 VP1 and VP4, Gas-POX 205 VP1 and ZP2, Gas-POX 206 VP1 and VP6, and Gas-POX 207 VP1 provide several hints that could lead to the formation of BTEX that were present in these quench water effluent samples.

These BTEX traces were measured in the entire test point (see Appendix: Table 9.7 for measured BTEX) but they were mostly below the threshold of measuring range (< 0.5). The instability in operating parameters and incomplete oxidation at the commencement and sometimes at the end of each test campaigns could be a major factor that may be responsible for the formation of BTEX compounds in the gasifier, which were collected in the quench chamber during the quenching of the hot gas. It could be observed that the xylene isomers (p- and m-xylene) were taken as the same due to the inseparable of both isomers. They both have close boiling points, which makes them impractical to separate by distillation [Peng et al., 2016] and [Wang et al., 2014]. p-xylene has a boiling point of 138.35 °C while m-xylene has 139 °C.
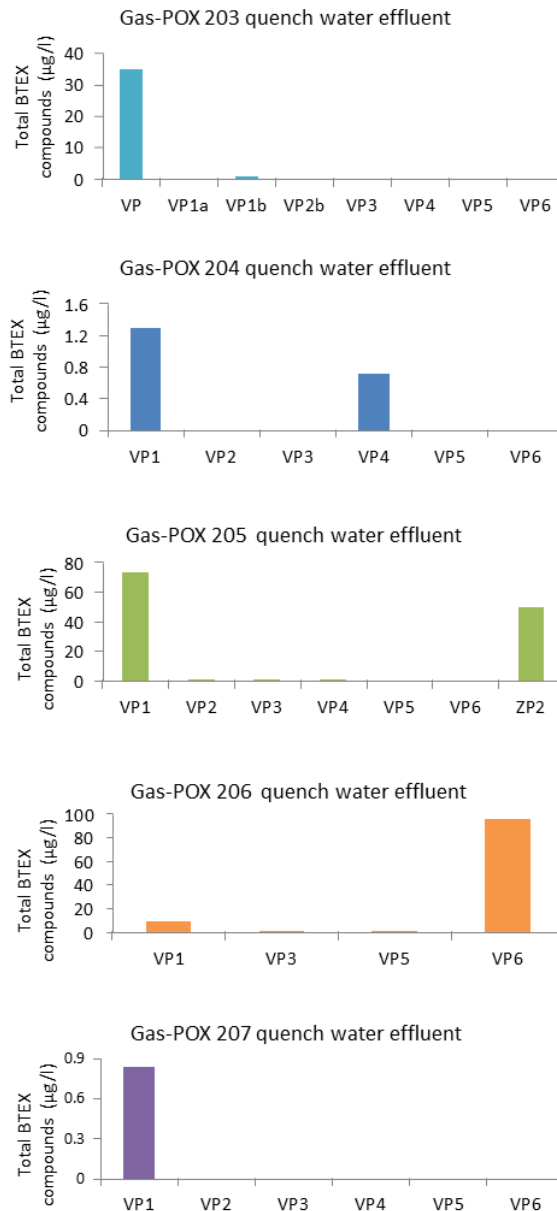
Figure 7.2: Traces of BTEX measured in the Gas-POX 203 – 207 quench water effluent sample.

Among the entire BTEX compounds, the most obvious is benzene as it can be seen in Fig. 7.3. Toluene was dominant in Gas-POX 203 VP, the formation of toluene through benzene reaction is mostly in the presence of catalyst and chloroalkane (e.g. chloromethane or chloroethane), which does not stop there according to Friedel–Crafts alkylation of benzene [Kim et al., 2014] and [Koltunov et al., 2004]. Based on the behaviour of tar compounds in gasification downstream processes [Bassil et al., 2012], toluene and other one ring aromatic compounds have been categorized to be in `Class 3´ among light

hydrocarbons that are not important in condensation and water solubility issues [Paasen et al., 2004]. According to the IARC classifications of carcinogenic agents, `Class 3´ compounds are not classifiable as to their carcinogenicity to humans due to the facts that the evidence of their carcinogenicity are inadequate in humans but sufficient in experimental animals.

The partial oxidation of the components of the natural gas could lead to the formation of vinyl free radicals leading to the formation of benzene, toluene and other trace of BTEX individual compounds with further oxidation or decomposition. Also, based on the reaction conditions, benzene may also be a main compound among the BTEX and its high selectivity are usually accompanied by coke formation [Collin et al., 1994], which makes it an important precursor of soot, first via PAHs formation.
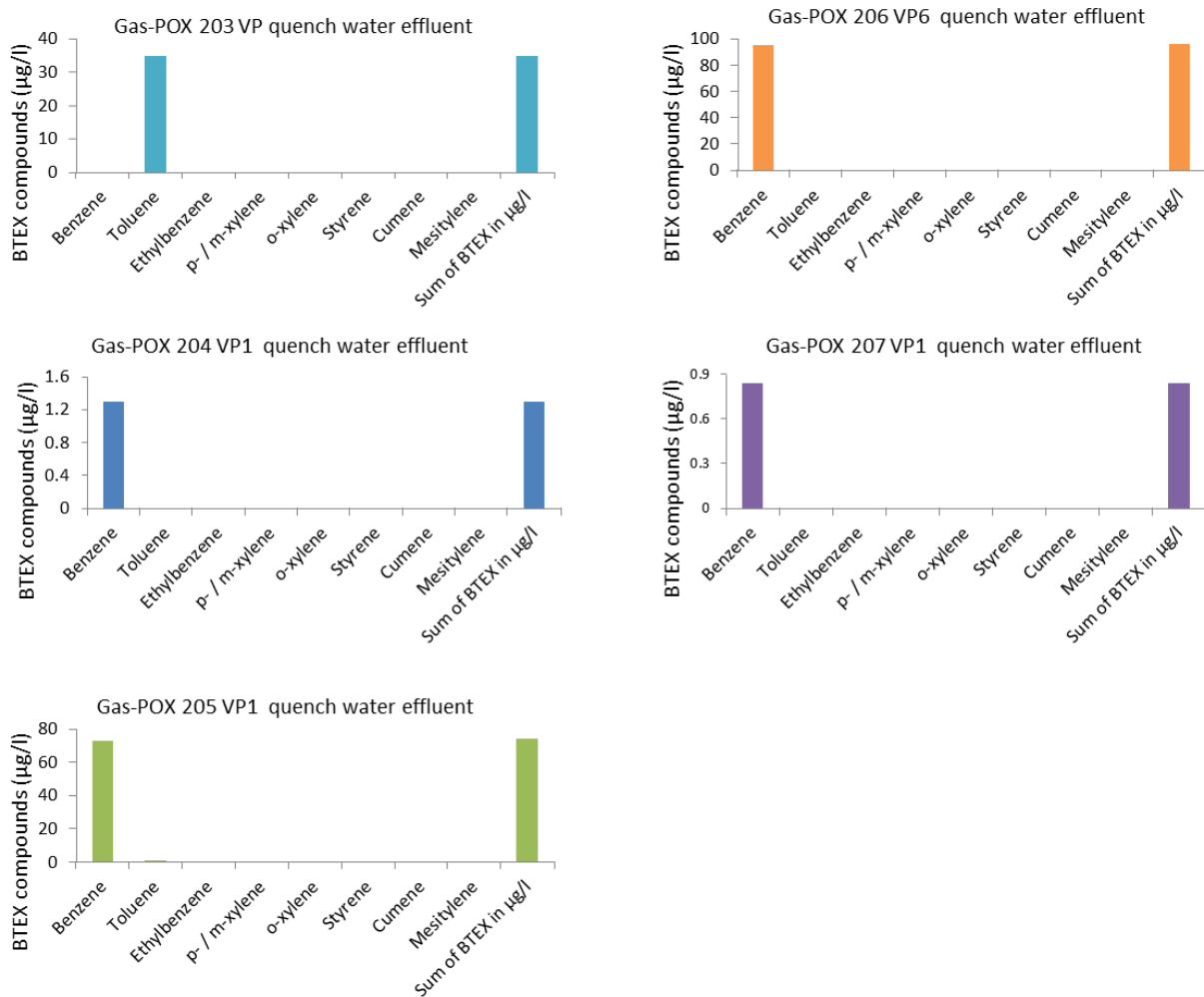
Figure 7.3: Individual component of BTEX measured in the Gas-POX 203 – 207 quench water effluent sample.

7.3 PAH compounds

Polycyclic aromatic hydrocarbons (PAHs) serve as precursors and building blocks for soot formation [Comandini et al., 2012]. They are mostly significant in combustion processes with low amount present in crude oil and are usually formed under fuel-rich conditions [Warnatz et al., 2006]. There annular structures are fused with various benzenic rings that can be substituted by alkyl groups. Their presence in the environment and different sources of formation make them very important. They have two or more fused aromatic rings, which are mainly carbon or hydrogen. PAHs are among the priority controlled pollutants in the US EPA and they are most commonly known contaminants in sewage sludge and many other thermochemical treatment products [Hu et al., 2014] like the quench water effluent. Another type of PAH that exist are called the heterocyclic PAHs because they contains other elements like nitrogen, sulphur and oxygen. These kinds of PAHs are seldom measured or report in most PAHs studies. Despite many growth mechanisms proposed for the formation of these multi-ring aromatic, their chemistry are yet to be fully understood. The important precursors to PAHs are considered to be phenolic compounds [Gong et al., 2016] and [Zhang et al., 2011].
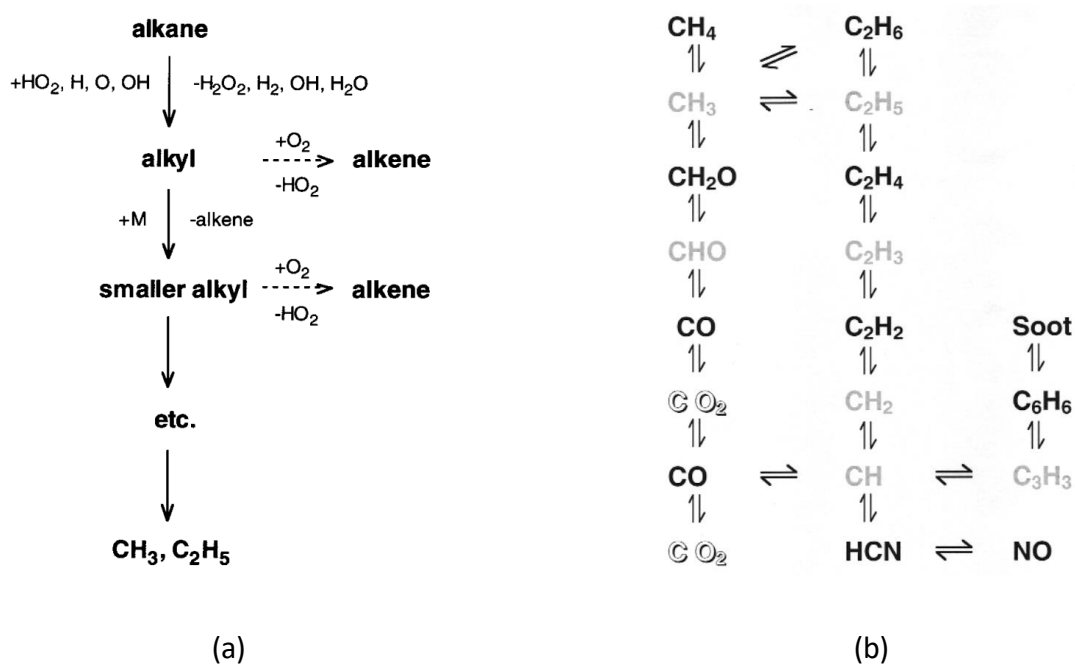
Figure 7.4: (a) Alkyl radical decomposition and (b) C_1 and C_2 hydrocarbons oxidation mechanism [Warnatz et al., 2000]

Based on Fig 7.4 as proposed by [Warnatz et al., 1981] and [Warnatz et al., 2000], the formation of acetylene under rich conditions of $CH_4 - O_2$ flame [Wagner et al., 1981] is the most important precursor of PAHs. It starts with the addition of C_2H_2 to phenyl radicals to form styryl radical [Bittner et al., 1981]. The second addition of C_2H_2 to styryl radical and the ring closure leads to the formation of naphthalene [Frenklach et al., 1991] Equation (7.1) and (7.2) provide a typical even-carbon-atom pathway [Frenklach et al., 2000], which involve the addition of acetylene to n-C_4H_3 and n-C_4H_5 to the form of the first aromatic ring:

$$n - C_4H_3 + C_2H_2 \rightarrow phenyl \tag{7.2}$$

$$n - C_4H_5 + C_2H_2 \rightarrow benzene + \text{H·} \qquad \text{Same as equation (7.1)}$$

Furthermore, acetylene is not the only species that can be envisioned to propagate the growth of aromatic rings of the PAHs [Sánchez et al., 2013]. Other proposals have included those involving methyl, propargyl, and cyclopentadienyl. Another formation of PAHs commences with C_3H_4 decomposition or reaction of CH or CH_2 with C_2H_2 to C_3H_3 leading to the formation of the benzene; the first ring [Stein et al., 1991] after recombination to an aliphatic C_6H_6 and rearrangement [Melius et al., 1992]. Oxidation reaction of C_3H_3 is known to be very slow [Warnatz et al., 2006].
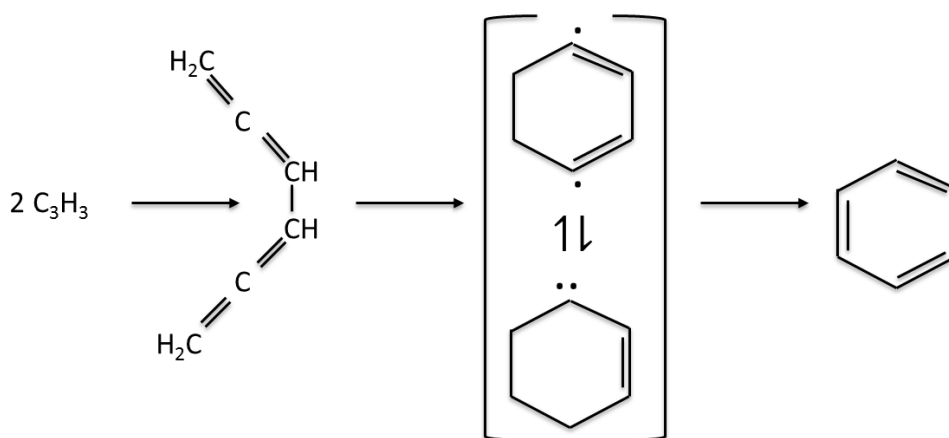
Figure 7.5: Recombination of C_3H_3 to form benzene

Among the 16 compounds of PAHs, naphthalene formation commences the path to other PAHs formation according to the Diels - Alder reaction mechanism in Fig.7.6. This mechanism provides an explanation for the formation these compounds [Cunliffe et al., 1998] and [Zhang et al., 2011].

[Bruinsma et al., 1988] reported the mechanism of condensed PAHs-formation, which were derived from product distribution and the pyrolytic formation of PAHs from benzene, toluene, ethylbenzene, styrene, phenylacetylene and n-decane in the temperature range of 900 – 1250 K.

(a) Dehydrogenation of alkanes to alkenes
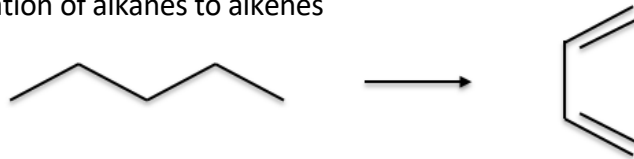
(b) Cyclization
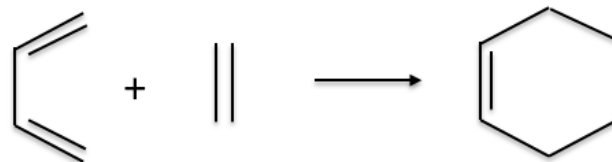
(c) An example of the formation of naphthalene and the route leading to the PAHs formation
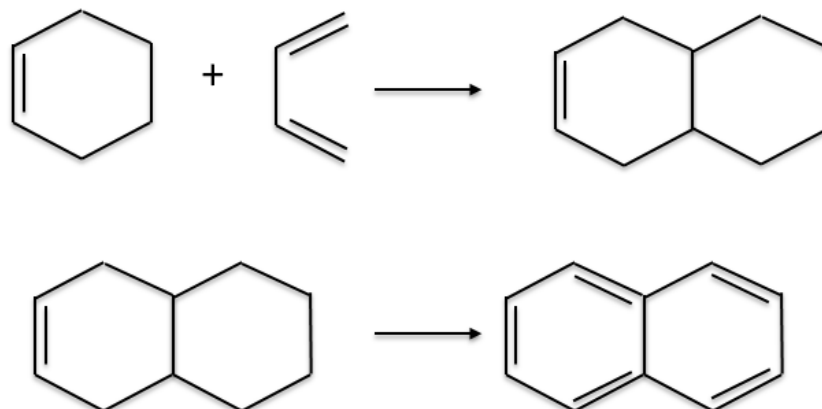
Figure 7.6: The Diels - Alder reaction for the formation of PAHs

7.3.1 PAHs in quench water effluent

Presented in Table 9.8 (in Appendix) are the PAH compounds that are present in the quench water effluent samples. Gas-POX 205 VP1 produces the most among the PAHs of about 63 µg/l analysed. A closer look at Fig 7.7 does provide more questions to the analysed less amount of BTEX in comparison to the PAHs present in the quench water effluent samples. The dominant compound type of the PAHs

from Fig. 7.8 is pyrene, which is a 4-ring aromatic. Other PAHs such as fluorene, phenanthrene, anthracene, fluoranthene, benzanthracene, chrysene, benzo(b)fluoranthene, benzo(k)flouranthene, benzo(a)pyrene, dibenz(a,h)anthracene, benzo(ghi)perylene, and indeno(1,2,3-cd)pyren all appear more than naphthalene and acenaphthylene. Naphthalene is the simplest form of the PAHs that could lead to the others, the correlation between more dominant benzene among the BTEX to the more pyrene among the PAHs shows complexities and poorly understood pathways to the formation of these traces. In addition, these PAHs were all in trace level while some were detected below the threshold (< 0.01, see Appendix Table 9.9 for measured PAHs). [Coll et al., 2001] reports that at 790 °C when varying the steam-to-carbon ratio during steam reforming of biomass, pyrene conversion remains stable and its reactivity is slightly higher than naphthalene.
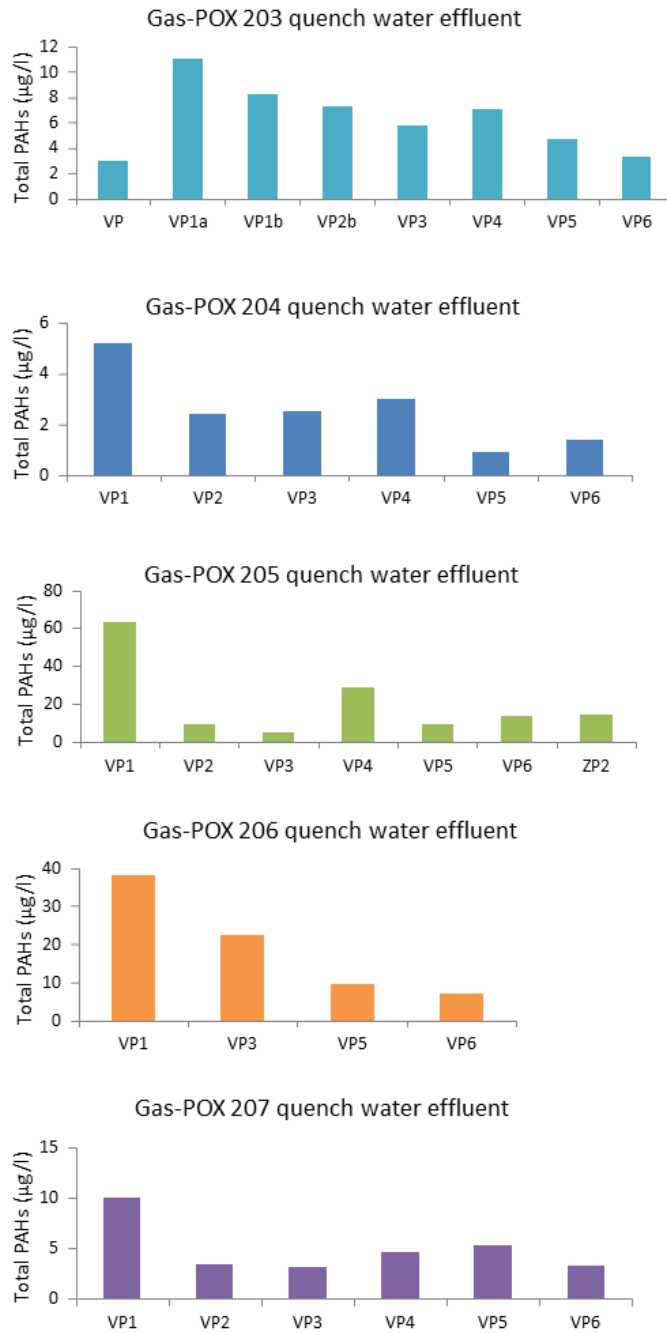
Figure 7.7: Amount of PAHs that were detected in Gas-POX 203 – 207 test points quench water effluent samples.
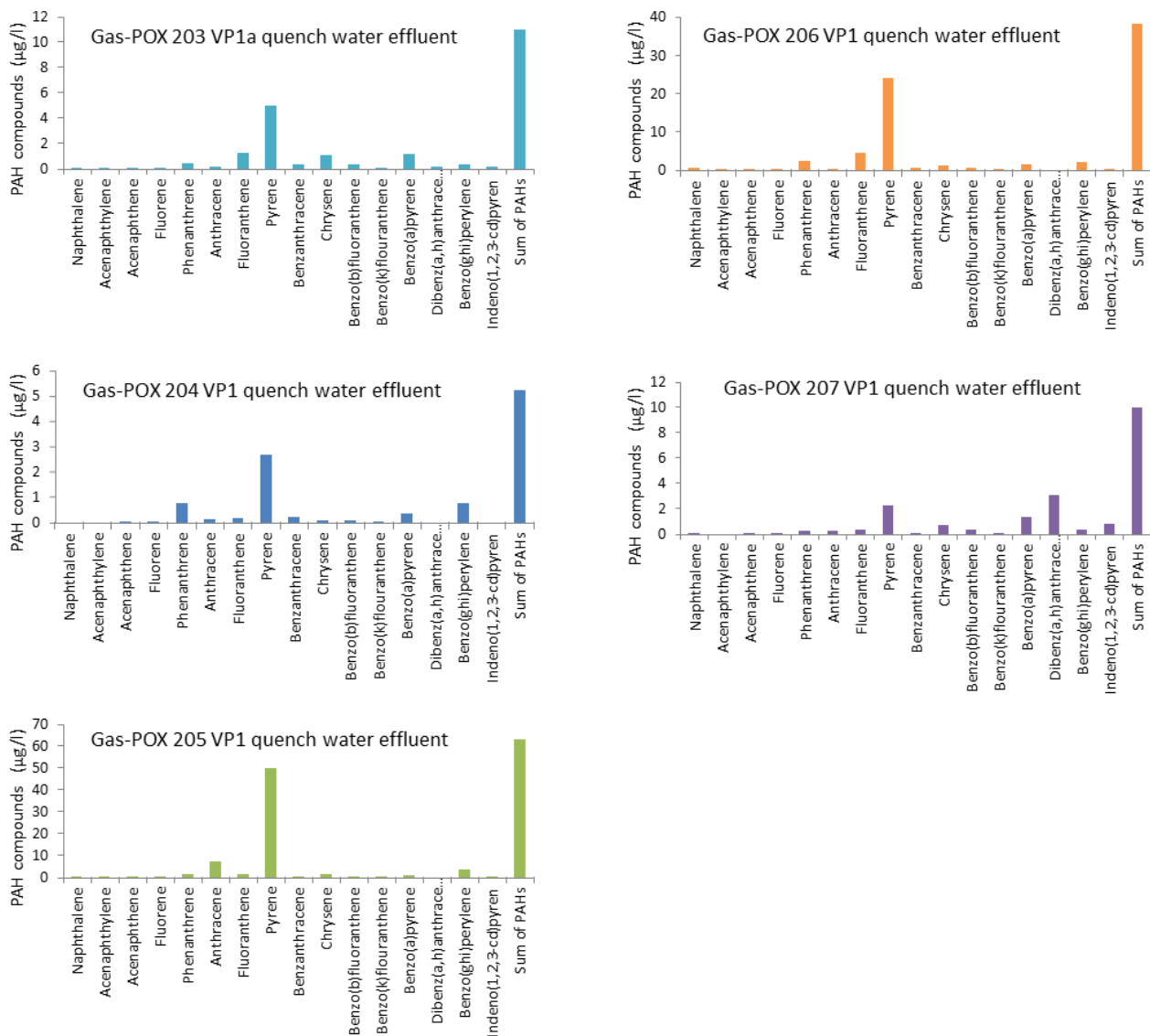
Figure 7.8: Distribution of PAH compounds in Gas-POX 203 – 207 quench water effluent samples.

During the formation of benzene (via acetylene (C_2H_2)), which is the most dominant of the BTEX based on the test campaigns under review (Fig. 7.3), the benzene decomposition pathway begins with the formation of smaller amounts of naphthalene, acenaphthylene, acenaphthene, fluorine, phenanthrene, anthracene, fluoranthene and most dominant amongst the PAHs is pyrene (Fig. 7.8). The results of the Gas-POX 205 VP1 quench water effluent analysis shows 50 µg/l of pyrene followed by 7.1 µg/l anthracene and 3.4 µg/l of benzo(ghi)perylene. It could be concluded that the dominant pathway to the formation of smaller amount of soot via the PAHs is pyrene as it can be seen in Fig. 7.9 (see Appendix: Table 9.9 for measured PAHs). The formation of smaller amount of soot shall be discussed in the next section.

7.4   Soot formation

Soot is generally agreed to be formed from further growth of the PAHs [Wagner et al., 1981] and [Homann et al., 1985]. It is mostly carbon with other elements like hydrogen and oxygen in very small amount. Aromatic compounds and soot chemistry relating to combustion processes have been broadly studied by [Kennedy et al., 1997] and [McEnally et al., 2006]. The formation of soot from gas phase hydrocarbons is complicated and it requires multi-step processes (Fig.7.9) that involves the formation of the first ring, then the formation of polycyclic aromatic hydrocarbons (PAHs), soot inception, and subsequently soot growth [Cuoci et al., 2013]. The soot volume fraction were measure in reactor core under gasification condition during the development of a laser-based absorption technique [Sepman et al., 2016]. The behaviour of soot during gasification by oxidants like H_2O, NO_2 and CO_2 were investigated [Stanmore et al., 2001]. It was confirmed that the molecular O_2 and the O and OH radicals all participate in soot oxidation [Cavaliere et al., 1994].
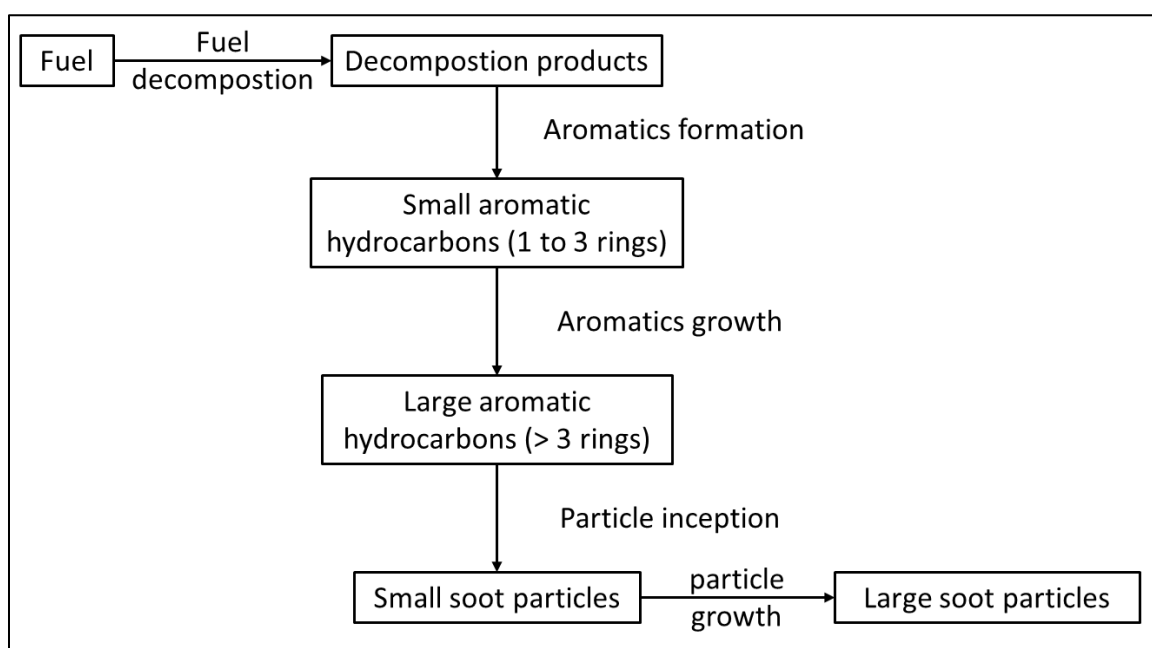
Figure 7.9: Some steps in soot formation [McEnally et al., 2006].

The problem of particulate matter emissions practically applies to mostly solid fuel combustion and gasification processes. Several models provide chemical kinetic description of the fuel and aromatic chemistry together with model for soot formation and agglomeration [Seshadri et al., 2011] and [D'anna et al., 2008]. The most important gaseous fuel is natural gas, and the methane constituent has lesser tendency to form aromatic compounds and soot. This is mainly due to the large methyl radical concentrations in methane flames [Cuoci et al., 2013] and the pathways to the formation of

PAHs in methane flame are different from those of larger hydrocarbons. Soot formations during partial oxidation of natural gas are known to be practically null [Hiller et al., 2000] but the analysed quench water effluent sample are seen to have very little suspension of particulates when viewed from transparent laboratory flask. Whereas, other constituent of the natural gas in this study includes: C_2H_6, C_3H_8 and C_4H_{10}. It is expected to have other pathways to soot from these other higher hydrocarbons apart from methane [Svensson et al., 2013].

In catalytic partial oxidation of natural gas [Bharadwaj et al., 1995], unwanted side reaction in the combustion was responsible for the formation of soot, later, deposit of coke and deactivate the catalyst. These gas phase carbon is also responsible for soot formation on the downstream surfaces resulting in heat transfer problem and plant facility damages [Bharadwaj et al., 1995].
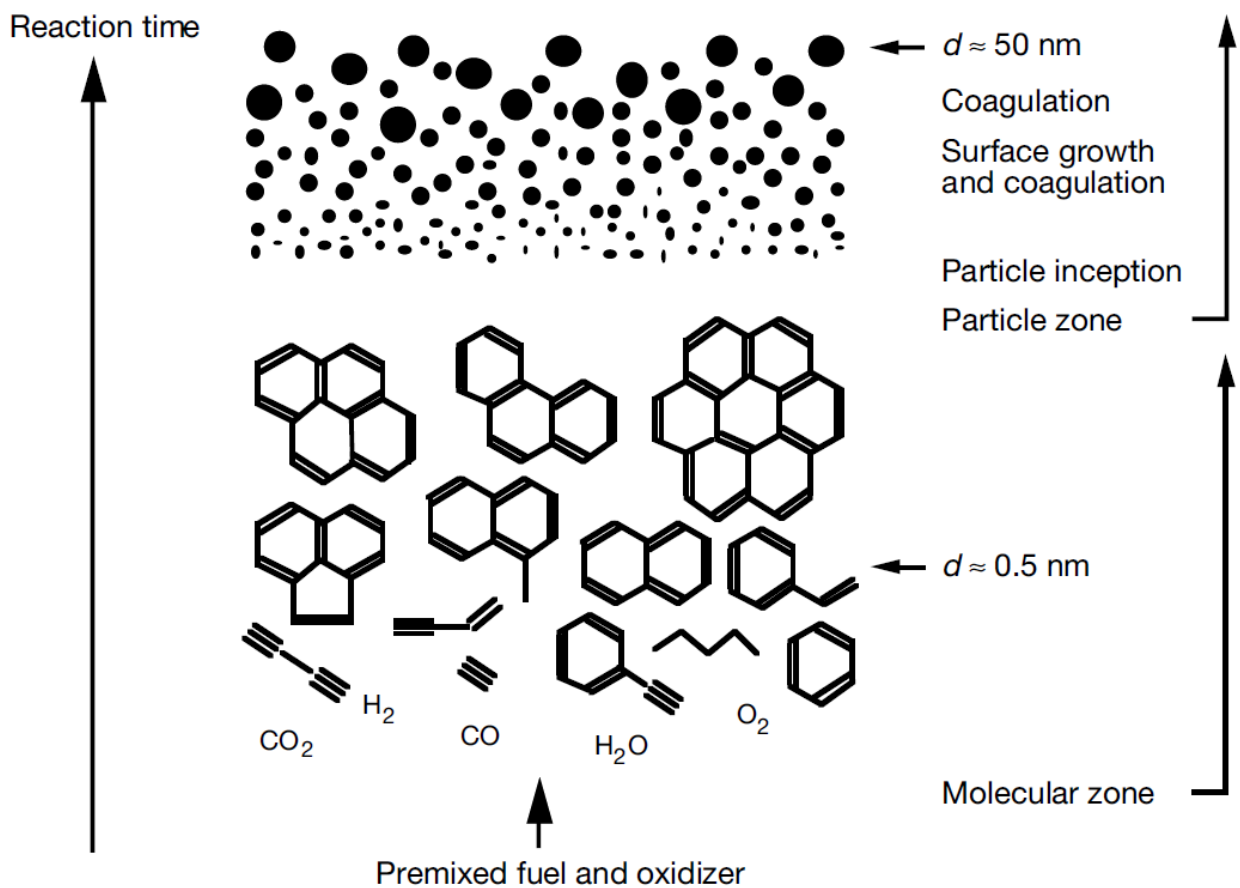
Figure 7.10: Illustration of soot formation path in homogenous mixture [Bockhorn et al., 1994]

Furthermore, in the production of acetylene and synthesis gas by partial oxidation of natural gas with oxygen [Michael Bachtler et al., 1998], soot is reported to be formed in the reaction zones contained in the aqueous quench medium after quenching. The formation of soot can nearly be prevented or

suppressed by the application of high pressures and relatively long residence times in the process. The low pressure and extremely short residence time of a few milliseconds are responsible for the production of acetylene, i.e. the incomplete conversion of the reactants to synthesis gas [Michael Bachtler et al., 1998]. The investigation of soot formation during isothermal pyrolysis of naphthalene, anthracene and pyrene by [Tesner et al., 2010] indicates that particle number densities of the soot formed during pyrolysis of PAHs were in higher magnitude and the apparent activation energy of soot aerosol formation is two times less than the parameters obtained during pyrolysis of benzene or acetylene [Tesner et al., 2010]. The sooting tendency of the hydrocarbons investigated as relative to methane can be arranged at 1350 °C in the following order in Table 7.1.

Table 7.1: Relative sooting tendency [Tesner et al., 2010]

Hydrocarbon	Sooting tendency
Methane	1
Ethylene	4
Acetylene	7.6
Diacetylene	50
Benzene	7.4
Toluene	5.5
Xylene	4
Naphthalene	112
Anthracene	91
Pyrene	74

7.4.1   Soots in quench water effluent

The result of the quench water effluent samples that were analysed indicates that the hot synthesis gas particulates were essentially composed of smaller soot particles, which was collected in the quench chamber during quench operations. The soot was below threshold of measuring range (see Appendix: Table 9.10 for measured soots)

Furthermore, there are close correlations between the amounts of BTEX, polycyclic aromatic hydrocarbons (PAHs) and soot in the quench water effluent as benzene and pyrene dominate the amount of species present. Based on the results in Figures 7.3 and 7.8 as well as the earlier discussed reaction mechanisms from acetylene to benzene (Fig 7.4) and then, the dominant reaction pathway for formation of small polycyclic aromatics via naphthalene and subsequently leading to pyrene as a major compound among 4-rings PAHs. As one of the larger aromatic hydrocarbons, pyrene can

undergo particle inception leading to the formation of smaller soot particles (see Fig.7.9 for steps and illustration).

7.5 Summary

The different results from the analysed quench water effluent samples of these test campaigns provide hints to the pathways for the trace amount of BTEX, PAHs and soot formation. The variations in operating parameters play a key role and influence the formation of BTEX, PAHs and soot.

From the analysed quench water effluent samples, it could be deduced that the order of the formation, decomposition and oxidation for the trace of BTEX, PAHs and soot formation in during the test campaigns is (in deceasing order):

benzene → toluene → pyrene → fluorene → phenanthrene → anthracene → fluoranthene → benzanthracene → chrysene → benzo(b)fluoranthene → benzo(k)flouranthene → benzo(a)pyrene → dibenz(a,h)anthracene → benzo(ghi)perylene → indeno(1,2,3-cd)pyren → small particles soot formation.

Soot formation in the Gas-POX test campaigns should not be expected since the larger the number of aromatic rings in the PAHs molecule, the stronger the tendency to soot formation. Pyrene with 4 aromatic rings is the only PAHs that is mostly suspected to lead to the traces of soot.

8 Summary and outlook

The HP POX quench water system has been extensively analysed and discussed. The quench water outlet stream contains molecularly and ionic dissolved species with complex interactions due to molecular trace component gas-liquid distributions according to the gas-liquid phase equilibrium between the raw gas and quench water phases. Also, molecular and ionic species distributions within the quench water phase according to the dissociations of the traces under electroneutrality condition constraint, as well as the temperature dependency of the Henry's and dissociation constant of the species.

The knowledge of the phase distribution of these species during quenching operations with further improvement in pH regulator designs could improve the separation process design for raw gas cleaning of residual traces in the quench chamber. The concerns from the effects of these trace components with respect to corrosion of plant surfaces, poisoning effects on catalyst in the downstream processes and complex problems resulting from handling waste water (or reuse) during the gasification process could be mitigated. This will ensure compliance toward the growing stringent governmental regulations on effluent discharge and to avoid undue environmental burden.

Moreover, investigation about the activity and reactivity of the surface of the internal wall of the quench chamber to act as catalyst and to enhance certain catalytic reaction of different trace components present in the quench water during quench and after quench need to be thoroughly looked into. It is possible that the remains of used catalyst particles from the ATR test campaigns might be washed into the quench system, which results into catalytic reactions leading to the formation of organic acid and other species in the quench water system.

Precautionary measure to check corrosion in the quench system is to be put in place, pH monitoring device or adjuster and the controller in order to avoid non-supply of the deionized water as this might result into adverse quality of the raw gas from the quench chamber.

In addition, reports about nitrogen bound in aromatic rings, which form HCN and nitrogen from amines, which releases NH_3 [Gräbner, 2015] or NH_3 formed during HCN devolatilization reaction in [Hämäläinen et al., 1996] or the rupturing of the nitrogen containing heteroaromatic ring systems leading to the formation of NH_3 and HCN [Chang et al., 2006] are possible pathways. Also

nitrogenated PAHs may lead to the formation or release NH_3 [Fullana et al., 2003] and [Cao et al., 2010]. Possibly the formamide in gas phase to produce HCN and it decomposition to form CO_2, CO and NH_3 [Cataldo et al., 2009] (see Appendix, comment on formamide). Reports in [Patnaik 2003] explain that ammonium carbamate (NH_2COONH_4) is usually formed when NH_3 reacts with CO_2 and this ammonium carbamate slowly decomposed on exposure to air at ambient temperatures, or rapidly breaks down on heating to NH_3, CO_2, and water; or liberates CO_2 when in contact with dilute mineral acids.

Although, many of these categories of traces reported above are not part of these investigation and are not to be expected especially salt formation like ammonium carbamate (hot gas from Gas-POX is the inlet stream for the investigated quench water system in this work).

Further laboratory analysis to have more information about other traces like acetylene, phenyl, BTEX compounds with nitrogen and –OH radicals especial the phenol group and heterocyclic PAHs (those PAHs with the addition of either nitrogen, sulphur or oxygen) will give more insights into the possible oxidation and decomposition reactions of many of the participating species in the gasifier and during quenching operations.

There is a need to create a comprehensive reaction mechanism for the formation of the dominant compounds of BTEX and PAHs from relating specific reaction schemes peculiar to natural gas gasification processes especially from the C_2, C_3 and C_4 hydrocarbons.

A review of the challenges encountered with the ASW design specification calculations and its compatibility with Microsoft Excel is inevitable. Being an Aspentech product, it would be interesting to see more robustness in ASW in other to perform the same task as with interfaces to Aspen plus written in Python and excel VBA.
It could be helpful to implement these kinds of configurations and interface with Aspen Plus in MATLAB software provided it has more room for improved calculations than Python, VBA and ASW.

There is a need for a specialized agenda (or programme) to execute sensitivity studies for the entire 47 test points in order to investigate all trace components discussed in this work, and those not covered in the scope of this work. The approach in the proposed specialized agenda could be used

for other feedstocks and other gasification processes in such a way to enhance strategies like raw gas cleaning in quench chamber, quench water treatment and re-use. In this work sensitivity studies regarding quench water temperature and pH values change were executed for the GasPOX 201 VP 1 test point (chapter 4), but the trace distributions were calculated for all 47 test points (chapers 5, 6 and 7).

Bibliography

Chapter 1

Anindra Mazumdar, James Scott Kain (2015): pH adjustment within gasification system. Patent: US9108869 B2

Brüggemann, Philipp (2010): Formation and evolution of by-products and trace substances in the high pressure partial oxidation of gaseous and liquid hydrocarbons. Ph.D. thesis, TU Bergakademie Freiberg.

Bucko Z., Uhelna S., Takahashi M., Vierrath H (2000): HTW Fluidized-bed gasification for 400 MW IGC power plant, Vresova, Czech Republic. Gasification Technology Conference, San Francisco, California, October 9 – 11, 2000.

Bunt, J. R.; Waanders, F. B. (2008): Trace element behaviour in the Sasol–Lurgi MK IV FBDB gasifier. Part 1 – The volatile elements. Hg, As, Se, Cd and Pb. Fuel, 87 (12): 2374–2387. DOI: 10.1016/j.fuel.2008.01.017.

Bunt, J. R.; Waanders, F. B. (2009): Trace element behaviour in the Sasol–Lurgi MK IV FBDB gasifier. Part 2 – The semi-volatile elements. Cu, Mo, Ni and Zn. Fuel, 88 (6): 961–969. DOI: 10.1016/j.fuel.2008.10.041.

Bunt, J. R.; Waanders, F. B. (2010): Trace element behaviour in the Sasol-Lurgi fixed-bed dry-bottom gasifier. Part 3 – The non-volatile elements. Ba, Co, Cr, Mn, and V. Fuel, 89 (3): 537–548. DOI: 10.1016/j.fuel.2009.04.018.

Chih-Hao Mark Tsang (2003): Gasification process employing ammonia injection for minimizing waste water treatment. Patent: WO2003022959 A1.

Cui, Hong; Turn, Scott Q.; Keffer, Vheissu; Evans, Donald; Tran, Thai; Foley, Michael (2013): Study on the fate of metal elements from biomass in a bench-scale fluidized bed gasifier. Fuel, 108: 1–12. DOI: 10.1016/j.fuel.2011.07.029.

Edwards, Thomas J.; Newman, John; Prausnitz, John M. (1975): Thermodynamics of aqueous solutions containing volatile weak electrolytes. AIChE Journal, 21 (2) 248–259. DOI: 10.1002/aic.690210205.

Furimsky, E. (1999): Gasification in Petroleum Refinery of 21st Century. Oil & Gas Science and Technology - Review. IFP, 54 (5): 597–618. DOI: 10.2516/ogst: 1999051.

H. Stahl, S. G. Thomsen (1996): "Survey of Worldwide Experience with Metal Dusting," Annual symposium; 40th Ammonia plant safety and related facilities. American Institute of Chemical Engineers (AIChE). Volume 36. Page 180–191. ISBN: 0816907080

Higman, Chris; van der Burgt, Maarten (2003): Gasification. Boston: Elsevier/Gulf Professional Publishing.

Hoekman, S. Kent; Robbins, Curtis; Wang, Xiaoliang; Zielinska, Barbara; Schuetzle, Dennis; Schuetzle, Robert (2013): Characterization of trace contaminants in syngas from the thermochemical conversion of biomass. Biomass Conversion and Biorefinery, 3 (4): 271–282. DOI: 10.1007/s13399-013-0081-7.

International Gasification Organisation [IGO] (2003): A Worldwide Industry. www.gasification.org

Kimberly K. Denney, Norman G. Block (1989): Control of pH in water quench of a partial oxidation process. Patent: US4854942 A.

Miller, Bruce G.; Tillman, David A. (2008): Combustion engineering issues for solid fuel systems. Amsterdam, London: Elsevier/Academic Press.

Mondal, P.; Dang, G. S.; Garg, M. O. (2011): Syngas production through gasification and cleanup for downstream applications — Recent developments. Fuel Processing Technology, 92 (8): 1395–1410. DOI: 10.1016/j.fuproc.2011.03.021.

Nishiyama, Y.; Kudo, T.; Otsuka, N. (2006): Effect of Syngas Composition on Metal Dusting of Alloy 800H in Simulated Reforming Gas Atmospheres. Corrosion, 62 (1): 54–63. DOI: 10.5006/1.3278252.

Öhrman, Olov G. W.; Molinder, Roger; Weiland, Fredrik; Johansson, Ann-Christine (2014): Analysis of trace compounds generated by pressurized oxygen blown entrained flow biomass gasification. Environmental Progress & Sustainable Energy, 33 (3): 699–705. DOI: 10.1002/ep.11975.

Öhrman, Olov; Häggström, Caroline; Wiinikka, Henrik; Hedlund, Jonas; Gebart, Rikard (2012): Analysis of trace components in synthesis gas generated by black liquor gasification. Fuel, 102: 173–179. DOI: 10.1016/j.fuel.2012.05.052.

Pitchai, R.; Klier, K. (1986): Partial Oxidation of Methane. Catalysis Reviews, 28 (1): 13–88. DOI: 10.1080/03602458608068085.

Pröll, Tobias; Siefert, Ingmar G.; Friedl, Anton; Hofbauer, Hermann (2005): Removal of NH_3 from Biomass Gasification Producer Gas by Water Condensing in an Organic Solvent Scrubber. Industrial & Engineering Chemistry Research, 44 (5): 1576–1584. DOI: 10.1021/ie049669v.

Pudasainee, Deepak; Paur, Hanns-Rudolf; Fleck, Sabine; Seifert, Helmut (2014): Trace metals emission in syngas from biomass gasification. Fuel Processing Technology, 120: 54–60. DOI: 10.1016/j.fuproc.2013.12.010.

Reed, G. P.; Dugwell, D. R.; Kandiyoti, R. (2001): Control of Trace Elements in Gasification: Distribution to the Output Streams of a Pilot Scale Gasifier. Energy Fuels, 15 (4): 794–800. DOI: 10.1021/ef000156k.

Shoko E.; McLellan B.; Dicks A. L.; Diniz da Costa, J. C. (2006): Hydrogen from coal: Production and utilisation technologies. International Journal of Coal Geology, 65 (3-4): 213–222. DOI: 10.1016/j.coal.2005.05.004.

Stemmler, Michael; Tamburro, Angela; Müller, Michael (2013): Laboratory investigations on chemical hot gas cleaning of inorganic trace elements for the "UNIQUE" process. Fuel, 108: 31–36. DOI: 10.1016/j.fuel.2011.05.027.

Stiegel, Gary J.; Ramezan, Massood (2006): Hydrogen from coal gasification: An economical pathway to a sustainable energy future. International Journal of Coal Geology, 65 (3-4): 173–190. DOI: 10.1016/j.coal.2005.05.002.

Wiinikka, Henrik; Carlsson, Per; Marklund, Magnus; Grönberg, Carola; Pettersson, Esbjörn; Lidman, Marcus; Gebart, Rikard (2012): Experimental investigation of an industrial scale black liquor gasifier. Part 2: Influence of quench operation on product gas composition. Fuel, 93: 117–129. DOI: 10.1016/j.fuel.2011.06.066.

Woolcock, Patrick J.; Koziel, Jacek A.; Cai, Lingshuang; Johnston, Patrick A.; Brown, Robert C. (2013): Analysis of trace contaminants in hot gas streams using time-weighted average solid-phase microextraction: proof of concept. Journal of Chromatography A, 1281: 1–8. DOI: 10.1016/j.chroma.2013.01.036.

Woolcock, Patrick J.; Koziel, Jacek A.; Johnston, Patrick A.; Brown, Robert C.; Broer, Karl M. (2015): Analysis of trace contaminants in hot gas streams using time-weighted average solid-phase microextraction: Pilot-scale validation. Fuel, 153: 552–558. DOI: 10.1016/j.fuel.2015.02.101.

Chapter 2

Aasberg-Petersen, K.; Bak Hansen, J.-H; Christensen, T.S; Dybkjaer, I.; Christensen, P.Seier; Stub Nielsen, C. et al. (2001): Technologies for large-scale gas conversion. Applied Catalysis A: General, 221 (1-2): 379–387. DOI: 10.1016/S0926-860X(01)00811-0.

Aasberg-Petersen, Kim; Christensen, Thomas S.; Stub Nielsen, Charlotte; Dybkjær, Ib (2003): Recent developments in autothermal reforming and pre-reforming for synthesis gas production in GTL applications. Fuel Processing Technology, 83 (1-3): 253–261. DOI: 10.1016/S0378-3820(03)00073-0.

Brüggemann, Philipp (2010): Formation and evolution of by-products and trace substances in the high pressure partial oxidation of gaseous and liquid hydrocarbons. Ph.D. thesis, TU Bergakademie Freiberg.

Cassella, Ricardo Jorgensen; Oliveira, Leandra Guimarães de; Santelli, Ricardo Erthal (1999): On Line Dissolution of ZnS For Sulfide Determination in Stabilized Water Samples with Zinc Acetate, Using Spectrophotometry by Methylene Blue Method. Spectroscopy Letters, 32 (3): 469–484. DOI: 10.1080/00387019909349999.

Curry-Hyde, H. E.; Howe, R. (1994): Studies in surface science and catalysis. Volume 81. 1st Edition. Natural Gas Conversion II: proceedings of the Third Natural Gas Conversion Symposium, Sydney, July 4-9, 1993, Elsevier. ISBN: 9780080887609.

Guiberti, T. F.; Garnier, C.; Scouflaire, P.; Caudal, J.; Labegorre, B.; Schuller, T.; Darabiha, N. (2016): Experimental and numerical analysis of non-catalytic partial oxidation and steam reforming of $CH_4/O_2/N_2/H_2O$ mixtures including the impact of radiative heat losses. International Journal of Hydrogen Energy, 41 (20): 8616–8626. DOI: 10.1016/j.ijhydene.2016.03.009.

Guo, Wenyuan; Wu, Yanzeng; Dong, Liang; Chen, Caixia; Wang, Fuchen (2012): Simulation of non-catalytic partial oxidation and scale-up of natural gas reformer. Fuel Processing Technology, 98: 45–50. DOI: 10.1016/j.fuproc.2012.01.019.

Higman, Chris; van der Burgt, Maarten (2003): Gasification. Boston: Elsevier/Gulf Professional Publishing.

Huff, M.; Torniainen, P. M.; Hickman, D. A.; Schmidt, L. D. (1994): Partial Oxidation of CH_4, C_2H_6, and C_3H_8 on Monoliths at Short Contact Times. Studies in surface science and catalysis. Volume 81. 1st Edition. Natural Gas Conversion II: proceedings of the Third Natural Gas Conversion Symposium, Sydney, July 4-9, 1993, Elsevier: 315–320. ISBN: 9780080887609.

Konnov, Alexander A.; Zhu, Jian Ning; Bromly, John H.; Zhang, Dong-Ke (2004): Noncatalytic Partial Oxidation Of Methane Into Syngas Over A Wide Temperature RANGE. Combustion Science and Technology, 176 (7): 1093–1116. DOI: 10.1080/00102200490426451.

Langensiepen, H.-W. (1979): Balancing and balance uncertainties in pilot plants. Computers & Chemical Engineering, 3 (1-4):79–83. DOI: 10.1016/0098-1354(79)80016-2.

Li, Chao'en; Burke, Nick; Gerdes, Karl; Patel, Jim (2013): The undiluted, non-catalytic partial oxidation of methane in a flow tube reactor – An experimental study using indirect induction heating. Fuel, 109: 409–416. DOI: 10.1016/j.fuel.2013.02.055.

Lurgi GmbH (2008): Multi-Purpose Gasification. Company brochure.

Ma, Jian; Dasgupta, Purnendu K.; Blackledge, William; Boss, Gerry R. (2010) Temperature Dependence of Henry's Law Constant for Hydrogen Cyanide. Generation of Trace Standard Gaseous Hydrogen Cyanide: Environmental Science & Technology, 44 (8): 3028–3034. DOI: 10.1021/es1001192.

Meyer B, Seifert P, Tehsmer R, Baitalow F, Günther K-H, Brüggemann P, Prescher R, Bader A, Tischer P, Schön C, Rehm M, Ortwein A, Keller P, Trompelt M, Böhning U, Weiterentwicklung der IGCC-Kohlekraftwerkstechnik mit CO$_2$- Abtrennung – COORAMENT.technical report (2010), TU Bergakademie Freiberg. edok01.tib.uni-hannover.de/edoks/e01fb11/665646453.pdf

Meyer B. (2007): Untersuchungen zur Hochdruck-Partialoxidation (HP POX) von gasfoermigen und fluessigen Kohlenwasserstoffen. Erdoel-Erdgas-Kohle, 123 (4): 159–167.

Pena, M. A.; Gómez, J. P.; Fierro, J.L.G. (1996): New catalytic routes for syngas and hydrogen production. Applied Catalysis A: General, 144 (1-2): 7–57. DOI: 10.1016/0926-860X(96)00108-1.

Pitchai, R.; Klier, K. (1986): Partial Oxidation of Methane. Catalysis Reviews, 28 (1): 13–88. DOI: 10.1080/03602458608068085.

Pomeroy, Richard. (1954): Auxiliary Pretreatment by Zinc Acetate in Sulfide Analyses. Analytical Chemistry, 26 (3): 571–572. DOI: 10.1021/ac60087a047.

Richter, Andreas; Seifert, Peter; Compart, Fred; Tischer, Paul; Meyer, Bernd (2015): A large-scale benchmark for the CFD modeling of non-catalytic reforming of natural gas based on the Freiberg test plant HP POX. Fuel, 152: 110–121. DOI: 10.1016/j.fuel.2014.12.004.

Rietema, K. (1961): A1. The role of chemical reaction engineering in process research and scaling up. Chemical Engineering Science, 14 (1): 3–10. DOI: 10.1016/0009-2509(61)85045-8.

Shanthi Krishnamoorthy, Balasubramanian, Natesan (1996): A Simple Spectrophotometric Method for the Determination of Hydrogen Sulfide Based on Schiff's Reaction. Microchemical Journal, 53 (2): 168–174. DOI: 10.1006/mchj.1996.0024.

Smirniotis Panagiotis, Gunugunuri Krishna (2015): Water gas shift reaction. Research developments and applications. 1st Edition. ISBN: 9780444633538.

Trippe, Frederik; Fröhling, Magnus; Schultmann, Frank; Stahl, Ralph; Henrich, Edmund (2011): Techno-economic assessment of gasification as a process step within biomass-to-liquid (BtL) fuel and chemicals production. Fuel Processing Technology, 92 (11): 2169–2184. DOI: 10.1016/j.fuproc.2011.06.026.

Uchijima, Toshio; Nakamura, Junji; Sato, Koichi; Aikawa, Keita; Kubushiro, Kaneshige; Kunimori, Kimio (1994): Production of Synthesis Gas by Partial Oxidation of Methane and Reforming of Methane with Carbon Dioxide. Studies in surface science and catalysis. Volume 81. 1st Edition. Natural Gas Conversion II: proceedings of the Third Natural Gas Conversion Symposium, Sydney, July 4-9, 1993, Elsevier: 325–327. ISBN: 9780080887609.

Wilhelm, D.J; Simbeck, D.R; Karp, A.D; Dickenson, R.L (2001): Syngas production for gas-to-liquids applications: technologies, issues and outlook. Fuel Processing Technology, 71 (1-3): 139–148. DOI: 10.1016/S0378-3820(01)00140-0.

Xu, Yueting; Dai, Zhenghua; Li, Chao; Li, Xinyu; Zhou, Zhijie; Yu, Guangsuo; Wang, Fuchen (2014): Numerical simulation of natural gas non-catalytic partial oxidation reformer. International Journal of Hydrogen Energy, 39 (17): 9149–9157. DOI: 10.1016/j.ijhydene.2014.03.204.

Zhou, Xinwen; Chen, Caixia; Wang, Fuchen (2010): Modeling of non-catalytic partial oxidation of natural gas under conditions found in industrial reformers. Chemical Engineering and Processing: Process Intensification, 49 (1): 59–64. DOI: 10.1016/j.cep.2009.11.006.

Zhou, Xinwen; Chen, Caixia; Wang, Fuchen (2010): Multi-dimensional modeling of non-catalytic partial oxidation of natural gas in a high pressure reformer. International Journal of Hydrogen Energy, 35 (4): 1620–1629. DOI: 10.1016/j.ijhydene.2009.12.063.

Chapter 3

Akesson, J.; Arzén, K.-E.; Gäfvert, M.; Bergdahl, T.; Tummescheit, H. (2010): Modeling and optimization with Optimica and JModelica.org—Languages and tools for solving large-scale dynamic optimization problems. Computers & Chemical Engineering, 34 (11): 1737–1749. DOI: 10.1016/j.compchemeng.2009.11.011.

Aspentech Manual (2008): Aspen HYSYS. Customization Guide. Aspen Technology, Inc.

Aspentech manual: property method. (2012): Aspen Physical Property System. Physical Property Models. Aspen Technology, Inc.

Aspentech white paper (2012): Enabling Model-Based Decision Support for Plant Optimization. An Industry White Paper.Ken Dooley, Stephen Sarafian. Aspen Technology, Inc.

Aspentech: ASW in Aspen HYSYS (2014): Jump Start: Aspen Simulation Workbook in Aspen HYSYS® V8. A Brief Tutorial (and supplement to training and online documentation). Vidya Mantrala, David Tremblay. Aspen Technology, Inc.

B. Mock, L. B. Evans, C.-C.Chen (1984): Phase Equilibria in Multiple-Solvent Electrolyte Systems: A New Thermodynamic Model. In: Proceedings of the 1984 Summer Computer Simulation Conference, 1984, 558–562, (held in Boston, Massachusetts, USA).

Chen, Chau-Chyun; Britt, H. I.; Boston, J. F.; Evans, L. B. (1982): Local composition model for excess Gibbs energy of electrolyte systems. Part 1: Single solvent, single completely dissociated electrolyte systems. AIChE Journal, 28 (4): 588–596. DOI: 10.1002/aic.690280410.

Chen, Chau-Chyun; Evans, L. B. (1986): A local composition model for the excess Gibbs energy of aqueous electrolyte systems. AIChE Journal, 32 (3): 444–454. DOI: 10.1002/aic.690320311.

Chen, Chau-Chyun; Song, Yuhua (2004): Generalized electrolyte-NRTL model for mixed-solvent electrolyte systems. AIChE Journal, 50 (8): 1928–1941. DOI: 10.1002/aic.10151.

Durante, Davide; Kilpiö, Teuvo; Suominen, Petteri; Herrera, Victor Sifontes; Wärnå, Johan; Canu, Paolo; Salmi, Tapio (2014): Modeling and simulation of a small-scale trickle bed reactor for sugar hydrogenation. Computers & Chemical Engineering, 66: 22–35. DOI: 10.1016/j.compchemeng.2014.02.025.

H. Renon, J. M.Prausnitz (1968): Local Compositions in Thermodynamic Excess Function for Liquid Mixtures. AIChE Journal, 14 (1) 135–144. DOI: 10.1002/aic.690140124

Haghtalab, Ali; Papangelakis, Vladimiros G.; Zhu, Xuetang (2004): The electrolyte NRTL model and speciation approach as applied to multicomponent aqueous solutions of H_2SO_4, $Fe_2(SO_4)_3$, $MgSO_4$ and $Al_2(SO_4)_3$ at 230–270 °C. Fluid Phase Equilibria, 220 (2): 199–209. DOI: 10.1016/j.fluid.2004.03.013.

Jaretun, Anders; Aly, Gharib (1999): New local composition model for electrolyte solutions: single solvent, single electrolyte systems. Fluid Phase Equilibria, 163 (2): 175–193. DOI: 10.1016/S0378-3812(99)00222-8.

Jaretun, Anders; Aly, Gharib (2000): New local composition model for electrolyte solutions: multicomponent systems. Fluid Phase Equilibria, 175 (1-2): 213–228. DOI: 10.1016/S0378-3812(00)00450-7.

Querol, E.; Gonzalez-Regueral, B.; Ramos, A.; Perez-Benedito, J. L. (2011): Novel application for exergy and thermoeconomic analysis of processes simulated with Aspen Plus®. Energy, 36 (2): 964–974. DOI: 10.1016/j.energy.2010.12.013.

Rangaiah, Gade Pandu (2016): Chemical process retrofitting and revamping: techniques and applications. Chichester, West Sussex: Wiley. ISBN: 978-1-119-01633-5

Chapter 4

Alvaro Pérez-Salado Kamps (2000): Influence of NH_4Cl, NH_4NO_3, and $NaNO_3$ on the Simultaneous Solubility of Ammonia and Carbon Dioxide in Water. Journal of Chemical & Engineering Data, 45 (5): 796-809. DOI: 10.1021/je000106+.

Anindra Mazumdar, James Scott Kain (2015): pH adjustment within gasification system. Patent: US9108869 B2

Ávila Filho, Salvador; Nascimento Lopes, José Rafael (2015): Cooling Water Systems: Mineral Scales and Deposits: 499–531, DOI: 10.1016/B978-0-444-63228-9.00019-X

Carroll, John J.; Mather, Alan E. (1989): The solubility of hydrogen sulphide in water from 0 to 90°C and pressures to 1 MPa. Geochimica et Cosmochimica Acta, 53 (6): 1163–1170. DOI: 10.1016/0016-7037(89)90053-7.

Chih-Hao Mark Tsang (2003): Gasification process employing ammonia injection for minimizing waste water treatment. Patent: WO2003022959 A1.

Dasgupta, Purnendu K.; Dong, Shen (1986): Solubility of ammonia in liquid water and generation of trace levels of standard gaseous ammonia. Atmospheric Environment, (1967) 20 (3): 565–570. DOI: 10.1016/0004-6981(86)90099-5.

David A. Dzombak, Rajat S. Ghosh, George M. Wong-Chong (2006): Cyanide in water and soil. Chemistry, risk, and management. CRC Press. ISBN: 9781566706667

David Bell, Brian Towler, Maohong Fan (2011): Coal Gasification and Its Applications (1st Edition). Oxford, U.K.Elsevier. ISBN: 9781437778519

Edwards, T. J.; Maurer, Gerd; Newman, John; Prausnitz, J. M. (1978): Vapor-liquid equilibria in multicomponent aqueous solutions of volatile weak electrolytes. AIChE Journal, 24 (6): 966–976. DOI: 10.1002/aic.690240605.

Falcke, Tarrant J.; Hoadley, Andrew F.A.; Brennan, David J.; Sinclair, Sarah E. (2011): The sustainability of clean coal technology: IGCC with / without CCS. Process Safety and Environmental Protection, 89 (1): 41–52. DOI: 10.1016/j.psep.2010.08.002.

Francis L. Smith (2007): Avoid Common Pitfalls When Using Henry's Law. Chemical Engineering Progress (CEP): 33-39. http://ws680.nist.gov/publication/get_pdf.cfm?pub_id=50449.

Gräbner, Martin (2015): Industrial Coal Gasification Technologies Covering Baseline and High-Ash Coal. Weinheim: Wiley-VCH Verlag GmbH & Co. KGaA. ISBN: 978-3-527-33690-6

Hales, Jeremy M.; Drewes, Dennis R. (1979): Solubility of ammonia in water at low concentrations. Atmospheric Environment, 13 (8): 1133 – 1147. DOI: 10.1016/0004-6981(79)90037-4.

Higman, Chris; van der Burgt, Maarten (2003): Gasification. Boston: Elsevier/Gulf Professional Publishing.

Hiller, Heinz; Reimert, Rainer; Marschner, Friedemann; Renner, Hans-Joachim; Boll, Walter; Supp, Emil et al. (2000): Ullmann's Encyclopedia of Industrial Chemistry. Gas Production. Weinheim, Germany: Wiley-VCH Verlag GmbH & Co. KGaA. ISBN: 9783527306732

Jacob A. Moulijn, Michiel Makkee, Annelies E. van Diepen (2013): Chemical process technology, 2nd Edition. ISBN: 978-1-4443-2024-4

Kaldis, S. P.; Skodras, G.; Sakellaropoulos, G. P. (2004): Energy and capital cost analysis of CO_2 capture in coal IGCC processes via gas separation membranes. Fuel Processing Technology, 85 (5): 337–346. DOI: 10.1016/S0378-3820(03)00204-2.

Kamps, Álvaro Pérez-Salado; Balaban, Anton; Jödecke, Michael; Kuranov, George; Smirnova, Natalia A.; Maurer, Gerd (2001): Solubility of Single Gases Carbon Dioxide and Hydrogen Sulfide in Aqueous Solutions of N -Methyldiethanolamine at Temperatures from 313 to 393 K and Pressures up to 7.6 MPa: New Experimental Data and Model Extension. Industrial & Engineering Chemistry Research, 40 (2): 696–706. DOI: 10.1021/ie000441r.

Kimberly K. Denney, Norman G. Block (1989): Control of pH in water quench of a partial oxidation process. Patent: US4854942 A.

Kuranov, George; Rumpf, Bernd; Smirnova, Natalia A.; Maurer, Gerd (1996): Solubility of Single Gases Carbon Dioxide and Hydrogen Sulfide in Aqueous Solutions of N -Methyldiethanolamine in the Temperature Range 313–413 K at Pressures up to 5 MPa. . Industrial & Engineering Chemistry Research, 35 (6): 1959–1966. DOI: 10.1021/ie950538r.

Leppälahti, Jukka; Kurkela, Esa; Simell, Pekka; Ståhlberg, Pekka (1993): Advances in Thermochemical Biomass Conversion. Formation and Removal of Nitrogen Compounds in Gasification Processes: 160-174. A. V. Bridgwater.Dordrecht: Springer Netherlands. ISBN: 978-94-011-1336-6

Li, Sheng; Gao, Lin; Zhang, Xiaosong; Lin, Hu; Jin, Hongguang (2012): Evaluation of cost reduction potential for a coal based polygeneration system with CO2 capture. Energy, 45 (1): 101–106. DOI: 10.1016/j.energy.2011.11.059.

Ma, Jian; Dasgupta, Purnendu K.; Blackledge, William; Boss, Gerry R. (2010): Temperature dependence of Henry's law constant for hydrogen cyanide. Generation of trace standard gaseous hydrogen cyanide. Environmental Science & Technology, 44 (8): 3028–3034. DOI: 10.1021/es1001192.

NALCO (2008): Cooling Water Treatment: Company report

Nič, Miloslav; Jirát, Jiří; Košata, Bedřich; Jenkins, Aubrey; McNaught, Alan (2009): IUPAC Compendium of Chemical Terminology. Research Triangle Park, NC: IUPAC. ISBN: 0-9678550-9-8

Ordorica-Garcia, Guillermo; Wong, Sam; Faltinson, John; Singh, Surindar (2009): CO_2 capture retrofit options for a gasification-based integrated bitumen extraction and upgrading facility. Energy Procedia, 1 (1): 3977–3984. DOI: 10.1016/j.egypro.2009.02.202.

Perry, Robert H.; Green, Don W.; Maloney, James O. (1984): Perry's chemical engineers' handbook. 6th Edition. London: McGraw-Hill. ISBN: 0-07-049479-7

Qian Zhu (2015): High temperature syngas coolers. IEA Clean Coal Centre. United Kingdom. https://www.usea.org/sites/default/files/media/High%20temperature%20Syngas%20coolers%20-%20ccc257.pdf.

Rumpf, B.; Maurer, G. (1992): Solubilities of hydrogen cyanide and sulfur dioxide in water at temperatures from 293.15 to 413.15 K and pressures up to 2.5 MPa. Fluid Phase Equilibria, 81: 241–260. DOI: 10.1016/0378-3812(92)85155-2.

Rumpf, B.; Pérez-Salado Kamps, Á.; Sing, R.; Maurer, G. (1999): Simultaneous solubility of ammonia and hydrogen sulfide in water at temperatures from 313 K to 393 K. Fluid Phase Equilibria, 158:923-932. DOI: 10.1016/S0378-3812(99)00110-7.

Rumpf, B.; Xia, J.; Maurer, G. (1997): An experimental investigation of the solubility of carbon dioxide in aqueous solutions containing sodium nitrate or ammonium nitrate at temperatures from 313 K to 433 K and pressures up to 10 MPa. The Journal of Chemical Thermodynamics, 29 (10): 1101–1111. DOI: 10.1006/jcht.1997.0225.

Salkuyeh, Yaser Khojasteh; Adams, Thomas A. (2013): Combining coal gasification, natural gas reforming, and external carbonless heat for efficient production of gasoline and diesel with CO_2 capture and sequestration. Energy Conversion and Management, 74: 492–504. DOI: 10.1016/j.enconman.2013.07.023.

Sander, R. (2015): Compilation of Henry's law constants (version 4.0) for water as solvent. Atmospheric Chemistry and Physics, 15 (8): 4399–4981. DOI: 10.5194/acp-15-4399-2015.

Schäfer, Dirk; Vogt, Mathias; Kamps, Álvaro Pérez-Salado; Maurer, Gerd (2007): Solubility of ammonia in liquid mixtures of (water+methanol). Fluid Phase Equilibria, 261 (1-2): 306–312. DOI: 10.1016/j.fluid.2007.07.049.

Tanaka, Yoshinobu (2010): Water dissociation reaction generated in an ion exchange membrane. Journal of Membrane Science, 350 (1-2): 347–360. DOI: 10.1016/j.memsci.2010.01.010.

Wright, R. H.; Maass, O. (1932): The electrical conductivity of aqueous solutions of hydrogen sulphide and the state of the dissolved gas. Canadian Journal of Research, 6 (6):588–595. DOI: 10.1139/cjr32-047.

Xia, Jianzhong; Rumpf, Bernd; Maurer, Gerd (1999): Solubility of carbon dioxide in aqueous solutions containing sodium acetate or ammonium acetate at temperatures from 313 to 433 K and pressures up to 10 MPa. Fluid Phase Equilibria, 155 (1): 107–125. DOI: 10.1016/S0378-3812(98)00464-6.

Yokozeki, A.; Shiflett, Mark B. (2007): Vapor–liquid equilibria of ammonia + ionic liquid mixtures. Applied Energy, 84 (12): 1258–1273. DOI: 10.1016/j.apenergy.2007.02.005.

Yoo, Ki-Pung; Lee, Soo Yong; Lee, Won Hong (1986): Ionization and Henry's law constants for volatile, weak electrolyte water pollutants. Korean Journal of Chemical Engineering, 3 (1): 67–72. DOI: 10.1007/BF02697525.

Chapter 5

Akiya, Naoko; Savage, Phillip E. (1998): Role of water in formic acid decomposition. AIChE Journal, 44 (2): 405–415. DOI: 10.1002/aic.690440217.

Alexander, Elliot R.; Wildman, Ruth Bowman (1948): Studies on the Mechanism of the Leuckart Reaction. Journal of the American Chemical Society, 70 (3): 1187–1189. DOI: 10.1021/ja01183a091.

Basagiannis, A. C.; Verykios, X. E. (2007): Catalytic steam reforming of acetic acid for hydrogen production. International Journal of Hydrogen Energy, 32 (15): 3343–3355. DOI: 10.1016/j.ijhydene.2007.04.039.

Becker, Brooks; Davidson, Arthur W. (1963): The Systems Formic Acid-Ammonia and Propionic Acid-Ammonia. Journal of the American Chemical Society, 85 (2): 157–159. DOI: 10.1021/ja00885a010.

Bell, Julie L.S.; Palmer, Donald A.; Barnes, H. L.; Drummond, S. E. (1994): Thermal decomposition of acetate. III. Catalysis by mineral surfaces. Geochimica et Cosmochimica Acta, 58 (19): 4155–4177. DOI: 10.1016/0016-7037(94)90271-2.

Bennett, Chris J.; Kaiser, Ralf I. (2007): The Formation of Acetic Acid (CH_3COOH) in Interstellar Ice Analogs. The Astrophysical Journal, 660 (2): 1289–1295. DOI: 10.1086/513267.

Bjerre, Anne Belinda; Soerensen, Emil (1992): Thermal decomposition of dilute aqueous formic acid solutions. Industrial & Engineering Chemistry Research, 31 (6): 1574–1577. DOI: 10.1021/ie00006a022.

Dar, Bashir A.; Wani, Abubakar; Rather, Shabir A.; Singh, Baldev (2013): Isothermal Studies of Sorption of Acetic Acid from Waste Water Using Shed Needles from Pine Trees. Arabian Journal for Science and Engineering, 38 (10): 2595–2599. DOI: 10.1007/s13369-012-0492-y.

David W. Savage, Robert P. Cahn, Norman N. Li (1973): Separation process. Patent: CA 1036724 A.

Gangadwala, J.; Radulescu, G.; Kienle, A.; Sundmacher, K. (2007): Computer aided design of reactive distillation processes for the treatment of waste waters polluted with acetic acid. Computers & Chemical Engineering, 31 (11): 1535–1547. DOI: 10.1016/j.compchemeng.2007.01.002.

Gangadwala, Jignesh; Radulescu, Gabriel; Kienle, Achim; Steyer, Frank; Sundmacher, Kai (2008): New processes for recovery of acetic acid from waste water. Clean Technologies and Environmental Policy, 10 (3): 245–254. DOI: 10.1007/s10098-007-0101-z.

Gibson, Harry W. (1969): Chemistry of formic acid and its simple derivatives. In: Chemical Reviews, 69 (5) 673–692. DOI: 10.1021/cr60261a005.

Gräbner, Martin (2015) Industrial Coal Gasification Technologies Covering Baseline and High-Ash Coal. Weinheim: Wiley-VCH Verlag GmbH & Co. KGaA. ISBN: 978-3-527-33690-6

Higman, Chris; van der Burgt, Maarten (2003): Gasification. Boston: Elsevier/Gulf Professional Publishing.

Iglesia, Enrique; Spivey, James J.; Fleisch, T. H. (2001): Natural gas conversion VI. Proceedings of the 6th Natural Gas Conversion Symposium, June 17-22, 2001, Elsevier (Studies in surface science and catalysis, 136, page 480).

Ivan Philip Greager, Laura J. Silva, Graham LEA (2014): Methods of making purified water from the fischer-tropsch process. Patent: WO 2016044348 A1.

Kittel, J.; Fleury, E.; Vuillemin, B.; Gonzalez, S.; Ropital, F.; Oltra, R. (2012): Corrosion in alkanolamine used for acid gas removal. From natural gas processing to CO_2 capture. Materials and Corrosion, 63 (3): 223 – 230. DOI: 10.1002/maco.201005847.

Lei, Zhigang; Li, Chengyue; Li, Yingxia; Chen, Biaohua (2004): Separation of acetic acid and water by complex extractive distillation. Separation and Purification Technology, 36 (2): 131–138. DOI: 10.1016/S1383-5866(03)00208-9.

Li, Yang; Liu, Chang-Jun; Eliasson, Baldur; Wang, Yu (2002): Synthesis of Oxygenates and Higher Hydrocarbons Directly from Methane and Carbon Dioxide Using Dielectric-Barrier Discharges: Product Distribution. Energy Fuels, 16 (4): 864–870. DOI: 10.1021/ef0102770.

Lino Locatelli, Lino Carnelli, Roberta Miglio, Roberto Zennaro (2008): Process for the purification of an aqueous stream coming from the Fischer-Tropsch reaction. Patent: US 9403693 B2.

Lu, Man; Zeng, Xu; Cao, Jiang-Lin; Huo, Zhi-Bao; Jin, Fang-Ming (2011): Production of formic and acetic acids from phenol by hydrothermal oxidation. Research on Chemical Intermediates, 37 (2-5): 201–209. DOI: 10.1007/s11164-011-0243-9.

Luis Kohler, Gert du Plessis, Francois Toit, Edward Koper, Trevor Phillips, Janette Walt (2004): Method of purifying Fischer-Tropsch derived water. Patent: US 20050131084 A1.

Maiella, P. G.; Brill, T. B. (1998): Spectroscopy of Hydrothermal Reactions. 10. Evidence of Wall Effects in Decarboxylation Kinetics of 1.00 m HCO_2X (X = H, Na) at 280–330 °C and 275 bar. The journal of physical chemistry. A, 102 (29): 5886–5891. DOI: 10.1021/jp981165l.

Man Lu, Xu Zeng, Jiang-Lin Cao, Zhi-Bao Huo, Fang-Ming Jin. (2011): Production of formic and acetic acids from phenol by hydrothermal oxidation. Research on Chemical Intermediates, 37: 201 – 209. DOI: 10.1007/s11164-011-0243-9

McCollom, Thomas M.; Seewald, Jeffrey S. (2003): Experimental constraints on the hydrothermal reactivity of organic acids and acid anions. I. Formic acid and formate. Geochimica et Cosmochimica Acta, 67 (19): 3625–3644. DOI: 10.1016/S0016-7037(03)00136-4.

McCollom, Thomas M.; Seewald, Jeffrey S. (2003): Experimental study of the hydrothermal reactivity of organic acids and acid anions. II. Acetic acid, acetate, and valeric acid. Geochimica et Cosmochimica Acta, 67 (19): 3645–3664. DOI: 10.1016/S0016-7037(03)00135-2.

Nguyen, Vinh Son; Orlando, Thomas M.; Leszczynski, Jerzy; Nguyen, Minh Tho (2013): Theoretical study of the decomposition of formamide in the presence of water molecules. The journal of physical chemistry. A, 117 (12): 2543–2555. DOI: 10.1021/jp312853j.

Özcan, Önder; İnci, İsmail; Aşçi, Yavuz Selim (2013): Multiwall Carbon Nanotube for Adsorption of Acetic Acid. Journal of Chemical & Engineering Data, 58 (3): 583–587. DOI: 10.1021/je301064t.

Park, Jung Mee; Laio, Alessandro; Iannuzzi, Marcella; Parrinello, Michele (2006): Dissociation mechanism of acetic acid in water. Journal of the American Chemical Society, 128 (35): 11318–11319. DOI: 10.1021/ja060454h.

Pearson, P.; Cousins, A. (2016): Absorption-Based Post-combustion Capture of Carbon Dioxide. Assessment of corrosion in amine-based post-combustion capture of carbon dioxide systems. 439 – 463. Elsevier.

Pitchai, R.; Klier, K. (1986): Partial Oxidation of Methane. Catalysis Reviews, 28 (1): 3–88. DOI: 10.1080/03602458608068085.

Rablen, Paul R.; Lockman, Jeffrey W.; Jorgensen, William L. (1998): Ab Initio Study of Hydrogen-Bonded Complexes of Small Organic Molecules with Water. The journal of physical chemistry. A, 102 (21): 3782–3797. DOI: 10.1021/jp980708o.

Silvia Imberti, Daniel T Bowron (2010): Formic and acetic acid aggregation in the liquid state. Journal of physics. Condensed matter: an Institute of Physics journal, 22 (40) 404212. DOI: 10.1088/0953-8984/22/40/404212.

Soffientini, Stefano; Bernasconi, Leonardo; Imberti, Silvia (2015): The hydration of formic acid and acetic acid. Journal of Molecular Liquids, 205: 85–92. DOI: 10.1016/j.molliq.2014.11.030.

Tran, Thu; Brown, Bruce; Nešić, Srdjan; Tribollet, Bernard (2014): Investigation of the Electrochemical Mechanisms for Acetic Acid Corrosion of Mild Steel. Corrosion, 70 (3): 223–229. DOI: 10.5006/0933.

Wang, Jian-guo; Liu, Chang-Jun; Eliassion, Baldur (2004): Density Functional Theory Study of Synthesis of Oxygenates and Higher Hydrocarbons from Methane and Carbon Dioxide Using Cold Plasmas. Energy Fuels, 18 (1): 148–153. DOI: 10.1021/ef0300949.

Wang, L. K. (2005): Physicochemical Treatment Processes. 2nd edition. Springer (Handbook of Environmental Engineering, Volume 3). http://www.springer.com/gb/book/9781588291653.

Webster, G. H., Von Klock, B., Vuong, D.-C., Stevenson, J. S., Johnson, S. R. (2000): Minimizing evaporator scaling and recovery of salts during gasification. Patent: US 6 086 722.

Wieringa, K. T. (1939): The formation of acetic acid from carbon dioxide and hydrogen by anaerobic spore-forming bacteria. Antonie van Leeuwenhoek, 6 (1): 251–262. DOI: 10.1007/BF02146190.

William A. Shaw, Mitchell Adam Edwards, Jeffrey Dean Brosdal (2014): Process of scrubbing volatiles from evaporator water vapor. Patent: US 8778037 B2.

Wu, Jian-Feng; Yu, Si-Min; Wang, Wei David; Fan, Yan-Xin; Bai, Shi; Zhang, Chuan-Wei et al. (2013): Mechanistic insight into the formation of acetic acid from the direct conversion of methane and carbon dioxide on zinc-modified H-ZSM-5 zeolite. Journal of the American Chemical Society, 135 (36): 13567–13573. DOI: 10.1021/ja406978q.

Xu, Zhanping; Afacan, Artin; Chuang, Karl T. (1999): Removal of acetic acid from water by catalytic distillation. Part 1. Experimental studies. The Canadian Journal of Chemical Engineering, 77 (4): 676–681. DOI: 10.1002/cjce.5450770408.

Yu, Jianli; Savage, Phillip E. (1998): Decomposition of Formic Acid under Hydrothermal Conditions. Industrial & Engineering Chemistry Research, 37 (1): 2–10. DOI: 10.1021/ie970182e.

Zhang, Fan; Wang, Meijuan; Zhu, Lingjun; Wang, Shurong; Zhou, Jinsong; Luo, Zhongyang (2017): A comparative research on the catalytic activity of La2O3 and γ-Al2O3 supported catalysts for acetic acid steam reforming. International Journal of Hydrogen Energy, 42 (6): 3667–3675. DOI: 10.1016/j.ijhydene.2016.06.264.

Zhang, Huanhuan; Wang, Yuming; Bai, Peng; Guo, Xianghai; Ni, Xiuxiu (2016): Adsorptive Separation of Acetic Acid from Dilute Aqueous Solutions. Adsorption Kinetic, Isotherms, and Thermodynamic Studies. Journal of Chemical & Engineering Data, 61 (1): 213–219. DOI: 10.1021/acs.jced.5b00481.

Chapter 6

Abdul R. Khan, Yanlong Shi, Carlo Cioffi (2004): Reduction of ammonia formation during fuel reforming. Patent: WO2004043851 A1.

Cao, Jing-Pei; Li, Liu-Yun; Morishita, Kayoko; Xiao, Xian-Bin; Zhao, Xiao-Yan; Wei, Xian-Yong; Takarada, Takayuki (2013): Nitrogen transformations during fast pyrolysis of sewage sludge. Fuel, 104 (110): 1–6. DOI: 10.1016/j.fuel.2010.08.015.

Cao, Jing-Pei; Zhao, Xiao-Yan; Morishita, Kayoko; Wei, Xian-Yong; Takarada, Takayuki (2010): Fractionation and identification of organic nitrogen species from bio-oil produced by fast pyrolysis of sewage sludge. Bioresource technology, 101 (19): 7648–7652. DOI: 10.1016/j.biortech.2010.04.073.

Cataldo, Franco; Patanè, Giacomo; Compagnini, Giuseppe (2009): Synthesis of HCN Polymer from Thermal Decomposition of Formamide. Journal of Macromolecular Science, Part A 46 (11): 1039–1048. DOI: 10.1080/10601320903245342.

Chang, L.-P.; Xie, Z.-L.; Xie, K.-C. (2006): Study on the Formation of NH_3 and HCN during the gasification of brown coal in steam. Process Safety and Environmental Protection, 84 (6): 446–452. DOI: 10.1205/psep05019.

Chang, Liping; Xie, Zongli; Xie, Ke-Chang; Pratt, Kerry C.; Hayashi, Jun-ichiro; Chiba, Tadatoshi; Li, Chun-Zhu (2003): Formation of NOx precursors during the pyrolysis of coal and biomass. Part VI. Effects of gas atmosphere on the formation of NH3 and HCN. Fuel, 82 (10): 1159–1166. DOI: 10.1016/S0016-2361(03)00024-3.

Fullana, Andres; Conesa, Juan A.; Font, Rafael; Martín-Gullón, Ignacio (2003): Pyrolysis of sewage sludge. Nitrogenated compounds and pretreatment effects. Journal of Analytical and Applied Pyrolysis, 68-69: 561–575. DOI: 10.1016/S0165-2370(03)00052-4.

Gräbner, Martin (2015) Industrial Coal Gasification Technologies Covering Baseline and High-Ash Coal. Weinheim: Wiley-VCH Verlag GmbH & Co. KGaA. ISBN: 978-3-527-33690-6

Hämäläinen, Jouni P.; Aho, Martti J. (1996): Conversion of fuel nitrogen through HCN and NH_3 to nitrogen oxides at elevated pressure. Fuel, 75 (12): 1377–1386. DOI: 10.1016/0016-2361(96)00100-7.

Hämäläinen, Jouni P.; Aho, Martti J.; Tummavuori, Jouni L. (1994): Formation of nitrogen oxides from fuel-N through HCN and NH_3. A model-compound study. Fuel, 73 (12): 1894–1898. DOI: 10.1016/0016-2361(94)90218-6.

Hansson, Karl-Martin; Samuelsson, Jessica; Tullin, Claes; Åmand, Lars-Erik (2004): Formation of HNCO, HCN, and NH3 from the pyrolysis of bark and nitrogen-containing model compounds. Combustion and Flame, 137 (3): 265–277. DOI: 10.1016/j.combustflame.2004.01.005.

Higman, Chris; van der Burgt, Maarten (2003): Gasification. Boston: Elsevier/Gulf Professional Publishing.

Hongrapipat, J.; Yip, A.C.K.; Marshall, A. T.; Saw, W. L.; Pang, S. (2014): Investigation of simultaneous removal of ammonia and hydrogen sulphide from producer gas in biomass gasification by titanomagnetite. Fuel, 135: 235–242. DOI: 10.1016/j.fuel.2014.06.037.

Kambara, Shinji; Takarada, Takayuki; Yamamoto, Yasuhiro; Kato, Kunio (1993): Relation between functional forms of coal nitrogen and formation of nitrogen oxide (NOx) precursors during rapid pyrolysis. Energy Fuels, 7 (6): 1013–1020. DOI: 10.1021/ef00042a045.

Leppälahti, Jukka (1995): Formation of NH_3 and HCN in slow-heating-rate inert pyrolysis of peat, coal and bark. Fuel, 74 (9): 1363–1368. DOI: 10.1016/0016-2361(95)00091-I.

Liu, Huan; Yi, Linlin; Hu, Hongyun; Xu, Kai; Zhang, Qiang; Lu, Geng; Yao, Hong (2017): Emission control of NOx precursors during sewage sludge pyrolysis using an integrated pretreatment of Fenton peroxidation and CaO conditioning. Fuel, 195: 208–216. DOI: 10.1016/j.fuel.2017.01.067.

Ma, Wenchao; Du, Guiyue; Li, Jian; Fang, Yuanhao; Hou, Li'an; Chen, Guanyi; Ma, Degang (2017): Supercritical water pyrolysis of sewage sludge. Waste Management, 59: 371–378. DOI: 10.1016/j.wasman.2016.10.053.

Patnaik Pradyot (2003): Handbook of inorganic chemicals. 1st Edition. ISBN-13: 978-0070494398 http://www.loc.gov/catdir/bios/mh041/2002029526.html.

Schweitzer, Daniel; Gredinger, Andreas; Schmid, Max; Waizmann, Gebhard; Beirow, Marcel; Spörl, Reinhold; Scheffknecht, Günter (2017): Steam gasification of wood pellets, sewage sludge and manure. Gasification performance and concentration of impurities. Biomass and Bioenergy. DOI: 10.1016/j.biombioe.2017.02.002.

Simell, Pekka; Kurkela, Esa; Ståhlberg, Pekka; Hepola, Jouko (1996): Catalytic hot gas cleaning of gasification gas. Catalysis Today, 27 (1-2): 55–62. DOI: 10.1016/0920-5861(95)00172-7.

Slack, A. V.; James, G. R. (1973): Ammonia, Part 2. Fertilizer science and technology series, Volume 2.

Thomsen, Tobias Pape; Sarossy, Zsuzsa; Gobel, Benny; Stoholm, Peder; Ahrenfeldt, Jesper; Frandsen, Flemming Jappe; Henriksen, Ulrik Birk (2017): Low temperature circulating fluidized bed gasification and co-gasification of municipal sewage sludge. Part 1. Process performance and gas product characterization. Waste Management, 66: 123–133. DOI: 10.1016/j.wasman.2017.04.028.

Uebel, Konrad; Rößger, Philip; Prüfert, Uwe; Richter, Andreas; Meyer, Bernd (2016a): A new CO conversion quench reactor design. Fuel Processing Technology, 148: 198–208. DOI: 10.1016/j.fuproc.2016.02.022.

Uebel, Konrad; Rößger, Philip; Prüfert, Uwe; Richter, Andreas; Meyer, Bernd (2016b): CFD-based multi-objective optimization of a quench reactor design. Fuel Processing Technology, 149: 290–304. DOI: 10.1016/j.fuproc.2016.04.008.

Xu, Deshun; Lewis, Randy S. (2012): Syngas fermentation to biofuels. Effects of ammonia impurity in raw syngas on hydrogenase activity. Biomass and Bioenergy, 45: 303–310. DOI: 10.1016/j.biombioe.2012.06.022.

Chapter 7

Allou, Lyassine; El Maimouni, Lahcen; Le Calvé, Stéphane (2011): Henry's law constant measurements for formaldehyde and benzaldehyde as a function of temperature and water composition. Atmospheric Environment, 45 (17): 2991–2998. DOI: 10.1016/j.atmosenv.2010.05.044.

Am Daifullah, Abdel Hakim; Mohamed, Mohamed Mokhtar (2004): Degradation of benzene, toluene ethylbenzene andp-xylene (BTEX) in aqueous solutions using UV/H$_2$O$_2$ system. Journal of Chemical Technology and Biotechnology, 79 (5): 468–474. DOI: 10.1002/jctb.992.

André Steynberg, Mark Dry (2006): Fischer-Tropsch technology. (Studies in surface science and catalysis, 152). Reprinted. Amsterdam: Elsevier http://www.loc.gov/catdir/enhancements/fy0634/2006274114-d.html.

Asadullah, Mohammad (2014): Biomass gasification gas cleaning for downstream applications. A comparative critical review. Renewable and Sustainable Energy Reviews, 40: 118–132. DOI: 10.1016/j.rser.2014.07.132.

Bassil, Georgio; Mokbel, Ilham; Abou Naccoul, Ramy; Stephan, Juliette; Jose, Jacques; Goutaudier, Christelle (2012): Tar removal from biosyngas in the biomass gasification process. (Liquid+liquid) equilibrium {water+solvent (paraxylene and methyl hexadecanoate)+model molecules of tar (benzene, toluene, phenol)}. The Journal of Chemical Thermodynamics, 48: 123–128. DOI: 10.1016/j.jct.2011.12.009.

Bharadwaj, S. S.; Schmidt, L. D. (1995): Catalytic partial oxidation of natural gas to syngas. Fuel Processing Technology, 42 (2-3): 109–127. DOI: 10.1016/0378-3820(94)00098-E.

Bhavya, B.; Singh, R.; Bhaskar, T. (2015): Gasification for Synthetic Fuel Production: Preparation of feedstocks for gasification for synthetic liquid fuel production. Elsevier: 57–71.

Bruinsma, O.S.L.; Moulijn, J. A. (1988): The pyrolytic formation of polycyclic aromatic hydrocarbons from benzene, toluene, ethylbenze,e, styrene, phenylacetylene and n-decane in relation to fossil fuels utilization. Fuel Processing Technology, 18 (3): 213–236. DOI: 10.1016/0378-3820(88)90048-3.

Cavaliere, A.; Barbella, R.; Ciajolo, A.; D'anna, A.; Ragucci, R. (1994): Fuel and soot oxidation in diesel-like conditions. Symposium (International) on Combustion, 25 (1): 167–174. DOI: 10.1016/S0082-0784(06)80641-7.

Coll, Roberto; Salvadó, Joan; Farriol, Xavier; Montané, Daniel (2001): Steam reforming model compounds of biomass gasification tars: conversion at different operating conditions and tendency

towards coke formation. Fuel Processing Technology, 74 (1): 19–31. DOI: 10.1016/S0378-3820(01)00214-4.

Coll, Roberto; Salvadó, Joan; Farriol, Xavier; Montané, Daniel (2001): Steam reforming model compounds of biomass gasification tars: conversion at different operating conditions and tendency towards coke formation. Fuel Processing Technology, 74 (1): 19–31. DOI: 10.1016/S0378-3820(01)00214-4.

Comandini, A.; Malewicki, T.; Brezinsky, K. (2012): Chemistry of polycyclic aromatic hydrocarbons formation from phenyl radical pyrolysis and reaction of phenyl and acetylene. The Journal of Physical Chemistry. A, 116 (10): 2409–2434. DOI: 10.1021/jp207461a.

Cunliffe, Adrian M.; Williams, Paul T. (1998): Composition of oils derived from the batch pyrolysis of tyres. Journal of Analytical and Applied Pyrolysis, 44 (2): 131–152. DOI: 10.1016/S0165-2370(97)00085-5.

Cuoci, Alberto; Frassoldati, Alessio; Faravelli, Tiziano; Jin, Hanfeng; Wang, Yizun; Zhang, Kuiwen et al. (2013): Experimental and detailed kinetic modeling study of PAH formation in laminar co-flow methane diffusion flames. Proceedings of the Combustion Institute, 34 (1): 1811–1818. DOI: 10.1016/j.proci.2012.05.085.

D'anna, A.; Kent, J. H. (2008): A model of particulate and species formation applied to laminar, nonpremixed flames for three aliphatic-hydrocarbon fuels. Combustion and Flame, 152 (4): 573–587. DOI: 10.1016/j.combustflame.2007.08.003.

Dórea, Haroldo S.; Bispo, José R.L.; Aragão, Kennedy A.S.; Cunha, Bruno B.; Navickiene, Sandro; Alves, José P.H. et al. (2007): Analysis of BTEX, PAHs and metals in the oilfield produced water in the State of Sergipe, Brazil. Microchemical Journal, 85 (2): 234–238. DOI: 10.1016/j.microc.2006.06.002.

Frenklach, Michael (2002): Reaction mechanism of soot formation in flames: Physical Chemistry Chemical Physics, 4 (11): 2028–2037. DOI: 10.1039/b110045a.

Frenklach, Michael; Wang, Hai (1991): Detailed modeling of soot particle nucleation and growth. Symposium (International) on Combustion, 23 (1): 1559–1566. DOI: 10.1016/S0082-0784(06)80426-1.

Gai, Hengjun; Jiang, Yanbin; Qian, Yu; Kraslawski, Andrzej (2008): Conceptual design and retrofitting of the coal-gasification wastewater treatment process. Chemical Engineering Journal, 138 (1-3): 84–94. DOI: 10.1016/j.cej.2007.05.032.

Gong, Miao; Zhu, Wei; Zhang, Huiwen; Su, Ying; Fan, Yujie (2016): Polycyclic aromatic hydrocarbon formation from gasification of sewage sludge in supercritical water. The concentration distribution and effect of sludge properties. The Journal of Supercritical Fluids, 113: 112–118. DOI: 10.1016/j.supflu.2016.03.021.

Heonki Kim, Michael D. Annable, and P. Suresh C. Rao (1998): Influence of Air–Water Interfacial Adsorption and Gas-Phase Partitioning on the Transport of Organic Chemicals in Unsaturated Porous Media. Environmental Science & Technology, 32 (9): 1253–1259. DOI: 10.1021/es970868y.

Hermann Hofbauer, Karl Ripfel-Nitsche, Reinhard Rauch (2007): Gas Cleaning for Synthesis Applications. Work Package 2E: "Gas treatment". Vienna University of Technology, Institute of Chemical Engineering. ThermalNet network, Intelligent Energy – Europe Commision programme. https://ec.europa.eu/energy/intelligent/projects/en/projects/thermalnet.

Higman Christopher, Siegfried Bajohr and Rainer Reimert. (2002): Gasify POX Soot for Reduced Costs. Pittsburgh (19th Annual International Pittsburgh Coal Conference). http://www.higman.de/gasification/papers/pittsburgh.pdf.

Higman, Chris; van der Burgt, Maarten (2003): Gasification. Boston: Elsevier/Gulf Professional Publishing.

Hiller, Heinz; Reimert, Rainer; Marschner, Friedemann; Renner, Hans-Joachim; Boll, Walter; Supp, Emil et al. (2000): Gas Production. Ullmann's Encyclopedia of Industrial Chemistry. Weinheim, Germany: Wiley-VCH Verlag GmbH & Co. KGaA.

Holmen, Anders; Olsvik, Ola; Rokstad, O. A. (1995): Pyrolysis of natural gas: chemistry and process concepts. Fuel Processing Technology, 42 (2-3): 249–267. DOI: 10.1016/0378-3820(94)00109-7.

Homann, K. H. (1985): Formation of large molecules, particulates and ions in premixed hydrocarbon flames; Progress and unresolved questions. In: Symposium (International) on Combustion, 20 (1): 857–870. DOI: 10.1016/S0082-0784(85)80575-0.

Houben MP, Neeft J, Daey Ouwens C: An analysis and experimental investigation of the cracking and polymerisation of tar. 12TH European Conference and Technical. Exhibition on Biomass for Energy, Industry and Climate Protection, 581–584. http://infohouse.p2ric.org/ref/35/34185.pdf.

Hsu, Wei Ting; Liu, Mei Chen; Hung, Pao Chen; Chang, Shu Hao; Chang, Moo Been (2016): PAH emissions from coal combustion and waste incineration. Journal of Hazardous Materials, 318: 32–40. DOI: 10.1016/j.jhazmat.2016.06.038.

Hu, Yanjun; Li, Guojian; Yan, Mi; Ping, Chuanjuan; Ren, Jianli (2014): Investigation into the distribution of polycyclic aromatic hydrocarbons (PAHs) in wastewater sewage sludge and its resulting pyrolysis bio-oils. Science of the Total Environment, 473-474: 459–464. DOI: 10.1016/j.scitotenv.2013.12.051.

Jin, H.; Yang, X.; Yu, H.; Yin, D. (1999): Identification of Ammonia and Volatile Phenols as Primary Toxicants in a Coal Gasification Effluent. Bulletin of Environmental Contamination and Toxicology, 63 (3): 399–406. DOI: 10.1007/s001289900994

John W. Byrne, William B. Dolan, Kenneth F. Butwell (2001): Claus feed gas hydrocarbon removal. Patent: US 6508863 B1.

Kennedy, Ian M. (1997): Models of soot formation and oxidation. Progress in Energy and Combustion Science, 23 (2): 95–132. DOI: 10.1016/S0360-1285(97)00007-5.

Kim, Jeong-Chul; Cho, Kanghee; Ryoo, Ryong (2014): High catalytic performance of surfactant-directed nanocrystalline zeolites for liquid-phase Friedel–Crafts alkylation of benzene due to external surfaces. Applied Catalysis A: General, 470: 420–426. DOI: 10.1016/j.apcata.2013.11.019.

Koltunov, Konstantin Yu.; Walspurger, Stéphane; Sommer, Jean (2004): Friedel–Crafts alkylation of benzene with α,β-unsaturated amides. Tetrahedron Letters, 45 (18): 3547–3549. DOI: 10.1016/j.tetlet.2004.03.067.

Lederer, J. (2015): Hydrogen or Soot? Partial Oxidation of High-boiling Hydrocarbon Wastes. Chemical and Biochemical Engineering Quarterly, 29 (1): 5–11. DOI: 10.15255/CABEQ.2014.2108.

Lin, Sheng H.; Huang, Cheng Y. (1999): Adsorption of BTEX from aqueous solution by macroreticular resins. Journal of Hazardous Materials, 70 (1-2): 21–37. DOI: 10.1016/S0304-3894(99)00148-X.

McEnally, Charles S.; Pfefferle, Lisa D.; Atakan, Burak; Kohse-Höinghaus, Katharina (2006): Studies of aromatic hydrocarbon formation mechanisms in flames. Progress towards closing the fuel gap. Progress in Energy and Combustion Science, 32 (3): 247–294. DOI: 10.1016/j.pecs.2005.11.003.

Melius, Carl F.; Miller, James A.; Evleth, Earl M. (1992): Unimolecular reaction mechanisms involving C3H4, C4H4, and C6H6 hydrocarbon species. Symposium (International) on Combustion, 24 (1): 621–628. DOI: 10.1016/S0082-0784(06)80076-7.

Michael Bachtler, Rudolf R. cord, Peter Passler, Olaf Scheidsteger, Werner Kastenhuber, Gerd Schlindwein, Rainer Konig (1998): Process for the production of acetylene and synthesis gas. Patent: US5824834 A.

Mohammed, Shabin; Raj, Abhijeet; Shoaibi, Ahmed Al (2016): Effects of fuel gas addition to Claus furnace on the formation of soot precursors. Combustion and Flame, 168: 240–254. DOI: 10.1016/j.combustflame.2016.03.008.

Olsvik, Ola; Billaud, Francis (1994): Thermal coupling of methane: A comparison between kinetic model data and experimental data. In: Thermochimica Acta, 232 (1): 155–169. DOI: 10.1016/0040-6031(94)80055-3.

Parkhurst, B. R.; Meyer, J. S.; DeGraeve, G. M.; Bergman, H. L. (1981): A reevaluation of the toxicity of coal conversion process waters. Bulletin of Environmental Contamination and Toxicology, 26 (1): 9–15. DOI: 10.1007/BF01622046.

Peng, Jianlin; Zhang, Yan; Yang, Xiaohong; Qi, Meiling (2016): High-resolution separation performance of poly(caprolactone)diol for challenging isomers of xylenes, phenols and anilines by capillary gas chromatography. Journal of Chromatography A, 1466: 148–154. DOI: 10.1016/j.chroma.2016.09.005.

Pinto, Filomena; André, Rui Neto; Carolino, Carlos; Miranda, Miguel (2014): Hot treatment and upgrading of syngas obtained by co-gasification of coal and wastes. Fuel Processing Technology, 126: 19–29. DOI: 10.1016/j.fuproc.2014.04.016.

Raimondi, A.; Fino, D.; Saracco, G. (2009): New concept for soot removal from a syngas mixture. Journal of Power Sources, 193 (1): 338–341. DOI: 10.1016/j.jpowsour.2009.01.036.

Raj Abhijeet; Sinha Sourab (2015): Reaction Mechanism for the Oxidation of Aromatic Contaminants Present in Feed Gas to Claus Process. Energy Procedia, 66: 61–64. DOI: 10.1016/j.egypro.2015.02.032.

Richter H.; Howard J.B (2000): Formation of polycyclic aromatic hydrocarbons and their growth to soot—a review of chemical reaction pathways. Progress in Energy and Combustion Science, 26 (4-6): 565–608. DOI: 10.1016/S0360-1285(00)00009-5.

S.V.B van Paasen, J.H. A. Kiel (2004): Tar formation in a fluidised-bed gasifier. Impact of fuel properties and operating conditions. Energieonderzoek Centrum Nederland (ECN) (ECN-E-08-087).

Sánchez, Nazly E.; Millera, Ángela; Bilbao, Rafael; Alzueta, María U. (2013): Polycyclic aromatic hydrocarbons (PAH), soot and light gases formed in the pyrolysis of acetylene at different temperatures. Effect of fuel concentration. Journal of Analytical and Applied Pyrolysis, 103: 126–133. DOI: 10.1016/j.jaap.2012.10.027.

Sepman, A.; Ögren, Y.; Gullberg, M.; Wiinikka, H. (2016): Development of TDLAS sensor for diagnostics of CO, H_2O and soot concentrations in reactor core of pilot-scale gasifier. Applied Physics B, 122 (2): 89. DOI: 10.1007/s00340-016-6319-x.

Seshadri, Kalyanasundaram; Frassoldati, Alessio; Cuoci, Alberto; Faravelli, Tiziano; Niemann, Ulrich; Weydert, Patrick; Ranzi, Eliseo (2011): Experimental and kinetic modeling study of combustion of JP-8, its surrogates and components in laminar premixed flows. Combustion Theory and Modelling, 15 (4): 569–583. DOI: 10.1080/13647830.2011.552635.

Shabin Mohammed, Abhijeet Raj, Ahmed Al Shoaibi, P Sivashanmugam. (2015): Formation of polycyclic aromatic hydrocarbons in Claus process from contaminants in H2S feed gas. Chemical Engineering Science, 137: 91–105. DOI: 10.1016/j.ces.2015.06.029.

Sostaric A.; Stojic A.; Stanisic Stojic S.; Grzetic I. (2016): Quantification and mechanisms of BTEX distribution between aqueous and gaseous phase in a dynamic system. Chemosphere, 144: 721–727. DOI: 10.1016/j.chemosphere.2015.09.042.

Stanmore, B.R; Brilhac, J.F; Gilot, P. (2001): The oxidation of soot: a review of experiments, mechanisms and models. Carbon, 39 (15): 2247–2268. DOI: 10.1016/S0008-6223(01)00109-9.

Stein, Stephen E.; Walker, James A.; Suryan, Mahendra M.; Fahr, Askar (1991): A new path to benzene in flames. In: Symposium (International) on Combustion, 23 (1): 85–90. DOI: 10.1016/S0082-0784(06)80245-6.

Supawat Vivanpatarakij, Daranee Rulerkb, Eliseo Ranzi (2014): Removal of Tar from Biomass Gasification Process by Steam Reforming over Nickel Catalysts. Chemical engineering transactions, 37. International Conference on BioMass (IconBM). 4-7 May 2014, Florence, Italy. Milano: AIDIC Associazione Italiana di Ingegneria Chimica

Svensson, Helena; Tunå, Per; Hulteberg, Christian; Brandin, Jan (2013): Modeling of soot formation during partial oxidation of producer gas. Fuel, 106: 271–278. DOI: 10.1016/j.fuel.2012.10.061.

Tesner P. A.; Shurupov S. V. (2010): Soot Formation during Pyrolysis of Naphthalene, Anthracene and Pyrene. Combustion Science and Technology, 126 (1-6): 139–151. DOI: 10.1080/00102209708935671.

Torres, Walter; Pansare, Sourabh S.; Goodwin, James G. (2007): Hot Gas Removal of Tars, Ammonia, and Hydrogen Sulfide from Biomass Gasification Gas. Catalysis Reviews, 49 (4): 407–456. DOI: 10.1080/01614940701375134.

Torretta, Vincenzo; Collivignarelli, Maria Cristina; Raboni, Massimo; Viotti, Paolo (2015): Experimental treatment of a refinery waste air stream, for BTEX removal, by water scrubbing and biotrickling on a bed of Mitilus edulis shells. Environmental technology, 36 (18): 2300–2307. DOI: 10.1080/09593330.2015.1026289.

VOURLIOTAKIS G.; SKEVIS G., FOUNTI M. A., ALHAMAMRE Z.; TRIMIS D. (2008): Detailed kinetic modelling of the T-POX reforming process using a reactor network approach. International Journal of Hydrogen Energy, 33 (11): 2816–2825. DOI: 10.1016/j.ijhydene.2008.03.026.

Wagner H. Gg. (1981): Soot Formation — An Overview. Particulate Carbon: 1–29. Springer US. ISBN: 978-1-4757-6137-5

Wang, Li-Sheng; Wang, Xue-Yuan (2014): Selectivities at infinite dilution of xylene isomers in ionic liquids. Fluid Phase Equilibria, 374: 37–47. DOI: 10.1016/j.fluid.2014.04.016.

Warnatz J.; Maas U.; Dibble Robert W. (2006): Combustion. Physical and Chemical Fundamentals, Modeling and Simulation, Experiments, Pollutant Formation. 4th Edition. Springer. ISBN 978-3-540-45363-5

Warnatz, Jürgen (1981): The structure of laminar alkane-, alkene-, and acetylene flames. Symposium (International) on Combustion, 18 (1): 369–384. DOI: 10.1016/S0082-0784(81)80042-2.

Warnatz, Jürgen (2000): Hydrocarbon oxidation high-temperature chemistry. 10th International Conference on High Temperature Materials Chemistry (HTMC-X), Pure and Applied Chemistry, 72 (11): 2101–2110. http://citeseerx.ist.psu.edu/viewdoc/download?doi=10.1.1.545.8473&rep=rep1&type=pdf

Westmoreland, Phillip R.; Dean, Anthony M.; Howard, Jack B.; Longwell, John P. (1989): Forming benzene in flames by chemically activated isomerization. Journal of Physical Chemistry, 93 (25): 8171–8180. DOI: 10.1021/j100362a008.

Wiinikka Henrik; Gebart Rikard (2004): Experimental investigations of the influence from different operating conditions on the particle emissions from a small-scale pellets combustor. Biomass and Bioenergy, 27 (6): 645–652. DOI: 10.1016/j.biombioe.2003.08.020.

Wiinikka Henrik; Gebart Rikard (2006): The influence of fuel type on particle emissions in combustion of biomass pellets. Combustion Science and Technology, 177 (4): 741–763. DOI: 10.1080/00102200590917257.

Woolcock, Patrick J.; Brown, Robert C. (2013): A review of cleaning technologies for biomass-derived syngas. Biomass and Bioenergy, 52: 54–84. DOI: 10.1016/j.biombioe.2013.02.036.

Xu, Yueting; Dai, Zhenghua; Li, Chao; Li, Xinyu; Zhou, Zhijie; Yu, Guangsuo; Wang, Fuchen (2014): Numerical simulation of natural gas non-catalytic partial oxidation reformer. International Journal of Hydrogen Energy, 39 (17): 9149–9157. DOI: 10.1016/j.ijhydene.2014.03.204.

YANG, C.; QIAN, Y.; ZHANG, L.; FENG, J. (2006): Solvent extraction process development and on-site trial-plant for phenol removal from industrial coal-gasification wastewater. Chemical Engineering Journal, 117 (2):179–185. DOI: 10.1016/j.cej.2005.12.011.

Zalel, Amir; Yuval; Broday, David M. (2008): Revealing source signatures in ambient BTEX concentrations. Environmental Pollution, 156 (2): 553–562. DOI: 10.1016/j.envpol.2008.01.016.

Zhang, Beiping; Xiong, Sijiang; Xiao, Bo; Yu, Dongke; Jia, Xiaoyuan (2011): Mechanism of wet sewage sludge pyrolysis in a tubular furnace. International Journal of Hydrogen Energy, 36 (1): 355–363. DOI: 10.1016/j.ijhydene.2010.05.100.

Zhang, Beiping; Xiong, Sijiang; Xiao, Bo; Yu, Dongke; Jia, Xiaoyuan (2011): Mechanism of wet sewage sludge pyrolysis in a tubular furnace. International Journal of Hydrogen Energy, 36 (1): 355–363. DOI: 10.1016/j.ijhydene.2010.05.100.

9 Appendix

Chapter 2

Table 9.1: Natural gas feed analysis method [Brüggemann, 2010]

Feed	Analysis method	Sampling time interval	Result
Natural gas	GC-TCD (offline), MS5A column, Carrier gas: Argon	2 hours	concentration of CH_4, N_2, H_2 (LOQ 100 ppmv)
	GC-TCD, PPU column, Carrier gas: Helium		CO_2, C_2H_6, C_2H_4, C_2H_2, C_3H_4, H_2S, COS (LOQ 20 ppmv)
	GC-TCD, GasPro column, Carrier gas: Helium		C_3H_8, C_3H_6, n-/iso-C_4H_{10} (LOQ 20 ppmv)

Chapter 3
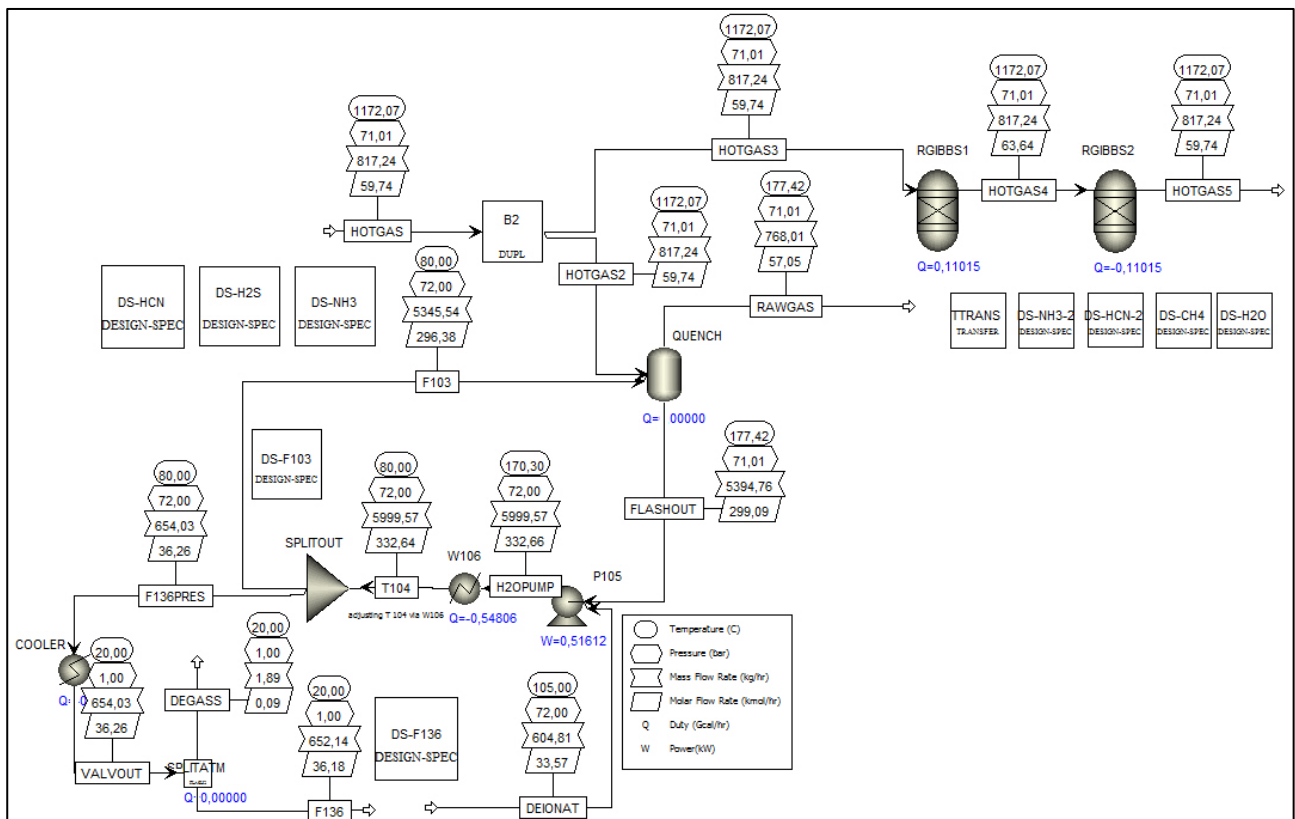
Figure 9.1: Aspen flow sheet set up for HP POX quench system GasPOX 201 VP1 (simplified and extension of Fig. 3.2, organic acids not taken into account). Tabulated values are given in Table 9.11.

Table 9.2: pH scale with examples of solution [NALCO 2008]

Relative concentration of Hydrogen ions compared to distilled water	pH =	Examples of solution at this pH
10,000,000	pH = 0	Battery acid, strong acid
1,000,000	pH = 1	Hydrochloric acid secreted by stomach lining
100,000	pH = 2	Lemon juice, vinegar
10,000	pH = 3	Grapefruit, orange juice, soda
1,000	pH = 4	Tomato juice, acid rain
100	pH = 5	Soft drinking water, black coffee
10	pH = 6	Urine, saliva
1	pH = 7	"Pure" water
1/10	pH = 8	Sea water
1/100	pH = 9	Baking soda
1/1,000	pH = 10	Great salt lake, milk of magnesia
1/10,000	pH = 11	Ammonia solution
1/100,000	pH = 12	Soapy water
1/1,000,000	pH = 13	Bleaches, oven cleaner
1/10,000,000	pH = 14	Liquid drain cleaner

(left-margin labels: More Basic ↑ ; Neutral ; More Acidic ↓)

The pH scale indicates the relative acidity or basicity of water, which runs from 0 − 14 with 0 representing maximum acidity and 14 representing maximum basicity. Typical solutions and pH range are given in Table 9.2.

Henry´s constant: Aspen Plus and Literatures
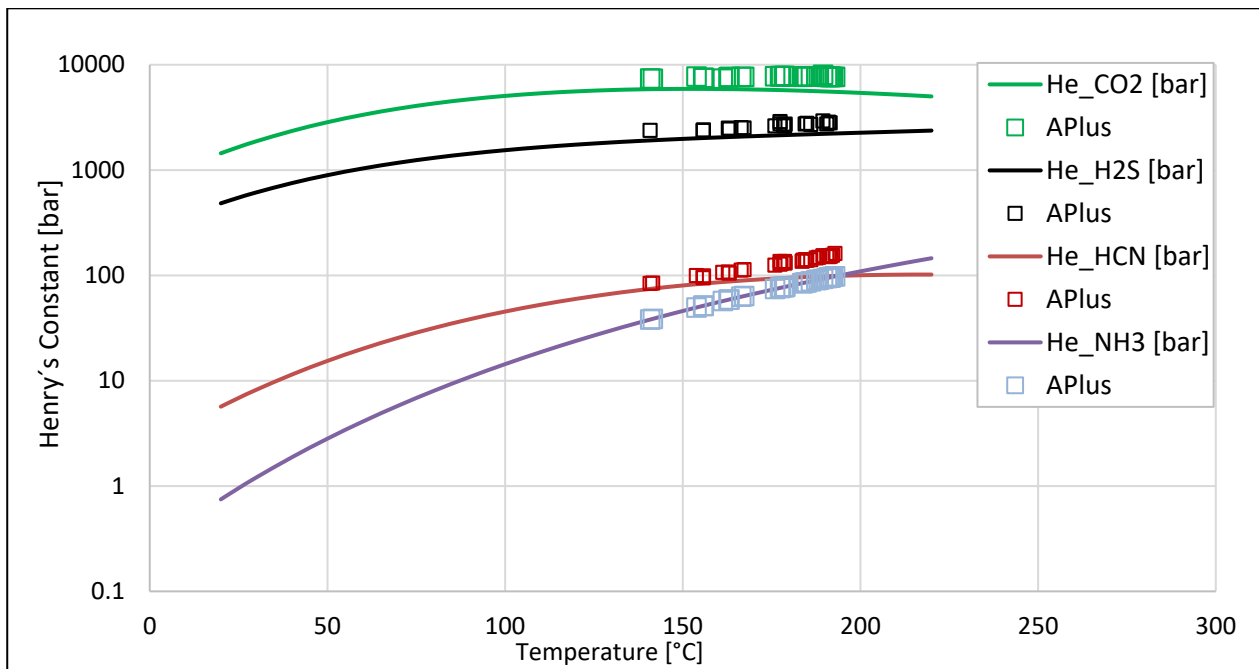
Figure 9.2: Comparison between the Henry´s constant profiles: Aspen Plus (markers) and Literatures (solid lines) ([Edwards et al., 1978] for CO_2, [Alvaro et al., 2000] for NH_3, [Kamps et al., 2001] for H_2S, and [Rumpf et al., 1992] for HCN as it can be seen in Fig. 4.3)
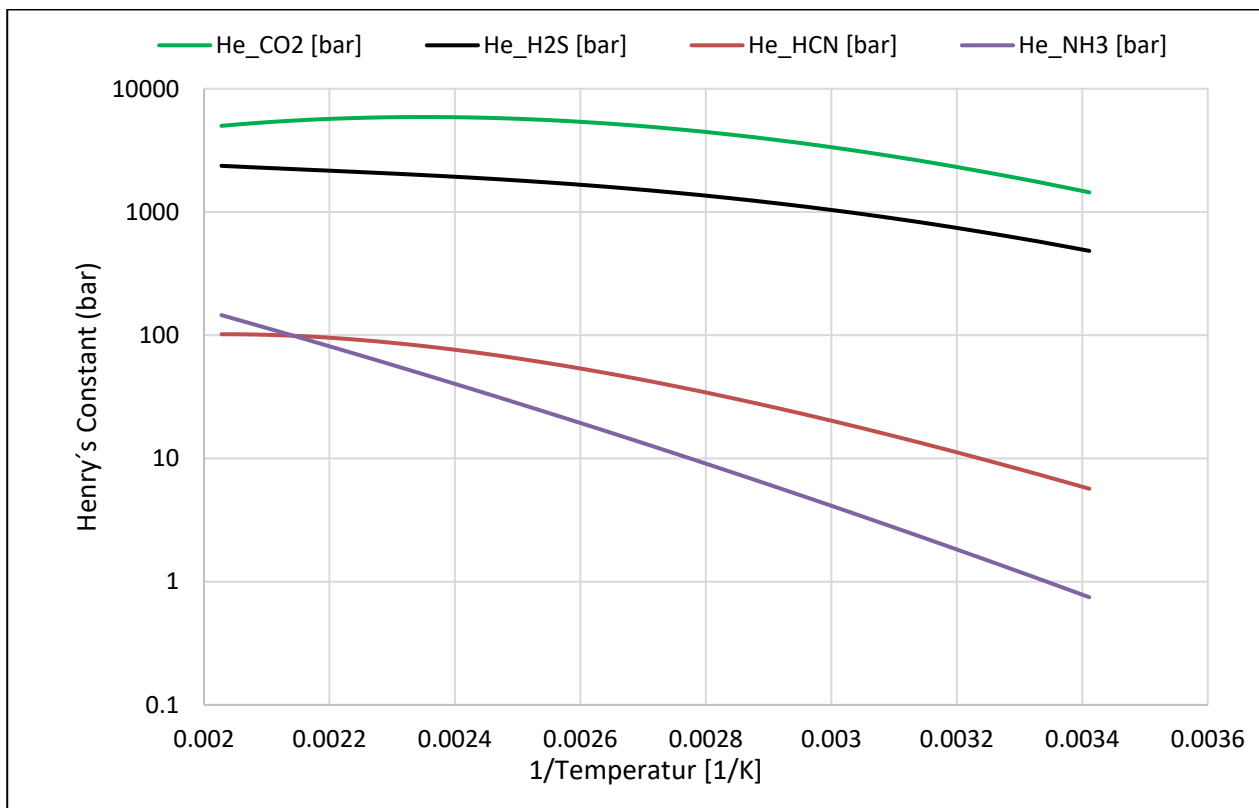
Figure 9.3: Henry´s constant profiles derived from literatures ([Edwards et al., 1978] for CO2, [Alvaro Pérez-Salado et al., 2000] for NH_3, [Kamps et al., 2001] for H_2S, and [Rumpf et al., 1992] for HCN as it can be seen in Fig. 4.3)

Dissociation constant: Aspen Plus and Literatures
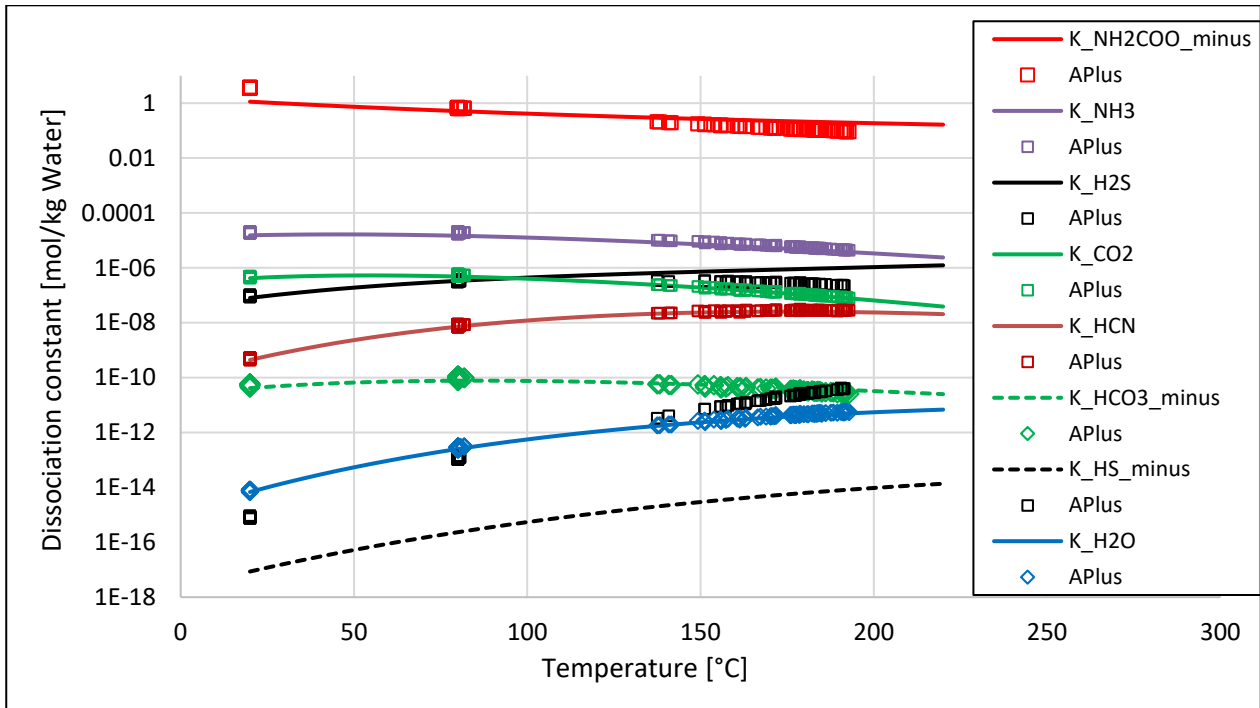
Figure 9.4: Comparison between the dissociation constant profiles: Aspen Plus (markers) and Literatures (solid or dashed lines) [Alvaro et al., 2000], [Kamps et al., 2001], and [Edwards et al., 1978] as in Fig.4.4.
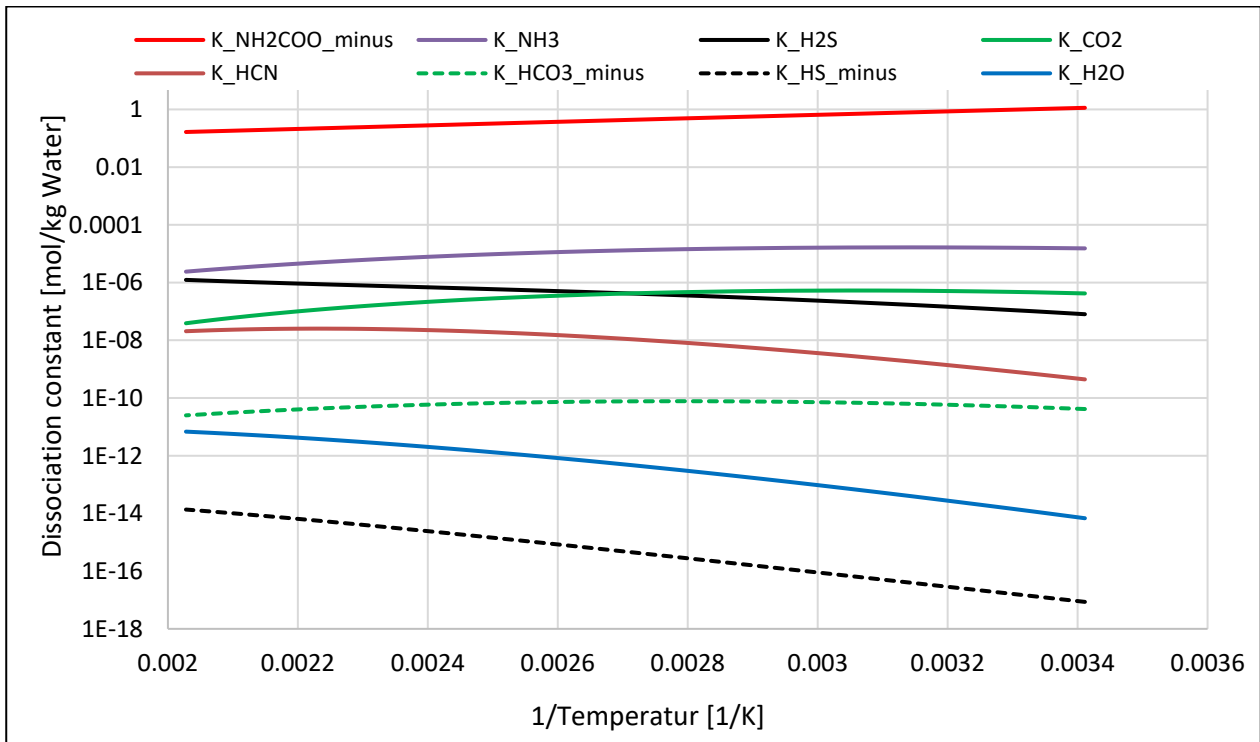
Figure 9.5: Dissociation constant profiles derived from literatures [Kamps et al., 2001], and [Edwards et al., 1978] as in Fig.4.4.

T [°C]	1/T [1/K]	He_CO2 [bar]	He_H2S [bar]	He_HCN [bar]	He_NH3 [bar]	K_NH2COO_minus	K_NH3	K_CO2	K_H2S	K_HCN	K_HCO3_minus	K_HS_minus	K_H2O mol²/kg²	pKw	pHneutral	H'neutral mol/kg	pHneutral	pOHneutral	pKw
20	0.00341122	1443.435103	483.6224649	5.674017907	0.747326358	1.135725885	1.52974E-05	4.19598E-07	8.00024E-08	4.41304E-10	4.14255E-11	8.60529E-18	6.80302E-15	14.16729848	7.083649242	8.24804E-08	7.08364924	7.08364924	14.1672985
25	0.00335402	1654.39165	547.4400649	6.856453692	0.954737612	1.052090044	1.57456E-05	4.49239E-07	9.4945E-08	6.08374E-10	4.60246E-11	1.19197E-17	1.00384E-14	13.99833619	6.99916809	1.00192E-07	6.99916809	6.99916809	13.9983362
30	0.0032987	1877.170064	613.8240249	8.209345505	1.207228439	0.976739509	1.60947E-05	4.74519E-07	1.11326E-07	8.23101E-10	5.05192E-11	1.63414E-17	1.45329E-14	13.83764765	6.91882383	1.20552E-07	6.91882383	6.91882383	13.8376477
40	0.00319336	2350.52068	752.140532	11.427008	1.879567988	0.847068945	1.64952E-05	5.10808E-07	1.48156E-07	1.42931E-09	5.88908E-11	2.98211E-17	2.88845E-14	13.5393551	6.76966776	1.69954E-07	6.76966776	6.76966776	13.5393355
50	0.00309454	2846.509368	894.2736637	15.41893827	2.816451731	0.740311788	1.65164E-05	5.27705E-07	1.89832E-07	2.32816E-09	6.60128E-11	5.24314E-17	5.38103E-14	13.26913433	6.63456716	2.31971E-07	6.63456716	6.63456716	13.2691343
60	0.00300165	3346.775361	1036.205553	20.14695944	4.100514192	0.651650962	1.6198E-05	5.26551E-07	2.35526E-07	3.56886E-09	7.15171E-11	8.9025E-17	9.45751E-14	13.02422302	6.51211151	3.07531E-07	6.51211151	6.51211151	13.024223
70	0.00291418	3833.240847	1174.496624	25.59544137	5.808083964	0.577426105	1.55941E-05	5.10038E-07	2.8436E-07	5.18842E-09	7.52129E-11	1.46289E-16	1.57715E-13	12.80212624	6.40106312	3.97134E-07	6.40106312	6.40106312	12.8021262
80	0.00283166	4289.502212	1306.451979	31.69205153	8.026039436	0.514822505	1.47658E-05	4.81514E-07	3.3551E-07	7.18032E-09	7.7048E-11	2.50806E-16	2.50806E-13	12.60066402	6.30033201	5.00804E-07	6.30033201	6.3003201	12.6006664
90	0.00275368	4701.831051	1430.174194	38.32613992	10.84684494	0.461654294	1.37752E-05	4.44455E-07	3.88279E-07	9.4978E-09	7.7212E-11	3.60785E-16	3.82024E-13	12.4179098	6.2089549	6.18081E-07	6.2089549	6.2089549	12.4179098
100	0.00267989	5059.75509	1544.530583	45.35449212	14.36704552	0.41620789	1.28804E-05	4.02105E-07	4.42149E-07	1.20518E-08	7.58295E-11	5.43328E-16	5.59557E-13	12.25215546	6.12607729	7.48036E-07	6.12607773	6.12607773	12.2521555
110	0.00260994	5356.253075	1649.065378	52.60942635	18.68569685	0.377128074	1.15332E-05	3.5727E-07	4.96801E-07	1.47177E-08	7.31884E-11	7.97302E-16	7.90894E-13	12.10188186	6.050940928	8.89322E-07	6.05094093	6.05094093	12.1018819
120	0.00254356	5587.636336	1743.883632	59.9083486	23.90279872	0.343334169	1.03767E-05	3.12228E-07	5.52118E-07	1.73494E-08	6.95715E-11	1.14163E-15	1.0821E-12	11.96573398	5.98286988	1.04024E-06	5.98286699	5.98286699	11.965734
130	0.0024847	5753.205705	1829.527481	67.06383972	30.11778898	0.313957731	9.24526E-06	2.68718E-07	6.08177E-07	1.97905E-08	6.52564E-11	1.59708E-15	1.43714E-12	11.84249987	5.92124935	1.19881E-06	5.92124993	5.92124993	11.842499
135	0.00245008	5811.792527	1869.168782	70.53033174	33.63063553	0.300700948	8.69732E-06	2.47941E-07	6.36558E-07	2.08952E-08	6.29177E-11	1.87325E-15	1.63915E-12	11.7853814	5.892690698	1.28029E-06	5.8926907	5.8926907	11.7853814
140	0.00242043	5854.771454	1906.85809	73.89341732	37.42814291	0.288295774	8.16468E-06	2.27975E-07	6.65234E-07	2.19008E-08	6.04972E-11	2.18538E-15	1.85741E-12	11.7310271	5.865546356	1.36287E-06	5.86554636	5.86554636	11.7310927
145	0.00239149	5882.671954	1942.738403	77.1324907	41.52369163	0.276674385	7.64935E-06	2.08906E-07	6.94261E-07	2.27935E-08	5.80212E-11	2.53617E-15	2.09163E-12	11.679515	5.8397575	1.44625E-06	5.8397575	5.8397575	11.679515
150	0.00236323	5896.112272	1976.956555	80.22826353	45.92811028	0.265775341	7.15293E-06	1.90798E-07	7.23706E-07	2.35617E-08	5.5513E-11	2.92822E-15	2.34194E-12	11.63053547	5.815267733	1.53014E-06	5.81526773	5.81526773	11.6305355
155	0.00233563	5895.78317	2009.568221	83.16294693	50.66249495	0.255542901	6.67662E-06	1.73694E-07	7.53645E-07	2.41965E-08	5.29958E-11	3.36401E-15	2.60587E-12	11.5840698	5.79202489	1.61427E-06	5.79202349	5.79202349	11.58047
160	0.00230867	5882.432558	2041.032446	85.92040268	55.70761139	0.245926421	6.2213E-06	1.5762E-07	7.84162E-07	2.46915E-08	5.04864E-11	3.84585E-15	2.88438E-12	11.53994772	5.769973859	1.69835E-06	5.76997386	5.76997386	11.5399477
165	0.00228232	5856.851192	2071.210756	88.48626321	61.10386991	0.236879819	5.78751E-06	1.42685E-07	8.15348E-07	2.50428E-08	4.8002E-11	4.37579E-15	3.17594E-12	11.49814088	5.749070438	1.78209E-06	5.74907044	5.74907044	11.4981409
170	0.00225657	5819.859528	2100.365822	90.84802045	66.85130296	0.228361103	5.37556E-06	1.28588E-07	8.47305E-07	2.52494E-08	4.55566E-11	4.95564E-15	3.47909E-12	11.4585343	5.729267172	1.86523E-06	5.72926717	5.72926717	11.4585343
175	0.0022314	5772.295822	2128.660369	92.99508445	72.95954532	0.22203196	4.98549E-06	1.15611E-07	8.80142E-07	2.53126E-08	4.31623E-11	5.56887E-15	3.7928E-12	11.42104046	5.710520228	1.94751E-06	5.71052023	5.71052023	11.4210405
180	0.00220677	5715.00549	2156.256301	94.91981294	79.43781697	0.21275738	4.61717E-06	1.03632E-07	9.13975E-07	2.52362E-08	4.08289E-11	6.27056E-15	4.11562E-12	11.3855772	5.692787858	2.02867E-06	5.69278786	5.69278786	11.385757
185	0.00218269	5648.831734	2183.314038	96.61251375	86.29490841	0.205605337	4.27028E-06	9.26183E-08	9.49833E-07	2.50258E-08	3.86645E-11	7.00741E-15	4.44569E-12	11.35206058	5.676030288	2.10848E-06	5.67603029	5.67603029	11.3520606
190	0.00215913	5574.607394	2209.992028	98.07142199	93.53916843	0.19884649	3.94436E-06	8.25313E-08	9.8515E-07	2.46892E-08	3.63755E-11	7.79766E-15	4.78168E-12	11.3204192	5.6602096	2.18671E-06	5.6602096	5.6602096	11.3204192
195	0.00213607	5493.147991	2236.446421	99.29265442	101.1784942	0.19245393	3.63883E-06	7.33283E-08	1.02277E-06	2.42356E-08	3.42668E-11	8.64105E-15	5.12178E-12	11.29057928	5.64528638	2.26313E-06	5.64528964	5.64528964	11.2905793
200	0.00211349	5405.245876	2262.830886	100.2751436	109.2203235	0.186402947	3.35304E-06	6.49628E-08	1.06195E-06	2.36752E-08	3.22418E-11	9.55683E-15	5.46422E-12	11.26247179	5.63123589	2.33757E-06	5.63123589	5.63123589	11.2624718
205	0.00209139	5311.665438	2289.209556	101.019554	117.6716293	0.180670822	3.08625E-06	5.7386E-08	1.10286E-06	2.30194E-08	3.0303E-11	1.04837E-14	5.80723E-12	11.23603097	5.618015435	2.40982E-06	5.61801544	5.61801544	11.2360309
210	0.00206975	5213.13926	2315.992071	101.528184	126.5389159	0.175236645	2.83766E-06	5.0548E-08	1.14568E-06	2.22802E-08	2.84516E-11	1.14798E-14	6.14903E-12	11.21119362	5.605598809	2.47972E-06	5.60559681	5.60559681	11.211936
215	0.00204855	5110.365154	2343.063732	101.8048543	135.8282172	0.170081147	2.60644E-06	4.43981E-08	1.19059E-06	2.14689E-08	2.66886E-11	1.25228E-14	6.48794E-12	11.18789993	5.593949966	2.54712E-06	5.59394997	5.59394997	11.1878999
220	0.00202778	5004.003987	2370.655717	101.8547877	145.5450968	0.165186553	2.39174E-06	3.88859E-08	1.23781E-06	2.06007E-08	2.50117E-11	1.36097E-14	6.82194E-12	11.1660237	5.583046186	2.61188E-06	5.58304619	5.58304619	11.1660924

Figure 9.6: Calculated pH values, temperature range and species

Chapter 5

Table 9.3: Gas-POX test campaigns and with designated serial numbers

Serial numbers	Test Points
1	GasPOX 201 VP1 08.04.2014 20:00
2	GasPOX 201 VP2 09.04.2014 05:00
3	GasPOX 201 VP3 09.04.2014 14:00
4	GasPOX 201 VP4 09.04.2014 22:45
5	GasPOX 201 VP5 10.04.2014 07:30
6	GasPOX 201 VP6 10.04.2014 16:30
7	GasPOX 201 VP7 11.04.2014 02:00
8	GasPOX 202 VP1 04.06.2014 12:00
9	GasPOX 202 VP2 04.06.2014 22:45
10	GasPOX 202 VP3 05.06.2014 07:30
11	GasPOX 202 VP4 05.06.2014 16:15
12	GasPOX 202 VP5 06.06.2014 03:30
13	GasPOX 202 VP6 06.06.2014 11:00
14	GasPOX 203 VP1A 09.12.2014 21:30
15	GasPOX 203 VP1B 10.12.2014 18:45
16	GasPOX 203 VP2 11.12.2014 02:30
17	GasPOX 203 VP3 11.12.2014 06:30
18	GasPOX 203 VP4 12.12.2014 04:00
19	GasPOX 203 VP5 12.12.2014 12:30
20	GasPOX 203 VP6 12.12.2014 21:30
21	GasPOX 203 ZP3 13.12.2014 06:45
22	GasPOX 204 VP1 18.03.2015 12:30
23	GasPOX 204 VP2 19.03.2015 01:15
24	GasPOX 204 VP3 19.03.2015 10:30
25	GasPOX 204 VP4 20.03.2015 13:30
26	GasPOX 204 VP5 21.03.2015 01:00
27	GasPOX 204 VP6 21.03.2015 12:00
28	GasPOX 205 VP1 25.06.2015 09:00
29	GasPOX 205 VP2 25.06.2015 17:30
30	GasPOX 205 VP3 26.06.2015 01:30
31	GasPOX 205 VP5 26.06.2015 23:15
32	GasPOX 205 VP4 27.06.2015 07:45
33	GasPOX 205 VP6 27.06.2015 14:30
34	GasPOX 205 ZP2 27.06.2015 20:00
35	GasPOX 206 VP1 29.10.2015 07:00
36	GasPOX 206 VP2 29.10.2015 12:30
37	GasPOX 206 VP3 29.10.2015 19:30
38	GasPOX 206 VP3 29.10.2015 23:30
39	GasPOX 206 VP5 30.10.2015 05:00
40	GasPOX 206 ZP5 30.10.2015 09:00

41	**GasPOX 206 VP6 30.10.2015 15:00**
42	**GasPOX 207 VP1 09.03.2016 05:00**
43	**GasPOX 207 VP2 09.03.2016 14:30**
44	**GasPOX 207 VP3 10.03.2016 07:15**
45	**GasPOX 207 VP4 11.03.2016 08:00**
46	**GasPOX 207 VP6 11.03.2016 21:00**
47	**GasPOX 207 VP5 12.03.2016 05:45**

Figure 9.7: Aspen Plus flow sheet setup for organic acid compounds calculations (GasPOX 201 VP1, see also Table 9.12)

Comment on formamide (Chapter 5)

Another dehydration pathway for formamide decomposition in the presence of water molecules was investigated by [Nguyen et al., 2013]. The investigation by [Nguyen et al., 2013] explains that when formamide decomposes, more reactants are produced that lead to formation of more complex biomolecules. Small molecules produced as a result of many reactive channels of the decomposition of formamides include traces of: H_2, CO, H_2O, HCN, HNC (hydrogen isocyanide), NH_3, and HNCO (isocyanic acid) [Nguyen et al., 2013]. [Becker et al., 1963] reports that at 80 °C in aqueous phase, a system of methyl substituted formamides with formic acid and ammonia result in the formation of stronger additional base compounds like N-methylformamide (NMF) and N,N-dimethylformamide (DMF) as these new compounds are regarded as a substituted ammonium formate. In addition, the dehydration of formamide by heating over a metallic catalyst at temperature range between 350 – 600 °C can lead to the formation of some yield of hydrogen cyanide [Gibson, 1969].

Chapter 5: Correlation coefficient (r)

$$r = \frac{n\Sigma x_i y_i - \Sigma x_i \Sigma y_i}{\sqrt{n\Sigma x_i^2 - (\Sigma x_i)^2}\sqrt{n\Sigma y_i^2 - (\Sigma y_i)^2}}$$

(8.1)

Correlation coefficient scale

Negative correlation			No correlation		Positive correlation		
Strong	Moderate	Weak			Weak	Moderate	Strong
-1	-0.8	-0.5	-0.2	0 0.2	0.5	0.8	1

Based on of Pearson correlation coefficient, when the r is close to 1, the correlation is described as strong. When the value of r is between 0.5 and 0.8, the variables are said be moderately correlated and when it is between 0.2 and 0.5, the correlation is said to be weak. r = 1indicates a perfect positive correlation and r = -1 a perfect negative correlation. When r is close to zero it is considered that no correlation exists between the two variables.

Table 9.4: Summary of correlation coefficient (r) from Figures in Chapter 5

	Variables		Correlation Coefficient (r)	Interpretation	Figure references
	y_i	x_i			
1	m_eq [HCOOH + HCOO-]	m_real [NH_3 + NH_4^+] mol/kg	-0.31	Negative weak correlation	Fig. 5.1
2	m_real [HCOOH + HCOO-]	m_real [NH_3 + NH_4^+] mol/kg	+0.81	Positive strong correlation	Fig. 5.1
3	m_eq [HCOOH + HCOO-]	T_Quench water [°C]	-0.83	Negative strong correlation	Fig. 5.2 & 5.6
4	m_real [HCOOH + HCOO-]	T_Quench water [°C]	+0.79	Positive strong correlation	Fig. 5.2 & 5.6
5	m_eq [CH_3COOH + CH_3COO^-]	m_real [NH_3 + NH_4^+] mol/kg	-0.34	Negative weak correlation	Fig. 5.3
6	m_real [CH_3COOH + CH_3COO^-]	m_real [NH_3 + NH_4^+] mol/kg	+0.60	Positive moderate correlation	Fig. 5.3
7	m_eq [CH_3COOH + CH_3COO^-]	T_Quench water [°C]	-0.30	Negative weak correlation	Fig. 5.4 & 5.10
8	m_real [CH_3COOH + CH_3COO^-]	T_Quench water [°C]	+0.49	Positive weak correlation	Fig. 5.4 & 5.10
9	K_{eq} HCOOH	T_Quench water [°C]	-0.97	Negative strong correlation	Fig. 5.8
10	K_{real} HCOOH	T_Quench water [°C]	+0.83	Positive strong correlation	Fig. 5.8
11	K_{eq} CH_3COOH	T_Quench water [°C]	-0.62	Negative moderate correlation	Fig. 5.12
12	K_{real} CH_3COOH	T_Quench water [°C]	+0.56	Positive moderate correlation	Fig. 5.12

The correlation coefficient for all the considered real trace concentrations and reaction quotients for the trace formation (two varibales x and y in Table 9.4) in Chapter 5 show strongly or moderately positive correlations.

Higher temperatures lead to higher amount of organic acid formation (positive correlations). These higher amount of organic acids in the quench water phase leads (beside the other dissolved anionic species) to a higher amount of dissolved ammonium cations from dissolved NH_3 out of the hot gas (positive correlations between m_real [NH_3 + NH_4^+] and organic acids).
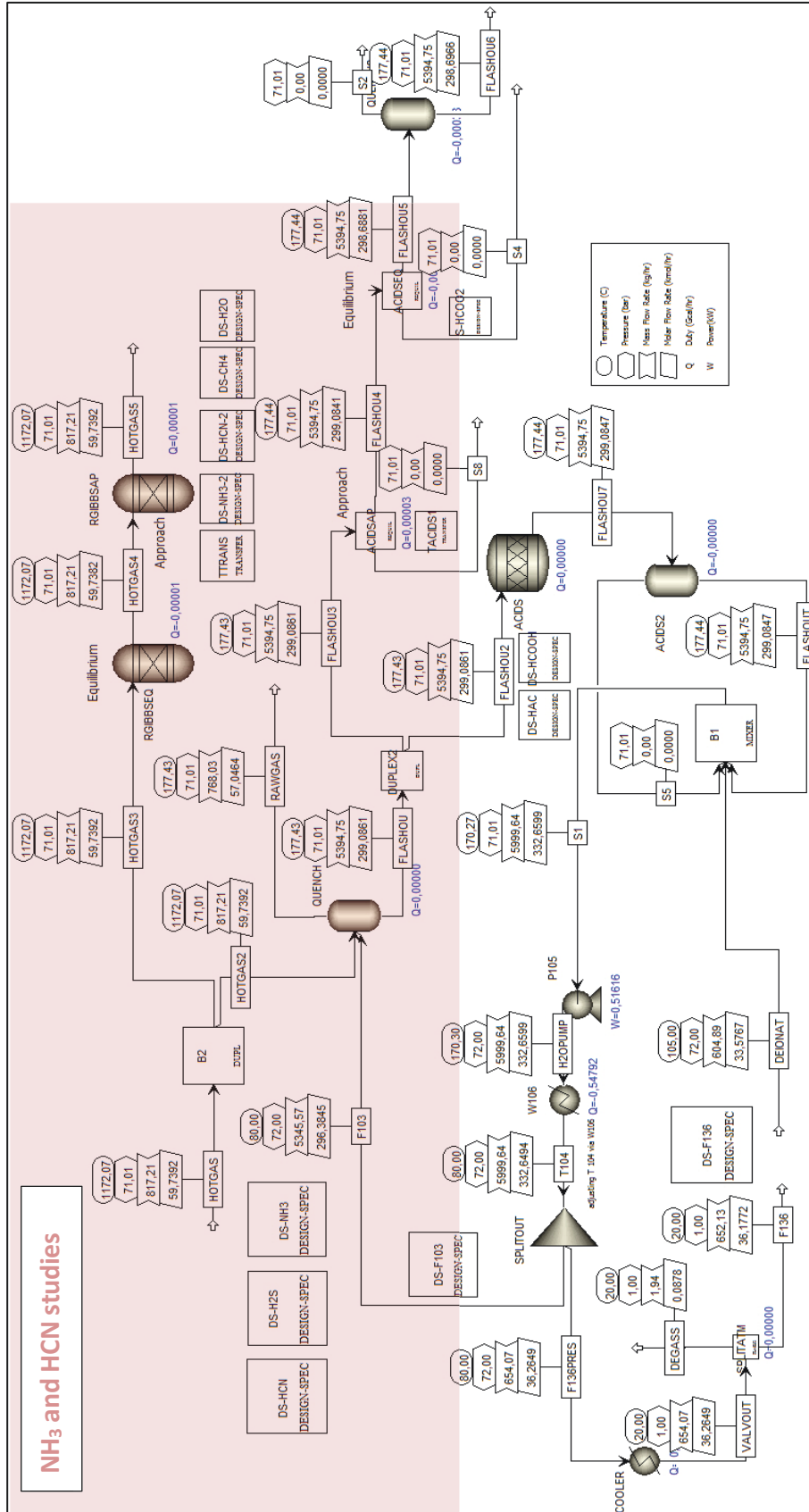
Figure 9.8: Aspen Plus flow sheet setup for nitrogen compounds calculations (GasPOX 201 VP1, see also Table 9.12, organic acids are taken into account in the aqueous streams of the quench system)
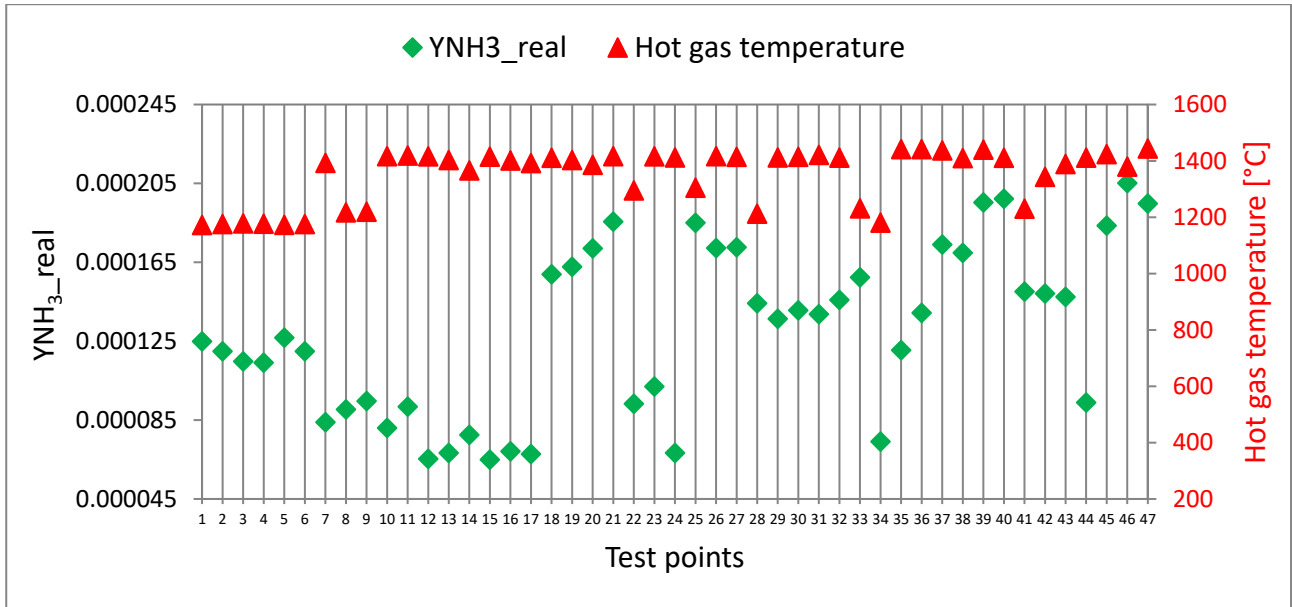
Figure 9.9: Yield of ammonia in gasifier (calculated real) and hot gas temperature against the 47 test points
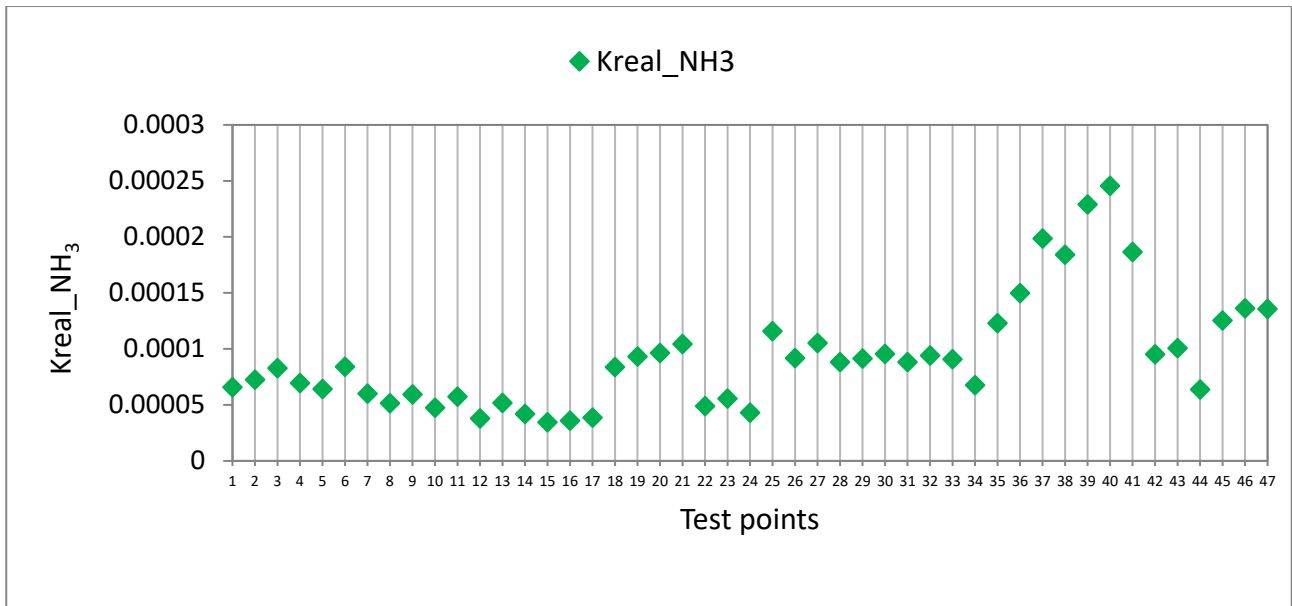
Figure 9.10: K_{real} or reaction quotient for ammonia formation in the gasifier against the 47 test points.
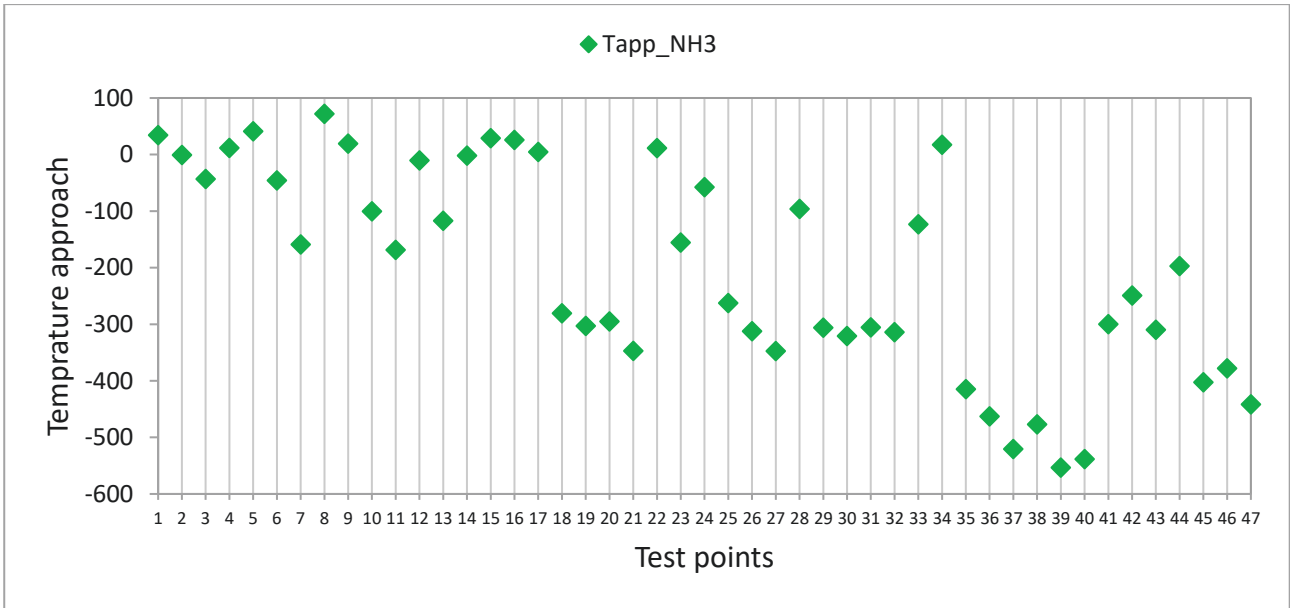
Figure 9.11: Temperature approach studies for ammonia and the 47 test points
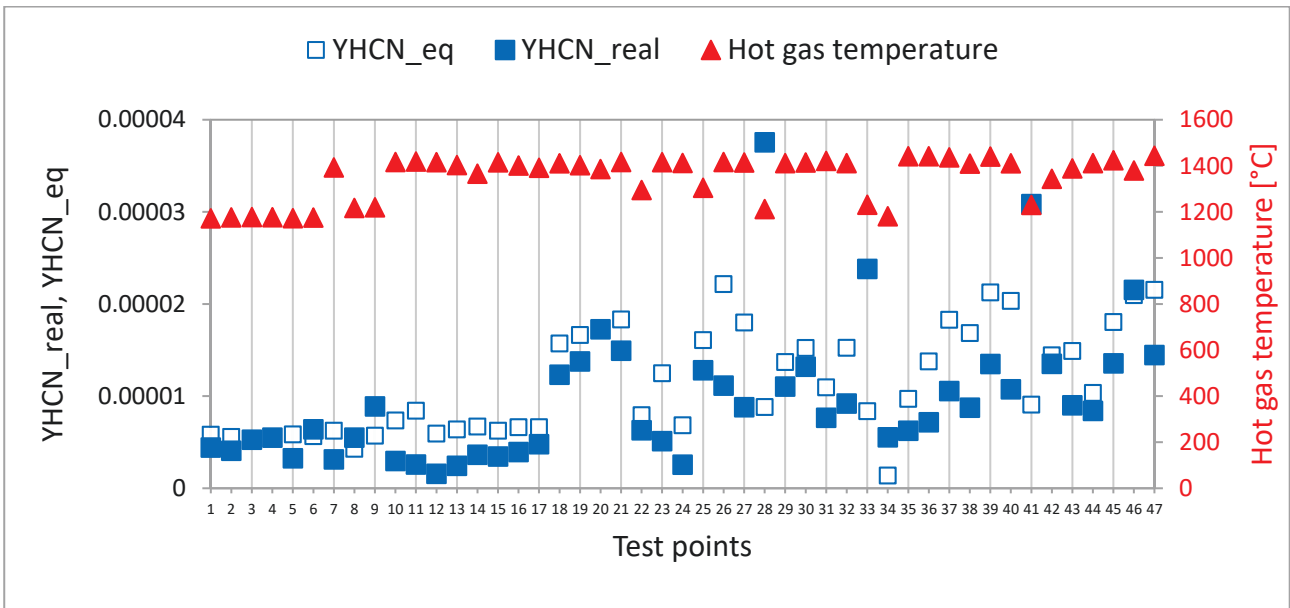
Figure 9.12: Yield of HCN from the gasifier (calculated real and equilibrium) and hot gas temperature and the 47 test points
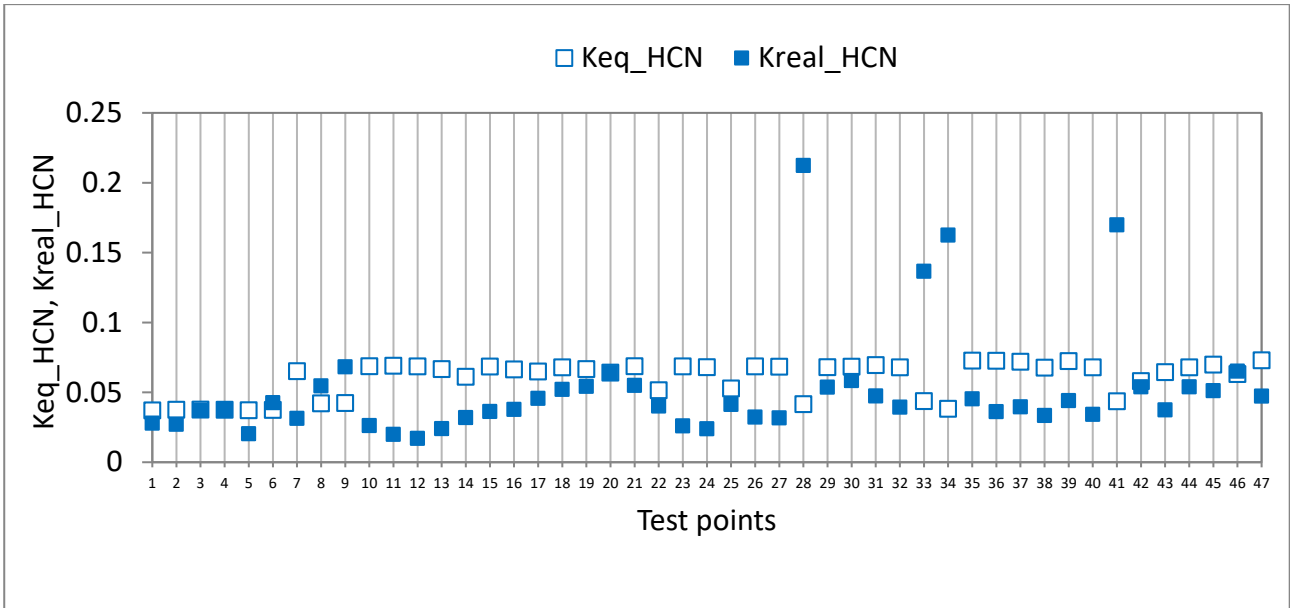
Figure 9.13: Comparison between equilibrium constant and reaction quotient for HCN and 47 test points
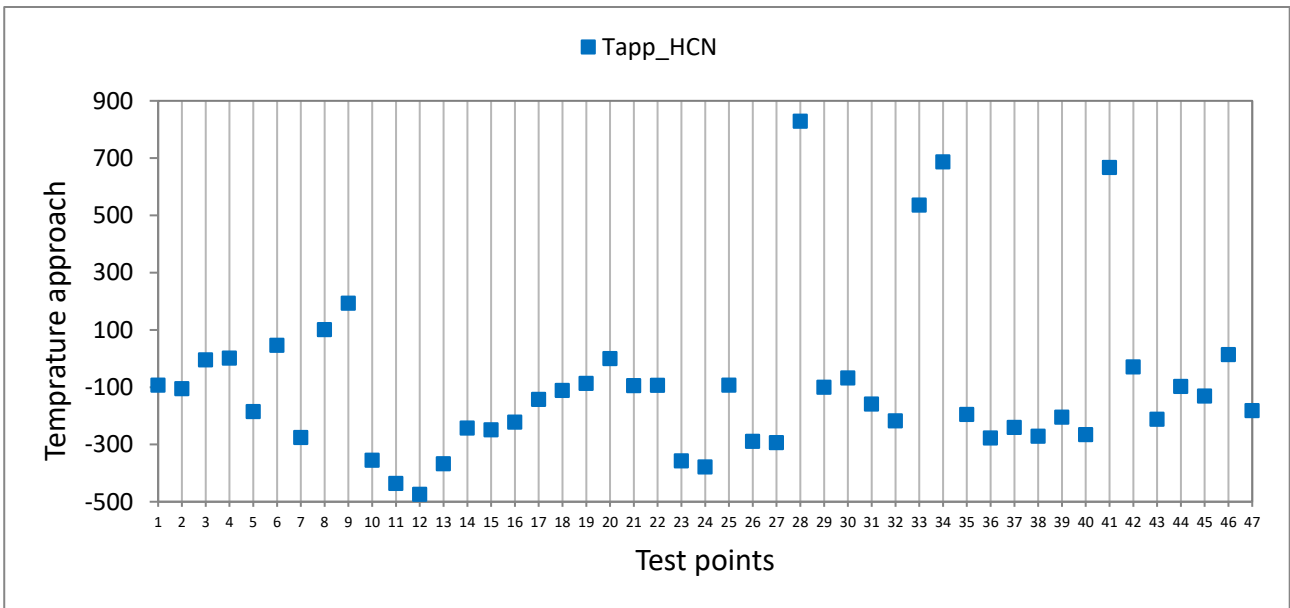
Figure 9.14: Temperature approach studies for HCN and the 47 test points

Table 9.5: Comparison among reactions temperatures and heat of reactions

Temperature, T [°C]	25	1000	1200	1400
	Heat of reaction, $\Delta H_{Reaction}$ [kJ/mol]			
Reactions				
$CH_4 + CO_2 \leftrightarrow 2\,CO + 2\,H_2$ CO_2 - reforming of CH_4	247.3	259.6	258.0	255.9
$CH_4 + H_2O_G \leftrightarrow CO + 3\,H_2$ Steam - reforming of CH_4 (reverse: methanation with CO)	206.2	227.5	227.6	227.1
$NH_3 \leftrightarrow 3/2\,H_2 + 1/2\,N_2$ reverse of NH3 formation	45.9	55.9	56.0	55.7
$H_2 + CO_2 \leftrightarrow CO + H_2O_G$ reverse of CO - shift reaction / water gas shift reaction	41.2	32.2	30.4	28.8
$NH_3 + CO \leftrightarrow HCN + H_2O$	49.7	52.8	53.0	53.1
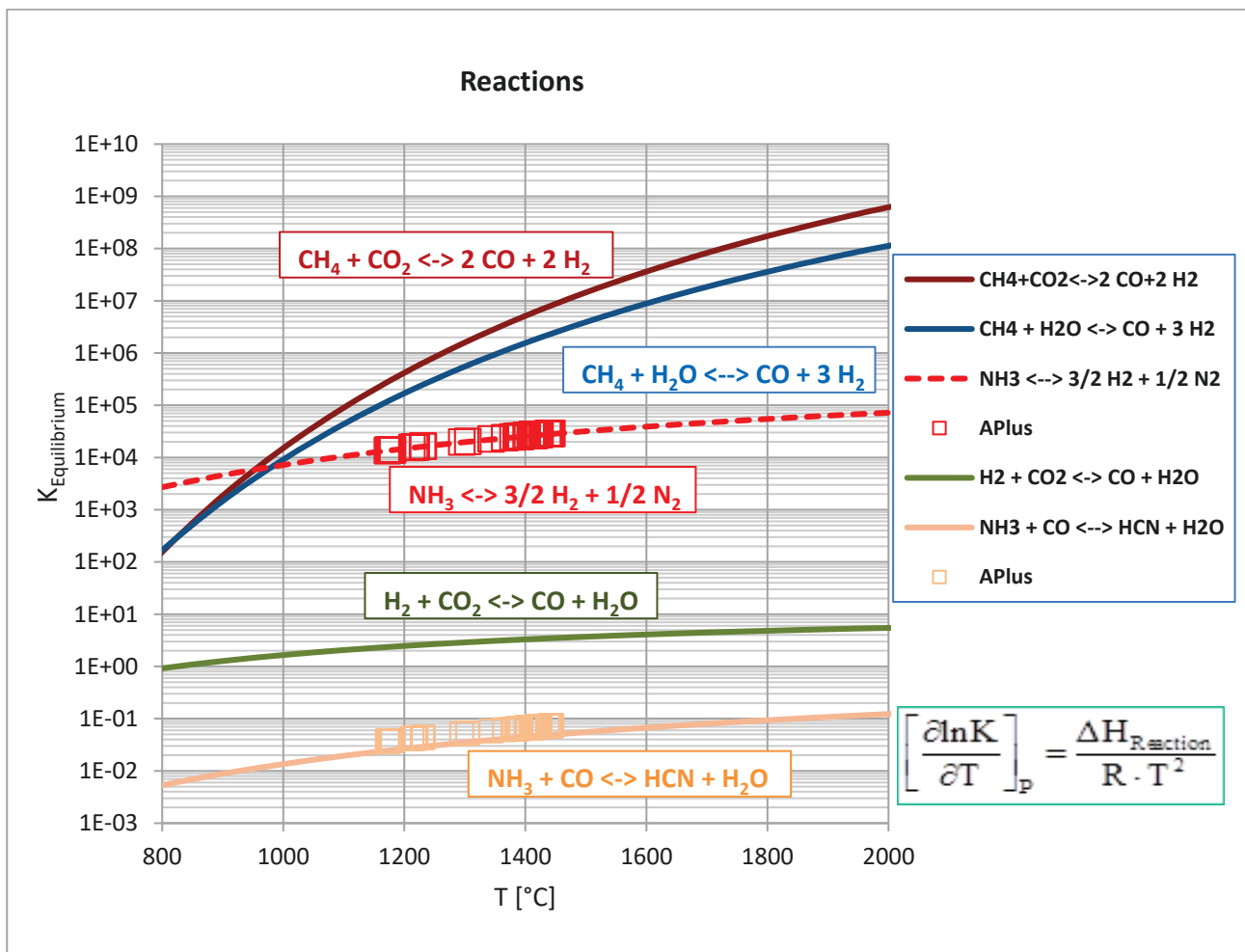
Figure 9.15: Comparison among equilibrium constants of reactions against temperature, T [°C]
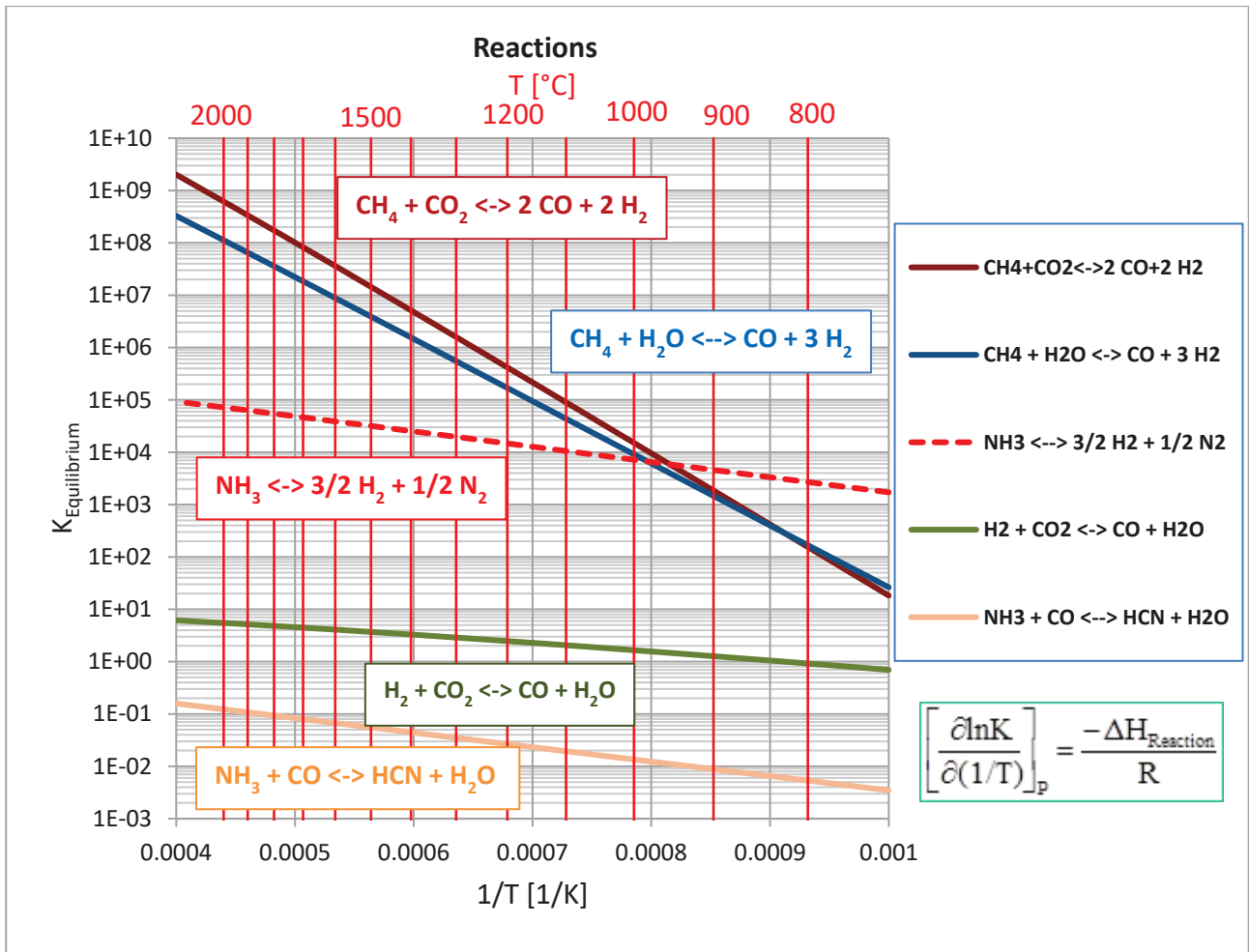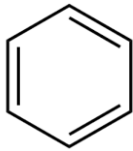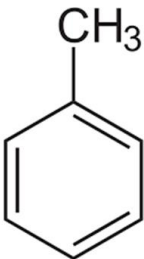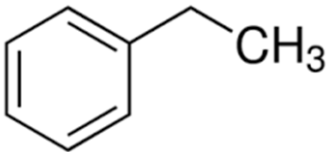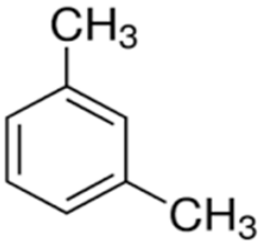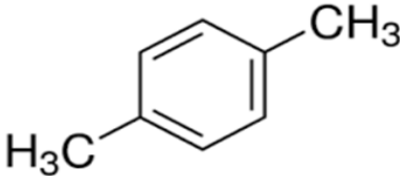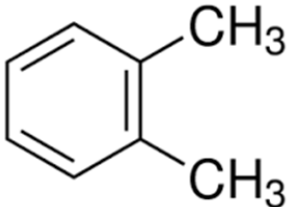
Figure 9.16: Comparison among equilibrium constants of reactions against temperature, 1/T [1/K]

Chapter 7

Table 9.6: Content of BTEX compounds in Gas-POX quench water samples

BTEX compounds	Chemical formula	Structure	IUPAC name
	CAS Number		
Benzene	C_6H_6		Benzene or Benzol
	71-43-2		
Toluene	C_7H_8		Toluene or Methylbenzene
	108-88-3		
Ethylbenzene	C_8H_{10}		Ethylbenzene or Ethylbenzol
	100-41-4		
m-xylene	C_8H_{10}		1,3-Xylene
	108-38-3		
p- xylene	C_8H_{10}		1,4-Xylene
	106-42-3		
o-xylene	C_8H_{10}		1,2-Xylene
	95-47-6		
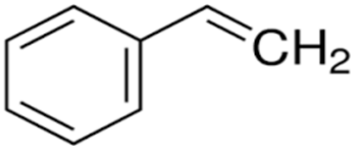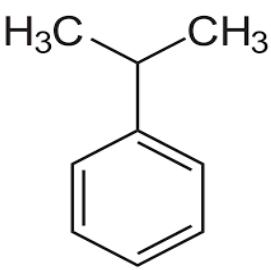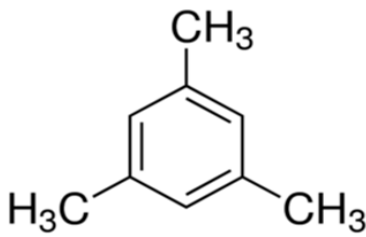
Styrene	C_8H_8 100-42-5		Ethenylbenzene
Cumene	C_9H_{12} 98-82-8		Isopropylbenzene or (Propan-2-yl)benzene
Mesitylene	C_9H_{12} 108-67-8		1,3,5-Trimethylbenzene

Table 9.7: BTEX in quench water effluent samples results

Gas-POX 203 (VP1a, VP1b, and VP2b) quench water analysis report for BTEX

Quench water analysis				
Report number: 1408115				
Date: 05.06 – 12.12. 2014				
Method: DIN 38407-F 9-1				
Gas-POX 203	VP	VP1a	VP1b	VP2b
Sample name	Quench water 05.06.14 13:00 p.m.	Quench water 11.12.14 03:30 a.m.	Quench water 11.12.14 00:45 a.m.	Quench water 11.12.14 03:30 a.m.
Laboratory number	1414926	1414927	1414928	1414929
Parameter (µg/l)				
Benzene	< 0.5	0.89	< 0.5	< 0.5
Toluene	35	< 0.5	< 0.5	< 0.5
Ethylbenzene	< 0.5	< 0.5	< 0.5	< 0.5
p- / m-xylene	< 1.0	< 1.0	< 1.0	< 1.0
o-xylene	< 0.5	< 0.5	< 0.5	< 0.5
Styrene	< 0.5	< 0.5	< 0.5	< 0.5
Cumene	< 0.5	< 0.5	< 0.5	< 0.5
Mesitylene	< 0.5	< 0.5	< 0.5	< 0.5
Sum of BTEX in µg/l	**35**	**0.89**	**n.n**	**n.n**

Gas-POX 203 (VP3, VP6, VP4, and VP5) quench water analysis report for BTEX

Quench water analysis				
Report number: 1408115				
Date: 05.06 – 12.12. 2014				
Method: DIN 38407-F 9-1				
Gas-POX 203	VP3	VP6	VP4	VP5
Sample name	Quench water 11.12.14 10:30 a.m.	Quench water 12.12.14 03:30 a.m.	Quench water 12.12.14 10:00 a.m.	Quench water 12.12.14 18:30 p.m.
Laboratory number	1414930	1414931	1414932	1414933
Parameter (µg/l)				
Benzene	< 0.5	0.89	< 0.5	< 0.5
Toluene	< 0.5	< 0.5	< 0.5	< 0.5
Ethylbenzene	< 0.5	< 0.5	< 0.5	< 0.5
p- / m-xylene	< 1.0	< 1.0	< 1.0	< 1.0
o-xylene	< 0.5	< 0.5	< 0.5	< 0.5
Styrene	< 0.5	< 0.5	< 0.5	< 0.5
Cumene	< 0.5	< 0.5	< 0.5	< 0.5
Mesitylene	< 0.5	< 0.5	< 0.5	< 0.5
Sum of BTEX in µg/l	**n.n**	**n.n**	**n.n**	**n.n**

Gas-POX 204 (VP1, VP2, and VP3) quench water analysis report for BTEX

Quench water analysis			
Report number: 1501658			
Date: 18 – 21.03. 2015			
Method: DIN 38407-F 9-1			
Gas-POX 204	VP1	VP2	VP3
Sample name	Quench water 18.03.15 18:30 p.m.	Quench water 19.03.15 07:15 a.m.	Quench water 19.03.15 16:30 p.m.
Laboratory number	1503093	1503094	1503095
Parameter (µg/l)			
Benzene	1.3	< 0.5	< 0.5
Toluene	< 0.5	< 0.5	< 0.5
Ethylbenzene	< 0.5	< 0.5	< 0.5
p- / m-xylene	< 1.0	< 1.0	< 1.0
o-xylene	< 0.5	< 0.5	< 0.5
Styrene	< 0.5	< 0.5	< 0.5
Cumene	< 0.5	< 0.5	< 0.5
Mesitylene	< 0.5	< 0.5	< 0.5
Sum of BTEX in µg/l	**1.3**	**n.n**	**n.n**

Gas-POX 204 (VP4, VP5, and VP6) quench water analysis report for BTEX

Quench water analysis			
Report number: 1501658			
Date: 18 – 21.03. 2015			
Method: DIN 38407-F 9-1			
Gas-POX 204	VP4	VP5	VP6
Sample name	Quench water 20.03.15 19:30 p.m.	Quench water 21.03.15 06:00 a.m.	Quench water 21.03.15 18:00 p.m.
Laboratory number	1503096	1503097	1503098
Parameter (µg/l)			
Benzene	0.72	< 0.5	< 0.5
Toluene	< 0.5	< 0.5	< 0.5
Ethylbenzene	< 0.5	< 0.5	< 0.5
p- / m-xylene	< 1.0	< 1.0	< 1.0
o-xylene	< 0.5	< 0.5	< 0.5
Styrene	< 0.5	< 0.5	< 0.5
Cumene	< 0.5	< 0.5	< 0.5
Mesitylene	< 0.5	< 0.5	< 0.5
Sum of BTEX in µg/l	**0.72**	**n.n**	**n.n**

Gas-POX 205 (VP1, VP2, VP3, and VP5) quench water analysis report for BTEX

Quench water analysis				
Report number: 1503649				
Date: 27.06. 2015				
Method: DIN 38407-F 9-1				
Gas-POX 205	VP1	VP2	VP3	VP5
Sample name	Quench water 25.06 15 13:00 p.m.	Quench water 25.06 15 21:30 p.m.	Quench water 26.06 15 05:30 a.m.	Quench water 27.06 15 03:15 a.m.
Laboratory number	1506521	1506522	1506523	1506524
Parameter (µg/l)				
Benzene	73	0.83	0.71	0.76
Toluene	0.82	< 0.5	< 0.5	< 0.5
Ethylbenzene	< 0.5	< 0.5	< 0.5	< 0.5
p- / m-xylene	< 1.0	< 1.0	< 1.0	< 1.0
o-xylene	< 0.5	< 0.5	< 0.5	< 0.5
Styrene	< 0.5	< 0.5	< 0.5	< 0.5
Cumene	< 0.5	< 0.5	< 0.5	< 0.5
Mesitylene	< 0.5	< 0.5	< 0.5	< 0.5
Sum of BTEX in µg/l	**74**	**0.83**	**0.71**	**0.76**

Gas-POX 205 (VP4, VP6, and ZP2) quench water analysis report for BTEX

Quench water analysis			
Report number: 1503649			
Date: 27.06. 2015			
Method: DIN 38407-F 9-1			
Gas-POX 205	VP4	VP6	ZP2
Sample name	Quench water 27.06 15 09:45 a.m.	Quench water 27.06 15 16:30 p.m.	Quench water 27.06 15 22:00 p.m.
Laboratory number	1506525	1506526	1506527
Parameter (µg/l)			
Benzene	1.1	< 0.5	50
Toluene	< 0.5	< 0.5	< 0.5
Ethylbenzene	< 0.5	< 0.5	< 0.5
p- / m-xylene	< 1.0	< 1.0	< 1.0
o-xylene	< 0.5	< 0.5	< 0.5
Styrene	< 0.5	< 0.5	< 0.5
Cumene	< 0.5	< 0.5	< 0.5
Mesitylene	< 0.5	< 0.5	< 0.5
Sum of BTEX in µg/l	**1.1**	**n.n**	**50**

Gas-POX 206 (VP1, VP3, VP5, and VP6) quench water analysis report for BTEX

Quench water analysis				
Report number: 1506566				
Date:29 – 30.10, 2015				
Method: DIN 38407-F 9-1				
Gas-POX 206	VP1	VP3	VP5	VP6
Sample name	Quench water 29.10.15 11:00 a.m.	Quench water 29.10.15 23:30 p.m.	Quench water 30.10.15 09:00 a.m.	Quench water 30.10.15 19:00 p.m.
Laboratory number	1512043	1512044	1512045	1512046
Parameter (µg/l)				
Benzene	9.3	0.78	0.72	95
Toluene	< 0.5	< 0.5	< 0.5	< 1.0
Ethylbenzene	< 0.5	< 0.5	< 0.5	< 0.5
p- / m-xylene	< 1.0	< 1.0	< 1.0	< 1.0
o-xylene	< 0.5	< 0.5	< 0.5	< 0.5
Styrene	< 0.5	< 0.5	< 0.5	< 0.5
Cumene	< 0.5	< 0.5	< 0.5	< 0.5
Mesitylene	< 0.5	< 0.5	< 0.5	< 0.5
Sum of BTEX in µg/l	**9.3**	**0.78**	**0.72**	**96**
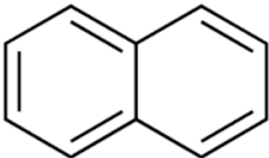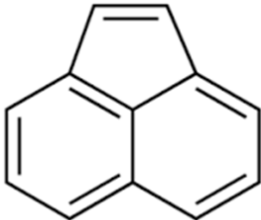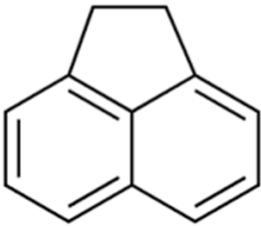
Gas-POX 207 (VP1, VP2 and VP3) quench water analysis report for BTEX
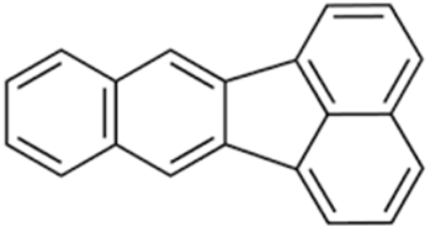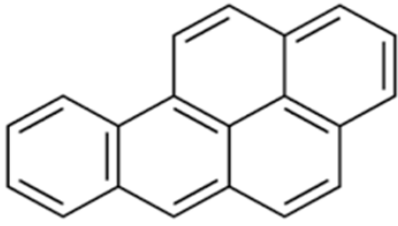
Quench water analysis			
Report number: 1601472			
Date: 09 – 12 .03 2016			
Method: DIN 38407-F 9-1			
Gas-POX 207	VP1	VP2	VP3
Sample name	Quench water 09.03 16 09:00 a.m.	Quench water 09.03 16 18:30 p.m.	Quench water 10.03 16 23:15 p.m.
Laboratory number	1603195	1603196	1603197
Parameter (µg/l)			
Benzene	0.84	< 0.5	50
Toluene	< 0.5	< 0.5	< 0.5
Ethylbenzene	< 0.5	< 0.5	< 0.5
p- / m-xylene	< 1.0	< 1.0	< 1.0
o-xylene	< 0.5	< 0.5	< 0.5
Styrene	< 0.5	< 0.5	< 0.5
Cumene	< 0.5	< 0.5	< 0.5
Mesitylene	< 0.5	< 0.5	< 0.5
Sum of BTEX in µg/l		**0.84**	**n.n**	**50**

Gas-POX 207 (VP4, VP5 and VP6) quench water analysis report for BTEX

Quench water analysis			
Report number: 1601472			
Date: 09 – 12 .03 2016			
Method: DIN 38407-F 9-1			
Gas-POX 207	VP4	VP5	VP6
Sample name	Quench water 11.03 16 11:00 a.m.	Quench water 12.03 16 01:00 a.m.	Quench water 12.03 16 09:45 p.m.
Laboratory number	1603198	1603199	1603200
Parameter (µg/l)			
Benzene	0.84	< 0.5	< 0.5
Toluene	< 0.5	< 0.5	< 0.5
Ethylbenzene	< 0.5	< 0.5	< 0.5
p- / m-xylene	< 1.0	< 1.0	< 1.0
o-xylene	< 0.5	< 0.5	< 0.5
Styrene	< 0.5	< 0.5	< 0.5
Cumene	< 0.5	< 0.5	< 0.5
Mesitylene	< 0.5	< 0.5	< 0.5
Sum of BTEX in µg/l		**n.n**	**n.n**	**n.n**

Table 9.8: Content of PAH compounds in Gas-POX quench water samples

PAH compounds	Chemical formula CAS Number	Structure	IUPAC name
Naphthalene	$C_{10}H_8$ 91-20-3		Naphthalene
Acenaphthylene	$C_{12}H_8$ 208-96-8		Acenaphthylene
Acenaphthene	$C_{12}H_{10}$ 83-32-9		1,2-Dihydroacenaphthylene
Fluorene	$C_{13}H_{10}$ 86-73-7		9H-Fluorene
Phenanthrene	$C_{14}H_{10}$ 85-01-8		Phenanthrene
Anthracene	$C_{14}H_{10}$ 120-12-7		Anthracene
Fluoranthene	$C_{16}H_{10}$ 206-44-0		Fluoranthene

Pyrene	C$_{16}$H$_{10}$		Pyrene
	129-00-0		
Benzanthracene	C$_{18}$H$_{12}$		benz[a]anthracene
	56-55-3		
Chrysene	C$_{18}$H$_{12}$		Chrysene
	218-01-9		
Benzo(b)fluoranthene	C$_{20}$H$_{12}$		Benzo(b)fluoranthene
	205-99-2		
Benzo(k)flouranthene	C$_{20}$H$_{12}$		Benzo(k)flouranthene
	207-08-9		
Benzo(a)pyrene	C$_{20}$H$_{12}$		
	50-32-8		
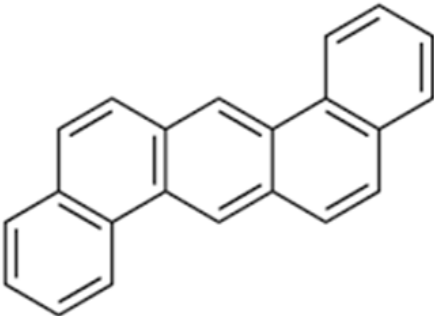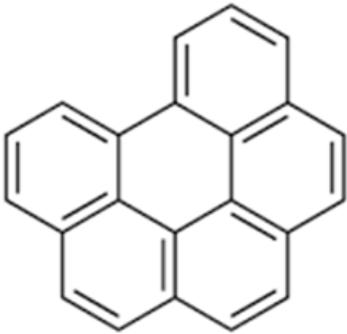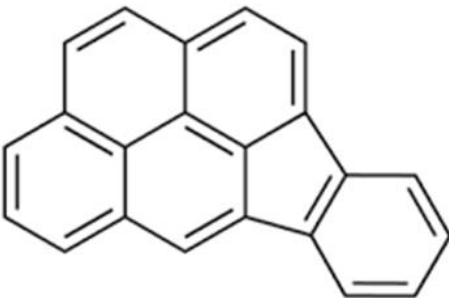
Dibenz(a,h)anthracene	C$_{22}$H$_{14}$		Dibenz(a,h)anthracene
	53-70-3		
Benzo(ghi)perylene	C$_{22}$H$_{12}$		Benzo(ghi)perylene
	191-24-2		
Indeno(1,2,3-cd)pyren	C$_{22}$H$_{12}$		Indeno(1,2,3-cd)pyren
	193-39-5		

Table 9.9: PAHs in quench water effluent samples results

Gas-POX 203 (VP1a, VP1b, and VP2b) quench water analysis report for PAH

Quench water analysis / Extraction				
Report number: 1408115				
Date: 05.06 – 12.12. 2014				
Method: DIN 38407-F 18				
Gas-POX 203		VP1a	VP1b	VP2b
Sample name	Quench water 05.06.14 13:00 p.m.	Quench water 11.12.14 03:30 a.m.	Quench water 11.12.14 00:45 a.m.	Quench water 11.12.14 03:00 a.m.
Laboratory number	1414926	1414927	1414928	1414929
Parameter (µg/l)				
Naphthalene	0.17	0.032	0.060	0.056
Acenaphthylene	< 0.01	0.013	< 0.01	< 0.01
Acenaphthene	0.050	0.042	0.032	0.025
Fluorene	0.043	0.040	0.013	0.012
Phenanthrene	0.46	0.47	0.38	0.27
Anthracene	0.065	0.18	0.13	0.15
Fluoranthene	0.43	1.3	1.2	0.76
Pyrene	1.1	5.0	3.6	2.9
Benzanthracene	0.16	0.34	0.26	0.19
Chrysene	0.11	1.1	1.0	0.92
Benzo(b)fluoranthene	0.11	0.37	0.25	0.21
Benzo(k)flouranthene	0.16	0.11	0.071	0.061
Benzo(a)pyrene	0.026	1.2	0.86	0.77
Dibenz(a,h)anthracene	< 0.01	0.19	0.091	0.024
Benzo(ghi)perylene	0.14	0.34	0.15	0.16
Indeno(1,2,3-cd)pyren	0.10	0.21	0.071	0.75
Sum of PAH in µg/l	**3.0**	**11**	**8.2**	**7.3**

Gas-POX 203 (VP3, VP6, VP4, and VP5) quench water analysis report for PAH

Quench water analysis / Extraction				
Report number: 1408115				
Date: 05.06 – 12.12. 2014				
Method: DIN 38407-F 18				
Gas-POX 203	VP3	VP6	VP4	VP5
Sample name	Quench water 05.06.14 10:30 a.m.	Quench water 11.12.14 03:30 a.m.	Quench water 11.12.14 10:00 a.m.	Quench water 11.12.14 18:30 a.m.
Laboratory number	1414930	1414931	1414932	1414933
Parameter (µg/l)				
Naphthalene	< 0.01	< 0.01	0.24	0.15
Acenaphthylene	< 0.01	< 0.01	< 0.01	< 0.01
Acenaphthene	0.027	0.016	0.028	0.028
Fluorene	0.027	0.014	0.040	0.030
Phenanthrene	0.21	0.12	0.24	0.18
Anthracene	0.070	< 0.01	0.076	0.060
Fluoranthene	0.46	0.13	0.66	0.38
Pyrene	1.8	0.92	2.9	1.5
Benzanthracene	0.12	0.085	0.19	0.12
Chrysene	0.74	0.54	0.92	0.67
Benzo(b)fluoranthene	0.23	0.13	0.24	0.18
Benzo(k)flouranthene	0.052	< 0.01	0.060	0.042
Benzo(a)pyrene	0.058	0.55	0.94	0.72
Dibenz(a,h)anthracene	0.15	0.24	0.16	0.18
Benzo(ghi)perylene	0.32	0.42	0.31	0.35
Indeno(1,2,3-cd)pyren	0.99	0.12	0.088	0.074
Sum of PAH in µg/l	**5.8**	**3.3**	**7.1**	**4.7**

Gas-POX 204 (VP1, VP2, and VP3) quench water analysis report for PAH

Quench water analysis / Extraction			
Report number: 1501658			
Date: 18 – 21.03. 2015			
Method: DIN 38407-F 9-1			
Gas-POX 204	VP1	VP2	VP3
Sample name	Quench water 18.03.15 18:30 p.m.	Quench water 19.03.15 07:15 a.m.	Quench water 19.03.15 16:30 p.m.
Laboratory number	1503093	1503094	1503095
Parameter (µg/l)			
Naphthalene	< 0.01	0.11	0.14
Acenaphthylene	< 0.01	< 0.01	< 0.01
Acenaphthene	0.018	0.024	0.040
Fluorene	0.011	0.020	0.037
Phenanthrene	0.79	0.22	0.16
Anthracene	0.14	< 0.01	< 0.01
Fluoranthene	0.21	0.029	0.012
Pyrene	2.7	0.67	0.51
Benzanthracene	0.26	0.056	0.38
Chrysene	0.12	0.048	0.072
Benzo(b)fluoranthene	0.11	0.048	0.027
Benzo(k)flouranthene	0.066	0.027	< 0.01
Benzo(a)pyrene	0.37	0.11	0.14
Dibenz(a,h)anthracene	< 0.01	< 0.01	< 0.01
Benzo(ghi)perylene	0.80	0.96	1.0
Indeno(1,2,3-cd)pyren	< 0.01	0.027	0.025
Sum of PAH in µg/l	**5.2**	**2.4**	**2.5**

Gas-POX 204 (VP4, VP5, and VP6) quench water analysis report for PAH

Quench water analysis / Extraction			
Report number: 1501658			
Date: 18 – 21.03. 2015			
Method: DIN 38407-F 9-1			
Gas-POX 204	VP4	VP5	VP6
Sample name	Quench water 20.03.15 19:30 p.m.	Quench water 21.03.15 06:00 a.m.	Quench water 21.03.15 18:00 p.m.
Laboratory number	1503096	1503097	1503098
Parameter (µg/l)			
Naphthalene	0.075	0.018	< 0.01
Acenaphthylene	< 0.01	< 0.01	< 0.01
Acenaphthene	0.022	< 0.01	< 0.01
Fluorene	0.025	< 0.01	< 0.01
Phenanthrene	0.43	0.062	0.22
Anthracene	0.012	< 0.01	< 0.01
Fluoranthene	0.44	0.053	0.084
Pyrene	0.49	0.11	0.18
Benzanthracene	0.28	0.063	0.16
Chrysene	0.061	0.055	0.15
Benzo(b)fluoranthene	0.13	0.053	0.065
Benzo(k)flouranthene	0.066	0.024	0.023
Benzo(a)pyrene	0.30	0.055	0.16
Dibenz(a,h)anthracene	< 0.01	< 0.01	< 0.01
Benzo(ghi)perylene	0.69	0.38	0.36
Indeno(1,2,3-cd)pyren	0.013	0.020	0.012
Sum of PAH in µg/l	**3.0**	**0.89**	**1.4**

Gas-POX 205 (VP1, VP2, VP3, and VP5) quench water analysis report for PAH

Quench water analysis				
Report number: 1503649				
Date: 27.06. 2015				
Method: DIN 38407-F 9-1				
Gas-POX 205	VP1	VP2	VP3	VP5
Sample name	Quench water 25.06 15 13:00 p.m.	Quench water 25.06 15 21:30 p.m.	Quench water 26.06 15 05:30 a.m.	Quench water 27.06 15 03:15 a.m.
Laboratory number	1506521	1506522	1506523	1506524
Parameter (µg/l)				
Naphthalene	0.33	0.070	0.041	0.032
Acenaphthylene	0.015	< 0.01	< 0.01	< 0.01
Acenaphthene	0.045	0.014	0.013	0.010
Fluorene	0.20	0.013	0.034	0.037
Phenanthrene	1.7	0.18	0.22	0.28
Anthracene	7.1	2.1	1.2	0.48
Fluoranthene	1.2	0.14	0.073	0.65
Pyrene	50	2.5	1.2	3.3
Benzanthracene	0.16	0.060	0.059	0.14
Chrysene	1.2	0.50	0.34	1.6
Benzo(b)fluoranthene	0.24	0.15	0.071	0.22
Benzo(k)flouranthene	0.062	0.038	0.025	0.058
Benzo(a)pyrene	0.73	0.042	0.26	0.68
Dibenz(a,h)anthracene	< 0.01	< 0.01	< 0.01	0.047
Benzo(ghi)perylene	3.4	2.8	0.16	1.9
Indeno(1,2,3-cd)pyren	0.23	0.18	0.13	0.29
Sum of PAH in µg/l	**63**	**9.2**	**5.3**	**9.7**

Gas-POX 205 (VP4, VP6, and ZP2) quench water analysis report for BTEX

Quench water analysis			
Report number: 1503649			
Date: 27.06. 2015			
Method: DIN 38407-F 18			
Gas-POX 205	VP4	VP6	ZP2
Sample name	Quench water 27.06 15 09:45 a.m.	Quench water 27.06 15 16:30 p.m.	Quench water 27.06 15 22:00 p.m.
Laboratory number	1506525	1506526	1506527
Parameter (µg/l)			
Naphthalene	0.089	0.13	0.28
Acenaphthylene	0.072	0.046	0.074
Acenaphthene	0.054	0.014	0.018
Fluorene	0.026	0.027	0.032
Phenanthrene	1.0	0.29	0.27
Anthracene	1.0	0.84	0.38
Fluoranthene	1.1	0.40	0.31
Pyrene	1.4	4.1	6.2
Benzanthracene	7.3	0.14	0.089
Chrysene	0.50	1.4	0.86
Benzo(b)fluoranthene	4.2	0.33	0.24
Benzo(k)flouranthene	0.86	0.12	0.093
Benzo(a)pyrene	0.25	0.98	0.74
Dibenz(a,h)anthracene	2.7	0.35	0.43
Benzo(ghi)perylene	7.0	3.9	4.1
Indeno(1,2,3-cd)pyren	1.2	0.57	0.49
Sum of PAH in µg/l	**28.5**	**13.6**	**14.6**

Gas-POX 206 (VP1, VP3, VP5, and VP6) quench water analysis report for PAH

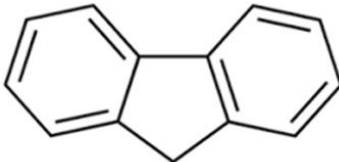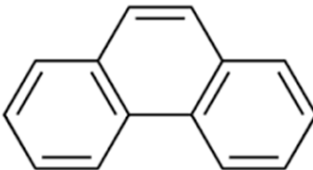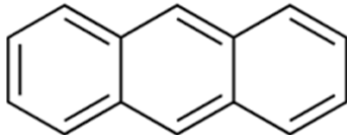| Quench water analysis				
Report number: 1506566				
Date:29 – 30.10, 2015				
Method: DIN 38407-F 9-1				
Gas-POX 206	VP1	VP3	VP5	VP6
Sample name	Quench water 29.10.15 11:00 a.m.	Quench water 29.10.15 23:30 p.m.	Quench water 30.10.15 09:00 a.m.	Quench water 30.10.15 19:00 p.m.
Laboratory number	1512043	1512044	1512045	1512046
Parameter (µg/l)				
Naphthalene	0.51	0.45	0.19	0.40
Acenaphthylene	0.33	0.17	0.095	0.08
Acenaphthene	0.023	0.068	0.028	0.010
Fluorene	0.11	0.062	0.019	0.010
Phenanthrene	2.3	1.1	0.34	0.22
Anthracene	0.14	0.46	0.24	0.010
Fluoranthene	4.6	2.5	0.97	0.39
Pyrene	24	11	4.24	2.81
Benzanthracene	0.53	0.32	0.13	0.067
Chrysene	1.2	1.8	0.95	0.44
Benzo(b)fluoranthene	0.52	0.40	0.23	0.20
Benzo(k)flouranthene	0.14	0.11	0.061	0.053
Benzo(a)pyrene	1.5	1.5	0.85	0.69
Dibenz(a,h)anthracene	< 0.01	< 0.01	< 0.01	< 0.01
Benzo(ghi)perylene	2.2	2.2	1.16	1.36
Indeno(1,2,3-cd)pyren	0.22	0.25	0.21	0.20
Sum of PAH in µg/l	**38.3**	**22.4**	**9.71**	**6.94**

Gas-POX 207 (VP1, VP2 and VP3) quench water analysis report for PAH

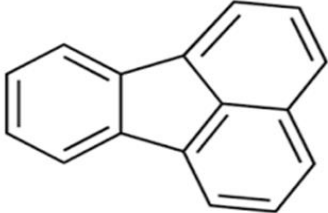| Quench water analysis			
Report number: 1601472			
Date: 27.06. 2015			
Method: DIN 38407-F 18			
Gas-POX 207	VP1	VP2	VP3
Sample name	Quench water 09.03 16 09:00 a.m.	Quench water 09.03 16 18:30 p.m.	Quench water 10.03 16 23:15 p.m.
Laboratory number	1603195	1603196	1603197
Parameter (μg/l)			
Naphthalene	0.062	0.085	0.15
Acenaphthylene	< 0.01	< 0.01	< 0.01
Acenaphthene	0.038	0.042	0.053
Fluorene	0.062	0.061	0.073
Phenanthrene	0.28	0.23	0.12
Anthracene	0.22	0.077	0.063
Fluoranthene	0.35	0.19	0.18
Pyrene	2.28	1.14	1.05
Benzanthracene	0.074	0.031	0.041
Chrysene	0.71	0.31	0.35
Benzo(b)fluoranthene	0.36	0.093	0.082
Benzo(k)flouranthene	0.093	0.027	0.028
Benzo(a)pyrene	1.3	0.38	0.35
Dibenz(a,h)anthracene	3.1	0.082	0.041
Benzo(ghi)perylene	0.30	0.85	0.40
Indeno(1,2,3-cd)pyren	0.81	0.24	0.14
Sum of PAH in μg/l	**10.0**	**3.84**	**3.12**

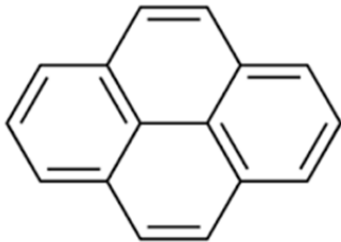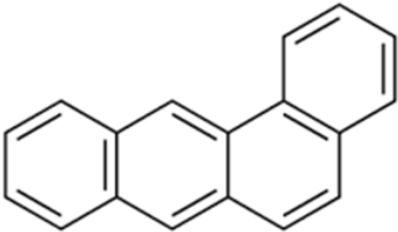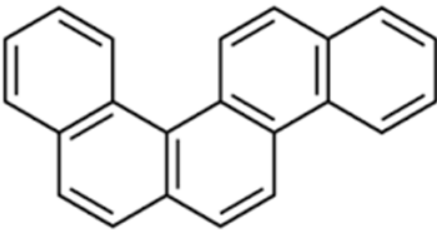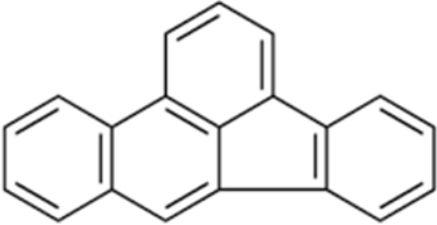**Gas-POX 207 (VP4, VP5 and VP6) quench water analysis report for PAH**

Quench water analysis			
Report number: 1601472			
Date: 09 – 12 .03 2016			
Method: DIN 38407-F 18			
Gas-POX 207	VP4	VP5	VP6
Sample name	Quench water 11.03 16 11:00 a.m.	Quench water 12.03 16 01:00 a.m.	Quench water 12.03 16 09:45 p.m.
Laboratory number	1603198	1603199	1603200
Parameter (µg/l)			
Naphthalene	< 0.01	0.039	0.050
Acenaphthylene	< 0.01	< 0.01	< 0.01
Acenaphthene	0.015	0.016	0.018
Fluorene	0.013	0.015	0.016
Phenanthrene	0.10	0.17	0.15
Anthracene	0.094	0.087	0.068
Fluoranthene	0.39	0.41	0.19
Pyrene	1.53	1.47	0.73
Benzanthracene	0.081	0.13	0.041
Chrysene	0.54	0.98	0.49
Benzo(b)fluoranthene	0.18	0.15	0.081
Benzo(k)flouranthene	0.050	0.053	0.031
Benzo(a)pyrene	0.54	0.57	0.35
Dibenz(a,h)anthracene	0.059	0.058	0.84
Benzo(ghi)perylene	0.74	0.85	0.048
Indeno(1,2,3-cd)pyren	0.26	0.25	0.19
Sum of PAH in µg/l	**4.59**	**5.29**	**3.29**

Table 9.10: Soot in quench water effluent samples results

Gas-POX 206 quench water analysis report for soot

Quench water analysis					
Turbidity measurement: GAS-POX Experiment					
Xion 500 Method			Measuring range 40 – 400 FAU		
Sample name	Water 05.11.15	Quench water 05.11.15 12:00 p.m.	Quench water 05.11.15 11:00 a.m.	Quench water 05.11.15 09:00 a.m.	Quench water 05.11.15 19:00 p.m.
Measured values FAU	-7.49	3.80	0.213	0.924	-2.25
Turbidity unit FAU	< 40	< 40	< 40	< 40	< 40
Soot fraction (mg/l)	< 50	< 50	< 50	< 50	< 50
Comments	Negative result	Below threshold of measuring range	Below threshold of measuring range	Below threshold of measuring range	Negative result
Sample bottle vigorously shaken, 8 ml pipetted in a measuring cuvette, Measuring cuvette was closed for 15 s, Measurement on the photometer Xion 500 Determination of carbon black content from calibration curve 50 – 500 mg/l Carbon black content					

FAU (Formazine Attenuation Units)

Table 9.11: Aspen Plus flow sheet setup stream details (GasPOX 201 VP1, according to Fig.3.2 and Fig.9.1, organic acids not taken into account)

	Units	DEGASS	DEIONAT	F103	F136	F136PRES	FLASHOUT	H2OPUMP	HOTGAS	HOTGAS2	HOTGAS3	HOTGAS4	HOTGAS5	RAWGAS	T104	VALVOUT
From		SPLITATM		SPLITOUT	SPLITATM	SPLITOUT	QUENCH	P105		B2	B2	RGIBBS1	RGIBBS2	QUENCH	W106	COOLER
To			P105	QUENCH		COOLER	P105	W106	B2	QUENCH	RGIBBS1	RGIBBS2			SPLITOUT	SPLITATM
Substream: MIXED																
Phase:		Vapor	Liquid	Liquid	Liquid	Liquid	Liquid	Liquid	Vapor	Vapor	Vapor	Vapor	Vapor	Vapor	Liquid	Mixed
Component Mole Fraction																
H_2O		0.0235876	1	0.9931589	0.9954762	0.9931589	0.9923915	0.9931592	0.1860173	0.1860173	0.1860173	0.1529753	0.1860173	0.1519179	0.9931589	0.9931589
CO_2		0.0928307	0	0.00028786	6.55E-05	0.00028786	0.00039216	0.00034485	0.0413129	0.0413129	0.0413129	0.0297907	0.0413129	0.0430027	0.00028786	0.00028667
CO		0.4997677	0	0.0022766	0.00108762	0.0022766	0.00253198	0.00227647	0.2365049	0.2365049	0.2365049	0.2616423	0.2365049	0.2462291	0.0022766	0.0022766
H_2		0.2017593	0	0.00048394	2.90E-06	0.00048394	0.00053823	0.00048392	0.4841684	0.4841684	4.84E-01	5.37E-01	0.4841684	0.5067306	0.00048394	0.00048394
CH_4		0.1806506	0	0.00353793	0.00311464	0.00353793	0.00393479	0.00353773	0.0455476	0.0455476	0.0455476	0.0121148	0.0455476	0.0454501	0.00353793	0.00353793
H_2S		9.22E-06	0	3.82E-08	1.90E-08	3.82E-08	3.85E-08	3.40E-08	1.45E-06	1.45E-06	1.45E-06	1.36E-06	1.45E-06	1.49E-06	3.82E-08	4.09E-08
NH_3		1.42E-07	0	1.41E-06	2.01E-07	1.41E-06	7.34E-05	5.82E-05	1.56E-04	1.56E-04	1.56E-04	1.57E-04	1.56E-04	8.33E-05	1.41E-06	2.01E-07
HCN		6.81E-06	0	1.72E-06	1.71E-06	1.72E-06	1.84E-06	1.66E-06	4.34E-06	4.34E-06	4.34E-06	9.94E-06	4.33E-06	3.44E-06	1.72E-06	1.72E-06
N_2		0.00138184	0	3.31E-06	1.72E-08	3.31E-06	3.68E-06	3.31E-06	6.29E-03	6.29E-03	6.29E-03	5.89E-03	6.29E-03	6.58E-03	3.31E-06	3.31E-06
COS		5.98E-06	0	6.38E-07	6.26E-07	6.38E-07	7.10E-07	6.38E-07	1.07E-06	1.07E-06	1.07E-06	1.01E-06	1.07E-06	7.18E-07	6.38E-07	6.38E-07
ACETI-01		0	0	0	0	0	0	0	0	0	0	0	0	0	0	0
FORMI-01		0.00E+00	0	0.00E+00	0.00E+00	0.00E+00	0.00E+00	0.00E+00	0.00E+00	0.00E+00	0	0	0.00E+00	0.00E+00	0.00E+00	0
HCL		0	0	0	0	0	0	0	0	0	0	0	0	0	0	0
NH_4^+		0	0	0.0001238	0.00012531	0.0001238	6.59E-05	6.69E-05	0.00E+00	0.00E+00	0.00E+00	0	0.00E+00	0.00E+00	1.24E-04	0.00012501
NA^+		0	0	0	0	0	0	0	0	0	0	0	0	0	0	0
H_3O^+		0	1.47E-08	2.26E-08	4.36E-09	2.26E-08	1.21E-08	1.22E-08	0.00E+00	0.00E+00	0.00E+00	0.00E+00	0.00E+00	0.00E+00	2.26E-08	4.35E-09
NH_2COO^-		0	0	6.45E-09	5.03E-09	6.45E-09	3.01E-08	2.70E-08	0.00E+00	0.00E+00	0.00E+00	0.00E+00	0.00E+00	0.00E+00	6.45E-09	5.01E-09
HS^-		0	0	1.00E-08	7.24E-09	1.00E-08	1.51E-08	1.42E-08	0.00E+00	0.00E+00	0.00E+00	0.00E+00	0.00E+00	0.00E+00	1.00E-08	7.23E-09
HCO_3^-		0	0	1.24E-04	1.25E-04	1.24E-04	6.56E-05	6.67E-05	0.00E+00	0.00E+00	0.00E+00	0.00E+00	0.00E+00	0.00E+00	1.24E-04	0.00012495
OH^-		0	1.47E-08	3.91E-09	5.58E-10	3.91E-09	1.14E-07	1.00E-07	0.00E+00	0.00E+00	0.00E+00	0.00E+00	0.00E+00	0.00E+00	3.91E-09	5.57E-10
CL^-		0	0	0	0	0	0	0	0	0	0	0	0	0	0	0
CH_3COO^-		0	0	0	0	0	0	0	0	0	0	0.00E+00	0	0	0	0

Component	Units	1	2	3	4	5	6	7	8	9	10	11	12	13	14	15
HCOO⁻		0	0	0.00E+00	0.00E+00	0.00E+00	0.00E+00	0.00E+00	0.00E+00	0.00E+00	0.00E+00	0	0.00E+00	0.00E+00	0.00E+00	0
CN-		0	0	1.07E-08	3.45E-09	1.07E-08	7.50E-08	6.69E-08	0.00E+00	0.00E+00	0.00E+00	0.00E+00	0.00E+00	0.00E+00	1.07E-08	3.44E-09
S²⁻		0	0	9.48E-16	2.44E-17	9.48E-16	5.05E-13	3.45E-13	0.00E+00	0.00E+00	0.00E+00	0.00E+00	0.00E+00	0.00E+00	9.48E-16	2.44E-17
CO₃²⁻		0	0	9.46E-09	2.75E-08	9.46E-09	3.27E-09	3.73E-09	0.00E+00	0.00E+00	0.00E+00	0.00E+00	0.00E+00	0.00E+00	9.46E-09	2.75E-08
Component Mole Flow																
H₂O	KMOL/HR	0.00203935	33.57191	294.351	36.01186	36.01394	296.8146	330.3839	11.11285	11.11285	11.11285	9.73535	11.11285	8.666328	330.365	36.0139
CO₂	KMOL/HR	0.00802597	0	0.085314	0.00236916	0.0104382	0.1172906	0.1147167	2.468076	2.468076	2.468076	1.895883	2.468076	2.453149	0.0957522	0.0103951
CO	KMOL/HR	0.0432089	0	0.6747349	0.039345	0.082554	0.757289	0.757289	14.12903	14.12903	14.12903	16.65092	14.12903	14.04648	0.757289	0.082554
H₂	KMOL/HR	0.0174437	0	0.1434306	0.000105047	0.0175487	0.1609794	0.1609794	28.92469	28.92469	28.92469	34.20107	28.92469	28.90715	0.1609794	0.0175487
CH₄	KMOL/HR	0.0156187	0	1.048566	0.1126736	0.1282923	1.176858	1.176858	2.72106	2.72106	2.72106	0.7709905	2.72106	2.592768	1.176858	0.1282923
H₂S	KMOL/HR	7.97E-07	0	1.13E-05	6.87E-07	1.38E-06	1.15E-05	1.13E-05	8.68E-05	8.68E-05	8.68E-05	8.68E-05	8.68E-05	8.50E-05	1.27E-05	1.48E-06
NH₃	KMOL/HR	1.23E-08	0	0.000417878	7.27E-06	5.11E-05	0.0219459	0.0193728	0.00929062	0.00929062	0.00929062	1.00E-02	0.00929062	0.00474998	0.000469005	7.28E-06
HCN	KMOL/HR	5.89E-07	0	0.000508396	6.19E-05	6.22E-05	0.000551715	0.000551887	0.000259099	0.000259099	0.000259099	0.000632722	0.000258974	0.000196508	0.000570599	6.25E-05
N₂	KMOL/HR	0.000119471	0	0.000981566	6.24E-07	0.000120095	0.00110166	0.00110166	0.3755611	0.3755611	0.3755611	0.3750131	0.3755612	0.375441	0.00110166	0.000120095
COS	KMOL/HR	5.17E-07	0	0.000189214	2.26E-05	2.32E-05	0.000212365	0.000212365	6.41E-05	6.41E-05	6.41E-05	6.41E-05	6.41E-05	4.09E-05	0.000212365	2.32E-05
ACETI-01	KMOL/HR	0	0	0	0	0	0	0	0	0	0	0	0	0	0	0
FORMI-01	KMOL/HR	0.00E+00	0	0	0.00E+00	0.00E+00	0	0	0	0	0	0	0	0	0	0
HCL	KMOL/HR	0	0	0	0	0	0	0	0	0	0	0	0	0	0	0
NH₄⁺	KMOL/HR	0	0	0.0366919	0.00453318	0.00448927	0.0196974	0.0222705	0	0	0	0	0	0	0.0411812	0.00453318
NA⁺	KMOL/HR	0	0	0	0	0	0	0	0	0	0	0	0	0	0	0
H₃O⁺	KMOL/HR	0	4.95E-07	6.70E-06	1.58E-07	8.20E-07	3.63E-06	4.07E-06	0.00E+00	0.00E+00	0.00E+00	0	0.00E+00	0.00E+00	7.53E-06	1.58E-07
NH₂COO⁻	KMOL/HR	0	0	1.91E-06	1.82E-07	2.34E-07	9.01E-06	8.99E-06	0.00E+00	0.00E+00	0.00E+00	0.00E+00	0.00E+00	0.00E+00	2.15E-06	1.82E-07
HS⁻	KMOL/HR	0	0	2.97E-06	2.62E-07	3.63E-07	4.50E-06	4.71E-06	0.00E+00	0.00E+00	0.00E+00	0.00E+00	0.00E+00	0.00E+00	3.33E-06	2.62E-07
HCO₃⁻	KMOL/HR	0	0	0.0366838	0.00453076	0.00448828	0.019629	0.0222027	0	0	0	0.00E+00	0	0	0.0411721	0.00453076
OH⁻	KMOL/HR	0	4.95E-07	1.16E-06	2.02E-08	1.42E-07	3.41E-05	3.34E-05	0.00E+00	0.00E+00	0.00E+00	0.00E+00	0.00E+00	0.00E+00	1.30E-06	2.02E-08
CL⁻	KMOL/HR	0	0	0	0	0	0	0	0	0	0	0	0	0	0	0
CH₃COO⁻	KMOL/HR	0	0	0	0	0	0	0	0	0	0	0.00E+00	0	0	0	0
HCOO⁻	KMOL/HR	0	0	0	0	0	0	0	0	0	0	0	0	0	0	0
CN⁻	KMOL/HR	0	0	3.17E-06	1.25E-07	3.88E-07	2.24E-05	2.23E-05	0.00E+00	0.00E+00	0.00E+00	0.00E+00	0.00E+00	0.00E+00	3.56E-06	1.25E-07

Component	Units															
S^{2-}	KMOL/HR	0	0	2.81E-13	8.83E-16	3.44E-14	1.51E-10	1.15E-10	0.00E+00	0.00E+00	0.00E+00	0.00E+00	0.00E+00	0.00E+00	3.15E-13	8.83E-16
CO_3^{2-}	KMOL/HR	0	0	2.80E-06	9.95E-07	3.43E-07	9.79E-07	1.24E-06	0.00E+00	0.00E+00	0.00E+00	0.00E+00	0.00E+00	0.00E+00	3.15E-06	9.95E-07
Component Mass Flow																
H_2O	KG/HR	0.0367394	604.8073	5302.816	648.7638	648.8013	5347.198	5951.959	200.2012	200.2012	200.2012	175.3851	200.2012	156.1263	5951.618	648.8005
CO_2	KG/HR	0.3532215	0	3.754655	0.104266	0.459383	5.161937	5.048659	108.6195	108.6195	108.6195	83.43742	108.6195	107.9626	4.214038	0.4574876
CO	KG/HR	1.210301	0	18.8996	1.10207	2.312372	21.21197	21.21197	395.7599	395.7599	395.7599	466.399	395.7599	393.4475	21.21197	2.312372
H_2	KG/HR	0.0351644	0	0.2891389	0.000211763	0.0353762	0.3245151	0.3245151	58.30871	58.30871	58.30871	68.94525	58.30871	58.27334	0.3245151	0.0353762
CH_4	KG/HR	0.2505674	0	16.82189	1.807596	2.058163	18.88005	18.88005	43.65331	43.65331	43.65331	12.36882	43.65331	41.59515	18.88005	2.058163
H_2S	KG/HR	2.72E-05	0	0.000385519	2.34E-05	4.72E-05	0.000392637	0.000385453	0.00295767	0.00295767	0.00295767	0.00295767	0.00295767	0.00289813	0.000432687	5.06E-05
NH_3	KG/HR	2.10E-07	0	0.00711669	1.24E-04	0.000870729	0.373751	0.329930	0.1582244	0.1582244	0.1582244	0.1705267	0.1582244	0.0808948	0.00798742	0.000123939
HCN	KG/HR	1.59E-05	0	0.0137397	0.00167226	0.00168106	0.0149104	0.0149151	0.00700232	0.00700232	0.00700232	0.0170997	0.00699894	0.00531077	0.0154208	0.00168817
N_2	KG/HR	0.00334628	0	0.027497	1.75E-05	0.00336428	0.0308613	0.0308613	10.52077	10.52077	10.52077	10.50542	10.52078	10.51741	0.0308613	0.00336428
COS	KG/HR	3.10E-05	0	0.0113673	0.00135975	0.00139079	0.0127581	0.0127581	0.0038504	0.0038504	0.0038504	0.0038504	0.0038504	0.00245961	0.0127581	0.00139079
ACETI-01	KG/HR	0	0	0	0	0	0	0	0	0	0	0	0	0	0	0
FORMI-01	KG/HR	0.00E+00	0	0	0	0	0	0	0	0	0	0	0	0	0	0
HCL	KG/HR	0	0	0	0	0	0	0	0	0	0	0	0	0	0	0
NH_4^+	KG/HR	0	0	0.6618477	0.0817691	0.0809772	0.355302	0.4017149	0	0	0	0	0	0	0.742825	0.0817691
NA^+	KG/HR	0	0	0	0	0	0	0	0	0	0	0	0	0	0	0
H_3O^+	KG/HR	0	9.42E-06	0.000127544	3.00E-06	1.56E-05	6.90E-05	7.74E-05	0	0	0	0	0	0	0.00014315	3.00E-06
NH_2COO^-	KG/HR	0	0	1.15E-04	1.09E-05	1.41E-05	0.000541196	0.000539781	0	0	0	0.00E+00	0	0	0.000128898	1.09E-05
HS^-	KG/HR	0	0	9.81E-05	8.67E-06	1.20E-05	1.49E-04	1.56E-04	0.00E+00	0.00E+00	0.00E+00	0.00E+00	0.00E+00	0.00E+00	1.10E-04	8.67E-06
HCO_3^-	KG/HR	0	0	2.238365	0.2764562	0.2738646	1.197721	1.354762	0	0	0	0	0	0	2.512229	0.2764562
OH^-	KG/HR	0	8.42E-06	1.97E-05	3.44E-07	2.41E-06	0.000580119	0.000568024	0	0	0	0.00E+00	0	0	2.21E-05	3.44E-07
CL^-	KG/HR	0	0	0	0	0	0	0	0	0	0	0	0	0	0	0
CH_3COO^-	KG/HR	0	0	0	0	0	0	0	0	0	0	0	0	0	0	0
$HCOO^-$	KG/HR	0	0	0	0	0	0	0	0	0	0	0	0	0	0	0
CN^-	KG/HR	0	0	8.25E-05	3.25E-06	1.01E-05	0.000583906	0.000579446	0	0	0	0.00E+00	0	0	9.26E-05	3.25E-06
S^{2-}	KG/HR	0	0	9.01E-12	2.83E-14	1.10E-12	4.84E-09	3.68E-09	0.00E+00	0.00E+00	0.00E+00	0.00E+00	0.00E+00	0.00E+00	1.01E-11	2.83E-14
CO_3^{2-}	KG/HR	0	0	1.68E-04	5.97E-05	2.06E-05	5.88E-05	7.44E-05	0.00E+00	0.00E+00	0.00E+00	0.00E+00	0.00E+00	0.00E+00	1.89E-04	5.97E-05
Total Mole Flow	KMOL/HR	0.0864581	33.57191	296.3786	36.17551	36.26202	299.0902	332.6596	59.74098	59.74098	59.74098	63.64002	59.74098	57.04638	332.6406	36.26197

Total Mass Flow	KG/HR	1.889415	604.8073	5345.543	652.1394	654.0289	5394.764	5999.571	817.2354	817.2354	817.2354	817.2354	817.2354	768.0139	5999.571	654.0289
Total Volume Flow	CUM/HR	2.105579	0.631389	5.62477	0.6650318	0.6881924	6.193782	6.815753	102.1621	102.1621	102.1621	108.8626	102.1621	30.26388	6.312962	2.770611
Temperature	C	20	105	79.99752	20	79.99752	177.4174	170.3033	1172.073	1172.073	1172.073	1172.073	1172.073	177.4174	79.99752	20
Pressure	BAR	1	72.0003	72.0003	1	72.0003	71.01355	72.0003	71.01355	71.01355	71.01355	71.01355	71.01355	71.01355	72.0003	1
Vapor Fraction		1	0	0	0	0	0	0	1	1	1	1	1	1	0	0.00238427
Liquid Fraction		0	1	1	1	1	1	1	0	0	0	0	0	0	1	0.9976157
Solid Fraction		0	0	0	0	0	0	0	0	0	0	0	0	0	0	0
Molar Enthalpy	KCAL/MOL	-26.56895	-66.8462	-67.00904	-68.20758	-67.00904	-65.19139	-65.35769	-12.15431	-12.15431	-12.15431	-9.678846	-12.15431	-19.07302	-67.00904	-68.1083
Mass Enthalpy	KCAL/KG	-1215.774	-3710.53	-3715.253	-3783.614	-3715.253	-3614.265	-3623.902	-888.4962	-888.4962	-888.4962	-753.7143	-888.4962	-1416.702	-3715.253	-3776.196
Enthalpy Flow	GCAL/HR	-0.0022971	-2.24416	-19.86004	-2.467444	-2.429883	-19.49811	-21.74186	-0.7261105	-0.7261105	-0.7261105	-0.615962	-0.7261105	-1.088047	-22.28993	-2.469741
Molar Entropy	CAL/MOL-K	9.52014	-34.7121	-35.72624	-39.14055	-35.72624	-31.25979	-31.58042	9.095839	9.095839	9.095839	9.803593	9.095839	-0.1523003	-35.72624	-39.02453
Mass Entropy	CAL/GM-K	0.4356341	-1.92682	-1.980808	-2.171207	-1.980808	-1.733069	-1.751046	0.6649177	0.6649177	0.6649177	0.7634286	0.6649177	-0.0113125	-1.980808	-2.163676
Molar Density	KMOL/CUM	0.0410614	53.17149	52.69169	54.39667	52.69169	48.28879	48.80746	0.5847664	0.5847664	0.5847664	0.5845904	0.5847664	1.884966	52.69169	13.08808
Mass Density	KG/CUM	0.8973376	957.8993	950.3576	980.6139	950.3576	870.9968	880.2507	7.999396	7.999396	7.999396	7.507036	7.999396	25.37725	950.3576	236.0595
Average Molecular Weight		21.85352	18.01528	18.0362	18.0271	18.0362	18.03725	18.03517	13.67965	13.67965	13.67965	12.84153	13.67965	13.46297	18.0362	18.03622
Liq Vol 60F cum/hr		4.56E-03							2.805002	2.805002	2.805002	3.062739	2.805002	2.747557		

Table 9.12: Aspen Plus flow sheet setup for organic acid and nitrogen compounds calculations for GasPOX 201 VP1 (according to Figures 9.7 and 9.8, organic acids are taken into account)

	Units	DEGASS	DEIONAT	F103	F136	F136 PRES	FLASHOU	FLASHOU 2	FLASHOU 3	FLASHOU 4	FLASHOU 5	FLASHOU 6	FLASHOU 7	FLASHOU T	H2OPUMP	HOT GAS	HOT GAS2	HOT GAS3	HOT GAS4	HOT GAS5	RAW GAS	S1	S2	S4	S5	S8	T104	VALVOUT
From		SPLIT ATM		SPLIT OUT	SPLIT ATM	SPLIT OUT	QUENCH	DUPLEX2	DUPLEX2	ACID SAP	ACID SEQ	QUENCH2	ACIDS	ACIDS2	P105		B2	B2	RGIBBSEQ	RGIBBSAP	QUENCH	B1	QUENCH2	ACIDSEQ	ACIDS2	ACIDSAP	W106	COOLER
To			B1	QUENCH	SPLIT OUT	COOLER	DUPLEX2	ACIDS	ACIDSAP	ACIDSEQ	QUENCH2		ACIDS2	B1	W106	B2	QUENCH	RGIBBSEQ	RGIBBSAP			P105			B1		SPLIT OUT	SPLIT ATM
Substream: MIXED																												
Phase:		Vapor	Liquid	Liquid	Liquid	Liquid	Liquid	Liquid	Liquid	Liquid	Liquid	Liquid	Liquid	Liquid	Liquid	Vapor	Vapor	Vapor	Vapor	Vapor	Vapor	Missing	Missing	Missing	Missing	Missing	Liquid	Mixed
Component Mole Fraction																												
H_2O		0.0235896	1	0.9931396	0.9954922	0.9931396	0.9923697	0.9923697	0.9923697	0.9923697	0.9930231	0.9929947	0.9923697	0.9923697	0.9931398	0.1860229	0.1860229	0.1860229	0.186028	0.1860229	0.1519623	0.9931398					0.9931396	0.9931397
CO_2		0.1023892	0	7.22E-05	0.00031978	0.00031978	0.00039239	0.00039239	0.00039239	0.00039239	0.0001275	0.00015595	0.000396	0.000396	0.00035125	0.0413141	0.0413141	0.0413141	0.0413148	0.0413141	0.0430238	0.00035129					0.00031978	0.00031982
CO		0.4938115	0	0.00226658	0.00107387	0.00226658	0.00252904	0.00252904	0.00252904	0.00252243	0.00159813	0.00159808	0.00252095	0.00252095	0.00226651	0.236512	0.236512	0.236512	0.2365137	0.236512	0.2461926	0.00226651					0.00226658	0.00226658
H_2		0.1985742	0	0.00048352	2.86E-06	0.00048352	0.00053778	0.00053778	0.00053778	0.00053778	7.68E-06	7.68E-06	0.00053778	0.00053778	0.0004835	0.484183	0.484183	0.484183	0.4841664	0.484183	0.5067303	0.0004835					0.00048352	0.00048352
CH_4		0.1802517	0	0.00353424	0.00310544	0.00353424	0.00393085	0.00393085	0.00393085	0.00393088	0.00393609	0.00393598	0.00393087	0.00393087	0.00353413	0.045549	0.045549	0.045549	0.0455497	0.045549	0.0454522	0.00353413					0.00353424	0.00353424
H_2S		1.10E-05	0	4.74E-08	2.26E-08	4.74E-08	5.02E-08	5.02E-08	5.02E-08	5.02E-08	5.02E-08	5.87E-08	5.12E-08	5.12E-08	4.52E-08	1.89E-06	1.89E-06	1.89E-06	1.89E-06	1.89E-06	1.94E-06	4.52E-08					4.74E-08	4.91E-08
NH_3		6.11E-08	0	6.12E-07	8.60E-08	6.12E-07	4.50E-05	4.50E-05	4.50E-05	4.50E-05	4.51E-05	6.76E-05	4.06E-05	4.06E-05	3.17E-05	0.00012486	0.00012486	0.00012486	0.00013905	0.00012486	5.12E-05	3.18E-05					6.12E-07	8.59E-08
HCN		6.82E-06	0	1.72E-06	1.71E-06	1.72E-06	1.89E-06	1.89E-06	1.89E-06	1.89E-06	1.89E-06	1.92E-06	1.89E-06	1.89E-06	1.70E-06	4.42E-06	4.42E-06	4.42E-06	6.54E-06	4.41E-06	3.53E-06	1.70E-06					1.72E-06	1.72E-06
N_2		0.00135998	0	3.31E-06	1.70E-08	3.31E-06	3.68E-06	3.68E-06	3.68E-06	3.68E-06	3.69E-06	3.68E-06	3.68E-06	3.68E-06	3.31E-06	0.00628668	0.00628668	0.00628668	0.00627862	0.00628668	0.00658132	3.31E-06					3.31E-06	3.31E-06
COS		5.98E-06	0	6.38E-07	6.25E-07	6.38E-07	7.10E-07	7.10E-07	7.10E-07	7.10E-07	7.11E-07	7.11E-07	7.10E-07	7.10E-07	6.38E-07	1.07E-06	1.07E-06	1.07E-06	1.07E-06	1.07E-06	7.18E-07	6.38E-07					6.38E-07	6.38E-07
ACETI-01		0	0	0	0	0	0	0	0	0	0.00013271	0.00013267	0	0	0	0	0	0	0	0	0	0					0	0
FORMI-01		5.77E-09	0	6.62E-07	1.28E-07	6.62E-07	3.50E-07	3.50E-07	3.50E-07	6.97E-06	0.00093463	0.00083244	4.54E-07	4.54E-07	3.86E-07	0	0	0	0	0	4.00E-08	3.87E-07					6.62E-07	1.27E-07
HCL		0	0	0	0	0	0	0	0	0	0	0	0	0	0	0	0	0	0	0	0	0					0	0
NH_4^+		0	0	0.00012459	0.00012542	0.00012459	9.42E-05	9.42E-05	9.42E-05	9.42E-05	9.44E-05	0.00013937	9.86E-05	9.86E-05	9.35E-05	0	0	0	0	0	0	9.34E-05					0.00012459	0.00012511
NA^+		0	0	0	0	0	0	0	0	0	0	0	0	0	0	0	0	0	0	0	0	0					0	0
H_3O^+		0	1.47E-08	5.31E-08	1.03E-08	5.31E-08	2.88E-08	2.88E-08	2.88E-08	2.88E-08	2.89E-08	2.87E-05	3.35E-08	3.35E-08	3.19E-08	0	0	0	0	0	0	3.18E-08					5.31E-08	1.02E-08

NH_2COO^-		0	0	1.33E-09	1.01E-09	1.33E-09	8.01E-09	8.01E-09	8.01E-09	8.01E-09	8.02E-09	5.16E-15	6.31E-09	6.31E-09	5.97E-09	0	0	0	0	0	0	5.98E-09				1.33E-09	1.01E-09
HS^-		0	0	5.29E-09	3.65E-09	5.29E-09	8.49E-09	8.49E-09	8.49E-09	8.49E-09	8.50E-09	1.07E-11	7.49E-09	7.49E-09	7.52E-09	0	0	0	0	0	0	7.50E-09				5.29E-09	3.65E-09
HCO_3^-		0	0	5.86E-05	5.87E-05	5.86E-05	2.84E-05	2.84E-05	2.84E-05	2.84E-05	2.85E-05	1.21E-08	2.48E-05	2.48E-05	2.71E-05	0	0	0	0	0	0	2.70E-05				5.86E-05	5.85E-05
OH^-		0	1.47E-08	1.66E-09	2.37E-10	1.66E-09	4.93E-08	4.93E-08	4.93E-08	4.93E-08	4.94E-08	5.30E-11	4.27E-08	4.27E-08	4.01E-08	0	0	0	0	0	0	3.99E-08				1.66E-09	2.36E-10
CL^-		0	0	0	0	0	0	0	0	0	0	0	0	0	0	0	0	0	0	0	0	0				0	0
CH_3COO^-		0	0	0	0	0	0	0	0	0	0	2.71E-08	0	0	0	0	0	0	0	0	0	0				0	0
$HCOO^-$		0	0	6.60E-05	6.67E-05	6.60E-05	6.57E-05	6.57E-05	6.57E-05	6.57E-05	6.58E-05	0.00016799	7.37E-05	7.37E-05	6.63E-05	0	0	0	0	0	0	6.63E-05				6.60E-05	6.66E-05
CN^-		0	0	4.57E-09	1.47E-09	4.57E-09	3.32E-08	3.32E-08	3.32E-08	3.32E-08	3.33E-08	3.64E-11	2.88E-08	2.88E-08	2.74E-08	0	0	0	0	0	0	2.73E-08				4.57E-09	1.46E-09
S^{2-}		0	0	2.13E-16	5.22E-18	2.13E-16	1.28E-13	1.28E-13	1.28E-13	1.28E-13	1.28E-13	1.83E-19	9.79E-14	9.79E-14	7.69E-14	0	0	0	0	0	0	7.52E-14				2.13E-16	5.21E-18
CO_3^{2-}		0	0	1.90E-09	5.46E-09	1.90E-09	6.34E-10	6.34E-10	6.34E-10	6.34E-10	6.35E-10	3.10E-16	4.81E-10	4.81E-10	6.30E-10	0	0	0	0	0	0	6.22E-10				1.90E-09	5.45E-09
Component Mole Flow																											
H_2O	KMOL/HR	0.002007077	33.577	294.3512	36.01433	36.0164	296.804	296.804	296.804	296.802	296.6042	296.6041	296.8026	296.8026	330.378	11.11285	11.11285	11.11285	11.11298	11.11285	8.668909	330.3676	0	0	0	0	330.3676	36.0164
CO_2	KMOL/HR	0.00898805	0	0.0947763	0.00261042	0.0115967	0.1173577	0.1173577	0.1173577	0.1173577	0.0380836	0.0465819	0.1184385	0.1184385	0.1168476	2.468076	2.468076	2.468076	2.468076	2.468076	2.454355	0.116859	0	0	0	0	0.106373	0.0115984
CO	KMOL/HR	0.0433483	0	0.6717795	0.0388496	0.082198	0.7563991	0.7563991	0.7563991	0.7544197	0.4773419	0.4773419	0.7539776	0.7539776	0.7539776	14.12903	14.12903	14.12903	14.12891	14.12903	14.04441	0.7539776	0	0	0	0	0.7539776	0.082198
H_2	KMOL/HR	0.0174314	0	0.1433065	0.00010332	0.0175347	0.1608413	0.1608413	0.1608413	0.1608413	0.00229323	0.00229323	0.1608413	0.1608413	0.1608413	28.92469	28.92469	28.92469	28.92323	28.92469	28.90716	0.1608413	0	0	0	0	0.1608413	0.0175347
CH_4	KMOL/HR	0.015823	0	1.047493	0.1123467	0.1281698	1.175663	1.175663	1.175663	1.175663	1.175663	1.175663	1.175663	1.175663	1.175663	2.72106	2.72106	2.72106	2.72106	2.72106	2.59289	1.175663	0	0	0	0	1.175663	0.1281698
H_2S	KMOL/HR	9.63E-07	0	1.41E-05	8.17E-07	1.72E-06	1.50E-05	1.50E-05	1.50E-05	1.50E-05	1.50E-05	1.75E-05	1.53E-05	1.53E-05	1.50E-05	0.00011282	0.00011282	0.00011282	0.00011282	0.00011282	0.0001109	1.50E-05	0	0	0	0	1.58E-05	1.78E-05
NH_3	KMOL/HR	5.37E-09	0	0.00018138	3.11E-06	2.22E-05	0.0134602	0.0134602	0.0134602	0.0134602	0.0134602	2.02E-05	0.012156	0.012156	0.0105568	0.00745874	0.00745874	0.00745874	0.00830679	0.00745875	0.00291832	0.0105688	0	0	0	0	0.00020358	3.12E-06
HCN	KMOL/HR	5.99E-07	0	0.00051025	6.19E-05	6.24E-05	0.00056427	0.00056427	0.00056427	0.00056427	0.00056427	0.00057419	0.00056559	0.00056559	0.0005651	0.00026376	0.00026376	0.00026376	0.0003909	0.00026363	0.00020116	0.00056514	0	0	0	0	0.00057268	6.25E-05
N_2	KMOL/HR	0.00011938	0	0.0009807	6.13E-07	0.00012	0.00110069	0.00110069	0.00110069	0.00110069	0.00110069	0.00110069	0.00110069	0.00110069	0.00110069	0.3755611	0.3755611	0.3755611	0.3750735	0.3755612	0.3754411	0.00110069	0	0	0	0	0.00110069	0.00012
COS	KMOL/HR	5.25E-07	0	0.00018909	2.26E-05	2.31E-05	0.00021223	0.00021223	0.00021223	0.00021223	0.00021223	0.00021223	0.00021223	0.00021223	0.00021223	6.41E-05	6.41E-05	6.41E-05	6.41E-05	6.41E-05	4.10E-05	0.00021223	0	0	0	0	0.00021223	2.31E-05
ACETI-01	KMOL/HR	0	0	0	0	0	0	0	0	0	0.0396374	0.0396293	0	0	0	0	0	0	0	0	0	0	0	0	0	0	0	0
FORMI-01	KMOL/HR	5.07E-10	0	0.00019635	4.62E-06	2.40E-05	0.00010476	0.00010476	0.00010476	0.00208412	0.2791619	0.2486482	0.00013581	0.00013581	0.00012829	0	0	0	0			2.28E-06	0	0	0	0	0.00012888	4.62E-05
HCL	KMOL/HR	0	0	0	0	0	0	0	0	0	0	0	0	0	0	0	0	0	0	0	0	0	0	0	0	0	0	0

	Units	1	2	3	4	5	6	7	8	9	10	11	12	13	14	15	16	17	18	19	20	21	22	23	24	25	26	27
NH_4^+	KMOL/HR	0	0	0.0369257	0.00453727	0.00451818	0.0281852	0.0281852	0.0281852	0.0281852	0.0281852	0.0416277	0.0294899	0.0294899	0.031089	0	0	0	0	0	0	0.0310771	0	0	0	0	0.0414439	0.00453727
NA^+	KMOL/HR	0	0	0	0	0	0	0	0	0	0	0	0	0	0	0	0	0	0	0	0	0	0	0	0	0	0	0
H_3O^+	KMOL/HR	0	4.95E-07	1.57E-05	3.71E-07	1.93E-06	8.62E-06	8.62E-06	8.62E-06	8.62E-06	8.62E-06	0.00856241	1.00E-05	1.00E-05	1.06E-05	0	0	0	0	0	0	1.06E-05	0	0	0	0	1.77E-05	3.71E-07
NH_2COO^-	KMOL/HR	0	0	3.93E-07	3.65E-08	4.81E-08	2.40E-06	2.40E-06	2.40E-06	2.40E-06	2.40E-06	1.54E-12	1.89E-06	1.89E-06	1.99E-06	0	0	0	0	0	0	1.99E-06	0	0	0	0	4.42E-07	3.65E-08
HS^-	KMOL/HR	0	0	1.57E-06	1.32E-07	1.92E-07	2.54E-06	2.54E-06	2.54E-06	2.54E-06	2.54E-06	3.19E-09	2.24E-06	2.24E-06	2.50E-06	0	0	0	0	0	0	2.50E-06	0	0	0	0	1.76E-06	1.32E-07
HCO_3^-	KMOL/HR	0	0	0.0173612	0.00212241	0.0021243	0.00849927	0.00849927	0.00849927	0.00849927	0.00849927	3.61E-06	0.00741908	0.00741908	0.00900974	0	0	0	0	0	0	0.00899843	0	0	0	0	0.0194855	0.00212241
OH^-	KMOL/HR	0	4.95E-07	4.93E-07	8.57E-09	6.03E-08	1.48E-05	1.48E-05	1.48E-05	1.48E-05	1.48E-05	1.58E-08	1.28E-05	1.28E-05	1.34E-05	0	0	0	0	0	0	1.33E-05	0	0	0	0	5.53E-07	8.57E-09
CL^-	KMOL/HR	0	0	0	0	0	0	0	0	0	0	0	0	0	0	0	0	0	0	0	0	0	0	0	0	0	0	0
CH_3COO^-	KMOL/HR	0	0	0	0	0	0	0	0	0	0	8.08E-06	0	0	0	0	0	0	0	0	0	0	0	0	0	0	0	0
$HCOO^-$	KMOL/HR	0	0	0.0195753	0.00241461	0.00239521	0.0196646	0.0196646	0.0196646	0.0196646	0.0196646	0.0501784	0.022055	0.022055	0.0220626	0	0	0	0	0	0	0.022062	0	0	0	0	0.0219705	0.00241461
CN^-	KMOL/HR	0	0	1.35E-06	5.30E-08	1.66E-07	9.94E-06	9.94E-06	9.94E-06	9.94E-06	9.94E-06	1.09E-08	8.62E-06	8.62E-06	9.11E-06	0	0	0	0	0	0	9.07E-06	0	0	0	0	1.52E-06	5.30E-08
S^{2-}	KMOL/HR	0	0	6.33E-14	1.89E-16	7.74E-15	3.82E-11	3.82E-11	3.82E-11	3.82E-11	3.82E-11	5.47E-17	2.93E-11	2.93E-11	2.56E-11	0	0	0	0	0	0	2.50E-11	0	0	0	0	7.10E-14	1.89E-16
CO_3^{2-}	KMOL/HR	0	0	5.64E-07	1.98E-07	6.90E-08	1.90E-07	1.90E-07	1.90E-07	1.90E-07	1.90E-07	9.26E-14	1.44E-07	1.44E-07	2.10E-07	0	0	0	0	0	0	2.07E-07	0	0	0	0	6.33E-07	1.98E-07
Component Mass Flow																												
H_2O	KG/HR	0.0373054	604.8991	5302.083	648.8083	648.8456	5347.006	5347.006	5347.006	5346.971	5343.407	5343.406	5346.982	5346.982	5951.853	200.2012	200.2012	200.2034	200.2012	200.2012	156.1728	5951.853	0	0	0	0	5951.664	648.8456
CO_2	KG/HR	0.3955623		4.171086	0.114884	0.5103683	5.16489	5.16489	5.16489	5.16489	1.676055	2.050061	5.212454	5.212454	5.142442	108.6195	108.6195	108.6195	108.6195	108.6195	108.0157	5.142939	0	0	0	0	4.681454	0.5104463
CO	KG/HR	1.214204	0	18.81681	1.088195	2.302399	21.18704	21.18704	21.18704	21.1316	13.37054	13.37054	21.11921	21.11921	21.11921	395.7599	395.7599	395.7599	395.7599	395.7599	393.3896	21.11921	0	0	0	0	21.11921	2.302399
H_2	KG/HR	0.0351397	0	0.2888888	0.00020828	0.035348	0.3242368	0.3242368	0.3242368	0.3242368	0.00462288	0.00462288	0.3242368	0.3242368	0.3242368	58.30871	58.30871	58.30871	58.30576	58.30871	58.27337	0.3242368	0	0	0	0	0.3242368	0.035348
CH_4	KG/HR	0.2538456	0	16.80468	1.802352	2.056197	18.86088	18.86088	18.86088	18.86088	18.86088	18.86088	18.86088	18.86088	18.86088	43.65331	43.65331	43.65331	43.65331	43.65331	41.59712	18.86088	0	0	0	0	18.86088	2.056197
H_2S	KG/HR	3.28E-05	0	0.00047927	2.78E-05	5.86E-05	0.00051137	0.00051137	0.00051137	0.00051137	0.00051137	0.00059781	0.00052155	0.00052155	0.00051261	0.003845	0.003845	0.003845	0.003845	0.003845	0.00377982	0.00051286	0	0	0	0	0.00053791	6.07E-05
NH_3	KG/HR	9.14E-08	0	0.000308906	5.30E-05	0.00037797	0.2292358	0.2292358	0.2292358	0.2292358	0.2292358	0.00034406	0.207025	0.207025	0.1797891	0.1270265	0.1270265	0.1270265	0.1414693	0.1270266	0.0497005	0.1799932	0	0	0	0	0.00346704	5.31E-05
HCN	KG/HR	1.62E-05		0.0137898	0.00167416	0.0016873	0.0152496	0.0152496	0.0152496	0.0152496	0.0152496	0.0155179	0.0152853	0.0152853	0.015272	0.00712824	0.00712824	0.00712824	0.0105643	0.0071248	0.00543646	0.0152731	0	0	0	0	0.0154771	0.00169035
N_2	KG/HR	0.00334434	0	0.0274726	1.72E-05	0.00336152	0.0308342	0.0308342	0.0308342	0.0308342	0.0308342	0.0308342	0.0308342	0.0308342	0.0308342	10.52077	10.52077	10.52077	10.50711	10.52078	10.51741	0.0308342	0	0	0	0	0.0308342	0.00336152
COS	KG/HR	3.15E-05	0	0.01136	0.00135849	0.00139	0.01275	0.01275	0.01275	0.01275	0.01275	0.01275	0.01275	0.01275	0.01275	0.0038504	0.0038504	0.0038504	0.0038504	0.0038504	0.0024604	0.01275	0	0	0	0	0.01275	0.00139

Component	Units																										
ACETI-01	KG/HR	0	0	0	0	0	0	0	0	0	2.380331	2.379846	0	0	0	0	0	0	0	0	0	0	0	0	0	0	0
FORMI-01	KG/HR	2.33E-08	0	0.0090037255	0.00021273	0.00110579	0.00482185	0.00482185	0.00482185	0.0959231	12.84862	11.4442	0.00625086	0.00625086	0.0059047	0	0	0	0	0	0.00010509	0.00593168	0	0	0	0	0.010143	0.00021275
HCL	KG/HR	0	0	0	0	0	0	0	0	0	0	0	0	0	0	0	0	0	0	0	0	0	0	0	0	0	0	0
NH_4^+	KG/HR	0	0	0.6660644	0.081843	0.0814987	0.5084044	0.5084044	0.5084044	0.5084044	0.5084044	0.7508788	0.5319382	0.5319382	0.5607835	0	0	0	0	0	0.5605672	0	0	0	0	0	0.7475631	0.081843
NA^+	KG/HR	0	0	0	0	0	0	0	0	0	0	0	0	0	0	0	0	0	0	0	0	0	0	0	0	0	0	0
H_3O^+	KG/HR	0	9.42E-06	0.00029939	7.07E-06	3.66E-05	0.00016405	0.00016405	0.00016405	0.00016405	0.00016405	0.1628798	0.00019052	0.00019052	0.00020206	0	0	0	0	0	0.00020122	0	0	0	0	0	0.00033602	7.07E-06
NH_2COO^-	KG/HR	0	0	2.36E-05	2.19E-06	2.89E-06	0.00014382	0.00014382	0.00014382	0.00014382	0.00014382	9.25E-11	0.00011337	0.00011337	0.00011925	0	0	0	0	0	0.0001195	0	0	0	0	0	2.65E-05	2.19E-06
HS^-	KG/HR	0	0	5.19E-05	4.37E-06	6.35E-06	8.40E-05	8.40E-05	8.40E-05	8.40E-05	8.40E-05	1.06E-07	7.41E-05	7.41E-05	8.28E-05	0	0	0	0	0	8.25E-05	0	0	0	0	0	5.82E-05	4.37E-06
HCO_3^-	KG/HR	0	0	1.059341	0.1295043	0.1296196	0.5186056	0.5186056	0.5186056	0.5186056	0.5186056	0.00022049	0.4526949	0.4526949	0.5497534	0	0	0	0	0	0.5490636	0	0	0	0	0	1.188961	0.1295043
OH^-	KG/HR	0	8.42E-06	8.38E-06	1.46E-07	1.03E-06	0.00025101	0.00025101	0.00025101	0.00025101	0.00025101	2.69E-07	0.00021717	0.00021717	0.00022711	0	0	0	0	0	0.00022552	0	0	0	0	0	9.41E-06	1.46E-07
CL^-	KG/HR	0	0	0	0	0	0	0	0	0	0	0	0	0	0	0	0	0	0	0	0	0	0	0	0	0	0	0
CH_3COO^-	KG/HR	0	0	0	0	0	0	0	0	0	0	0.00047729	0	0	0	0	0	0	0	0	0	0	0	0	0	0	0	0
$HCOO^-$	KG/HR	0	0	0.8812471	0.1087017	0.1078282	0.8852675	0.8852675	0.8852675	0.8852675	0.8852675	2.258946	0.9928823	0.9928823	0.9932209	0	0	0	0	0	0.9931945	0	0	0	0	0	0.9890753	0.1087017
CN^-	KG/HR	0	0	3.52E-05	1.38E-06	4.31E-06	0.00025853	0.00025853	0.00025853	0.00025853	0.00025853	2.83E-07	0.00022418	0.00022418	0.00023696	0	0	0	0	0	0.00023588	0	0	0	0	0	3.95E-05	1.38E-06
S^{2-}	KG/HR	0	0	2.03E-12	6.06E-15	2.48E-13	1.22E-09	1.22E-09	1.22E-09	1.22E-09	1.22E-09	1.75E-15	9.39E-10	9.39E-10	8.20E-10	0	0	0	0	0	8.02E-10	0	0	0	0	0	2.28E-12	6.06E-15
CO_3^{2-}	KG/HR	0	0	3.38E-05	1.19E-05	4.14E-06	1.14E-05	1.14E-05	1.14E-05	1.14E-05	1.14E-05	5.56E-12	8.63E-06	8.63E-06	1.26E-05	0	0	0	0	0	1.24E-05	0	0	0	0	0	3.80E-05	1.19E-05
Total Mole Flow	KMOL/HR	0.0877831	33.57701	296.3845	36.17741	36.26519	299.0861	299.0861	299.0861	299.0841	298.6881	298.6966	299.0847	299.0847	332.6601	59.73918	59.73918	59.73918	59.7382	59.73918	57.04644	332.6601					332.6497	36.2652
Total Mass Flow	KG/HR	1.939482	604.8992	5345.572	652.1374	654.0768	5394.75	5394.75	5394.75	5394.75	5394.75	5394.75	5394.75	5394.75	5999.649	817.2052	817.2052	817.2052	817.2052	817.2052	768.0275	5999.649	0	0	0	0	5999.649	654.0768
Total Volume Flow	CUM/HR	2.137767	0.6314851	5.626738	0.6651938	0.6884799	6.194821	6.194821	6.194821	6.195052	6.209748	6.207094	6.194882	6.194882	6.817684	102.1591	102.1591	102.1591	102.1574	102.1591	30.26476	6.81711	0	0	0	0	6.315218	2.80296
Temperature	C	20	105	79.99752	20	79.99752	177.4319	177.4319	177.4319	177.4382	177.4382	177.4382	177.4382	177.4382	170.4049	1172.073	1172.073	1172.073	1172.073	1172.073	177.4319	170.2656					79.99752	20
Pressure	BAR	1	72.0003	72.0003	1	72.0003	71.01355	71.01355	71.01355	71.01355	71.01355	71.01355	71.01355	71.01355	72.0003	71.01355	71.01355	71.01355	71.01355	71.01355	71.01355	71.01355	71.01355	71.01355	71.01355	71.01355	72.0003	1
Vapor Fraction		1	0	0	0	0	0	0	0	0	0	0	0	0	0	1	1	1	1	1	1	0					0	0.00242059

Property	Units	1	2	3	4	5	6	7	8	9	10	11	12	13	14	15	16	17	18	19	20	21	22	23	24	25	26	27
Liquid Fraction		0	1	1	1	1	1	1	1	1	1	1	1	1	1	0	0	0	0	0	0	1					1	0.9975794
Solid Fraction		0	0	0	0	0	0	0	0	0	0	0	0	0	0	0	0	0	0	0	0	0					0	0
Molar Enthalpy	KCAL/MOL	-27.30369	-66.84623	-67.00651	-68.2046	-67.00651	-65.19051	-65.19051	-65.19051	-65.19084	-65.28987	-65.28928	-65.19081	-65.19081	-65.35537	-12.15477	-12.15477	-12.15477	-12.15517	-12.15477	-19.07623	-65.35821					-67.00651	-68.10559
Mass Enthalpy	KCAL/KG	-1235.796	-3710.529	-3715.166	-3783.66	-3715.166	-3614.176	-3614.176	-3614.176	-3614.17	-3614.867	-3614.938	-3614.176	-3614.176	-3623.733	-888.5358	-888.5358	-888.5358	-888.5501	-888.5358	-1416.917	-3623.89					-3715.166	-3776.105
Enthalpy Flow	GCAL/HR	-0.0023968	-2.244496	-19.85969	-2.467466	-2.430004	-19.49757	-19.49757	-19.49757	-19.49754	-19.50131	-19.50169	-19.49757	-19.49757	-21.74113	-0.726116	-0.726116	-0.726116	-0.7261277	-0.726116	-1.088231	-21.74207					-22.28969	-2.469863
Molar Entropy	CAL/MOL-K	9.430608	-34.71213	-35.72419	-39.13957	-35.72419	-31.25891	-31.25891	-31.25891	-31.25881	-31.32381	-31.32487	-31.25894	-31.25894	-31.57592	9.096026	9.096026	9.096026	9.096041	9.096026	-0.1529537	-31.58125					-35.72419	-39.022
Mass Entropy	CAL/GM-K	0.42684	-1.926816	-1.980722	-2.171273	-1.980722	-1.733	-1.733	-1.733	-1.732984	-1.734288	-1.734396	-1.732995	-1.732995	-1.750777	0.6649359	0.6649359	0.6649359	0.6649262	0.6649359	-0.0113608	-1.751073					-1.980722	-2.163569
Molar Density	KMOL/CUM	0.041063	53.17149	52.67429	54.38628	52.67429	48.28001	48.28001	48.28001	48.2779	48.09988	48.12181	48.27932	48.27932	48.79371	0.5847663	0.5847663	0.5847663	0.5847664	0.5847663	1.884913	48.79783					52.67429	12.93818
Mass Density	KG/CUM	0.9072469	957.8993	950.0304	980.372	950.0304	870.8483	870.8483	870.8483	870.816	868.7551	869.1265	870.8398	870.8398	880.0128	7.999341	7.999341	7.999341	7.999473	7.999341	25.37695	880.0869					950.0304	233.3521
Average Molecular Weight		22.09401	18.01528	18.03594	18.02609	18.03594	18.03745	18.03745	18.03745	18.03757	18.06148	18.06097	18.03753	18.03753	18.03537	13.67955	13.67955	13.67955	13.67978	13.67955	13.4632	18.03537					18.03594	18.03594
Liq Vol 60F cum/hr		4.63E-03														2.804906	2.804906	2.804906	2.804849	2.804906	2.747468		0	0	0	0		